UNIVERSITÀ DELLA CALABRIA

UNIVERSITA' DELLA CALABRIA

Dipartimento di Biologia, Ecologia e Scienze della Terra (DiBEST)

Dottorato di Ricerca in

Scienze della Vita

Indirizzo

Biotecnologie

XXXIII CICLO

The effect of cholesterol on the function of eukaryotic membrane transporters for amino acids

Settore Scientifico Disciplinare: BIO/10 BIOCHIMICA

Coordinatore: Ch.mo Prof.ssa Maria Carmela Cerra

Firma _____ Firma oscurata in base alle linee guida del Garante della privacy

Supervisore/Tutor: Ch.mo Prof. Cesare Indiveri

Firma_____ INDIVERI CESARE 25.11.2020 17:04:56 UT

Dottoranda: Dott.ssa Jessica Cosco

Firma _ Firma oscurata in base alle linee guida del Garante della privacy

Contents

Abstract

Amino acid transport in mammalian cells is mediated by different amino acid transporters. Amino acid flow, which is important under physiological conditions, becomes particularly relevant under pathological conditions such as in cancer cells where high demand for these nutrients is required to satisfy the uncontrolled growth and proliferation. Therefore, to guarantee a sufficient supply of nutrients a lot of amino acid transporters are highly expressed in cancer cells. In this context, the amino acid transporters hLAT1 and hASCT2 are widely studied for their role as potential targets for drug development.

hASCT2 belongs to SLC1 family and assembles at the plasma membrane as a trimeric complex. Studies conducted using the recombinant protein showed that this transporter is strongly stimulated by cholesterol. The stimulation is due to an improvement of protein insertion in the phospholipid bilayer and direct interaction with the protein. In fact, cholesterol increased the Vmax of the transport, without affecting the external Km, indicating that it increases the rate of conformational changes. Thanks to docking analysis, 6 putative cholesterol binding sites were predicted, some of these matched with the electron densities identified on the cryo-EM structure of ASCT2. Two poses are on the TM6, where a CRAC and a CARC motif has been identified. Experimental demonstrated the direct binding of cholesterol to the protein. In particular, Koshland's reagent and SH-reagents have been used for the target of tryptophan and cysteine residues close to the cholesterol poses.
hLAT1 belongs to SLC7 family and it forms a heterodimer complex (HAT) with the glycoprotein 4F2hc (also known as CD98 in mice), a member of SLC3 family. hLAT1 is the sole component involved in the transport of essential amino acids, as previously demonstrated (Napolitano, Scalise et al. 2015). In this work, the influence of cholesterol has been evaluated on the recombinant protein hLAT1. Moreover, putative regulators involved in energy metabolism have been tested on the transport. The transport activity increased up 75 µg cholesterol/ mg phospholipids. Moreover, the internal substrate affinity increased in the presence of cholesterol suggesting a stabilization of the inward conformation of hLAT1. The transporter is also stimulated by ATP at physiological concentration. This effect occurs only in the presence of cholesterol and was seen also on the native protein. This finding suggested that cholesterol and ATP binding sites are close to each other. The computational analysis confirmed this hypothesis. In fact, a hydrophobic region between the TMs 1, 5 and 7 was found to be close to a hydrophilic one. Docking results for ATP suggested an electrostatic interaction of the ϒ-phosphate of ATP with Lys 204, which was confirmed by site-directed mutagenesis. This residue is conserved in the other SLC7 proteins and for a serendipity event, it has been seen that Lys204 is also important in the substrate binding and pH-sensitive.

In this work, the attention was focused also on another amino acid transporter CAT2, from *Solanum lycopersicum*. The specific interest in tomato resides in the well-recognized role for this species in biotechnology. In fact, tomato has been used as the primary model for the study of climacteric fruit ripening.
SlCAT2 belongs to APC superfamily, as LAT1, and it is involved in the transport of cationic amino acids like arginine, lysine and the non-proteogenic amino acid ornithine. The experimental data on CAT2 highlighted an

asymmetric regulation by cations and osmotic pressure, in line with the localization of the transporter in vacuoles. Like the other human transporters, CAT2 is also stimulated by cholesterol. On the basis of the 3D structure of the amino acid transporter GkApcT, the homology model of SlCAT2 was built and putative substrate binding residues and cholesterol binding domains were proposed.

Altogether, the described results open new perspectives for studying the response of membrane transporters to metabolic and membrane changes. Moreover the identification of hydrophobic or hydrophilic sites interacting with cholesterol or physiological effectors, respectively, could be important for applications in human pathology.

Abbreviations

ATP-binding cassette (ABC) transporters

SLC Solute carrier

APC Amino acid-polyamine-organocation (APC) superfamily

ATF Amino acid transport family

EAAT excitatory amino acid transporters

GkApcT Proton-coupled broad-specificity amino acid transporter from *Geobacillus Kaustophilus*

ASCTs Alanine serine cysteine transporters

GLAST Glutamate aspartate transporter

GLT Glutamate transporter

EAT Ethanolamine transporter

AAT Amino acid transporter

YAT Yeast amino acid transporter

APA Basic amino acid/polyamine transporter

ACT Amino acid/choline transporter

ABT Archaeal/bacterial transporter

GGA Glutamate:GABA antiporter

SGP Spore germination protein

CATs Cationic amino acid transporters

LATs Light subunits of amino acid transporters

ASD Autism spectrum disorders

BCAA Branched chain amino acids

LNAA Large neutral amino acids

CD98 Cluster of differentiation 98

BAT Neutral and basic amino acid transport protein

BBB Blood brain barrier

CNS central nervous system

DAT Dopamine transporter

SERT serotonin transporter

mTOR Mammalian target of rapamycin

TEMED Tetramethylethylenediamine

TX-100 Triton X-100

GSNO S-Nitrosoglutathione

DTE Dithioerythritol

DDM N-Dodecyl β-D-maltopyranoside

AdiC L-arginine/agmatine antiporter

BCH 2-aminobicyclo-(2,2,1)-heptane-2-carboxylic acid

$C_{12}E_8$ Octaethylene glycol monododecyl ether

E. coli Escherichia coli

P. Pastoris Pichia pastoris

LeuT Na^+-coupled leucine transporter

MTSEA 2-Aminoethyl methanethiosulfonate hydrobromide

NEM N-ethylmaleimide

ECL Electro Chemi Luminescence

EDTA Ethylenediaminetetraacetic acid

EGTA Ethylene glycol-bis(β-aminoethyl ether)-*N*,*N*,*N*′,*N*′-tetraacetic acid

SDS Sodium dodecyl sulfate

PLP Pyridoxal 5'- phosphate

CHEMS Cholesteryl hemisuccinate

MCD Methyl-β-ciclodextrin

MeAIB N-methyl-aminoisobutyric acid

CRAC-CARC Cholesterol recognition amino acid consensus sequence

CHAPTER I

Introduction

1.1. Biological membranes and transport activity

Biological membranes are selectively permeable barriers that separate the inner space (cytoplasm) of the cell from the outer space, maintaining their architecture and physiology. In addition to the plasma membrane that defines the external boundaries, other intracellular membranes divide the internal space of eukaryotic cells into discreet compartments with several components involved in specific processes (Nelson D.L. Fourth Edition).

Membranes regulate molecule traffic between the internal and external environment, safeguarding nutrient assumption, retaining metabolic intermediates and eliminating scrap products. Moreover, they are involved in cell-to-cell communication and signal transduction.

They are formed by a phospholipid bilayer which gives stability and fluidity. Peripheral or integral proteins partially or fully embedded, respectively, in the membrane, are involved in signal transduction and transport phenomena. Ions, amino acids, sugars, or other molecules are not able to diffuse through the hydrophobic bilayer, with very few exceptions. The presence of transport proteins guarantees the flux of the molecules needed for cell functioning (Nelson D.L. Fourth Edition).

In particular, they guarantee the uptake into the cytoplasmic compartment and the distribution to the organelles of all nutrients that are used as a source of energy as well as atoms such as carbon, nitrogen, sulfur, and phosphorus needed for anabolic processes. The membrane transporters contribute to the regulation of metabolic pathways and guarantee the excretion of end products. Some specific transporters, called primary active transporters, create the membrane potential by hydrolyzing ATP. More recently, it was discovered that membrane transporters are also involved in the uptake or efflux of drugs or toxic compounds (Saier 2000).

The concentration of transport proteins in the membrane bilayer changes on the basis of membrane type and function. Membrane proteins represent a significant fraction (30%) of all proteins encoded in the genomes of all organisms, highlighting the importance of these proteins for cell life (Fagerberg, Jonasson et al. 2010, Nelson D.L. Fourth Edition).

1.2. Membrane transport proteins

Transporters can be classified using different criteria based on functional, molecular or evolutionary aspects. Two major groups can be distinguished, channels and permeases on the basis on the features below described:

1. **Channels** are transmembrane proteins that are involved in the transport of ions, with a high turnover rates ($10^7 - 10^8$ ions/s). Ions move from one side of the membrane to the other, on the basis of their concentration gradient;
2. **Permeases** exhibit turnover rates orders of magnitude lower than those of channels. In contrast, they show a higher specificity towards the substrates and they can employ different energy-

coupled mechanisms, besides the simple concentration gradient. Moreover, they show saturable kinetic of transport, like enzymes.

On the basis of the transport driving force, permeases can be further subdivided into primary or secondary active transporters.

- **Primary active transporters** utilize the primary source of energy generated from ATP hydrolysis;
- **Secondary active transporters** represent the largest group and can be subdivided in uniporters, symporters and antiporters on the basis of the transport modes.
    - **Uniporters** catalyse the transport of a single molecular species using, as driving force, the concentration gradient of the molecule itself on the two sides of the membrane;
    - **Symporters** also called cotransporters, mediate the transport of a substrate coupled, generally, to an ion, in the same direction. The driving force derives from the concentration gradient of the ion, thus the substrate can be transported also against its concentration gradient;
    - **Antiporters**, also called countertransporters, catalyse the exchange of two (or more) substrates in opposite direction (Saier 2000, Scalise, Pochini et al. 2013).

1.3. Amino acid metabolism and transport

The human body is able to synthesize only some amino acids (non-essential). The other amino acids (essential) derive from the diet proteins. Protein degradation, in their constituent amino acids, takes place in the gastrointestinal segment. The resulting dipeptides and amino acids are efficiently absorbed by enterocytes of the small intestine and distributed to tissues through the blood. Amino acids are necessary for the synthesis of proteins and bioactive molecules, such as hormones, neurotransmitters, polyamine, creatine, phosphatidylserine, etc., as well as for energy metabolism. Moreover, amino acids can be involved in the regulation of certain endocrine metabolisms (Broer 2008, Broer and Broer 2017). For example, glucose and amino acids can modulate insulin, glucagon and glucagon-like peptides secretion (Hyde, Taylor et al. 2003).

1.4. Mammalian amino acid transporters

Mammalian cells have a broad range of mechanisms for the transmembrane transport of amino acids. Amino acid transporters are classified on the basis of substrate specificity, transport mechanism and regulatory properties, ion or pH dependence. Studies of Halvor Christensen in nonepithelial cells showed that amino acid transporters

accept groups of amino acids, not individual amino acids, such as small neutral amino acids, large neutral amino acids, anionic amino acids, and cationic amino acids (Hyde, Taylor et al. 2003, Broer 2008). Initially, amino acid transporters have been defined as "systems", a term used to indicate a transport activity functionally identified and very similar in different cell types. In particular, Christensen's work identified:

- **System L** which includes neutral amino acid transporters that prefer leucine or other large hydrophobic neutral amino acids;
- **System A** regroups amino acid transporters that prefer alanine or other small and polar neutral amino acids;
- **System ASC** with amino acid transporters that prefer alanine, serine and cysteine;
- **System y^+** for cationic amino acids;
- **System X^{-AG}** for anionic amino acids.

Moreover, all transporters can be divided in Na^+- dependent or Na^+-independent.

- **Na^+-dependent amino acid transporters** utilize the energy stored in the transmembrane sodium gradient, maintained by the sodium pump or Na^+-K^+-ATPase, to move ions or other solutes against their concentration gradient across the membrane;
- **Na^+-independent amino acid transporters** move amino acids across the membrane independently of Na^+.

Except for the Na^+-independent system L, lowercase acronyms indicate Na^+-independent transporters, whereas uppercase acronyms are used for Na^+-dependent transporters (Bode 2001). This classification is still considered effective from a functional point of view. In the last decades, with the advent of bioinformatics, a new classification has been introduced on the basis of the sequence homology among transporters. Similar amino acid sequences in proteins reflect similar 3D structures and mechanism of action. Therefore, proteins are assigned to a certain family on the basis of their sequence homology with the other proteins belonging to this family, the number of transmembrane domains and the biological function.

1.5. The solute carrier (SLC) superfamily

A high number of transporters has been identified and characterized in the last decades and on the basis of functional properties, transporters are divided into two main superfamilies: the Solute Carrier (SLC) and the ATP-binding cassette (ABC) transporters. SLC members are involved in the transport of nutrients and other compounds essential for cell survival, such as sugars, digested peptides, amino acids, nucleosides and inorganic

ions. On the other hand, ABC proteins are involved in the efflux or metabolites, drugs and toxic compounds. Many transporters are still orphans since their substrates and functions remain to be identified (Fredriksson, Nordstrom et al. 2008, Schlessinger, Yee et al. 2013, Zhang, Zhang et al. 2019). SLC member localization also varies in cells, with the majority localized to the plasma membrane, while other transporters are localized in mitochondria, endoplasmic reticulum, lysosomes, synaptic vesicles or peroxisomes. The SLC nomenclature system was introduced in the 1990s by Matthias A. Hediger and Phyllis McAlpine. An overview of all currently known SLC genes is provided in the SLC tables (slc.bioparadigms.org) and the HGNC database (www.genenames.org/cgi-bin/genefamilies/set/752). At present, the SLC superfamily (Solute Carrier Transporters) includes more than 400 members grouped in 52 families (Hediger, Clemencon et al. 2013, Cesar-Razquin, Snijder et al. 2015, Zhang, Zhang et al. 2019). The classification is based on a common evolutionary origin (Schlessinger, Yee et al. 2013). SLC transporters are highly expressed in metabolically active organs, such as liver, kidney, brain and intestine, reflecting their importance in metabolism and in human diseases. In fact, SLC alterations are associated with Mendelian and complex multifactorial diseases. SLC related diseases range from neurological disorders, such as Parkinson disease, Alzheimer's disease, epilepsy, schizophrenia, autism, associated with dysfunction of SLC1 or SLC6 transporters autism (Pramod, Foster et al. 2013, Grewer, Gameiro et al. 2014), to less common diseases such as Barter and Gitelman syndrome, caused by mutations in SLC12 genes (Hebert, Mount et al. 2004). Furthermore, since their involvement in a lot of disorders, there is an increased interest in the targets of SLCs for drug development (Zhang, Zhang et al. 2019).

1.6. The SLC1 family

In mammals, the SLC1 family is composed of two groups, one is represented by five high-affinity glutamate transporters (EAAC1/SLC1A1, GLT-1/SLC1A2, GLAST/SLC1A3, EAAT4/SLC1A6 and EAAT5/SLC1A7), which exhibit the properties of the previously described system X^{-AG}, and the other group counts two neutral amino acid transporters (ASCT1/SLC1A4 and ASCT2/SLC1A5) sharing some features of the ASC system (Kanai and Hediger 2003). In humans, members of the first group share 44-55% sequence identity with each other. The other two proteins, ASCT1 and ASCT2, exhibit 57% identity with each other, but a low identity of 37-41% with the EAATs. The phylogenetic tree of SLC1 transporters is shown in Figure 1:

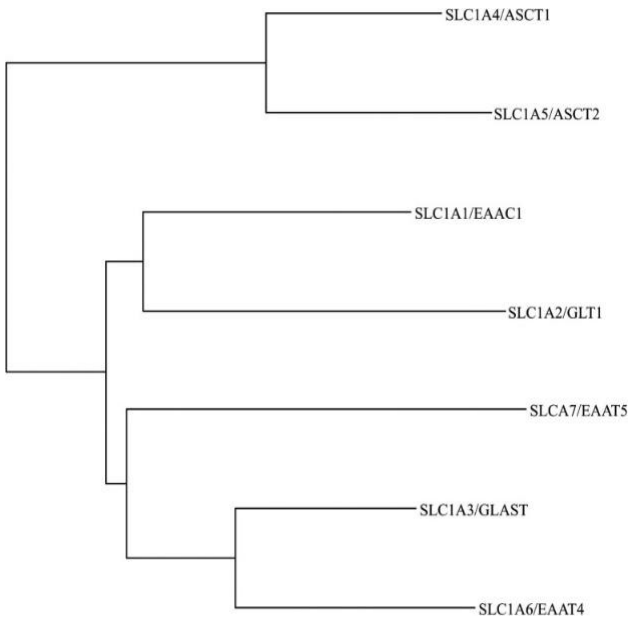

Figure 1 Phylogenetic tree of seven human SLC1 family members. (Adapted from Kanai Y. et al, The SLC1 high-affinity glutamate and neutral amino acid transporter family, 2013).

EAAC1, GLT1 and GLAST were the first transporters identified in 1992. Kanai and Hediger isolated a cDNA encoding EAAC1 after cloning in *Xenopus oocytes* (Kanai and Hediger 1992). Kanner et al. purified GLT1 and showed that this transporter mediates the transport of glutamate with high affinity using the reconstitution in liposomes (Danbolt, Storm-Mathisen et al. 1992, Pines, Danbolt et al. 1992). Stoffel et al. purified GLAST and identified its cDNA through partial amino acid sequencing (Storck, Schulte et al. 1992).

The other two glutamate transporters, EAAT4 and EAAT5, as well as ASCT1 and 2 were identified on the basis of their identity with the other members of SLC1 family. EAATs are the major transport mechanisms involved in the extracellular glutamate removal from CNS, regulating its concentration and avoiding the glutamate toxicity (Magi, Piccirillo et al. 2019). Loss of function of these transporters is associated with several diseases, like amyotrophic lateral sclerosis, Alzheimer's disease or schizophrenia (Kanai and Hediger 2003, O'Donovan, Sullivan et al. 2017, Malik and Willnow 2019). All SLC1 members are Na^+-dependent, although their stoichiometries are distinct. In fact, EAATs are concentrative transporters, i.e. substrate transport is coupled to the cotransport of three Na^+ ions and one H^+ ion and the contertransport of one K^+ (Figure 2). On the other hand, ASCTs are obligatory exchangers of neutral amino acids (Zerangue and Kavanaugh 1996, Broer, Wagner et al. 2000), where both the influx and the efflux event are coupled to the transport of two or more Na^+ ions. In addition to these ion fluxes, SLC1 members show a thermodynamically uncoupled Cl^- conductance. The significate of this flux has not been clarified, yet. It has been proposed that Cl^- could be used to balance Na^+ uptake, safeguarding the membrane potential and thus, the glutamate uptake.

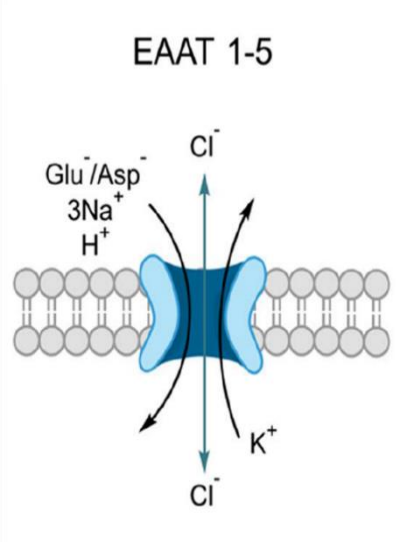

Figure 2 Stoichiometry of EAATs transporters (Adapted from Freidman et al., Amino Acid Transporters and Exchangers from the SLC1A Family: Structure, Mechanism and Roles in Physiology and Cancer, 2019).

1.6.1. ASCT2 (SLC1A5)

One of the most studied transporters belonging to SLC1 family is the plasma membrane transporter SLC1A5, also called ASCT2 (Alanine, Serine, Cysteine Transporter 2). ASCT2 gene was mapped on chromosome 19q13.32 (Larriba, Sumoy et al. 2001). This gene contains 8 exons and since the presence of different translation starts, three isoforms are reported either on NCBI and Ensemble databases. The first isoform, is the longest one, with 2873 nucleotides and 8 exons encoding for a peptide of 541 amino acids (NM 005628), with a molecular mass of 57 kDa. The second one (NM 001145144) with 1737 nucleotides differs in the 5' UTR from the first variant and encodes for a shorter peptide of 313 amino acids. The third isoform (NM 001145145) has 1927 nucleotides, lacking the first exon and it has been localized in mitochondria (Yoo, Park et al. 2020). It has a different translation start, coding a peptide of 339 amino acids. A longer transcript XM_005259167, identified by computational analysis, is reported only in the NCBI database (Figure 3). A lot of SNPs were reported for SLC1A5 gene. Some of these were well characterized: the variant rs3027956 and rs11668878 are associated with breast cancer and chronic lymphocytic leukemia (Savas, Kerr et al. 2006, Sille, Thomas et al. 2012). On the contrary, the other two variants, rs3027985 and rs1644343 are linked to longevity (D'Aquila, Crocco et al. 2018, Scalise, Pochini et al. 2018).

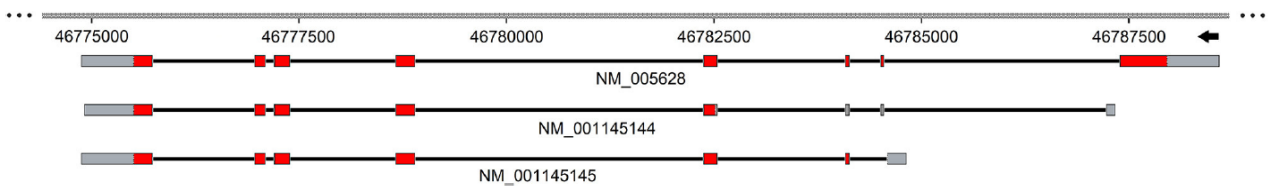

Figure 3 Schematic representation of human SLC1A5 gene. Exons and introns are represented with solid boxes and black straight lines, respectively. UTR sequence is in gray, while the codon region in red. (Adapted from Scalise et al. The Human SLC1A5 (ASCT2) Amino Acid Transporter: From Function to Structure and Role in Cell Biology, 2018).

ASCT2 is widely expressed in the human body. In particular, its expression has been found in lung, skeletal muscle, large intestine, kidney, testis, T-cells, brain and adipose tissue (Kanai, Clemencon et al. 2013). In all cells, ASCT2 has a unique localization at the plasma membrane (Kanai, Clemencon et al. 2013, Poffenberger and Jones 2014). Noteworthy, high levels of ASCT2 have been found in several cancer types, such as melanoma, lung, prostate, cervical, ovarian, renal, hepatic, colorectal and breast cancer (Scalise, Pochini et al. 2017).

1.6.2. Transport properties and structure of ASCT2

Human ASCT2 is a Na^+-dependent obligatory exchanger of neutral amino acids (Kekuda, Prasad et al. 1996, Utsunomiya-Tate, Endou et al. 1996, Broer, Brookes et al. 1999, Bode 2001). The studies of the antiport mode using radiolabelled substrates in intact cells and oocytes demonstrated that ASCT2 mediates the uptake and the efflux of alanine, glutamine and threonine (Kekuda, Prasad et al. 1996, Utsunomiya-Tate, Endou et al. 1996, Broer, Brookes et al. 1999, Bode 2001). Moreover, it has been seen that leucine, threonine, methionine, alanine, glutamine, and glutamate induce efflux of radiolabelled threonine from oocytes expressing human ASCT2, as well as rat ASCT2 (Torres-Zamorano, Leibach et al. 1998, Broer, Wagner et al. 2000). Patch clump measurement of alanine uptake on ASCT2 murine isoform revealed an anion current associated to counter transport of amino acids, like EAATs (Broer, Wagner et al. 2000). Using the recombinant *h*ASCT2 and the reconstitution in liposomes, additional data was obtained. In particular, it has been seen that glutamine is the preferred substrate of ASCT2 and amino acids such as alanine, serine, asparagine and threonine are able to induce both glutamine uptake and efflux. On the contrary, valine and cysteine induce only glutamine efflux (Oppedisano, Pochini et al. 2004, Oppedisano, Pochini et al. 2007, Scalise, Pochini et al. 2018). Moreover, it was demonstrated that Na^+ is a substrate of ASCT2 and it is transported together with neutral amino acids (Broer, Wagner et al. 2000, Oppedisano, Pochini et al. 2007). The cryo-EM structures of ASCT2 in the inward (Garaeva, Oostergetel et al. 2018) and outward facing conformation (Yu, Plotnikova et al. 2019) have been solved. ASCT2, as the other EAATs, assembles as a homotrimer, where each protomer is able to function independently (Grewer, Balani et al. 2005) and consists of two domains, a transport domain (TM3, TM6 and TM8 and helical loop 1 and 2) and a scaffold domain (TM1, TM2, TM4 and TM5) connected by the extracellular loop 2 (ECL2a and ECL2b) (Figure 4). Superposition between the inward and the outward state shows that the scaffold domains remain relatively rigid, while the transport domain moves toward the cytoplasm and the substrate binding site shifts. HP2 loop acts as a gate, open in the outward conformation and closed after glutamine binding (Garaeva, Oostergetel et al. 2018, Yu, Plotnikova et al. 2019).

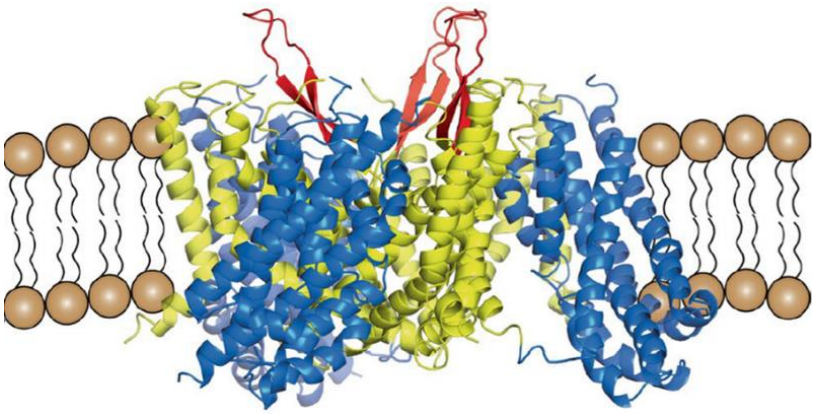

Figure 4 Structural model of ASCT2. Side view with the scaffold domains as yellow ribbons and the transport domains as blue ribbons (Adapted from Garaeva et al., Cryo-EM structure of the human neutral amino acid transporter ASCT2, 2018).

Residues belonging to the substrate binding sites are highly conserved in all SLC1 members (Figure 5), except for an arginine residue preserved in all EAATs and involved in substrate selectivity, which is substituted with a cysteine in ASCT2 (C467) and a threonine in ASCT1 (T459). The mutation of arginine with cysteine or threonine in EAATs introduces the neutral amino acid flux, demonstrating that this residue is important for substrate specificity. Scalise et al., demonstrated that C467 is involved in glutamine binding and translocation, in responsiveness to redox sensing molecules, such as GSH, H_2S and GSNO, as well as SH reagents, DTE and mercury. Moreover, mutation of cysteine with alanine determines a loss of sensitivity to all of these compounds, indicating an "ON/OFF" regulation of ASCT2 through C467 to the redox status in the cell. In fact, C467 could be involved in the formation of a disulfide bridge with the vicinal C308 and C309, leading to the interconversion between the active state (reduced cysteine) to the inactive state (oxidized cysteine) (Scalise, Pochini et al. 2018). Yu et al., identified an additional cavity in ASCT2 involving the residues Phe393, Val436, Ala433, Val463. These residues are not conserved in EAATs, only between ASCT1 and ASCT2, but their function is not clear, yet (Yu, Plotnikova et al. 2019). Moreover, it has been seen several cryo-EM densities in the structure of ASCT2, which may correspond to lipids, like cholesterol. Other SLC1 proteins have been found to interact with lipids, which stabilize their structure and regulate conformational changes. In ASCT2, lipids have been found not only on the surface, but also between the scaffold domain and transport domain suggesting a possible role in the regulation of the movement of the transport domain and thus in the regulation of conformational changes (Garaeva, Oostergetel et al. 2018).

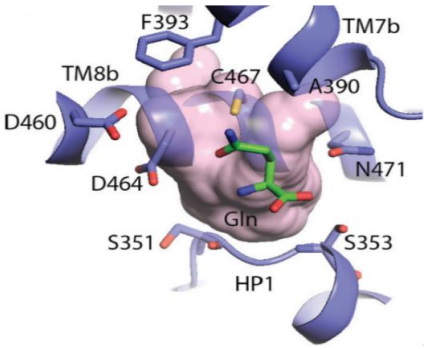

Figure 5 The substrate, L-glutamine-bound SLC1A5 structure (PDB ID: 6GCT) (Adapted from Garaeva et al., Cryo-EM structure of the human neutral amino acid transporter ASCT2, 2018).

1.7. SLC7 family

The SLC7 family consists of 15 members, two of which are pseudogenes. The 13 encoded proteins are classified in two subfamilies (Figure 6):

- **Cationic amino acid transporters** (CATs) with SLC7A1-4 and SLC7A14;
- **Glycoprotein-associated amino acid transporters** (LATs, SLC7A5-13 and SLC7A15), also called light chains or catalytic chains of the hetero(di)meric amino acid transporters (HATs).

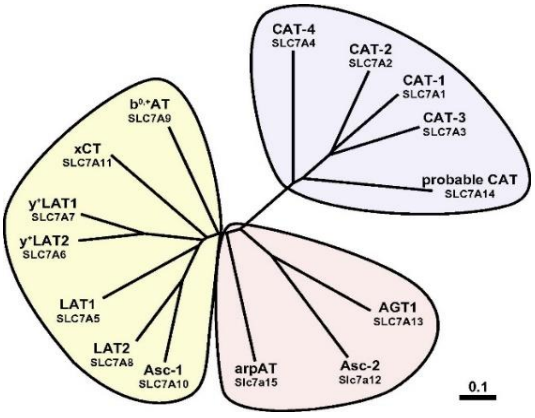

Figure 6 Phylogenetic tree of SLC7 family members. The SLC7 family is composed of the CATs (cluster colored in blue) and the light subunits (cluster colored in yellow/pink). (Adapted from Fotiadis D. et al., The SLC3 and SLC7 families of amino acid transporters, 2013).

Moreover, CATs and LATs belong to APC system, i.e. a superfamily of amino acids, polyamines and cationic transporters. APC transporters function as solute:cation symporters or solute:solute antiporters. This superfamily counts 10 families, which are: EAT (ethanolamine transporter) family; AAT (amino acid transporter) family; YAT (yeast amino acid transporter); LAT (l-type amino acid transporter) family; CAT (cationic amino acid transporter) family; APA (basic amino acid/polyamine transporter) family; ACT (amino acid/choline transporter) family; ABT (archaeal/bacterial transporter) family; GGA (Glutamate:GABA antiporter) family; SGP (Spore germination protein) family. Proteins belonging to APC superfamily vary in size from about 400 to 800 amino acid residues and according to hydropathy profile analysis, most APC transporters has 12 transmembrane domains with the N- and C- termini into the cytoplasm (Verrey, Jack et al. 1999, Jack, Paulsen et al. 2000, Casagrande, Ratera et al. 2008).

1.7.1. CAT family

The CAT proteins (Cationic Amino acid Transporter) are amongst the first mammalian amino acid transporters identified at the molecular level. CAT proteins form a subfamily of SLC7 which consists of four confirmed cationic amino acid transporters: CAT1 (SLC7A1), CAT2A and CAT2B (SLC7A2A and SLC7A2B) and CAT3 (SLC7A3). An additional transporter CAT4 (SLC7A4) has been allocated in the CAT branch, but its function is still unclear (Wolf, Janzen et al. 2002). CAT members are N-glycosylated and, on the basis of topology prediction and experimental data, they have 14 transmembrane domains with the N- and C- termini in the cytoplasmic space (Closs, Boissel et al. 2006, Fotiadis, Kanai et al. 2013).

The first member, CAT1 in mouse (mCAT1) was identified by Albritton et al. as the receptor for murine ecotropic leukemia viruses (Albritton, Kim et al. 1993, Closs, Boissel et al. 2006). Other three proteins associated with CAT1 have been identified in different mammalian species: CAT2A and B, CAT3 and CAT4. CAT2A and B are splicing variants, encoded by SLC7A2 gene, which differ only in a stretch of 42 amino acids localized between TM7 and TM 9. CATs transport cationic amino acids like arginine, lysine and ornithine in a Na^+-independent manner. They are trans-stimulated and show a low apparent Km for their substrates. Only CAT1 has a strong trans-stimulation and high affinity (Kim, Closs et al. 1991, Closs, Graf et al. 1997). Moreover, at acidic pH, CAT1 also mediates the transport of L-histidine. On the contrary, CAT2A is a low affinity cationic amino acid transporter and seems to be insensitive to trans-stimulation. The Km for cationic amino acids is 2-5 mM, while the other CATs show a Km of 0.1-0.4 mM (Verrey, Closs et al. 2004). It has been demonstrated that a region of 80 amino acids, localized into the 4^{th} intracellular loop on TM10 determines the substrate affinity and the trans-stimulation sensitivity of CATs. This region contains the short sequence of 42 amino acids which differ into two splicing variants, CAT2A and CAT2B. In particular, the low substrate affinity of CAT2A is due to the presence of two variants in this stretch: R369 and not Glu like the other transporters and a missing His at position 381 (Verrey, Closs et al. 2004). CAT1 is broadly expressed, except for the liver. In contrast, CAT2 variants have a more restricted expression pattern. In particular, CAT2A is strongly expressed in the liver, skeletal muscle and pancreas, while CAT2B is expressed in macrophages and T-cells. CAT3 is widely expressed in the developing mouse embryo, but seems also located in the brain in adult animals. Moreover, its expression has been found in peripheral tissues such as thymus and mammary gland (Closs, Boissel et al. 2006).

1.7.2. Physiological Function of the CAT Proteins

CATs seem to be the main transporters involved in the entry of cationic amino acids in non-epithelial cells. Cationic amino acids are involved in protein synthesis and other enzymatic reactions including the synthesis of nitric oxide (NO), urea, creatine and agmatine from arginine or the synthesis of polyamines, proline and glutamine from ornithine. There is increasing evidence that CAT-mediated transport can be an important

determinant of these processes (Mann, Yudilevich et al. 2003, Closs, Simon et al. 2004, San Martin and Sobrevia 2006). Studying the effect of CAT gene deletion in mice it has been seen that these transporters are crucial in mammals. In particular, CAT1 homozygous deletion is lethal (Perkins, Mar et al. 1997). In fact, mice suffered from severe anaemia, show a 25% reduction in size and die on day one after birth. Genetic ablation of CAT2, which affects both splice variants, leads to a decrease in sustained NO production by the inducible nitric oxide synthase in peritoneal macrophages and astrocytes, but not in fibroblasts (Nicholson, Manner et al. 2001, Nicholson, Manner et al. 2002, Manner, Nicholson et al. 2003). Moreover, it has been found that these mice exhibit baseline inflammation and an increase in dendritic cell activation in their lungs, although no pathogenic stimulus has been identified. This suggests that in the lung, CAT2B, which is more expressed than CAT2A, is indirectly involved in the suppression of inflammation since it guarantees arginine supply in macrophages for NO synthesis known to suppress dendritic cell activation. For CAT3, SLC7A4, and SLC7A14, knock-out animals have not been established so far. CAT3 is highly expressed in embryonic tissues, total ablation of this gene would most likely be fatal at an early stage due to interference with normal development (Closs, Boissel et al. 2006).

1.7.3. CAT family in plants

Amino acid transporters have been identified and analysed in several plant species, including Arabidopsis (Arabidopsis thaliana), tomato (*Solanum lycopersicum*), potato (*Solanum tuberosum*), broad bean (*Vicia faba L.*), barley (*Hordeum vulgare L.*), maize (*Zea mays L.*), pea (*Pisum sativum L.*), rice (*Oryza sativa L.*), and common bean (*Phaseolus vulgaris L.*) (Yao 2020). The first plant amino acid transporter to be reported, Amino Acid Permease 1 (AAP1), was identified on the basis of functional complementation of a yeast amino acid transporter mutant by heterologous expression of an Arabidopsis cDNA library (Frommer, Hummel et al. 1993, Hsu, Chiou et al. 1993).

The genomic sequence from *Arabidopsis thaliana* contains more than 50 genes putatively involved in amino acid transport. Based on sequence similarity, these transporters are classified into two major groups: the amino acid transporter family (ATF) superfamily and the amino acid polyamine choline (APC) transporters (Wipf, Ludewig et al. 2002). ATF superfamily is the largest group which counts 46 members (Tegeder 2012). The majority of these members have been expressed in *Saccharomyces cerevisiae* and *Xenopus laevis* oocytes and characterized demonstrating that these transporters are broadly expressed and show a cationic and neutral amino acid transport activity. Within Arabidopsis genome, 14 APC genes have been identified. Nine of these encode cationic amino acid transporters (CAT1-CAT9) with 14 transmembrane domains, sharing high similarity with human proteins, while the remaining five (LAT subfamily) have 12 TM domains (Regina, Galluccio et al. 2017). The LAT subfamily has not been characterized and only a few members of the CAT subfamily have been studied (Frommer, Hummel et al. 1995, Su, Frommer et al. 2004, Hammes, Nielsen et al. 2006). Proteomics data from *A. thaliana* revealed that CAT2, CAT4, CAT8 and CAT9 are localized in the vacuolar membrane (Jaquinod, Villiers et al.

2007), although CAT8 and CAT9 are also found in the plasma membrane (Yang, Krebs et al. 2014). The other ones are localized in the plasma or endoplasmic reticulum membranes (Su, Frommer et al. 2004, Yang, Krebs et al. 2014). *At*CAT1 and *At*CAT5 function as specific, high affinity basic amino acid transporters at the plasma membrane (Wipf, Ludewig et al. 2002, Su, Frommer et al. 2004). In particular, the expression profile of *At*CAT5 suggests its involvement in the reuptake of leaking amino acids at the leaf margin. On the contrary, *At*CAT6 transports large neutral and cationic amino acids suggesting a potential role in supplying amino acids to sink tissues (Hammes, Nielsen et al. 2006).

1.7.4. CAT2 transporter from Solanum lycopersicum

Tomato (*Solamum lycopersicum*) is one of the most widely cultivated vegetables with well-documented health benefits associated with the consumption of its fruits. The short life cycle, the small genome, the possibility of growth under different cultivation conditions and the typical character of the fruit development process make tomato an ideal model system for studying fruit development and ripening.

Amino acids play a key role in fruit development since they are involved in the synthesis of enzymes necessary for this stage (Boggio, Palatnik et al. 2000). In fact, the content of free amino acids increases markedly during the transition of tomato fruit to the ripening stage. Therefore, amino acid transporters are essential for cell life since they guarantee amino acid transport from source to sink tissues (Hammes, Nielsen et al. 2006). In 2013 Yang et al. isolated and identified for the first time CAT2 gene from tomato. Analysing its expression in different tomato tissues, it has been seen that CAT2 gene is highly expressed in flowers and fruits. In particular, it has been demonstrated that *Sl*CAT2 expression is dynamic since its transcripts increase from the mature green stage to the ripening stage in fruits (Boggio, Palatnik et al. 2000). These findings demonstrate that *Sl*CAT2 could have a key role in these processes (Yao, Nie et al. 2020). Recently *Sl*CAT2 has been characterized using the recombinant protein overexpressed in *E.coli* and the method of the reconstitution in liposomes (Regina, Galluccio et al. 2017). *Sl*CAT2 shows significant homology with the human CAT1 and CAT2B, sharing a sequence identity of 35 and 33%, respectively. This transporter, as the human CATs, is involved in the transport of cationic amino acids such as L-arginine, L-lysine and the non-proteogenic amino acid L-ornithine across the vacuolar membrane. Arginine is the higher affinity substrate and its transport is stimulated by internal substrates. Moreover, using radiolabelled arginine it has been seen that CAT2 is stimulated by internal ATP, which could act as an allosteric regulator of the transport. This finding suggests a possible regulation of CAT2 transporter in response to cell metabolism. CAT2 is also involved in the transport of acetylcholine. Although the function of this molecule in humans is well documented, in plants its role is poorly defined. It has been suggested that acetylcholine could be involved in the regulation of cell elongation, water homeostasis and photosynthesis (Di Sansebastiano, Fornaciari et al. 2014). In this scenario, CAT2 could have an essential role in the temporary storage of acetylcholine within the vacuole. Moreover, like the homologous GkApcT transporter, it has been

suggested that CAT2 might interact with cholesterol. In GkApcT transporter it has been observed that cholesterol seems to stabilize the complex formed with a single spanning transmembrane protein, MgtS (Jungnickel, Parker et al. 2018). In the case of CAT2, since its localization at the vacuolar membrane, cholesterol might be involved in the regulation of the transport activity.

1.7.5. The heteromeric amino acid transporters HATs

The heteromeric amino acid transporters, HATs are exchangers with a broad spectrum of substrates, such as neutral (System L and asc), aromatic (Transport arpAT), negatively charged (System X_c^-) or cationic plus neutral amino acids (Systems y^+L and $b^{0,+}$) (Fotiadis, Kanai et al. 2013). These transporters consist of a light and a heavy subunit linked by a disulfide bridge. The heavy subunits are represented from SLC3 members, 4F2hc (SLC3A2) or rBAT (SLC3A1), whereas the light subunits are the eukaryotic LATs from the SLC7 family. The cysteine residue, involved in the disulfide bridge, for SLC3 members is located four to five amino acids away from the TMD, while for LATs is the cysteine between TM3 and TM4 (Fotiadis, Kanai et al. 2013).

1.7.6. HATs and their heavy subunits

The SLC3 family includes two members (Table 1): rBAT (SLC3A1) and 4F2hc (SLC3A2, also named CD98) (Table 1). These proteins share about 27% sequence identity between them and they show N-glycosylation, with a molecular mass of ~94 kDa and ~85 kDa for the mature glycosylated forms of rBAT and 4F2hc, respectively. SLC3 proteins are type II membrane glycoproteins, with a single TM domain, the N- terminus in the internal space and the bulky C- terminus in the external site. The extracellular domain has a sequence and structural homology with insect maltases (35–40% amino acid identity) and bacterial α -glucosidases (~30% amino acid identity) (Palacin and Kanai 2004, Fort, de la Ballina et al. 2007, Gabrisko and Janecek 2009)

4F2hc was originally identified as lymphocyte activation antigen by means of a monoclonal antibody 4F2 (Palacin and Kanai 2004). The crystal structure of the extracellular domain of human 4F2hc has been solved at 2.1 Å resolution and more recently the cryo-EM of LAT1/4F2hc complex has been released (Lee, Wiriyasermkul et al. 2019, Yan, Zhao et al. 2019). As the enzymes mentioned above, 4F2hc shows a (β/α)8 barrel, also called A-domain, which correspond to the N-terminal of the protein and a C- terminal domain, which presents an anti-parallel β8 sandwich, although it lacks the key catalytic residues present in glucosidases, and consequently catalytic activity.

4F2hc could associate with several light chains (see Table 1). Residue 109 in 4F2hc is the cysteine involved in the disulfide bridge with the light chain and it is just 4 residues away from the transmembrane domain (Fort, de la Ballina et al. 2007).

rBAT was identified by expression in *Xenopus oocytes* and then it was demonstrated to be the heavy chain of the heterodimeric complex with $b^{0,+}$AT (SLC7A9). This complex mediates the antiport of cysteine and dibasic amino acids with neutral amino acids. The rBAT protein (685 amino acid residues for human rBAT) is longer than the 4F2hc protein (529 for human 4F2hc). Sequence homology of rBAT with glucosidases show that rBAT, despite 4F2hc, has an additional domain B and it is not clear if this heavy chain has also a glucosidase-like catalytic activity.

Human gene	Protein	Aliases	Predominant substrates	Transport type /coupling ions	Tissue distribution and cellular/subcellular expression	Link to disease	Human gene locus	Sequence accession ID	Splice variants and their specific features
SLC3A1	rBAT	NBAT D2	Heterodimerizes with light subunit $b^{0,+}$AT (SLC7A9): amino acid transport system $b^{0,+}$	Exchanger (see details in SLC7 table)	Epithelial cells in kidney and small intestine >liver, pancreas. In epithelial cells, apical plasma membrane	Classic cystinuria type I (genetic defect)	2p16.3-p21	L11696	
SLC3A2	4F2hc	CD98hc	Amino acid transport systems L, y^+L, x_c^- and asc with light subunits SLC7A5–8 and SLC7A10–11	Exchanger (see details in SLC7 table)	Ubiquitous. In epithelial cells, basolateral plasma membrane		11q13	NM_002394	

Table 1 SLC3 – heavy subunits of the heteromeric amino acid transporters. (Adapted from Fotiadis D. et al., The SLC3 and SLC7 families of amino acid transporters, 2013).

Recently, the crystal structure has been solved in complex with $b^{0,+}$AT. The rBAT interacts with $b^{0,+}$AT through a disulfide bond, like 4F2hc-LAT1, between rBAT-Cys114 and $b^{0,+}$AT-Cys144 (Palacin and Kanai 2004, Yan, Li et al. 2020).

4F2hc is a multifunctional protein, ubiquitously expressed, involved in a variety of activities such as cell activation, cell growth and cell adhesion. Moreover, 4F2hc expression is up-regulated in cancers and activated lymphocytic cells, suggesting a role for 4F2hc in cell growth and malignant transformation.

Furthermore, 4F2hc mediates β-integrin signaling and cell fusion. In fact, it has been hypothesized that the N-terminus of 4F2hc is associated with the C-terminus domain of integrin β-subunits (Feral, Nishiya et al. 2005). Moreover, 4F2hc is involved in the cell fusion induced by virus infection of eukaryotic cells (Ohgimoto, Tabata et al. 1995, Takesono, Moger et al. 2012).

rBAT is expressed mainly in kidney and small intestine. The rBAT protein is expressed in the apical plasma membrane of epithelial cells of the intestinal mucosa and the renal proximal tubule, in contrast with 4F2hc which is expressed in the basolateral plasma membrane (Broer and Palacin 2011). Moreover, rBAT mRNA is also detected in liver, pancreas and brain. The rBAT/$b^{0,+}$AT heterodimer is defective in cystinuria, a recessive disease, characterized by hyperexcretion of dibasic amino acids and cystine in urine.

1.7.7. HATs and their light subunits

The light subunits are highly hydrophobic and not glycosylated proteins. The first light subunits of HAT (LSHATs) were identified in 1998 (LAT-1, y^+LAT-1, and y^+LAT-2). Since then, four more mammalian LSHAT members have been cloned xCT, LAT-2, asc-1 and $b^{0,+}$AT. HATs differ from each other for substrate selectivity, ion coupling and tissue distribution. Six of these transporters can form heterodimers with 4F2hc. On the contrary only $b^{0,+}$AT interacts with rBAT, forming system $b^{0,+}$. All of these heterodimers act like amino acid exchangers: systems induced by LAT-1, LAT-2, y^+LAT-1, y^+LAT-2, and xCT, and system $b^{0,+}$ show a tight coupling exchange of substrates, whereas asc-1 might have some unidirectional flux of substrates in addition to the exchange transport (Chillaron, Roca et al. 2001).

Light subunits show twelve transmembrane domains, except for some proteins, with the N- and C-termini in the intracellular space. Moreover, the cysteine residue between TM3 and TM4, which is involved in the formation of the disulfide bridge with the heavy subunit, is conserved (Figure 7). These proteins show a similar structure with prokaryotic transporters AdiC (L-arginine/agmatine transporter), ApcT (broad-specificity amino acid transporter) and GadC (glutamate/ GABA antiporter). In particular, they show the so-called '5+5 inverted repeat' fold, i.e. TM1-5 at the N- terminus and TM6-10 at the C-terminus are related by a pseudo-two fold symmetry (Costa, Rosell et al. 2013).

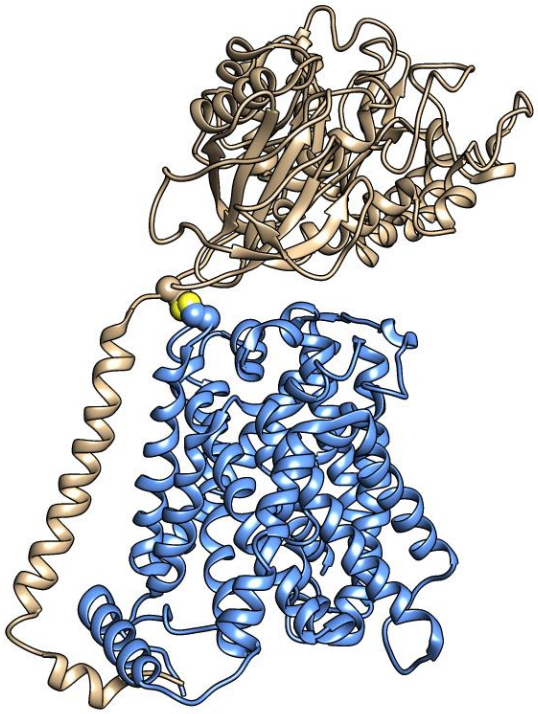

Figure 7 Model of human heterodimer 4F2hc/LAT1 proteins (PDB ID: 6IRT from Yan et al., 2019). The heterodimeric complex is represented as ribbon and cysteine residues as spheres using Chimera (LAT1 as cyan ribbon, while 4F2hc as tan ribbon).

1.7.8. LAT1 (SLC7A5)

The SLC7A5 gene, is localized at 16q24.2 (locus ID 8140) and contains 39477 nucleotides with 10 exons. In Ensemble, two different transcripts have been reported. One of these, NM_003486.6, codes for the active protein of 507 amino acids, with a molecular mass of 55 kDa. The other one derives from alternative splicing, but no information has been reported. Additional four transcripts are reported on NCBI databases, which, however, are only predicted. 352 single nucleotide polymorphisms (SNPs) have been identified in the SLC7A5 gene, but only five SNPs are in the coding region; three are synonymous SNPs and two non-synonymous (rs1060250 and rs17853937). The non-synonymous SNP rs1060250 (N230K) didn't show any functional implication while the relationship between rs17853937 (D223V) polymorphism and the protein activity is still not clear. In 2006, an amino acid substitution in position 41 (G41D) of the LAT1 gene has been described in a phenylketonuric patient population (del Amo, Urtti et al. 2008).

1.7.9. Transport properties and structure of LAT1

As a member of HATs, LAT1 forms a heterodimer with 4F2hc, through a disulfide bridge between cysteine 164 of LAT1 and cysteine 109 of 4F2hc. LAT1/4F2hc heterodimer is a Na^+-independent obligatory exchange with 1:1 stoichiometry of large neutral amino acids, such as leucine, isoleucine, valine, phenylalanine, tyrosine, tryptophan, methionine and histidine. LAT1/4F2hc has been extensively studied in cell systems. The transport of non amino acid substrates, such as L-DOPA, gabapentin and thyroid hormones (T3 and T4) mediated by LAT1 has been also described (Kageyama, Nakamura et al. 2000, del Amo, Urtti et al. 2008). LAT1 and LAT2 are sensitive to 2-aminobicyclo-(2,2,1)-heptane-2-carboxylic acid (BCH), commonly used to discriminate its activity from that of other amino acid transporters in cells.

LAT1/4F2hc was purified on a large scale and functionally characterized in the in vitro model of proteoliposomes (Galluccio, Pingitore et al. 2013). In particular, Napolitano et al., demonstrated that LAT1 is the sole transport competent subunit of the heterodimer, while 4F2hc does not exhibit any intrinsic transport function (Napolitano, Scalise et al. 2015), on the contrary 4F2hc is necessary for trafficking of the light chain to the plasma membrane (Palacin and Kanai 2004). The preference of LAT1 for amino acids was also investigated, demonstrating a functional and kinetic asymmetry of the transporter. In particular, histidine and tyrosine are the bidirectionally-transported substrates, while the others are preferentially inwardly transported and glutamine is a poor substrate. LAT1 is strongly inhibited by both inorganic ($HgCl_2$) and organic (Methyl-Hg) forms of mercury (Napolitano, Galluccio et al. 2017).

LAT1 is broadly expressed and mainly localized in basolateral membranes of polarized epithelia, with exception of BBB where it is localized on both membranes, apical and basolateral (Duelli, Enerson et al. 2000).

In particular, Tarlungeanu et al. demonstrated the importance of SLC7A5 at the BBB. In their study, SLC7A5 loss of function from the endothelial cells leads to ASD and motor dysfunctions in humans and mice. SLC7A5 regulates BCAA and LNAA levels at the BBB. In particular, it has been demonstrated that a lack of SLC7a5 expression at the BBB led to a significant decrease in brain BCAA levels, but not a significant reduction has been detected for LNAAs, indicating that other transporters could be involved in their transport (Tarlungeanu, Deliu et al. 2016).

The same study identified several patients with autistic traits and motor delays carrying homozygous mutations in SLC7A5. In particular, two mutations have been identified. The first one, A246V, affects the transporter's structure. This alanine is located in TM6, facing the extracellular compartment. Therefore, its substitution with the slightly larger valine impairs ligand accessibility, affecting the transport activity. The second one, P375L is located in TM9, facing the cytoplasmic side. Proline is probably involved in conformational changes important for transporter function. Therefore, its substitution with leucine disrupts the flexibility required for transport by SLC7A5. In conclusion, these two mutations are sufficient to affect the transport of BCAA at BBB. This is an important feature, since a fine-tuning of brain BCAA and LNAA concentrations is essential for normal brain functions and mutations affecting genes contributing to BCAA homeostasis and the downstream signaling cascade may underlie a larger subgroup of ASD (Tarlungeanu, Deliu et al. 2016).

The highest expression of LAT1 was also measured in testis, bone marrow, brain and placenta (Prasad, Wang et al. 1999, Fotiadis, Kanai et al. 2013). In particular, in placenta LAT1 is on both maternal and fetal surfaces of syncytiotrophoblasts (Ohgaki, Ohmori et al. 2017). It has been suggested that LAT1 has a key role in placenta since it provides the essential amino acids needed for growing foetus. In fact, knockout of LAT1 in mice is embryonically lethal and this finding could be due to its transport role at the placenta. Moreover, intracellular localization of LAT1/CD98 heterodimer in the lysosomal membrane of HeLa cells has been seen (Milkereit, Persaud et al. 2015).

As other transporters, it has been supposed that also hLAT1 interacts with cholesterol. In particular, Dickens et al., identified two putative cholesterol binding sites on hLAT1(Dickens, Chiduza et al. 2017) conserved in its homologous dDAT (Penmatsa, Wang et al. 2013) and hSERT (Laursen, Severinsen et al. 2018). In particular, it has been suggested that interaction with cholesterol in Site 1, between helices 1,5 and 7 could be involved in the stabilization of the outward conformation, such as dDAT and hSERT. Then, this interaction has been confirmed by the recently solved 3D structure of hLAT1 in complex with hCD98. In this structure, cholesterol-like density has been seen between the helices 3, 9, 10 and 12 (Yan, Zhao et al. 2019). Moreover, another cholesterol density was seen in the cryo-EM structure of LAT1 solved by Lee. The same authors showed that the addition of cholesterol to proteoliposomes harboring the LAT1-CD98 complex led to stimulation of leucine uptake (Lee, Wiriyasermkul et al. 2019, Yan, Zhao et al. 2019).

1.8. SLC38 Family

SLC38A family counts 11 members, 6 of which have been functionally characterized. All transporters are Na^+-dependent and mediate a net transport of neutral amino acids. In the past, these transporters were known as SNATs and divided into two systems: system A and system N. In particular, the first one includes transporters for small neutral amino acids, such as alanine: these transporters are inhibited by MeAIB (N-methyl-aminoisobutyric acid) and mediate a Na^+- dependent uniport, highly regulated by the amino acid concentration. Instead, system N is referred to transporters specific for glutamine, asparagine and histidine and they are Na^+ and H^+- dependent. A distinctive trait of the proteins belonging to system N is their tolerance to the NaCl substitution with LiCl and the activation of the transport in a pH range between 6 and 8 (Broer 2014). These transporters are broadly expressed in the human body. In particular, they are found in the brain, kidney and liver whose cells carry out a significant amino acid metabolism. SLC38 transporters are highly regulated in response to amino acid depletion and hormonal stimuli. For this reason, a putative role as transceptor has been suggested for some of them (Broer 2014).

1.8.1. SLC38A9 transporter

SLC38A9 gene is localized at chromosome 5q11.2 and codified for a protein of 561 amino acids with a molecular mass of 64 kDa. SLC38A9 is a member of SLC38 family and it has 11 TM domains with a 5+5 repeat fold and the helices 1 and 6 broken in the middle to form the helix 1A and 1B and 6A and 6B (Lei, Ma et al. 2018). This protein is highly glycosylated and is involved in cell growth regulation. SLC38A9 is localized at the lysosomal membrane where it is an important component of the machinery that controls mTORC1 activity in response to amino acid levels. It has been suggested that SLC38A9 probably acts as a glutamine sensor, interacting with RAG GTPase which is involved in the recruitment of mTORC1 at the lysosomal membrane (Rebsamen, Pochini et al. 2015, Wang, Tsun et al. 2015). Therefore SLC38A9 is the component of this machinery which acts like a transceptor, i.e., it has two functions: transporter and receptor. Commonly SLC38 members are involved in the transport of glutamine, leucine and arginine which are considered the main amino acids involved in the activation of mTORC1 (Rebsamen, Pochini et al. 2015). In particular, SLC38A9 catalyzes the uptake and the efflux of glutamine, while the transport of arginine occurs at low affinity and the efflux of arginine in proteoliposomes was poor and doesn't occur in vivo. Furthermore, it has been seen that intraliposomal arginine may stimulate glutamine efflux suggesting that arginine is involved in the regulation of the protein from the internal side.
Moreover, arginine doesn't inhibit glutamine uptake, on the contrary glutamine may inhibit arginine transport at a concentration higher than the Km for arginine (Scalise, Galluccio et al. 2019). SLC38A9 transport is dependent of internal Na^+, and it is most active at acidic pH (5.5-6.5), in line with its localization at the liposomal membrane. Two Na^+- binding sites were identified on SLC38A9, N128 and T453, highly conserved in this family (Rebsamen, Pochini et al. 2015, Scalise, Galluccio et al. 2019). Like other transporters, SLC38A9 transport is

stimulated by cholesterol. In fact, two putative cholesterol binding sites were found on its structure, a CARC and a CRAC motif (Castellano, Thelen et al. 2017). Mutations of two key residues in these motifs abolished the activation by cholesterol, confirming the interaction of cholesterol with these regions (Castellano, Thelen et al. 2017, Scalise, Galluccio et al. 2019).

1.9. The study of transport proteins through a multidisciplinary approach.

The best way to study the transport activity is to use different approaches that could confirm the results obtained. The study of transporters in intact cells or in vitro systems can give a lot of information regarding their function and mechanism of transport. Although the intact cell system is widely used, an emerging method is the proteoliposomal tool that allows the possibility to study the transporter in an isolated system. Protoliposomal tool requires the over-expression of the protein of interest in a heterologous system. This methodology, together with site-direct mutagenesis, allowing to obtain also mutants of the protein of interest, represents a possibility of a better understanding of the protein function and the involvement of specific residues in substrate recognition and transport mechanism. Moreover, computational analysis on the crystal structure of the protein of interest or homology model, could represent a primary tool to predict the transport mechanism or another tool to confirm experimental data. Thus, the better way to obtain trustworthy results is using a multidisciplinary approach, which confirms each other the made observations.

The study on transport proteins started in 1970' and the first model adopted was that of **intact cells**. In particular, transport activity was studied using labeled compounds and following their flux through native membranes of intact cells, isolated organelles (such as mitochondria) or microsomes, derived from the endoplasmic reticulum. Intact cell models are still widely used as tools for studying the functional properties of transport systems. In particular, in these years a lot of different cell lines have been used to study or expressing endogenous transporters or overexpressing specific transporters after transient transfection by appropriate plasmids. The advantage of over-expression of the protein of interest is to measure with a better resolution the transport activity through membranes than endogenous transporters. Although the study of transporters in intact cells has the advantage that the proteins are in their natural status and intact cells have a complete system to support transport, on the other hand, there is at least one disadvantage of the uptake assay in intact cells, in that live cells have a metabolic mechanism to modify or degrade substrates and will affect the subsequent measurement. Therefore, the use of intact cell systems as a unique method is not suitable for a comprehensive functional characterization of a transporter and even less for revealing structure/function relationships.

Reconstitution into liposomes is a powerful tool to analyze the function of a protein of interest. At first, liposomes were used to encapsulate and deliver enzymes or pharmaceutical compounds(Boddapati, D'Souza et al. 2010), and later, they are used as a tool for studying membrane transporters (Kasahara and Hinkle 1976, Newman, Foster et al. 1981), which are inserted into the membrane bilayer to obtain active proteoliposomes. Transport proteins could be isolated from biological samples using non-ionic detergent, but a more efficient

method is the production of recombinant proteins by overexpression in heterologous systems and purification by affinity chromatography. The proper incorporation of the purified transporters into liposomes, allows the investigation of transport and/or catalytic properties of this protein without interference by other membrane components and give the possibility to control internal and external compartments as well as the internal and the external site of the transport protein to produce detailed kinetic analysis. Moreover, through site direct mutagenesis is also possible to construct specific mutants in which selected amino acid residues are substituted, thus allowing the study of structure/function relationships (Scalise, Pochini et al. 2013).

Computational analysis could be helpful in the study in silico of transporters. The structure of the protein of interest could be used to obtain preliminary information on transport mechanism, substrate binding and inhibitor efficiency. 3D structures of various soluble proteins and transporters have been characterized in recent years by several experimental methods, such as Nuclear Magnetic Resonance (NMR), X-ray crystallography and cryo-electron microscopy, but due to the low solubility and stability, a lot of membrane proteins has not been solved yet. In the absence of high-resolution 3D structures, computational methods are used for the structure prediction. These methods can be broadly divided into two categories: homology modeling and *ab initio* modeling (Arinaminpathy, Khurana et al. 2009). Homology modeling (also known as comparative modeling) methods rely on sequence similarity with known protein structures, whereas ab initio modeling methods can be used when little or no experimental information is available for the protein or its homologs. The model generated can be used to predict the likelihood of interactions between a chemical entity and a particular transporter. In fact, through docking analysis is possible to obtain information about substrate interactions with residues of the protein and substrate affinity. Moreover, it is possible to identify allosteric sites or make a virtual screening of potential inhibitors for the protein of interest. The information obtained by in silico analysis could be integrated with experimental data, allowing a comprehensive characterization of the protein of interest.

CHAPTER II

Materials and Methods

2.1. Materials

2.1.1. RIPA Buffer 1X

- 20 mM Tris-HCl (pH 7.5)
- 150 mM NaCl
- 1 mM Na_2EDTA
- 1 mM EGTA
- 1% NP-40
- 1% sodium deoxycholate
- 2.5 mM sodium pyrophosphate
- 1 mM β-glycerophosphate
- 1 mM Na_3VO_4
- 1 μg/ml leupeptin

2.1.2. Washing buffer for SlCAT2 and hLAT1 pellets

- 0.1M Tris-HCl pH 8.0

2.1.3. Running buffer for PAGE 10X

- 250 mM Tris
- 14.4 % Glycine
- 1% SDS or 1% Sarkosyl

2.1.4. Loading dye for PAGE 3X

- 0.2 M Tris-HCl pH 6.8
- 7.5% SDS or 7.5% Sarkosyl
- 3% Glycerol
- 0.01% Bromophenol blu
- 100 mM DTE (when indicated)

2.1.5. Coomassie Brilliant Blue

- 0.25 g Coomassie Brilliant Blue
- 45 mL Methanol
- 45 mL Distilled H_2O

- 10 mL Acetic acid

2.1.6. Destaining solution

- 10% Acetic acid
- 40% Methanol
- 50% H_2O

2.1.7. Washing buffer for western blot analysis

- 50 mM Tris-HCl pH 7
- 150 mM NaCl

2.1.8. Lowry's solution

- 4 mg/mL NaOH and 20 mg/mL Na_2CO_3 in water
- 10 mg/mL Potassium Sodium Tartrate
- 5 mg/ mL $CuSO_4$
- 1% SDS

2.2. Experimental procedures

2.2.1. Protein purification by affinity chromatography

Affinity chromatography is a separating method of a molecule of interest from a mixture, based on a specific interaction between the molecule and its binding partner. This technique is commonly used to purify recombinant proteins, overexpressed in a heterologous system and genetically modified to have a specific tag to the N- or C- termini for binding the other substance. In this work, the proteins studied have a hexahistidine (6His)-tag to the N-terminus (*h*LAT1) and the C-terminus (*Sl*CAT2 and *h*ASCT2). The His-tag binds Ni^{2+} ions immobilized as Ni^{2+}-agarose. During this process, the protein of interest is immobilized on the column thanks to the coordination bonds between the 6His-tag and Ni^{2+} ions, while bacterial proteins are eluted. Then, the protein of interest is purified, adding high concentrations of imidazole, which acts as a metal ion ligand breaking bonds between His-tag and ions.

2.2.2. Size-exclusion chromatography

Size-exclusion chromatography or gel filtration chromatography is a technique of separation of molecules on the basis of their sizes. In particular, the chromatography column is packed with fine, porous beads which are composed of dextran polymers (Sephadex). Small molecules can enter in these porous beads and move through the column by a longer path than larger molecules. Therefore the passage of these small molecules will be retarded and they will be eluted after the larger ones. In our work, this technique is used to separate the purified protein fraction from imidazole before starting the study of the transport activity and also to separate proteoliposomes from the external substrate both after reconstitution procedure and transport assay.

A procedure has been used which is based on the removing of detergent from mixed micelles composed of protein, detergent and phospholipids. In particular, detergent removal can be performed by the batch-wise procedure, i.e. the mixed micelles are incubated with a hydrophobic resin (Amberlite XAD-4) for a time sufficient to remove virtually all the detergent. The main advantage of detergent removal is that the proteoliposomes are more sealed, unilamellar and, hence, virtually impermeable to hydrophilic compounds. Moreover, this procedure allows the protein insertion with a unidirectional orientation, which in most cases, corresponds to that of the transporter in the native membrane. This is due to the feature of the starting micelles that have a relatively small radius: this property forces the asymmetric protein to insert into the micelles with a right-side-out orientation. In this work, this last procedure has been used.

2.2.3. Polyacrylamide gel electrophoresis (PAGE)

The polyacrylamide gel consists of acrylamide, bisacrylamide, SDS, and a buffer at a specific pH. The polymerization process starts adding a source of free radicals and a stabilizer, i.e. ammonium persulfate and TEMED. The polymerization reaction creates a gel because of the added bisacrylamide, which can form cross-links between two acrylamide molecules. The acrylamide concentration of the gel can be varied, generally in the range from 5% to 25%. In our case, the concentration used was 12%. Molecules with a high molecular weight may be better separated using a lower percentage gel, while a higher percentage one is used to resolve smaller proteins.

Polyacrylamide gels are composed of a stacking gel and a separating gel. Stacking gels have higher porosity and a pH of 6.8, while separating gels have lower porosity and a pH of 8.8. Before loading on the gel, protein samples were solubilized with loading dye (see Materials and Methods, Section 2.1.4.) and then ran using a running buffer (see Materials and Methods, Section 2.1.3.). At the end of the electrophoresis run, gels were stained using Coomassie staining (see Materials and Methods, Section 2.1.5.) or Silver staining. In the Coomassie staining, the gel was incubated with Coomassie solution for 30 min and then washed with the destaining solution (see Materials and Methods, Section 2.1.6.) which allows the removal of unbound Coomassie and the detection of proteins as

blue bands. In the Silver staining, the gel was incubated for 20 min with destaining solution, 15 min with 10% glutaraldehyde, 15 min with water, 15 min with 0.16 mM DTE, 20 min with 0.1% silver nitrate. The detection of proteins was performed by adding 30 mM sodium carbonate plus 0.03% formaldehyde.

2.2.4. Western blotting

Western blot, also called immunoblot, is a technique used to identify a specific protein in a sample derived from tissue extract, homogenate or protein extracts. In our case, proteins studied are derived from cell extracts (SiHa cells) or they are recombinant purified proteins.

At first, proteins are separated through SDS PAGE (see Materials and Methods, Section 2.2.4.), then they are transferred to a nitrocellulose membrane, thanks to an electric field which allows the movement of the proteins from the gel onto the membrane maintain the same organization. Consequently, the membrane is buffered and incubated at first with a solution containing 3% Bovine serum albumin (BSA), to prevent the non-specific binding of the antibody in the next step. Then, the incubation with the specific antibody for the protein of interest is performed. After this, the membrane is washed with a washing buffer (see Materials and Methods, Section 2.1.7.) to remove the unbound antibody. A further incubation with a secondary antibody, linked to a reporter enzyme (peroxidase), is necessary for the detection of the reaction. This is performed by using Electro Chemi Luminescence (ECL). In particular, in the case of hASCT2, the protein was immuno-detected by ECL, after incubation with anti-His antibody 1:10,000 in 3% BSA for 1 h at room temperature, or with anti-His antibody 1:1,000 In 3 % BSA at 4 °C and then with secondary antibody anti-rabbit (1:5,000) in 1 % BSA for 1 h at room temperature.

2.2.5. Recombinant protein purification

All proteins were over-expressed in a heterologous system. In particular SlCAT2, hLAT1were overexpressed in *E.coli* with a 6His-tag to the C- terminus and N-terminus, respectively, while hASCT2 was overexpressed in *P. pastoris* with a 6His-tag to the C-terminus. Cell lysate pellets containing SlCAT2 and hLAT1 were washed with washing buffer (see Materials and Methods, Section 2.1.2.) and then proteins were solubilized with 100 mM DTE, 3.5 M urea, 0.8 sarkosyl, 10% glycerol, 200 mM NaCl and buffered at pH 8.0 with 10 mM Tris-HCl and centrifuged at 12000 x g, 4 °C for 10 min.

SlCAT2 supernatant was loaded on a column filled with His-select Ni-Chelating affinity gel (0.5 cm diameter, 3 cm height), while hLAT1 was loaded on His Trap HP column (5mL NiSepharose) using ÄKTA start. Both column were preequilibrated with 8 (SlCAT2) and 10 mL (hLAT1) of 20 mM Tris-HCl pH 8.0, 200 mM NaCl, 10% Glycerol and 0.1 % Sarkosyl.

For hLAT1, unbound bacterial proteins were washed out by using 10 mL of washing buffer, containing 20 mM Tris-HCl pH 8.0, 200 mM NaCl, 10% Glycerol, 0.1% DDM and 3 mM DTE. hLAT1 was eluted by 15 mL of washing buffer containing plus 400 mM imidazole. 2.8 mL of the purified protein was recovered and desalted using a PD-10 column adding 3.5 mL of a desalt buffer (20 mM Tris-HCl pH 8, 0.01% DDM and 10 mM DTE).

In the case of SlCAT2, unbound proteins were eluted using 5 mL of a washing buffer containing 20 mM Tris-HCl pH 8.0, 200 mM NaCl, 10% Glycerol, 0.1% DDM and 5 mM DTE. Then, the protein of interest was eluted with 3 mL washing buffer containing plus 10 mM imidazole and 3 ml of the same buffer containing 50 mM imidazole. Several fractions of 1 ml were collected. The third fraction of protein eluted with 10 mM imidazole and the first and the second fraction of 50 mM imidazole were pulled together for subsequent desalting using PD-10 column using the desalting buffer composed of 20 mM Tris HCl pH 8.0, 0.1% DDM, 10% glycerol, and 5 mM DTE.

The protocol for hASCT2 has to be described since it is different from the other two proteins. In particular, about 1.2 g of washed membranes containing hASCT2 were solubilized in a buffer composed of 25 mM Tris–HCl pH 7.4, 250 mM NaCl, 6 mM β -mercaptoethanol, 1 mM L-glutamine, 10% glycerol and 2% $C_{12}E_8$ (w/w), under rotatory stirring for 3 h at 4°C and then centrifugated at 18,000 x g for 45 min. After centrifugation, the supernatant was applied to 2 mL Ni-nitrilotriacetic acid (NTA) agarose resin preequilibrated with a buffer containing 20 mM Tris–HCl pH 7.4, 300 mM NaCl, 10% glycerol, 6 mM β-mercaptoethanol, 0.03% $C_{12}E_8$, 1 mM L-glutamine and 50 mM imidazole and incubated over-night, with gentle agitation, at 4 °C.
The next day, Ni-NTA resin bond ASCT2 was packed by gravity into a glass-column and washed with 30 ml of the same buffer above described. Protein was purified adding 10 ml of a buffer containing 20 mM Tris–HCl pH 7.4, 300 mM NaCl, 10% glycerol, 6 mM β-mercaptoethanol, 0.03% $C_{12}E_8$, 1 mM L-glutamine and 500 mM imidazole. 2.5 ml of purified protein were desalted on a PD-10 column from which 3.5 ml were collected. The column was pre-equilibrated and eluted with a buffer composed of 20 mM Tris–HCl pH 7.4, 100 mM NaCl, 10% glycerol, 6 mM β -mercaptoethanol, 0.03% $C_{12}E_8$ and 1 mM L-glutamine.

2.2.6. Extraction of 4F2hc/LAT1 complex from SiHa cells

Native 4F2hc/LAT1 complex was extracted from SiHa pellets and then reconstituted into liposomes. More specifically, 4F2hc/LAT1 was solubilized from these pellets with RIPA buffer (see Materials and Methods, Section 2.1.1.) and incubated for 30 min on ice. The sample was then subjected to centrifugation (12,000 g, 4°C, 15 min) and proteins were quantified using Lowry method for the following analysis. In particular, 5μL of the sample plus 45 μL of water were added 1 mL of Lowry's solution (Materials, section 2.1.8.) and 100 μL of 1.0N Folin's Phenol reagent.

2.2.7. Reconstitution of proteins into Liposomes

The desalted proteins were reconstituted by removing the detergent from mixed micelles containing detergent, protein, and phospholipids by incubation with Amberlite XAD-4 in a batch-wise procedure (see Materials and Methods, Section 2.2.3.).

- The initial mixture used for reconstitution of ***Sl*CAT2** (except when differently indicated) contains: 6µg of the purified protein, 80 µl of 10 % TX-100, 120 µL of 10% egg yolk phospholipids in the form of sonicated liposomes, 15 mM ATP, and 10 mM Tris Hepes pH 7.5 (except where differently indicated) in a final volume of 700 µL. This mixture was incubated with 0.5 g Amberlite XAD-4 under rotatory stirring (1200 rpm) at 23 °C for 40 min.
- For ***h*ASCT2**: 5 µg of the recombinant purified protein (50 µL) 5 µL of 0.3M EDTA, 340 µL of the mixture containing 100 µL of 10% egg yolk phospholipids (w/v) in the form of sonicated liposomes and 120 µL of 10% $C_{12}E_8$, 10 mM L-glutamine (except were differently indicated in the figure legend), 20 mM Hepes Tris pH 7.0 (or different pH as specified for each experiment) in a final volume of 700 µL. The mixture was incubated within Amberlite XAD-4 for 40 min.
- For ***h*LAT1**: 150 µg of cell extract or 4 µg of recombinant protein, 100 µL of 10% $C_{12}E_8$, 100 µL of 10 % phospholipids, 10 mM histidine, 10 mM DTE and 20 mM Hepes Tris pH 7.0 (except where differently indicated), in a final volume of 700 µL. The mixture was then incubated with 0.5 g Amberlite XAD-4 at room temperature for 40 min, in the case of extracted 4F2hc/LAT1 and 90 min for the recombinant protein under rotatory stirring (1200 rpm) at 23 °C.

2.2.8. Transport Measurements

Before measuring the transport activity, 600 µL of proteoliposomes were subjected to gel filtration chromatography to remove the excess of the external substrate. In particular, the sample was applied onto a Sephadex G-75 column (0.7 cm diameter × 15 cm height) pre-equilibrated with 10 mM Tris Hepes pH 7.5 in the case of *Sl*CAT2, 20 mM Hepes Tris pH 7.0 with 10 mM sucrose in the case of *h*ASCT2 and of *h*LAT1. After elution, proteoliposomes were divided into aliquots of 100 µL for transport assay.

➢ *Uptake experiments*

Transport activity was measured by adding 10 µL of the radiolabeled substrate to each 100 µL of proteoliposomes.

In particular:

- For ***Sl*CAT2**: [^{3}H]-arginine (100 µM) was added to proteoliposomes for starting the transport and 5 mM Pyridoxal Phosphate (PLP) was added to stop the transport according to the stop inhibitor method,

the same inhibitor was added at time zero to control samples (blank). For pH gradient experiments, the protein was reconstituted in liposomes with 10 mM Tris Hepes pH 5.5. Sephadex G-75 column was preequilibrated with 0.5 mM Tris Hepes pH 5.5, while the transport starts adding [^{3}H]-arginine (100 µM) buffered with 10 mM Tris Hepes at different pH as indicated in the figure legend. Osmotic experiments were performed varying the concentrations of sucrose in the extraliposomal/ intraliposomal compartment.

- For ***h*ASCT2**: 50 µM [^{3}H]-glutamine and 50mM Na-gluconate was added to 100 µL proteoliposomes, while to stop the transport reaction 100 µM HgCl2 was added;
- For ***h*LAT1**: 5 µM [^{3}H]-histidine was added to 100 µL of proteoliposomes. As inhibitor was added 15 µL Mercury(II) Chloride ($HgCl_2$).

After the transport for a specific time, 100 µL of proteoliposomes were subjected to gel filtration chromatography using a Sephadex G-75 column (0.6 cm diameter × 8 cm height), which allows the separation of external from internal radioactivity. The elution of loaded proteoliposomes was performed with 1 mL 50 mM NaCl and added to 4 mL scintillation mixture to be counted by a Liquid Scintillation Counter.

➢ *Efflux experiments*

To perform efflux measurements for SlCAT2, an uptake step was performed for 90 minutes to preloaded proteoliposomes with 100 µM [^{3}H]-arginine. External radioactivity was removed by another passage through Sephadex G-75 and efflux was measured at the indicated time.

2.3. Other materials

2.3.1. Preparation of cholesteryl hemisuccinate

Cholesteryl HemiSuccinate (CHEMS) was solubilized with 5% $C_{12}E_8$ and 20 mM Tris HCl pH 8.0 and then sonicated twice for 2 min (no pulse, 40 W) with a Vibracell VCX-130 sonifier (Hanson et al, 2008). To remove metal residues after sonication, the mixture was centrifuged for 5min at 10,000 g and the supernatant was then added to liposomes for 30 min under rotatory stirring (1,200 rpm) at 23 °C.

2.3.2. Insertion of cholesterol into liposomes

7.5 mg of cholesterol was weighted and added to 100 mg of egg yolk phospholipids. The mixture was solubilized by adding 1 mL chloroform. After short incubation under rotatory stirring (1200 rpm, 30 °C, 5 min) open tube is dried O.N. at room temperature overnight. The next day, when chloroform was completely evaporated, the lipid film was resuspended in 1mL water (10% final concentration) and sonicated to form unilamellar liposomes as previously described (see Materials and Methods, Section 2.2.3.).

2.3.3. Internal volume measurement

The colorimetric phosphate method was used to calculate the internal volume of proteoliposomes prepared with several amounts of cholesterol (Indiveri, Palmieri et al. 1994). The initial mixture of reconstitution contained several amounts of cholesterol previously solubilized as described in Materials and Methods, Section 2.3.1., sonicated liposomes and 50 mM dipotassium phosphate (K_2HPO_4). After reconstitution, liposomes were eluted from Sephadex G75, buffered without phosphate. Then 100 µL of the sample were incubated for 30 min with 150 µL of Solution R (10 mM hexammonium heptamolybdate 4-hydrate, 0.3 mM of H_2SO_4 and 0.1 mM $FeSO_4$) to allow the colorimetric reaction. Then, the absorbance was measured using spectrophotometer analysis (wavelength: 578 nm). The internal volume (µL) was calculated on the basis of nmol of phosphate included in liposomes.

2.3.4. Treatment of experimental data

Experimental values were corrected by subtracting the respective controls (blank) in the case of uptake measurements and subtracting the time zero value in the case of efflux experiments. These values were analyzed using Grafit software (Grafit® 5.0). In particular, different equations were adopted in line with experimental purposes.

- **First Order Rate Equation:** used where a process increases with time following a 1st order rate law:

$$A_t = A_\infty (1-e^{-kt})$$

- **Single Exponential Decay:** is the equation for a single exponential decay:

$$y = A_0.e^{-kt}$$

- **Michaelis-Menten Equation:** used to calculate kinetics parameters:

$$v = (Vmax .[S])/(Km.[S])$$

- **Lineweaver Burk Equation**: the Lineweaver Burk transformation was used to produce a double-reciprocal plot of the data:

$$1/V0 = [Km / (Vmax\cdot[S])] + 1/Vmax$$

- **IC50 Fully Range Corrected:** dose–response equation to calculate IC50 value:

$$y = 100\% / 1+(x / IC_{50})^{s}$$

2.4. Computational analysis

2.4.1. Molecular Docking

Molecular docking is a method that predicts how two or more molecules fit together, forming a stable complex. Based on the types of ligand, docking can be classified as: protein-small molecule (ligand) docking; protein-nucleic acid docking; protein-protein docking. In this work, we performed a protein-small molecule docking. At first, to perform docking analysis, the availability of the structure of the protein of interest is a fundamental requirement. Usually, the structure has been determined using a biophysical technique such as x-ray crystallography, NMR spectroscopy or cryo-electron microscopy (cryo-EM), but can also derive from homology modeling. Moreover, the availability of the database of ligands is the other input for starting docking analysis. The success of a docking program depends on two components: the search algorithm and the scoring function. The search space, in theory, consists of all possible orientations and conformations of the ligand within the protein. Most docking programs in use account for the whole conformational space of the ligand (flexible ligand), and several attempts to model a flexible protein receptor. Each "snapshot" of the pair is referred to as a pose. Ligand poses are evaluated on the basis of a scoring function, which returns a number indicating the likelihood that the pose represents a favorable binding interaction and ranks one ligand relative to another.

2.4.2. Protein preparation and grid generation

Cryo-EM structures of proteins of interest (in our case LAT1 and ASCT2) were downloaded from RCSB PDB. Before starting with docking analysis, proteins were prepared using Schrödinger Protein Preparation Wizard tool within Maestro v11.3, for LAT1, and Autodock Vina v4.2 for ASCT2. Protein preparation can be resumed in three essential steps: addition of missing hydrogen atoms, optimization of hydrogen bonds by flipping amino acid side chains and correcting charges, and minimization of the protein.

Docking analysis can be performed on the whole protein, this procedure is called blind docking, or on a selected area of interest. The grid box varied, dependent on the ligand, size and position.

Every ligand was downloaded in SDS format from PubChem and also prepared, optimizing their geometry and assign them appropriate protonation states.

In the case of ASCT2, we performed a blind rigid docking on full protein and also a docking on selected regions. The best conformation space of the ligand was searched employing the Lamarckian Genetic Algorithm. The best pose chosen has the lowest binding-energy conformation.

2.4.3. Induced Fit docking

Docking analysis on LAT1 was performed using Induced Fit docking, which considerate in the calculations the flexibility of the side chains in the binding site. In fact, the standard molecular docking is a rigid docking which places flexible ligands onto the rigid structure of the target. The workflow is composed of a job sequence in which ligand is docked with Glide (first step) then Prime is used to refine and optimize side chains of all residues within 5.0 Å of ligand poses (second step) and, at last, the ligands are redocked onto the relaxed receptor with Glide (third step).

2.4.4. Sitemap as a tool to identify putative binding sites

Schrödinger's SiteMap is a useful tool developed for identifying druggable sites on receptors. At first, SiteMap searches for one or more regions within the protein or on the protein surface, called sites, that may be suitable for binding of a ligand to the receptor. The search uses a grid of points, called site points, to locate the sites. In the second stage, site maps are generated, showing hydrophobic and hydrophilic regions. The hydrophilic maps are further divided into a donor, acceptor, and metal-binding regions. A Site Score is used to distinguish sites that could bind ligands to sites that could not. Typically a Site Score of 0.80 would aid in discriminating between a druggable and non-druggable site. Site Score of at least 1 and above indicated a reasonable chance for the site to be druggable.

CHAPTER III

Results

3.1. Functional and structural characterization of hASCT2 transporter

3.1.2. Effect of cholesterol on the hASCT2

hASCT2 was overexpressed in *P. pastoris* and then purified as described in Materials and Methods, Section 2.2.5. The effect of cholesterol was tested on the transport activity of hASCT2, since it has been found that cholesterol may interact with a lot of proteins modulating their function (Fantini and Barrantes 2013, Dickens, Chiduza et al. 2017, Pochini, Pappacoda et al. 2020). Therefore, different amounts of cholesterol, in the commercial form of cholesteryl hemisuccinate (CHEMS), was solubilized and then added to the mixture of lipids and detergent before reconstitution, as previously described in Materials and Methods, Section 2.3.1. The transport rate was measured as Na^+-[^{3}H]-glutamine$_{ex}$/glutamine$_{in}$ exchange at the indicated amount of CHEMS, expressed as μg CHEMS/ mg phospholipids. As shown in Figure 8A, hASCT2 is stimulated by the increasing amount of cholesterol with a maximum of activity at 75 μg CHEMS/mg phospholipids, then the transport activity decreased at a further increase of CHEMS. The increase of the transport, shown in the first part of the graph, might be due to the inclusion of cholesterol in proteoliposomes that allows the increase of internal volume and thus, not to a direct effect of cholesterol on the transporter. Therefore, the internal volume was measured at the indicated amount of cholesterol (see Materials and Methods, Section 2.3.3). As shown in Figure 8A the internal volume (indicated on the right Y axis in Figure 8A) did not change in all conditions. Another possibility is that cholesterol could improve the insertion of hASCT2 at the liposomal membranes and thus, this condition could explain the increase in the transport rate. Therefore, to better understand the mechanism of stimulation, the amount of protein incorporated into proteoliposomes at increasing cholesterol amount was also detected (Figure 8B). After reconstitution, proteoliposomes were run on SDS-PAGE and then, a Western Blot was performed (as described in Materials and Methods, Section 2.2.3 and 2.2.4.). As shown in Figure 8C, the amount of the protein increased by increasing the amount of cholesterol up 50 μg CHEMS/mg phospholipids. Noteworthy, the increase of protein amount did not exactly follow the increase of the transport activity, since as shown before the maximum of activity was at 75 μg CHEMS/mg phospholipids (Figure 8A). This data suggested that cholesterol has two different effects on hASCT2. In fact, on one side it seems to improve the insertion of hASCT2 into the membrane, but on the other side, it might directly interact with hASCT2 increasing the transport activity.

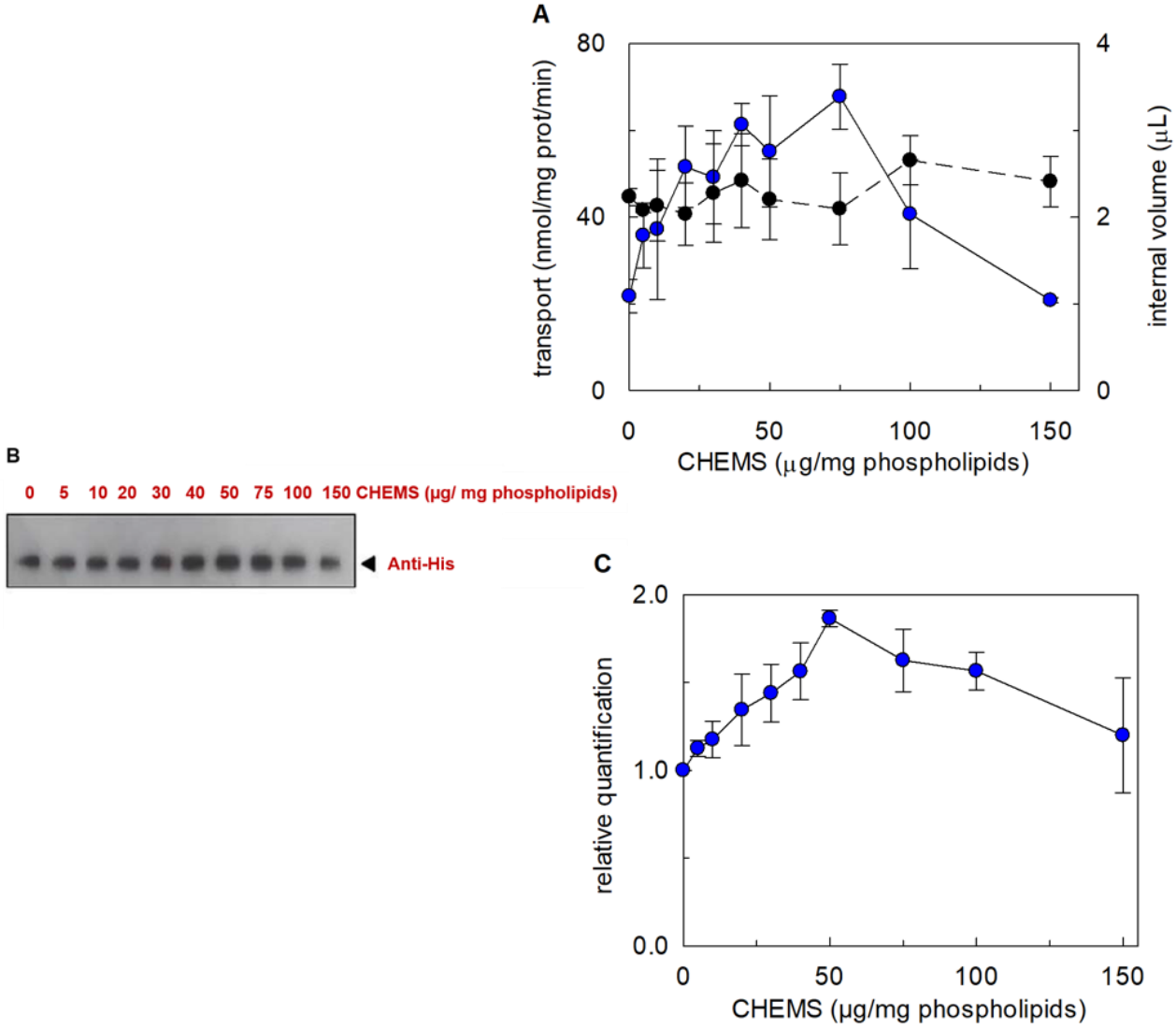

Figure 8 The effect of cholesterol on the transport of hASCT2. In (**A**) transport rate was measured in 20 min adding 50 µM of [^{3}H]-glutamine and 50 mM Na-gluconate to proteoliposomes prepared with the indicated amounts of CHEMS and containing 10 mM of glutamine (blue circle). In the right y-axis, the internal volume of proteoliposomes calculated at the indicated amounts of CHEMS, as described in Materials and Methods, Section 2.3.2. (black circle). In (**B**) Samples (a volume corresponding to 1% of the total reconstitution mixture) derived from (A) were subjected to SDS-PAGE and western blotting analysis, for evaluating the incorporation of hASCT2 into proteoliposomes prepared with the indicated amount of CHEMS. In (**C**) relative quantification of band intensity from western blotting of (**B**).

To investigate if cholesterol might influence the substrate affinity, kinetic analysis was performed. The external Km was measured as transport rate at the indicated glutamine concentrations in the absence or the presence of 75 µg CHEMS/mg phospholipids (Figure 9). As shown the Km was not significantly varied, while the Vmax increased from 113 ± 26.6 nmol · mg $^{-1}$· min^{-1} in the absence of cholesterol to 370 ± 79.3 nmol · mg $^{-1}$· min^{-1} in the presence of cholesterol. These data indicate that cholesterol interaction has not a direct effect on the binding site, but it probably influences the rate of conformational changes.

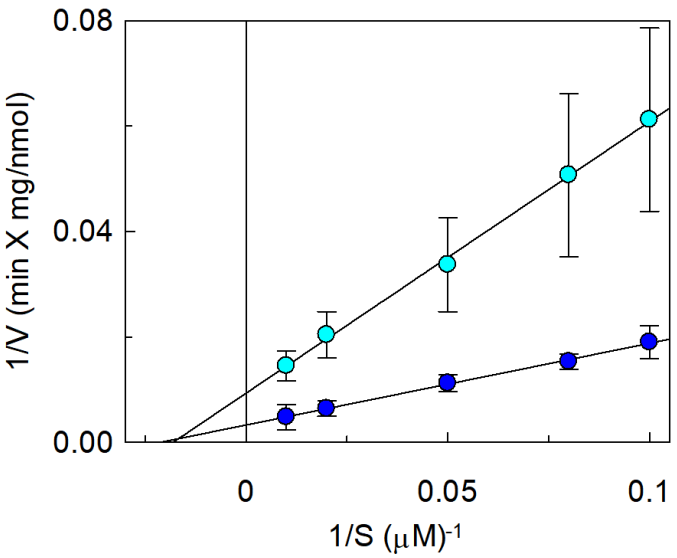

Figure 9 Effect of cholesterol on hASCT2 transport. Transport rate was measured in 15 min adding 50 μM of [^{3}H]-glutamine and 50 mM Na-gluconate to proteoliposomes prepared (cyan circle) or not (blue circle) with 75 μg CHEMS / mg phospholipids and containing 10 mM of glutamine. Data were plotted according to linear Lineweaver-Burk plot as reciprocal transport rate vs reciprocal glutamine concentration. Data are means ± SD of three independent experiments.

Moreover, the effect of cholesterol was also tested in the presence of other amino acids, transported by hASCT2 from the internal compartment. The transport rate was measured as heterologous exchange of Na^+-[^{3}H]glutamine$_{ex}$/asparagine$_{in}$, Na^+-[^{3}H]glutamine$_{ex}$ /threonine$_{in}$, or Na^+-[^{3}H]glutamine$_{ex}$ /serine$_{in}$ (Figure 10). Interesting, the transport rate of heterologous Na^+-[^{3}H]glutamine$_{ex}$ /serine$_{in}$ and Na^+-[^{3}H]glutamine$_{ex}$ /threonine$_{in}$ antiport increased six and nine times more, respectively, in the presence of cholesterol than the homologous Na^+-[^{3}H]-glutamine$_{ex}$/glutamine$_{in}$ antiport where the stimulation was of two times more or the heterologous Na^+-[^{3}H]glutamine$_{ex}$/asparagine$_{in}$ antiport, three times more.

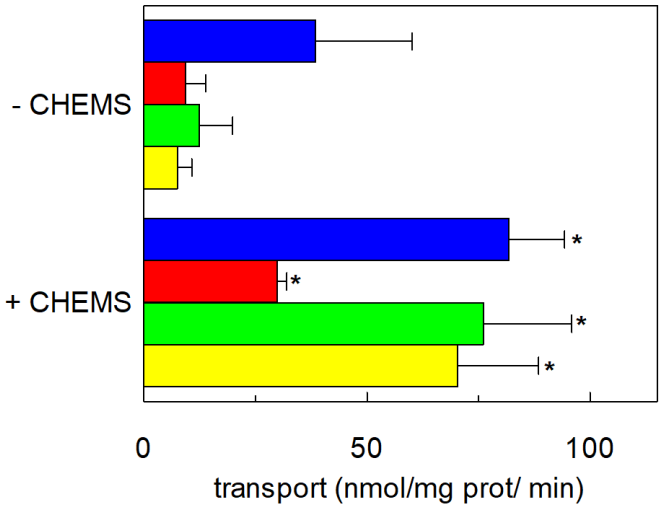

Figure 10 Effect of cholesterol on the transport activity of hASCT2. Transport activity was measured adding 50 μM [^{3}H]-glutamine and 50 mM Na-Gluconate to proteoliposomes prepared with 75 μg CHEMS/ mg phospholipids and containing 10 mM glutamine (blue bar) or asparagine (red bar) or threonine (green bar) or serine (yellow bar). Initial transport rates were calculated as k x limit (nmol/mg prot/min) from the first-order rate equation used to plot the time course data. Data are means ± SD of three independent experiments. (*), significantly different from the control sample (proteoliposomes prepared without CHEMS) as estimated by Student's t-test ($P < 0.05$).

The effect of cholesterol was also evaluated in intact HeLa cells. In particular, the effect was measured as sequestration of cholesterol by methyl-β-cyclodextrin (MCD), which is a known cholesterol depleting reagent (Dickens, Chiduza et al. 2017). A decrease in the transport rate, indicated as residual activity with respect to the control condition without MCD, was seen when HeLa cells were treated with 10 mM of MCD (Figure 11). This is in line with the results previously described (Figure 8A). In fact, a minor availability of cholesterol, due to the sequestration by MCD, determined a decrease of the transport activity.

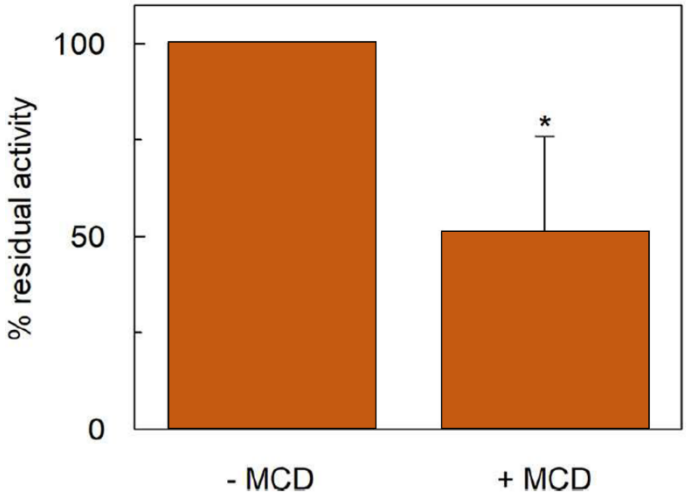

Figure 11 HeLa cells were treated with 10mM methyl-β-cyclodextrin (MCD) as described in Materials and Methods. Transport was measured adding 10μM [^{3}H]glutamine in the presence or in the absence of 100mM NaCl. Transport activity was calculated as the percent of residual activity with respect to the control condition (without MCD in the transport assay). (*), significantly different from the control sample (proteoliposomes prepared without MCD) as estimated by Student's t-test ($P < 0.05$).

3.1.3. Docking of cholesterol on the Cryo-EM structure of hASCT2

A direct interaction between ASCT2 and cholesterol has been hypothesized, in agreement with the finding of cholesterol-like densities in the Cryo-EM structure of ASCT2 (Garaeva, Oostergetel et al. 2018, Yu, Plotnikova et al. 2019). Therefore to understand the molecular mechanisms of cholesterol stimulation on the transport activity of ASCT2, docking analysis was performed. In particular, a blind docking (see Materials and Methods, Section 2.4.2.) was performed on ASCT2 trimer in an inward facing (PDB id: 6GCT). As shown in Figures 12 and 13, at least six sites were identified. Some of these, A, B, C and D, matched with the electron densities observed in the Cryo-EM structure. Interestingly, poses E and F are located on helix 6 where we found a CARC and a CRAC motif that are two putative cholesterol binding motifs (Fantini and Barrantes 2013, Fantini, Epand et al. 2019). Moreover, pose D on the TM3 is close to the R-W-L domain that is also considered a CARC/CRAC-like domain (Fantini and Barrantes 2013).

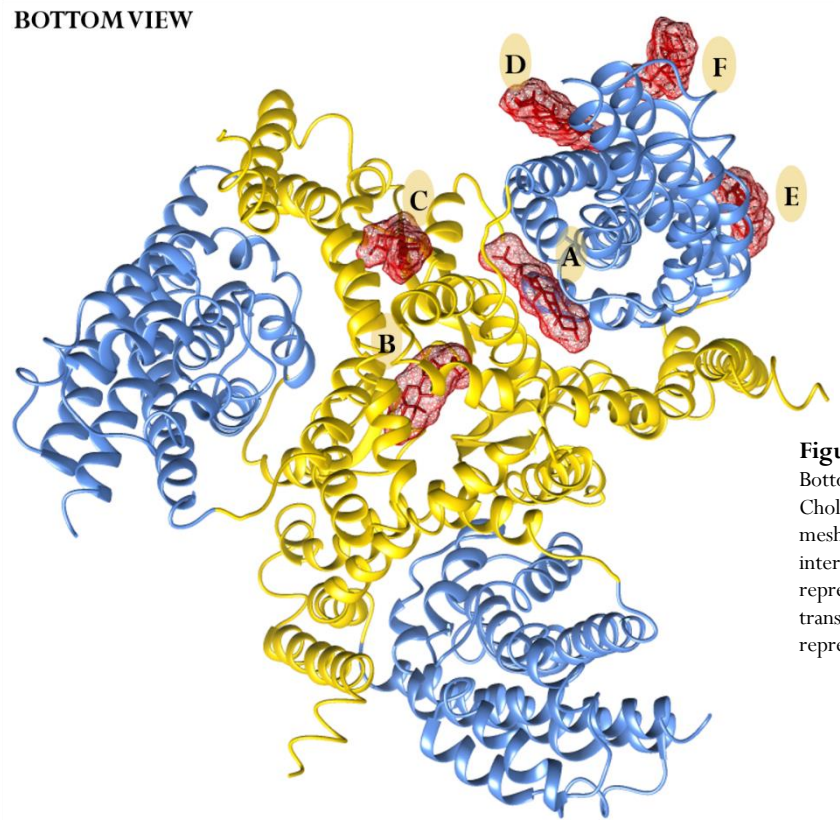

Figure 13 Cholesterol blind docking on hASCT2. Bottom view of the trimeric hASCT2 (PDB: 6GCT). Cholesterol poses are indicated as red sticks with mesh surface (A, B, C , D, E and F). Some of these interacts with the scaffold domain (TMs 1, 2, 4, 5 represented as gold ribbon) and the others with the transport domain (TMs 3, 6, 7, 8, HP1 and HP2 represented as blue ribbon) of a protomer.

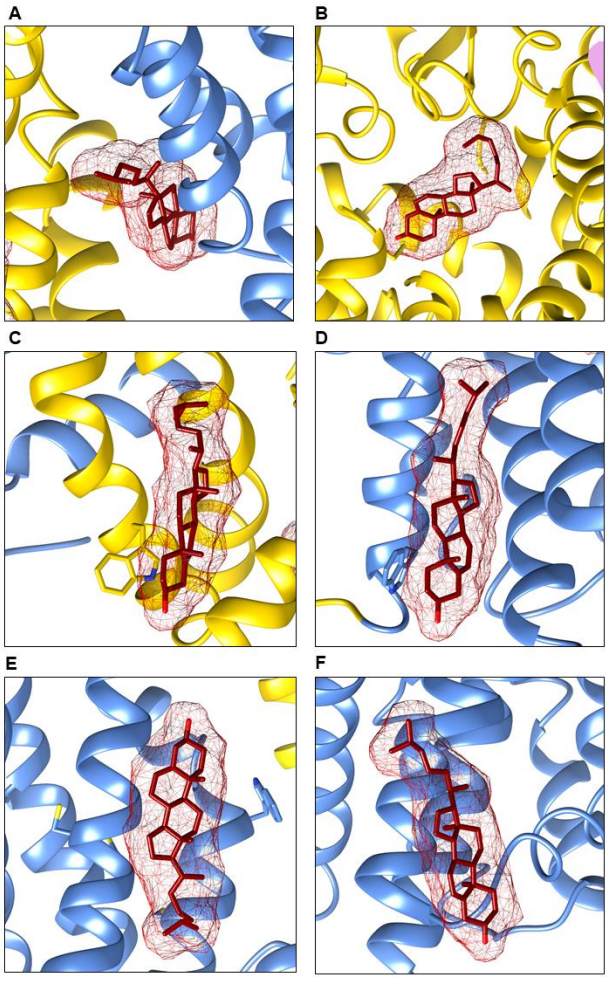

Figure 13 Zoom of cholesterol poses previously predicted in Figure 15. Cholesterol molecules are indicated as red sticks with mesh surfaces. Residues close to these poses are indicated as sticks (gold sticks if they belong to the scaffold domain or blue stick if belong to the transport domain). (**A**) Cholesterol is located between TMs 2, 4c and HP2 of a protomer. (**B**) Cholesterol is located between TMs 2, 4b and 5 of two protomers. C110 is represented in gold stick. (**C**) Cholesterol is located between TM4c of a protomer and TM2 and TM5 of the adjacent protomer; in gold stick residue W272. (**D**) Cholesterol is located between TMs 3, 6 and 8 of a protomer; in blue stick residue W130. (**E**) Cholesterol is located between TM6 which includes a CARC motif and TM8; in blue stick residues C308 and C309 (TM6) and W461 and C467 (TM8). (**F**) Cholesterol is located between TM6, which also includes a CRAC motif and HP1 of a protomer.

To analyze and to confirm these predictions, other experimental data were collected. In fact residues close to cholesterol molecules were used as targets of specific compounds and thus, the transport activity was measured in the absence or the presence of cholesterol, to evaluate if cholesterol could prevent the interaction with these compounds which are known to influence the transport activity.

3.1.4. Targeting tryptophan residues by the Koshland's reagent

At first, a reagent targeting tryptophan residues, the Koshland's reagent was employed in the presence or the absence of cholesterol (Figure 14). hASCT2 was incubated with 0.5 mM Koshland's reagent (Giangregorio, Tonazzi et al. 2019) for 15 min under rotatory stirring (1,200 rpm) at 23 °C before reconstitution. Then protein was reconstituted in liposomes containing or not 75 µg CHEMS/mg phospholipids. The Koshland's reagent shows a high reactivity at pH 7.0 and it acts modifying the indole ring of the tryptophan side chain (Loudon and Koshland 1970). As shown in Figure 14, the incubation of the protein with the reagent in the absence of cholesterol did not affect the transport activity of ASCT2, indicating that tryptophan residues are not crucial for transport. On the contrary, in the presence of cholesterol, the modification of tryptophan residues allowed a reduction of 30% of cholesterol stimulation, indicating that tryptophan residues might be important for cholesterol binding. These data confirmed the position of three of the predicted poses previously described, C, D and E which had in their proximity tryptophan residues (Figure 13).

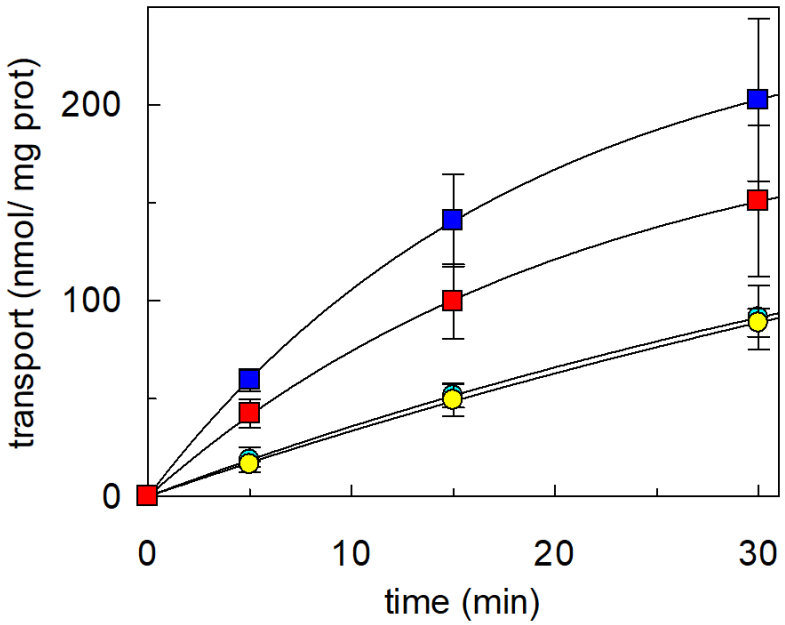

Figure 14 Effect of Koshland's reagent on hASCT2 transport. Transport rate was measured adding 50 µM [^{3}H]-glutamine and 50 mM Na-Gluconate in the absence (cyan circle and blue square) or the presence (yellow circle and red square) of 0.5 mM Koshland's reagent, to proteoliposomes prepared without (yellow and cyan circle) or with 75 µg CHEMS /mg phospholipids (red and blue square) and containing 10 mM glutamine.Values were plotted according to the first-order rate equation. Data are means ± SD of three independent experiments.

3.1.5. Targeting cysteine residues with SH-reagents

The reactivity towards SH reagents was also investigated considering that the poses B and E are close to cysteine residues (Figure 13). In a previous work (Scalise, Pochini et al. 2018), it was shown that hASCT2 is stimulated by DTE, a cysteine reducing agent. hASCT2 was reconstituted in liposomes prepared without or with 75 µg CHEMS/mg phospholipids. After reconstitution, the transport activity was measured as a function of the time in the presence of 10 mM DTE. Interestingly, these data showed that the interaction of hASCT2 with cholesterol prevented the stimulation by DTE. In fact, the condition without and with DTE are quite similar (Figure 15A). Moreover, also in the HeLa cells (data not shown), where hASCT2 should have an optimal cholesterol milieu, the addition of DTE had no effect. To further investigate the effect of cholesterol, hASCT2 was also treated with SH reagents which should inhibit the protein, as previously demonstrated (Scalise, Pochini et al. 2018). The transport activity, indicated as residual activity with respect to the control condition without any addition, was measured in the presence of 20 µM $HgCl_2$ (Figure 15B). As shown by the figure, in the absence of cholesterol (cyan bars), $HgCl_2$ exhibited a strong inhibition; this inhibition was lost in the presence of cholesterol (blue bars). The same effect was seen in the presence of 0.5 mM NEM, which is involved in the alkylation of SH cysteine residues (Figure 15B). Taken together these results indicated that some cysteine residues are masked by one or more cholesterol molecules (Figure 13 B, E).

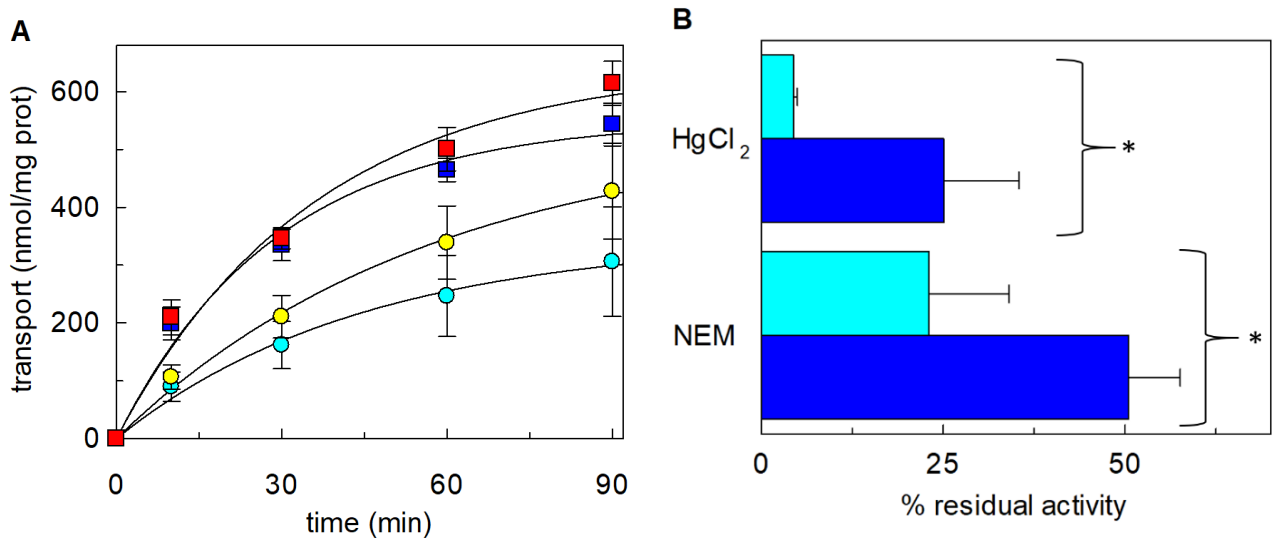

Figure 15 Effect of SH reagents on hASCT2 transport. In (**A**) the effect of DTE was investigated. Transport rate was measured adding 50 µM [3H]-glutamine and 50 mM Na-Gluconate in the absence (cyan circle and blue square) or the presence (yellow circle and red square) of 10 mM DTE, to proteoliposomes prepared without (yellow and cyan circle) or with CHEMS (red and blue square) and containing 10 mM glutamine. Values were plotted according to the first-order rate equation. In (**B**) effect of $HgCl_2$ and NEM. Transport rate was measured adding 50 µM [3H]-glutamine and 50 mM Na-Gluconate in the presence of 20 µM $HgCl_2$ and 0.5 mM NEM to proteoliposomes prepared without (cyan bars) or with (blue bars) CHEMS and containing 10 mM glutamine. (*), Significantly different from the control sample (proteoliposomes prepared without CHEMS) as estimated by Student's t-test ($P < 0.05$). In (A,B) data are means ± SD of three independent experiments.

Thanks to the availability in our laboratory of some cysteine mutants of the hASCT2, it has been possible to investigate the effect of SH reagents on these proteins, to obtain further data that may confirm some predicted poses. In particular, C467 that is the major target of SH reagents as previously shown (Scalise, Pochini et al. 2018) resulted to be close to the predictive pose E, together with C308 and C309 that lie on the CARC and CRAC motif close to this pose (Figure 13). The mutant C467A, together with other mutants C308A, C309A and C110 were used to test the effect of $HgCl_2$ and thus, they were reconstituted in proteoliposomes prepared in the absence or the presence of cholesterol. Then, the transport activity was measured as Na^+-[^{3}H]-$glutamine_{ex}$/$glutamine_{in}$ exchange in the presence of 20 µM $HgCl_2$. As shown in Figure 16A, the addition of $HgCl_2$ to proteoliposomes prepared with cholesterol had a different behaviour on the mutants respect the WT. In fact, measuring the protection index as the ratio between residual activity in the presence and the absence of cholesterol it has been confirmed that the protection seen by cholesterol on the WT was lost or reduced in the mutants. Only the mutant C110A showed a protection index similar to the WT. These data indicated that a cholesterol molecule may mask one or more cysteine residues, reducing the inhibition and thus, when cysteine is missing, as seen in the mutants, the protection by cholesterol is lower. Moreover, in the case of the mutant C110A, the higher protection index might mean either that this residue is not crucial for the transport activity either that it is not easily accessible by the reagent, since it is located in the core of the scaffold domain.

The treatment of these mutants with NEM showed similar behaviour to that obtained in the presence of $HgCl_2$, event if the protection by cholesterol, in this case, was less evident with respect to that previously described (Figure 16B).

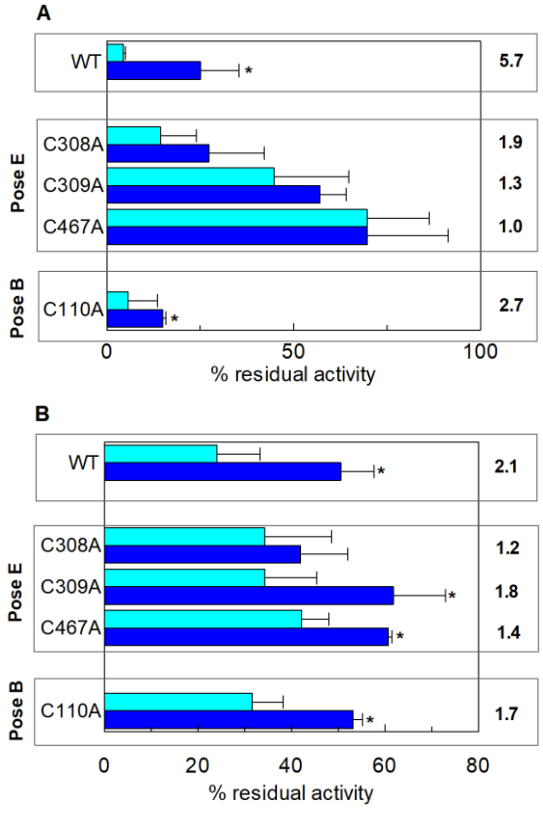

Figure 16 Effect of $HgCl_2$ and NEM on transport activity of hASCT2 WT and Cys mutants. The transport activity (indicated as residual activity with respect to the control without cholesterol) was measured adding 50 µM [^{3}H]-glutamine and 50 mM Na-Gluconate in the presence of 20 µM $HgCl_2$ (**A**) or 0.5 mM NEM (**B**) to proteoliposomes prepared without (cyan bars) or with 75 µg CHEMS/mg phospholipids (blue bars) and containing 10 mM glutamine. Dotted boxes indicated the protection index calculated as the ratio between residual activity in the presence of CHEMS and the residual activity in the absence of CHEMS. (*), significantly different from the control sample (proteoliposomes prepared without CHEMS) as estimated by Student's t-test ($P < 0.05$). Data are means ± SD of three independent experiments.

3.2. Functional and structural characterization of SlCAT2 transporter

3.2.1. Orientation of SlCAT2 reconstituted in proteoliposomes

SlCAT2 was overexpressed in *E.coli* with a 6His-tag to the C-terminus and purified as described in Materials and Methods, Section 2.2.5. On the basis of transmembrane topology predictions, it has been suggested that SlCAT2 is localized at the vacuolar membrane with the N- and C-termini exposed towards the vacuolar lumen (Regina, Galluccio et al. 2017). Therefore, to assess if the orientation of the recombinant protein at the proteoliposomal membrane was the same as the vacuolar membrane, i.e. the N- and C-termini exposed towards the intraliposomal compartment, a method based on side-specific targeting was performed. In particular, the recombinant protein was incubated with an Anti-His antibody against the 6His-tag at the C-terminus of the protein. The interaction between the 6His-tag and the antibody should create a steric hindrance affecting the transport activity, as already described for other transporters (Scalise, Pochini et al. 2014, Pochini, Scalise et al. 2015). The antibody was added before and after reconstitution. During the proteoliposome formation, the antibody added to the initial mixture of reconstitution can reach both sides of the protein. On the contrary, after reconstitution, the protein is inserted in the liposomal membrane and thus, the antibody, added to the external compartment, can bind only the external face of the protein. In both cases, the transport activity was measured by adding [^{3}H]-arginine to the proteoliposomes (See Materials and Methods, Section 2.2.8.). Significant inhibition was observed when the protein was incubated with the antibody before reconstitution (Figure 17A). On the contrary, the addition of the antibody to the external compartment had no effect on the transport activity. Moreover, the presence of the anti-His antibody in the external side of proteoliposomes previously incubated with anti-His antibody did not increase the inhibition (Figure 17A). To exclude a non-specific effect of the anti-His antibody, anti-Actin antibody was incubated with the protein before reconstitution, as a control. In this case, no effect was observed on the transport activity, demonstrating that the inhibition observed in the presence of internal anti-His antibody was specifically due to the interaction between the anti-His antibody and the 6His-tag at the C-terminus of the recombinant protein. To assess if the addition of the antibody could affect the liposomal membrane integrity, the same experiment was performed using liposomes without the recombinant protein. In the absence of SlCAT2 no effect was seen in all the conditions (yellow bars in Figure 17A). It has to be stressed that the [^{3}H]-arginine accumulated in the control liposomes was always less than 30% with respect to proteoliposomes. This data demonstrated that the C-terminus of the protein is exposed to the intraliposomal compartment, in line with membrane topology predictions. Moreover, the presence of the protein in liposomes was verified by running the solubilized proteoliposomes on SDS-PAGE (see Materials and Methods, Section 2.2.3.) and performing a Western blot analysis (see Materials and Methods, Section 2.2.4.). In Figure 17B, the lane 1 corresponds to the purified protein showing a molecular mass of 45 kDa, while lanes 2 and 3 correspond to the reconstituted protein without incubation (lane 2) or pre-incubated with the anti-His antibody (lane 3). As

shown in the figure, the corresponding band in lanes 2 and 3 was only 30% with respect to the protein added to the initial mixture.

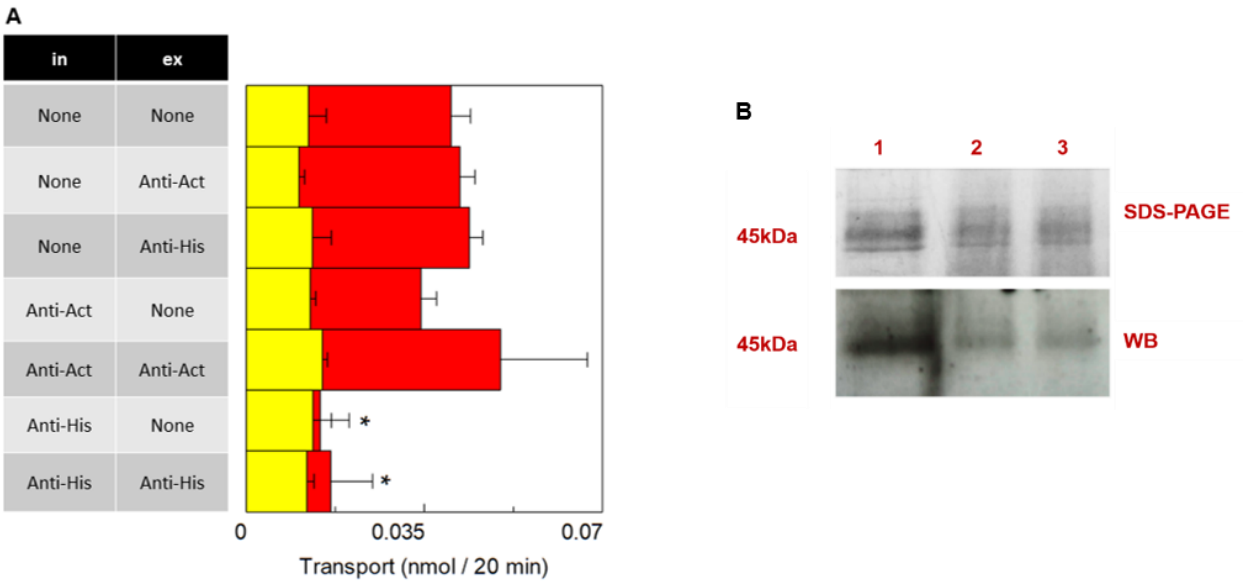

Figure 17 Sidedness of the reconstituted *Solanum lycopersicum* CAT2 in proteoliposomes. (**A**) The purified protein was pre-incubated with 6 µg of anti-His antibody or 0.6 µg of the antibody was added in the external compartment. Anti-actin antibody was used as control in both sides. Transport was measured in 20 min by adding 100 µM [^{3}H]-arginine to proteoliposomes (red bars) or liposomes (yellow bars) containing 200 mM sucrose and 15 mM ATP at pH 7.5. Results are the means ± SD from three experiments. (*), significantly different from the control (none) for $p < 0.05$ as calculated from 1-way ANOVA test. (**B**) SDS PAGE and WB of SlCAT2. In the lane 1 the purified protein with a molecular mass of 45 kDa. In the lane 2 and 3 the reconstituted protein without the antibody or after pre-incubation with anti-His antibody. Proteoliposomes were purified by size-exclusion chromatography as described in Materials and Methods, Section 2.2.2. and then run to SDS-PAGE.

3.2.2. Regulation of the SlCAT2 transport activity by pH and Osmolality

In *Arabidopsis thaliana* CAT1, CAT5 and CAT6 which share with SlCAT2 a sequence identity of 26.8%, 25% and 26.3% respectively, are pH-dependent transporters. To ascertain if SlCAT2 is also pH sensitive, the transport activity was measured at a pH ranging from 5.0 to 8.5 (Figure 18A). The desalted SlCAT2 was reconstituted as described in Materials and Methods, Section 2.2.7., except that 10 mM Tris Hepes at different pH was added to the initial mixture and then the transport activity was measured by adding [^{3}H]-arginine buffered with 10 mM Tris Hepes at the corresponding internal pH. As shown in Figure 18A the transport activity increased at neutral pH, with a maximum of activity at pH 7.5. Moreover, since SlCAT2 is localized at the vacuolar membrane of plant cells, and the vacuolar lumen has a more acidic pH (pH 5.5) with respect to the cytosolic pH, the effect of a pH gradient was also tested in proteoliposomes. To generate this gradient across the liposomal membranes, 10 mM Tris Hepes at pH 5.5 or pH 7.5(control condition) was added. Then, the transport activity was measured by adding [^{3}H]-arginine buffered with 10 mM of Tris Hepes at pH 7.5. As shown in Figure 18B in the presence of a pH gradient more acidic inside (pH 5.5_{in}, pH 7.5_{out}) the transport activity is slightly but not significantly increased with respect to the condition with an equal pH in the internal and external side.

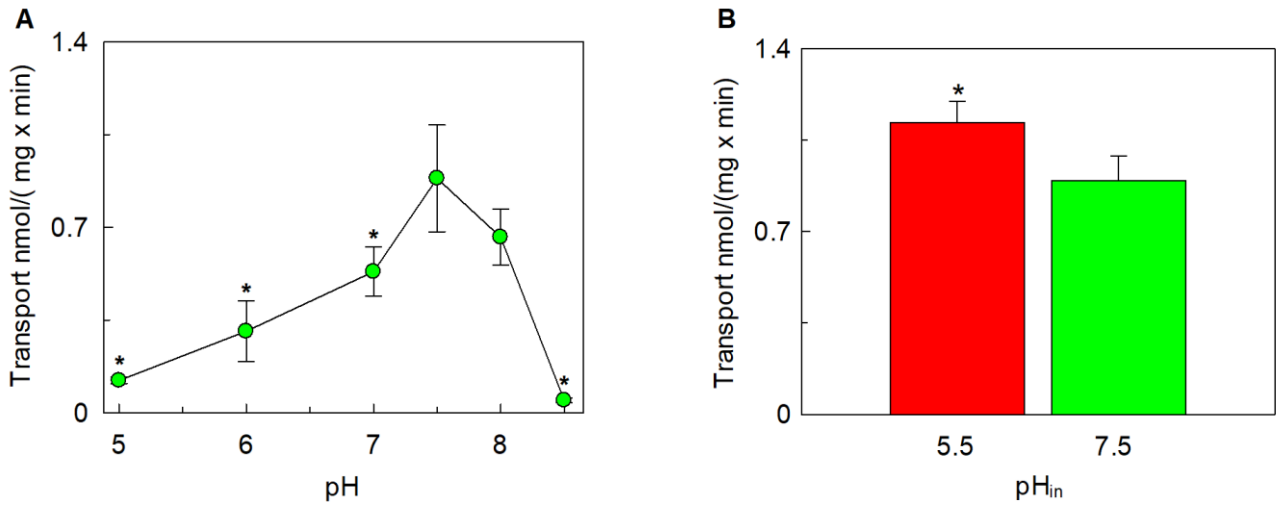

Figure 18 Effect of pH on the transport activity of SlCAT2. (**A**) Transport rate was measured as nmol/(mg x min) by adding 100 µM [^{3}H]-arginine to proteoliposomes containing 200 mM sucrose and 15 mM of ATP and 10 mM of Tris Hepes at the indicated pH. (**B**) The transport activity was measured by adding 100 µM [^{3}H]-arginine buffered with 10 mM of Tris Hepes at pH 7.5, to proteoliposomes prepared using 10 mM of Tris Hepes at pH 5.5 (red bars) or 7.5 (green bars) and containing 200 mM sucrose and 15 mM of ATP. Results are the means ± SD from three experiments. (*), significantly different from the control (none) for $p < 0.05$ as calculated from 1-way ANOVA test.

Vacuoles are known to be involved in the accumulation of several compounds and thus, they are subject to continuous osmotic oscillations in physiological conditions. Therefore, the influence of osmolality was also evaluated on the activity of SlCAT2. To generate the osmotic gradient across the proteoliposomal membrane, sucrose was used as an osmolyte and its concentration was varied in the initial mixture of reconstitution. In this condition, the transport activity increased by increasing the intraliposomal osmolality, reaching a plateau at 225 mOsmol (Figure 19A). To evaluate the side specificity of such a regulation, the transport activity was also measured changing the external osmolality (Figure 19B). In this case, the behaviour of SlCAT2 was different, in fact, the increase of the external osmolality caused a reduction in the transport activity to about 45% of the control at 50 mM sucrose. A further increase of the external osmolality did not affect the transport activity. Therefore, in agreement with the physiological phenomenon, also the transport of amino acid across the vacuolar membrane via SlCAT2 might be regulated by the increase of internal osmolality.

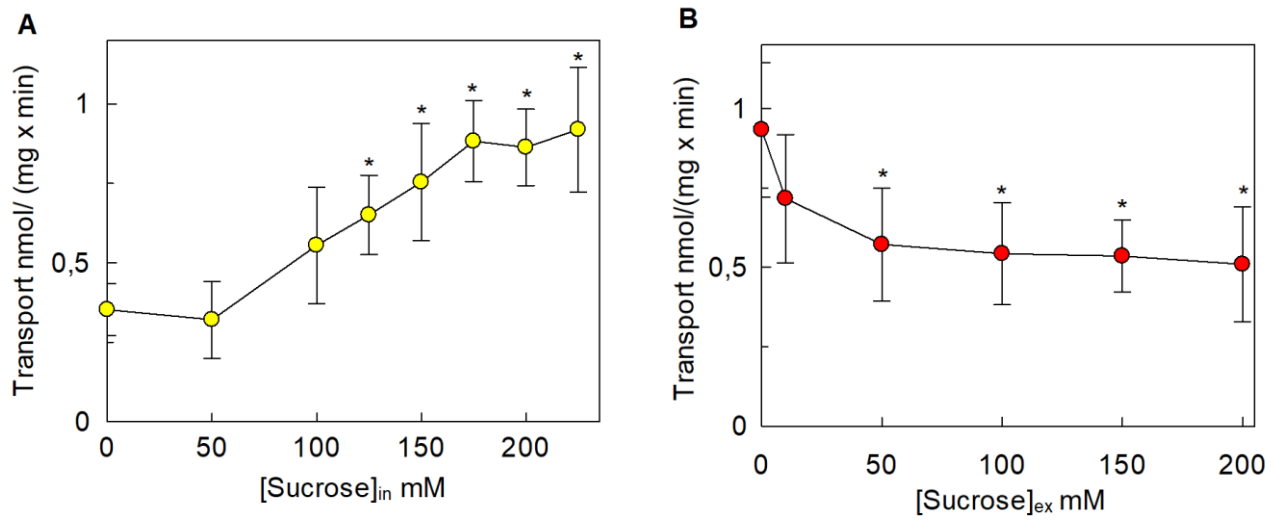

Figure 19 Effect of osmotic pressure on the transport activity of SlCAT2. SlCAT2 was purified and reconstituted in proteoliposomes as described in Materials and Methods, Section 2.2.3. (**A**) The transport activity (nmol/(mg x min)) was measured adding 100 µM [^{3}H]-arginine to proteoliposomes containing indicated concentrations of sucrose, 15 mM ATP and 10 mM of Tris Hepes at pH 7.5. (**B**) Transport rate was measured adding 100 µM [^{3}H]-arginine together indicated concentrations of sucrose to proteoliposomes containing 200 mM sucrose and 15 mM ATP, at pH 7.5. Results are the means ± SD from three experiments. (*), significantly different from the control (without sucrose in (A) and (B)) for $p < 0.05$ as calculated from 1-way ANOVA test.

3.2.3. Effect of Cations

The effect of cations was also tested on the transport activity of SlCAT2. In particular, KCl, NaCl, NH_4Cl, $CaCl_2$, or $MgCl_2$ were added to the extraliposomal compartment at concentrations close to their physiological values in the cytosol and the [^{3}H]-arginine uptake was measured. As shown in Figure 20 the transport activity was inhibited by external KCl and the same effect was observed in the presence of K-gluconate, indicating that the inhibition was specifically due to K^+ ions. Also Na^+ and NH_4^+ showed a similar inhibitory effect on SlCAT2. To exclude an osmotic effect, 40 mM of sucrose was used as an osmotic control. The inhibition by these ions was about 40% with respect to the condition with sucrose. It has to be highlighted that the addition of 40 mM of sucrose to the external compartment caused a reduction of the transport activity with respect to the condition without sucrose, in line with the results of Figure 19B. Among divalent cations, Mg^{2+} at low concentrations, which are close to the physiological ones, determined a decrease of transport activity by 33%, while Ca^{2+} had just a slight effect with respect to the condition with sucrose. In this case, as a control of osmolality, a condition with 1.2 mM of sucrose was used, which is similar to the condition without sucrose.

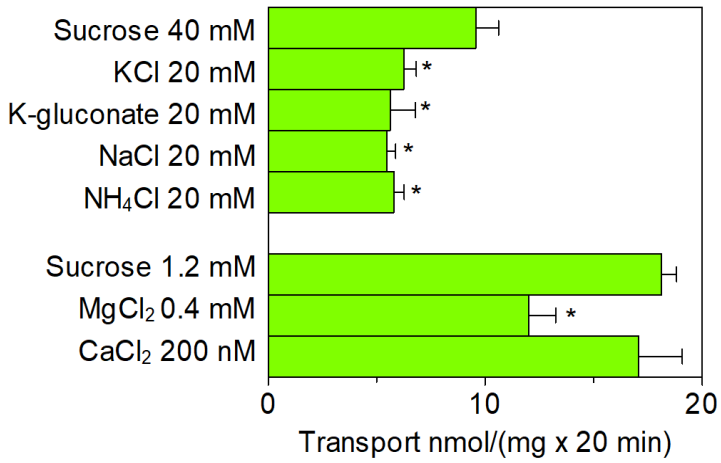

Figure 20 Effect of extraliposomal cations on the transport activity of SlCAT2. SlCAT2 was purified and reconstituted as described in Section. The transport rate was measured in 20 min by adding 100 µM [^{3}H]-arginine together with the indicated compounds to proteoliposomes containing 200 mM sucrose, 15 mM ATP and 10 mM of Tris Hepes at pH 7.5. . Results are the means ± SD from four experiments. (*), significantly different from the control (sucrose 40 Mm or sucrose 1.2 mM) for $p < 0.05$ as calculated from 1-way ANOVA test.

Dose-response analyses were performed for cations which exerted a stronger inhibition. Therefore, for each condition, the [^{3}H]-arginine uptake was measured together with several external concentrations of these cations. In particular, an IC_{50} value of 10.9 ± 0.8 mM, 11.3 ± 1.2 mM, 5.7 ± 1.49 mM, or 0.42 ± 0.18 mM was derived for Na^+ (Figure 21A), K^+ (Figure 21B), NH_4^+ (Figure 21C), or Mg^{2+} (Figure 21D), respectively.

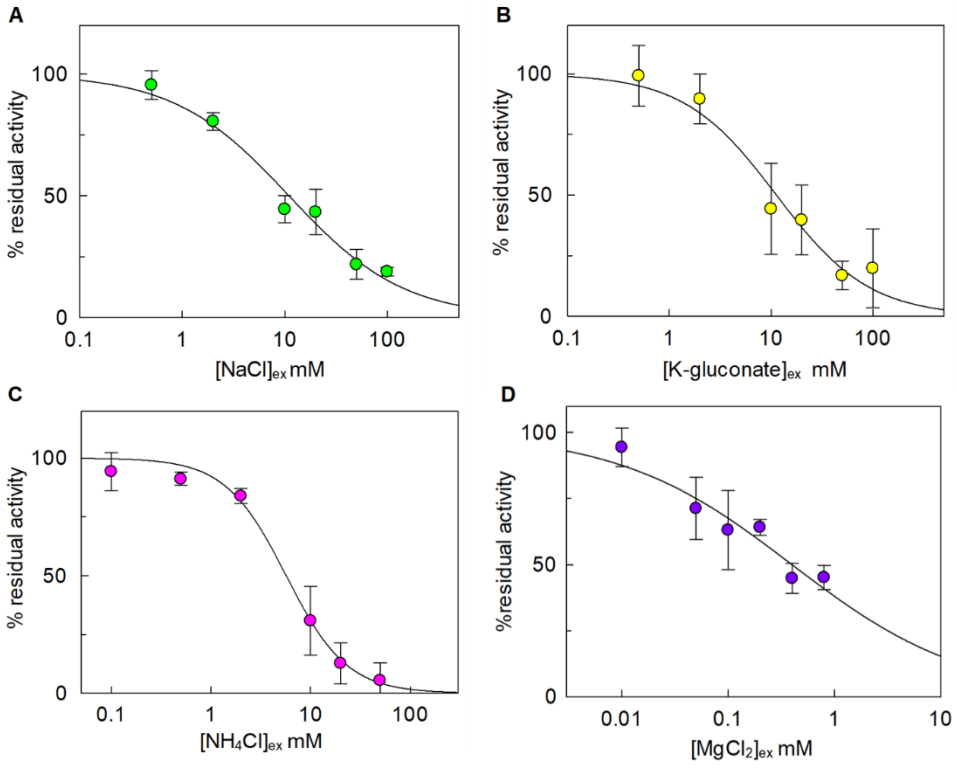

Figure 21 Dose-response curve for the inhibition of SlCAT2 by external cations. Transport was measured in 20 min (calculated as % residual activity with respect to the control condition without the compounds) by adding 100 µM [^{3}H]-arginine together with the indicated concentrations of NaCl (**A**), K-gluconate (**B**), NH_4Cl (**C**) or $MgCl_2$ (**D**) to proteoliposomes containing 200 mM sucrose and 15 mM ATP, at pH 7.5. Results are the means ± SD from three experiments.

The effect of cations was also tested in the intraliposomal compartment (Figure 22). In this case, K^+ and Na^+ activated the transport, but their activation compared with the osmotic control condition (sucrose 100 mM as control of KCl and sucrose 200 mM as control of NaCl) was not relevant. Ca^{2+} and NH_4^+ had the same effect as K^+ and Na^+. On the contrary, only Mg^{2+} showed a strong inhibitory effect.

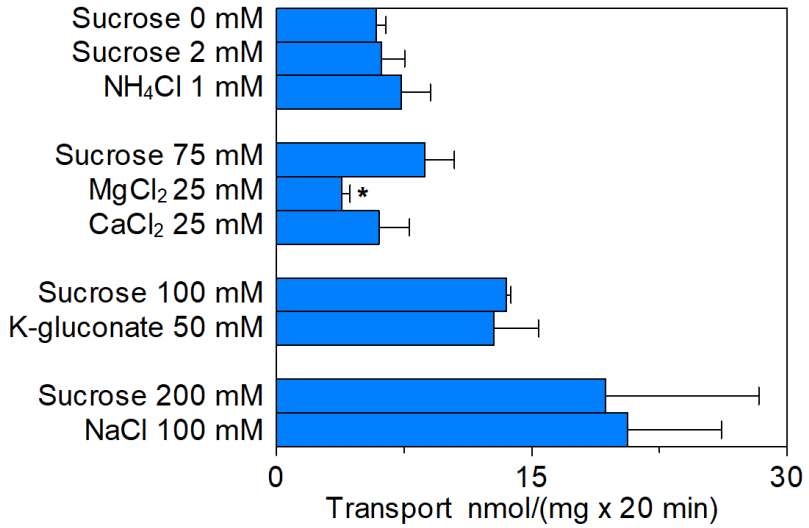

Figure 22 Effect of intraliposomal cations on the transport activity of SlCAT2. Transport was measure in 20 min by adding 100 µM [^{3}H]-arginine to proteoliposomes containing the indicated concentrations of compounds or sucrose, 15 mM ATP, at pH 7.5. Results are the means ± SD from four experiments. (*), Significantly different from the control (isoosmotic concentration of sucrose for each category of cations) for $p < 0.05$ as calculated from 1-way ANOVA test.

Therefore, a dose-response analysis in the presence of several internal concentrations of Mg^{2+} was performed (Figure 23A) and an IC_{50} value of 23.0 ± 9.9 mM was derived. The IC50 value derived for Mg^{2+} is two orders of magnitude higher than the external value. This minor inhibition in the internal compartment could be due to the known interaction of Mg^{2+} with ATP. In fact, all the experiments were performed in the presence of 15 mM ATP, since it has been demonstrated (Regina, Galluccio et al. 2017) that ATP stimulated the transport of SlCAT2 in the internal compartment. In the presence of Mg^{2+}, ATP could be complexed with Mg^{2+} and thus, it could not bind SlCAT2, and stimulate its transport. Therefore in order to dissect the effect of the sole Mg^{2+}, transport was measured in the absence of ATP. As shown in Figure 23B, no inhibition was observed, confirming the above suggested hypothesis. This data demonstrated that internal Mg^{2+} had no effect on the transport activity. Moreover, as shown in Figure 23B the higher scattering observed in the transport measurements was due to a low transport activity of SlCAT2 in the absence of ATP.

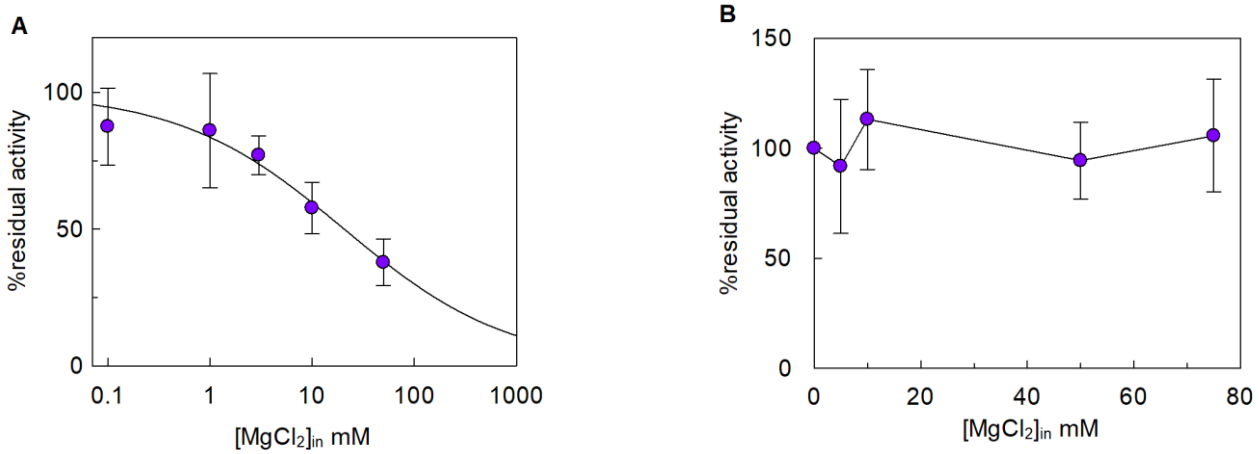

Figure 23 Effect of internal Mg^{2+} on the transport activity of SlCAT2. (**A**) Dose–response curve for the inhibition of Mg^{2+} in the presence of intraliposomal ATP. Transport was measured in 20 min by adding 100 µM [^{3}H]-arginine to proteoliposomes containing the indicated concentrations of Mg^{2+}, 200 mM sucrose, and 15 mM ATP, at pH 7.5. (**B**) Analysis of the inhibition of Mg^{2+} in the absence of intraliposomal ATP. Results are the means ± SD from three experiments.

The sidedness of SlCAT2 transport was further investigated by testing the effect of ATP on the extraliposomal side (data not shown). The addition of several concentrations of ATP at the external compartment caused a decrease of the transport, indicating a side-specific activation by ATP. However, since the ATP used is ATP-$(Na^+)_2$ salt, the inhibition is partially due to the increase of osmolality and the presence of Na^+ (Figure 19B and Figure 20). Thus, this inhibition might not be physiologically relevant, since the cytosolic free-ATP is in the micromolar range.

It has been observed that SlCAT2 is trans stimulated. Therefore, the effect of Mg^{2+} was also tested on the [^{3}H]-arginine efflux from proteoliposomes containing or not external Mg^{2+}. Interestingly, Mg^{2+} had just a slight effect on [^{3}H]-arginine efflux (Figure 24, purple circle).

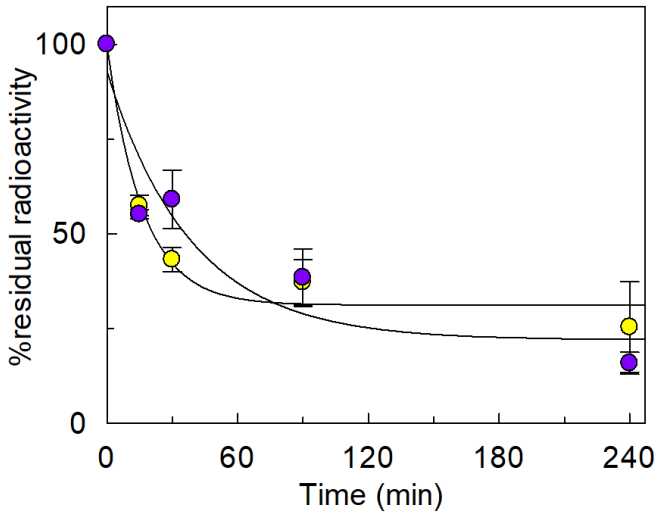

Figure 24 Efflux from proteoliposomes reconstituted with SlCAT2. Arginine efflux was measured at the indicated time. Internal residual radioactivity was measured as percent with respect to control (time 0), in the absence (yellow circle) or in the presence (purple circle) of 0.45 mM Mg^{2+} in the extraliposomal compartment. Data are plotted using the single exponential equation with offset as described in Materials and Methods, Section 2.3. Results are the means ± SD from three experiments.

3.2.4. *Effect of cholesterol*

The effect of cholesterol, as CHEMS, has been tested on the transport of SlCAT2.The transport activity of SlCAT2, measured at two different amounts of cholesterol, shown an increase of 30% in the presence of 1 µg CHEMS/mg to the control condition (without CHEMS) (Figure 25).

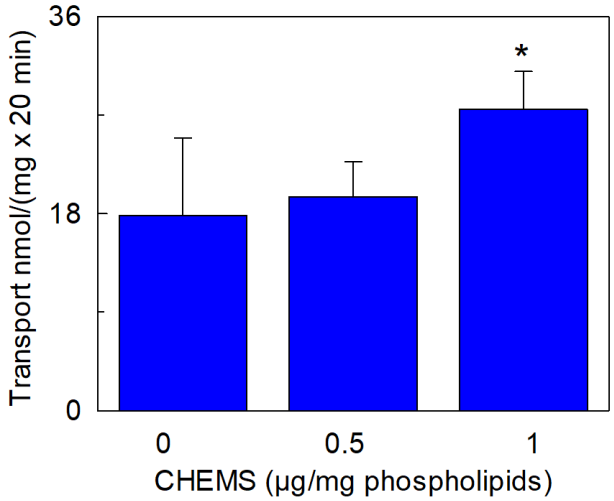

Figure 25 Effect of cholesteryl hemisuccinate (CHS) on the transport activity of SlCAT2. Transport was measured in 20 min by adding 100 µM [^{3}H]-arginine to proteoliposomes prepared without CHS or with 0.5 mg or 1 mg CHS and containing 200 mM sucrose, and 15 mM ATP, at pH 7.5. Results are the means ± SD from four experiments. (*), Significantly different, from the control (without CHS) for $p < 0.05$ as calculated from Student's t-test analysis.

3.2.5. *Homology model*

SlCAT2 showed 14 TM domains with the N- and C- termini exposed towards the vacuolar lumen. The 3D structure of SlCAT2 is still not available, yet. Therefore, the homology model of the transporter was built on the homologous prokaryotic transporter GkApcT (*G. kaustophilus*), which shares 27% of sequence identity with SlCAT2. GkApcT is a proton-coupled amino acid transporter, which has 12 TM helices and is localized at the plasma membrane. The homology model was built using SWISS-MODEL and lacks two helices (TM 11 and TM12) (Figure 26A). The Ramachandran plot of the homology model shows 84.8% or 93.9% of all residues are in favored or in allowed regions, respectively (figure not shown). SlCAT2 shows a LeuT fold, with the first five helices (orange) linked to the subsequent five helices (TM6-TM10 in cyan) by a pseudo-two-fold symmetry axis. The arginine binding site was also predicted on the basis of the position of the amino acid substrate in GkApcT (Figure 26B). As shown in figure Phe263 could act as the external substrate gating as the homologous Phe231 in GkApcT. Interestingly, this residue is also preserved in the LAT1 transporter (Phe252). Moreover, two putative cholesterol binding sites, corresponding to the known CRAC motif (L/V)-X_{1-5}-(Y)-X_{1-5}-(K/R), were identified on the homology model of SlCAT2 (Figure 26C).

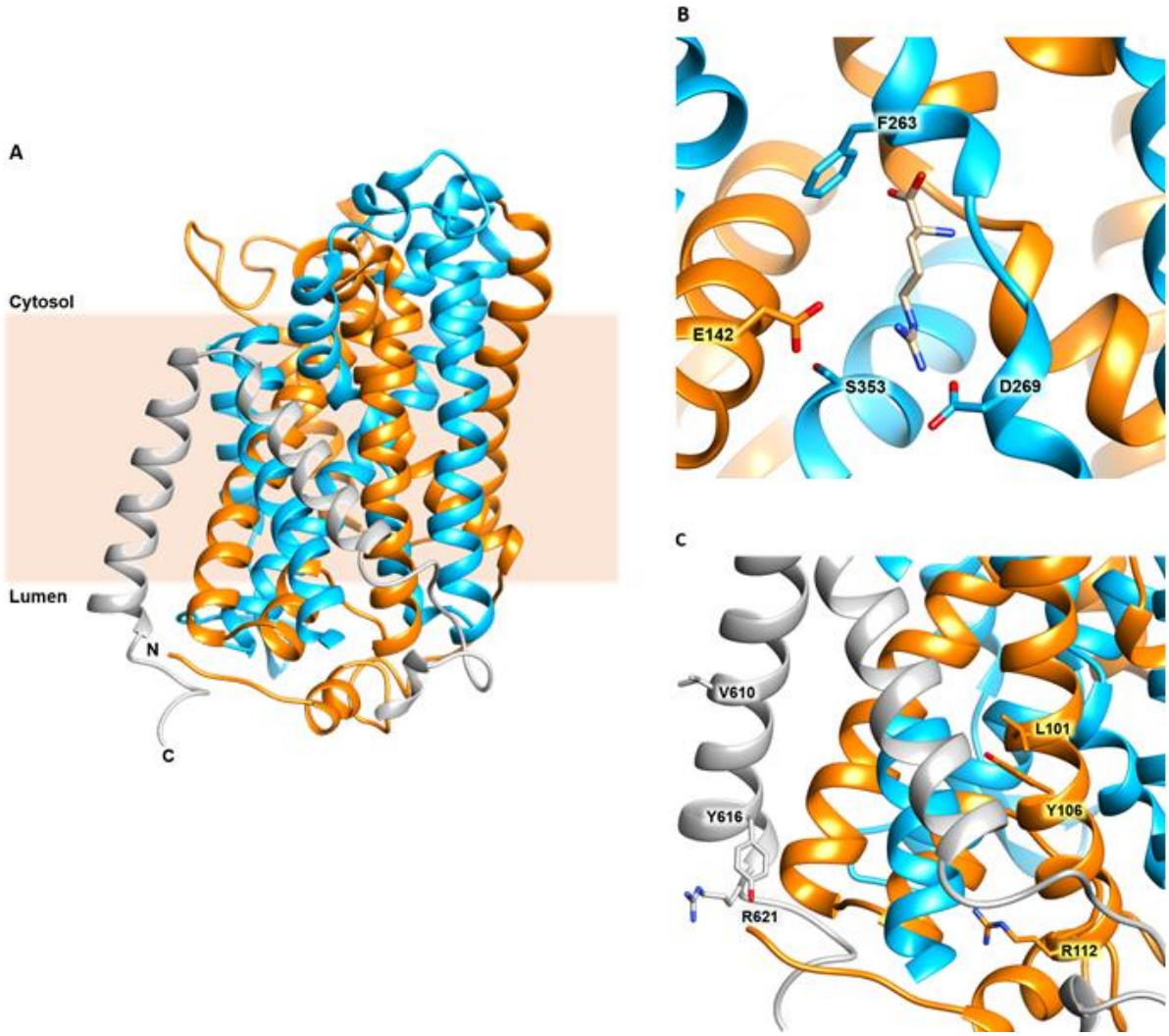

Figure 26 Homology model of SlCAT2. The homology model was build using GkApcT transporter (PDB ID: 5OQT) as a template. SlCAT2 show a '5+5 repeat fold' where the first five helices (TM1-5 in orange) are linked to the other five (TM6-10 in cyan) by a pseudo-2-fold symmetry. The additional two helices, which are not part of the fold are colored in gray. (**A**) Side and top view of the homology model. (**B**) Arginine docking in the putative binding site of SlCAT2, residues involved in the binding are represented as labelled ball and stick. (**C**) Residues of CRAC motifs. One is on TM2 (orange) and the other motif is on the TM14 (gray).

3.3. Structure/function relationships of LAT1 transporter

3.3.1. Effect of cholesterol on the transport activity of hLAT1 in proteoliposomes

hLAT1 was overexpressed in *E.coli* and then purified as described in Materials and Methods, Section 2.2.5. The effect of cholesterol on hLAT1 has been evaluated. At first, the desalted proteins were reconstituted in proteoliposomes prepared with an increased amount of cholesterol, indicated as µg of CHOL/mg of phospholipids It has to be highlighted that in this case, cholesterol has been used after improving the insertion of the lipid into the proteoliposome membrane (see Materials and Methods, Section 2.3.2.). After reconstitution, the transport rate was measured as [^{3}H]-histidine$_{ex}$/histidine$_{in}$ antiport. As shown in Figure 27 the transport activity increased by increasing the cholesterol concentration. Maximal activity was measured at 75 µg cholesterol/mg phospholipids.

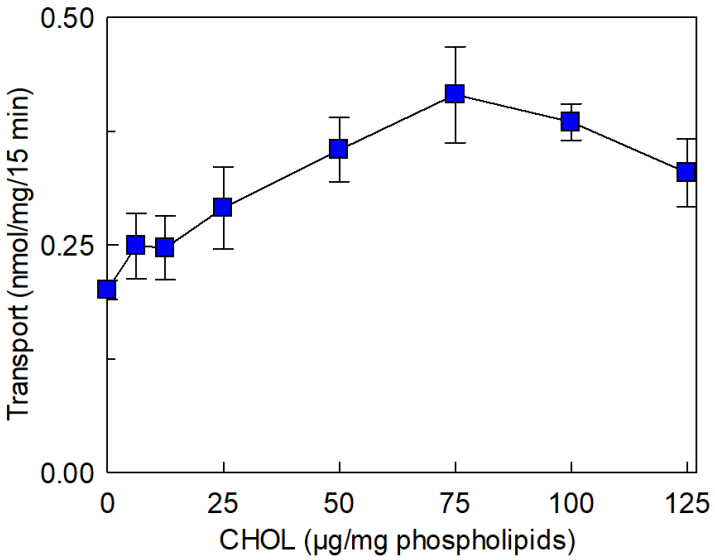

Figure 27 Effect of cholesterol (CHOL) on the transport activity of hLAT1. Transport rate (nmol/(mg x 15 min)) was measured adding 5 µM [^{3}H]-histidine to proteoliposomes containing 10 mM histidine prepared with the indicated amounts of CHOL. Results are means ± SD of at least three independent experiments.

The best condition, i.e. 75 µg cholesterol/mg phospholipids, was then used to perform the other experiments. In particular, the effect of cholesterol on substrate affinity on the external and internal side was evaluated. Therefore, kinetic parameters were measured in the absence and the presence of 75 µg cholesterol/mg phospholipids. Figure 28A shows the transport rate as a function of the external substrate concentrations plotted according to Michaelis-Menten. The Km measured in the absence of cholesterol was of 14.9 ± 2.7 µM, while in the presence of cholesterol the Km was slightly increased with respect to the control condition (22.6 ± 4.3 µM). These data are in agreement with previous data reported by Dickens et al., showing no variation of Km of L-DOPA after sequestration of cholesterol in cell systems by methyl-cyclodextrin. An increase of Vmax in the presence of cholesterol from 0.069 ± 0.0094 to 0.12 ± 0.012 nmol/mg/min was observed. On the contrary, the internal Km (Figure 28B) value decreased from 2.3 ± 0.6 mM in the absence of cholesterol to 0.87 ± 0.12

mM in the presence of cholesterol, while the Vmax increased from 0.061 ± 0.0087 nmol/mg/min to 0.10 ± 0.0038 nmol/mg/min. This data indicated that the interaction of cholesterol with hLAT1 stabilizes the transporter in an inward facing conformation and thus increasing the internal substrate affinity.

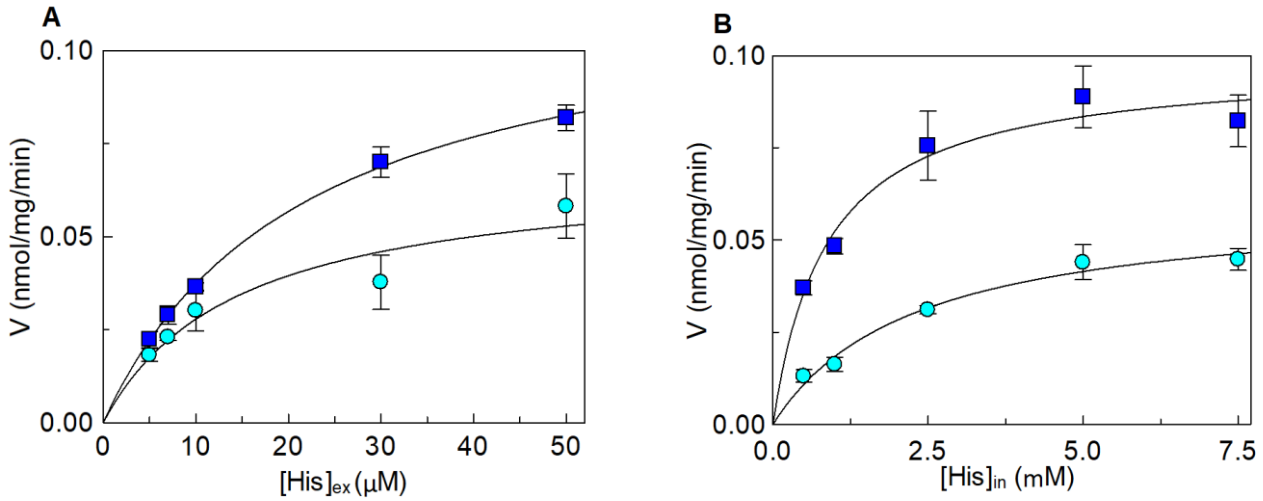

Figure 28 Effect of cholesterol on the kinetic of hLAT1. The purified protein was reconstituted using proteoliposomes prepared without (cyan circle) or with 75 μg cholesterol/mg phospholipids (blue square).In (**A**), transport rate was measured by adding [^{3}H]-histidine at the indicated concentrations to proteoliposomes containing 10 mM histidine. In (**B**),transport rate was measured by adding 30 μM [^{3}H]-histidine to proteoliposomes containing in the internal side indicated concentrations of histidine. Data were plotted according to the Michaelis–Menten equation as transport rate vs histidine concentration. Results are means ± SD of at least three independent experiments

3.3.2. Effect of nucleotides on the transport activity of hLAT1.

In the attempt of exploring possible cell regulators associated with energy metabolism, ATP and the other nucleotides were tested on the transport of hLAT1, since it has been found that these compounds influence the activity of other transporters, acting as allosteric regulators (Levine, Cloherty et al. 2002, Pochini, Scalise et al. 2012, Echtay, Bienengraeber et al. 2018, Cosco, Regina et al. 2019). At first, the [^{3}H]-histidine$_{ex}$/histidine$_{in}$ antiport was measured in the presence of several intraliposomal concentrations of ATP (Figure 29A). The recombinant protein was reconstituted in liposomes under the optimal condition of cholesterol concentration. As shown in Figure 29A the transport rate increased by increasing the intraliposomal ATP concentration up to 4 mM. Further increase of ATP concentrations caused a decrease of the transport activity. To assess if this effect was specifically due to ATP or if LAT1 might also be activated by the other nucleotides, CTP, UTP and GTP were also tested in comparison with ATP. Moreover, to exclude the possibility that the activation might be due to an osmotic effect or to the Na^+ cation present in the commercial formulation of ATP, sucrose or NaCl were used as control. As shown in Figure 29B, CTP, UTP and at a lower extent GTP stimulated the transport activity at the same concentration of ATP. On the contrary, no effect was observed in the presence of sucrose or NaCl, demonstrating that the stimulation is specifically due to the interaction of LAT1 with nucleotides. It has to be highlighted that 4 mM is in the range of the intracellular concentration of ATP, while the physiological

concentration of the other nucleotides is lower, in a range of 0.1 to 0.3 mM. Testing CTP, UTP and GTP at a concentration of 0.3 mM no effect was seen (data not shown), demonstrating that ATP activation is specific.

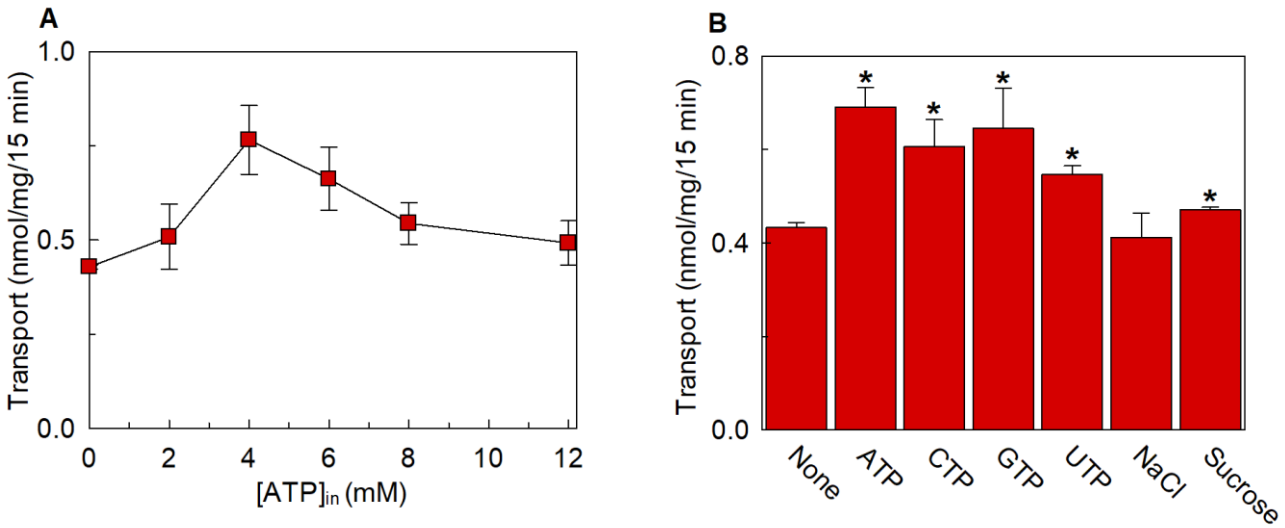

Figure 29 Effect of intraliposomal nucleotides on the transport activity of hLAT1. Proteoliposomes were prepared with 75 µg cholesterol/mg phospholipids. In (**A**) transport assay was started adding 5 µM [^{3}H]-histidine to proteoliposomes containing the indicated concentrations of ATP and 10 mM histidine. In (**B**) transport assay was started adding 5 µM [^{3}H]-histidine to proteoliposomes containing 4 mM of the indicated nucleotides and 10 mM histidine. Results are means ± SD of at least from three independent experiments. (*) Significantly different from the control (no addition in the intraliposomal compartment, none) as estimated by the Student's t-test ($p < 0.05$).

Very interestingly, the activation by ATP occurred only in the presence of cholesterol. In fact, in the absence of cholesterol, ATP had only a slight, if any, effect (Figure 30A). The addition of 75 µg cholesterol/mg phospholipids determined an increase of the transport activity in agreement with the data of Figure 27, but a maximum of activity was measured in the presence of cholesterol and 4 mM ATP. These data suggest that ATP and cholesterol binding sites may be close to each other. Since these experiments were performed using the recombinant protein and thus, in the absence of CD98, to exclude a possible influence of the heavy chain on the effect of cholesterol and ATP, the same experiment was performed using the protein extracted from SiHa cells, in complex with CD98 (Figure 30B). The reconstitution protocol was the same as that of the recombinant protein, with some minor variations as reported in Materials and Methods, Section 2.2.8. As shown in Figure 30B, also in this case, ATP and cholesterol showed a synergistic effect.

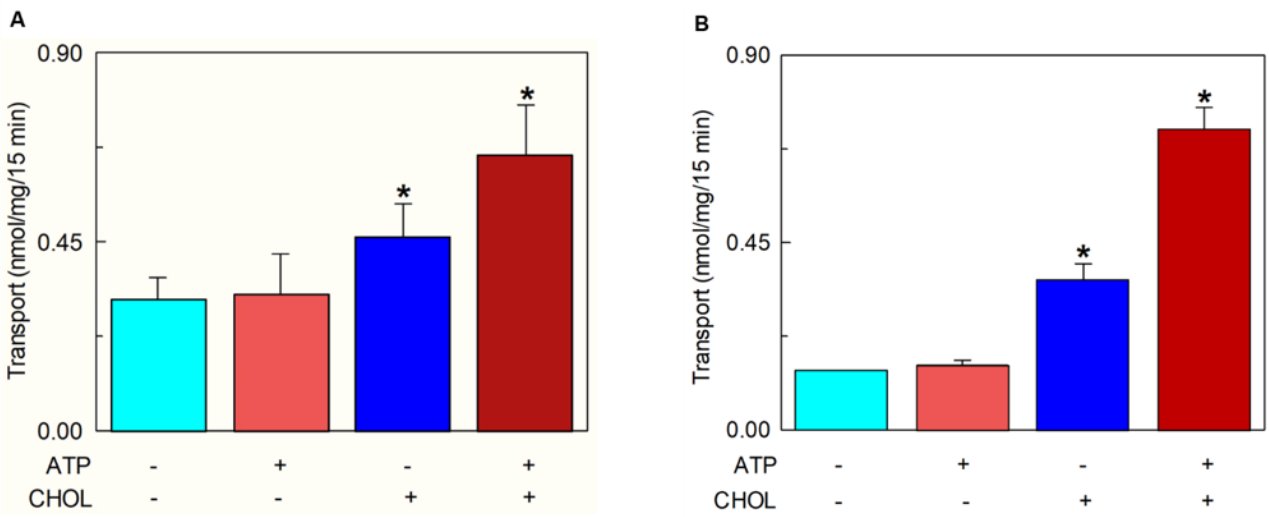

Figure 30 Synergistic effect of ATP and cholesterol on the transport activity of the recombinant hLAT1 and hLAT1 in complex with CD98. In (**A**), transport activity of the recombinant hLAT1. In (**B**) transport activity of the extracted hLAT1 in complex with CD98. In both cases, transport assay was started adding 5 µM [^{3}H]-histidine to proteoliposomes prepared without (−) or with (+) 75 µg cholesterol/mg phospholipids as indicated; without (−) or with (+) 4 mM ATP, buffered with 20 mM HepesTris pH 7.0 and containing 10 mM histidine. Results are means ± SD of at least from three independent experiments. (*) Significantly different from the control (no addition in the intraliposomal compartment, none) as estimated by the Student's t-test ($p < 0.05$).

To investigate if the effect could be influenced by phosphate groups, the transport activity was measured in the presence of 4 mM AMP, ADP or cAMP in comparison to ATP. As shown in Figure 31, transport activity decreased by decreasing the number of phosphate groups. These data indicated that three phosphates are necessary for full stimulation.

Since in cells, ATP is complexed with Mg^{2+}, the effect of ATP-Mg^{2+} was also tested on LAT1 and it has been seen that the effect exerted was in the same order of magnitude with respect to the sole ATP (data not shown).

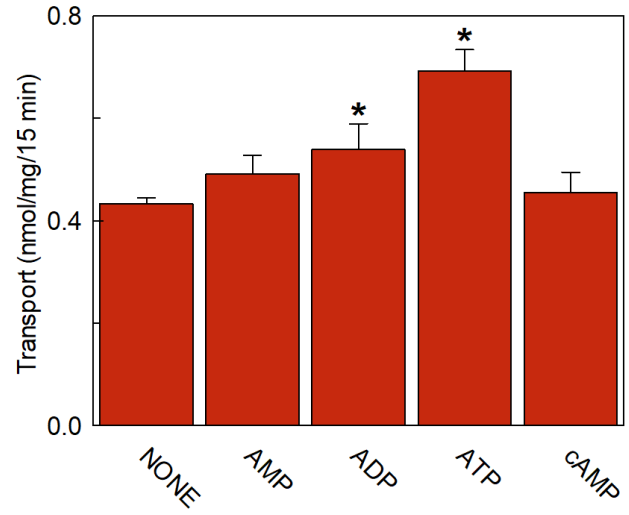

Figure 31 Effect of phosphate groups on the transport activity of hLAT1. Transport assay was started adding 5 µM [^{3}H]-histidine to proteoliposomes containing 4 mM of the indicated compounds and 10 mM histidine. Results are means ± SD of at least from three independent experiments. (*) Significantly different from the control (no addition in the intraliposomal compartment, none) as estimated by the Student's t-test ($p < 0.05$).

The kinetic parameters were also evaluated in the presence of 4 mM of ATP with respect to the control condition without ATP. The external Km value in the presence of intraliposomal ATP was slightly but not significantly higher with respect to the control condition (without ATP), of 33.9 ± 4.4 μM, while the Vmax significantly increased with respect to the control condition (Figure 32A). Also the internal Km was not influenced by the presence of ATP (0.57 ± 0.14 mM), with an increase of Vmax (Figure 32B). These data suggest that the effect of ATP was only secondary to the effect of cholesterol.

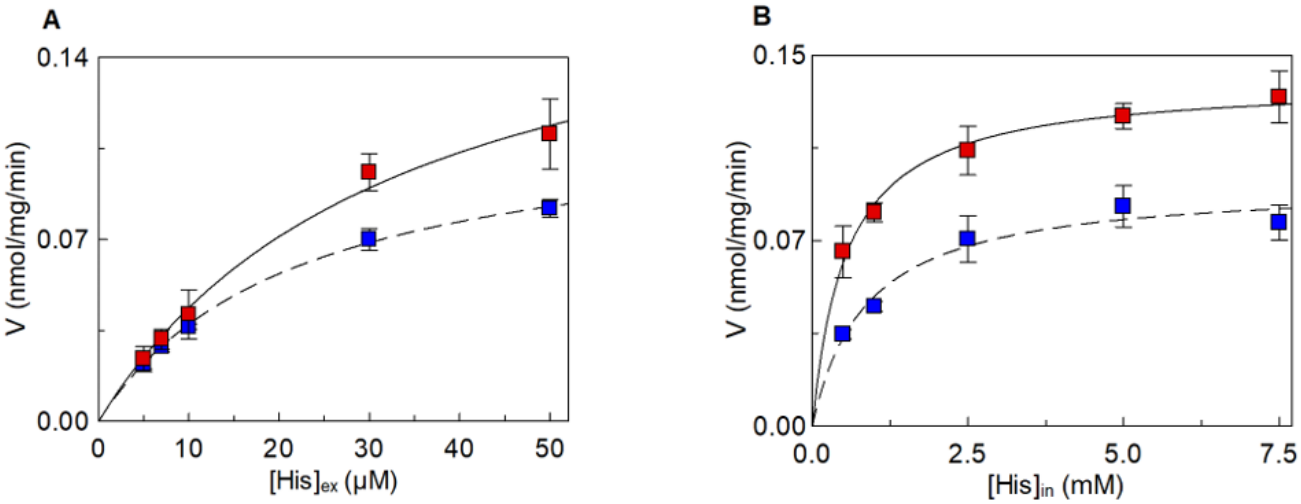

Figure 32 Effect of ATP on the kinetic parameters of hLAT1. In (**A**) transport activity was measured by adding [^{3}H]- histidine at the indicated concentrations to proteoliposomes prepared with 75 μg cholesterol/mg phospholipids as described in "Methods" and containing (red square) or not (blue square) 4 mM and 10 mM histidine (in dotted line, data from corresponding Fig. 2). In (**B**) transport activity was measured by adding [^{3}H]- histidine to proteoliposomes containing the indicated concentration of histidine. Data were plotted according to the Michaelis–Menten equation as transport rate vs histidine concentration. Results are means ± S.D. of at least three independent experiments.

The effect of ATP was also evaluated on the external side, showing a decrease of the transport activity of 25% at 4 mM (Figure 33). It has to be highlighted that this concentration is higher than the cytosolic ATP concentration. Therefore this inhibition maybe not relevant, but this different behavior of LAT1 confirms that the transporter has an asymmetric regulation and is inserted in the proteoliposomal membrane with a right-side-orientation.

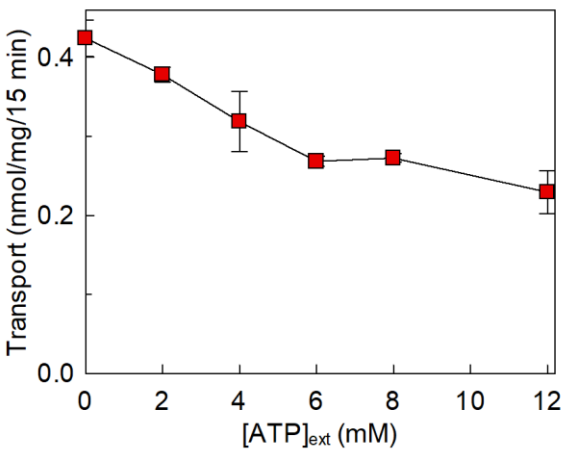

Figure 33 Effect of extraliposomal ATP on the transport activity of hLAT1. Transport assay was started adding 5 μM [^{3}H]-histidine, together with the indicated concentrations of ATP, to proteoliposomes prepared with 75 μg cholesterol/mg phospholipids and containing 4 mM of ATP and 10 mM histidine. Results are means ± SD of at least from three independent experiments.

3.3.3. Computational analysis of cholesterol and ATP interaction with hLAT1

To better analyze these data, computational analysis was performed as described in Materials and Methods, Section 2.4. Recently the Cryo-EM structure of LAT1 has been solved in an inward facing (PDB ID: 6IRT, chain B). At first, this structure has been used to identify putative hydrophilic or hydrophobic regions on the surface of LAT1 using SiteMap tool (see Materials and Methods, Section 2.4.4.). SiteMap identified ten sites with a sitescore ranging from 0.888 to 1.015, which is in the optimal range for a reliable SiteMap prediction. (Figure 34). In particular, the attention was focused on two of these sites**.** One of these, in fact, corresponded to cholesterol-like densities observed in the cryo-EM structure of hLAT1 (Yan, Zhao et al. 2019). In this site, we also found a putative cholesterol binding motif (**CRAC** motif), conserved in LAT1 orthologues (not shown). However, our interest was focused on the other putative site, close to a hydrophilic pocket. In particular, this site could be divided into two subsites. S**ubsite 1** corresponds to the hydrophobic region and the hydrophilic one and **subsite 2** corresponds to another hydrophobic region. Noteworthy is that these two hydrophobic surfaces correspond to regions already predicted to be involved in cholesterol binding (Dickens, Chiduza et al. 2017). However, the attention was focused on subsite 1, since the hydrophobic region is close to the hydrophilic pocket in agreement with our working hypothesis, based on biochemical data. Therefore, docking analysis was performed after generating a grid on subsite 1 of the large site. Moreover, to obtain more reliable information, Induced Fit docking was performed which takes into account the flexibility of the side chain of the binding site, therefore it is not a rigid docking (see Materials and Methods, Section 2.4.3.). 20 poses were carried out and after clustering, the pose with the lowest docking score (-5.54) was selected from the most populated cluster (Figure 34). In this site, cholesterol is located up the helix 1a, surrounded by hydrophobic residues of the helices 1a, 5 and 7, such as L53, V56, A57, L208, A209, I212, I284, V288, L291 and a hydrogen bond occurs between the hydroxyl group of cholesterol and the side chain of L53.

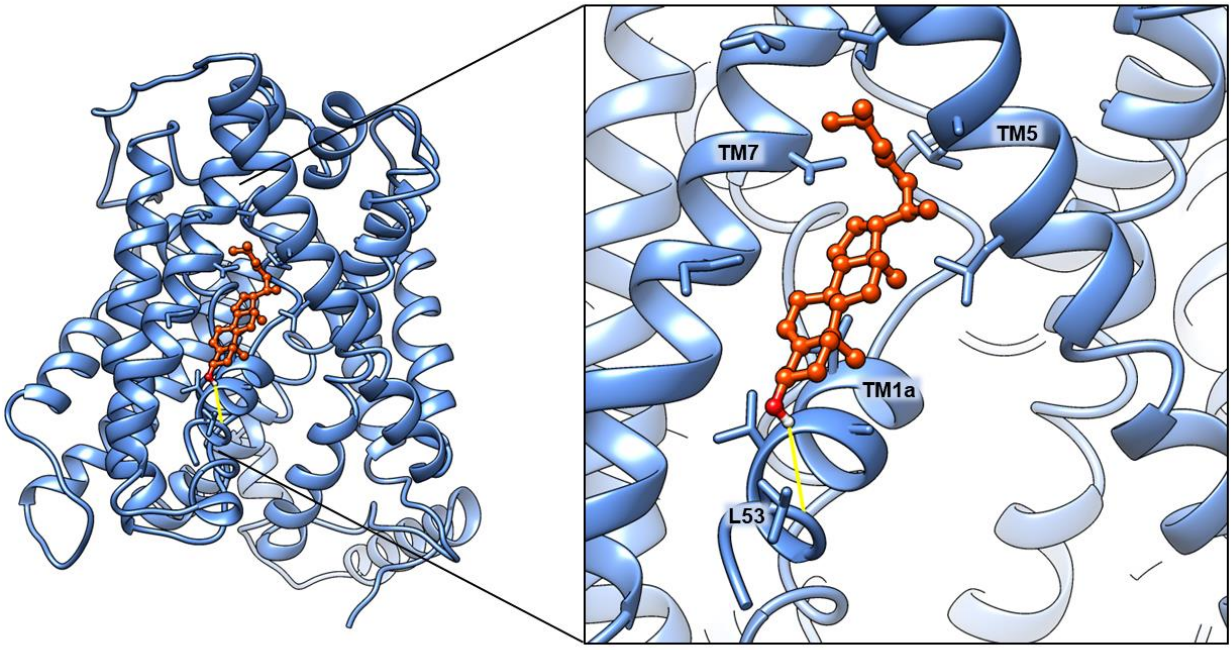

Figure 34 Cholesterol docking on hLAT1. Docking analysis were performed using InducedFit docking. The best pose (represented as orange ball and sticks) has a docking score of -5.54 and MMGBSA binding energy of -46.66 kcal/mol.

As said above, subsite 1 also contains a hydrophilic region close to the hydrophobic one, that might accommodate ATP. Thus, docking of ATP in this site was performed using InducedFit docking and in particular, the grid was generated using the same residues belonging to the cholesterol grid. In this case, ATP was accommodated between the helix 1a and 5 (Figure 35A). The ribose group of ATP makes hydrogen bonds with Gln197 and Asp198. Gln197 interacts also with the α-phosphate. The β-phosphate forms a hydrogen bond with Ser 338 and in particular, the attention was focused on the ϒ-phosphate, important for the full activation which is involved in an electrostatic interaction with Lys 204 (Figure 35A). Interestingly, ATP docking without cholesterol was different, with the nucleotide remaining in a more external position (Figure 35B). This result indicated that the presence of cholesterol might stabilize the binding of ATP in the subsite 1, in agreement with biochemical data which showed that ATP without cholesterol had no effect (Figure 30A). To confirm the ATP binding site, a blind docking was also performed using AutoDock Vina (data not shown). All the predicted ATP poses were located on the hydrophilic surface, confirming our ATP binding predictions.

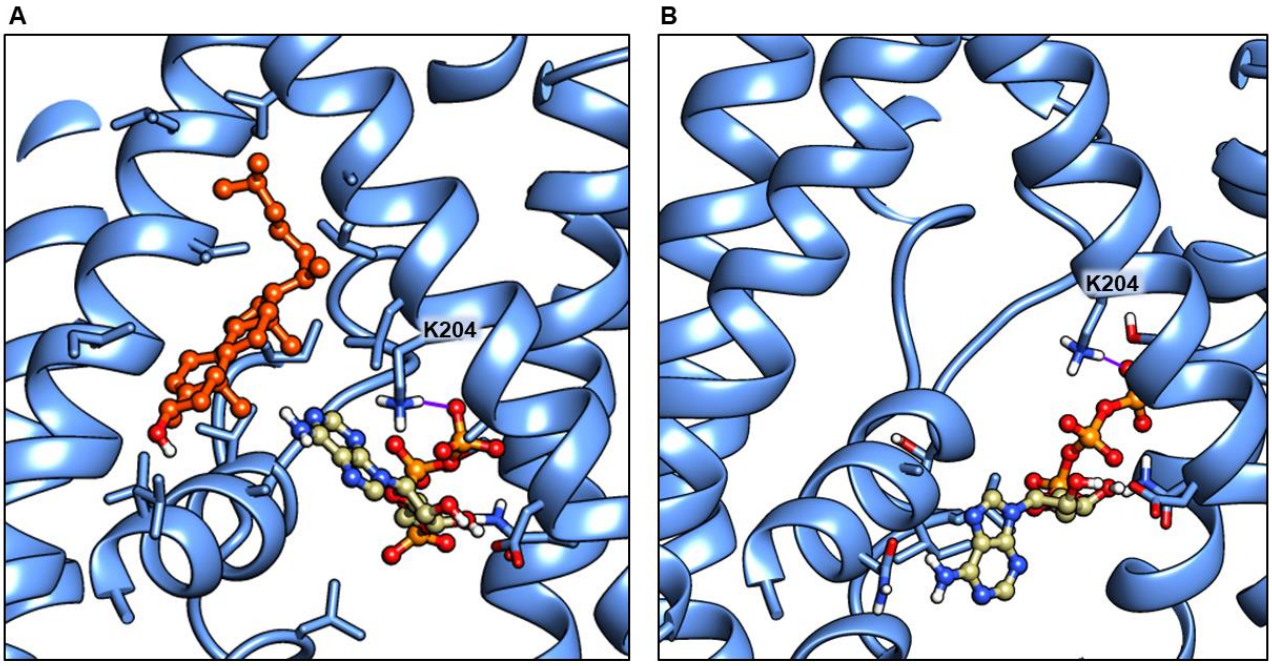

Figure 35 ATP docking on hLAT1. In (**A**) ATP docking in the presence of cholesterol (Figure 35). ATP interacts with Lys 204 through an electrostatic bond (in violet). This pose has a docking score of − 6.92 and a MMGBSA binding energy of − 8.97 kcal/mol. In (**B**), ATP docking in site 1 in the absence of cholesterol; in violet, electrostatic bond with Lys 204 represented in stick. The pose has a docking score of − 6.336.

3.3.4. Basic functional characterization of site-directed mutant hLAT1-K204Q

After docking analysis the attention was focused on Lys 204 since this residue is involved in an electrostatic bond with ϒ-phosphate, which was previously shown to be crucial for the ATP effect (Figure 31). Moreover, it has been found that Lys 204 is preserved in the other SLC7 transporters. Therefore, Lys 204 has been mutated to Gln, thus maintaining the hydrophilic nature and the size, but removing the positive charge. At first, the [^{3}H]-histidine$_{ex}$/histidine$_{in}$ was measured for the hLAT1- K204Q in comparison with the hLAT1-WT. As shown in Figure 36A a reduction of 15% of the transport activity was measured for the mutant with respect to the WT. Moreover, hLAT1-K204Q showed also a loss of sensitivity to competitive and covalent inhibitors (Figure 36B), indicating that this substitution might affect the substrate binding too.

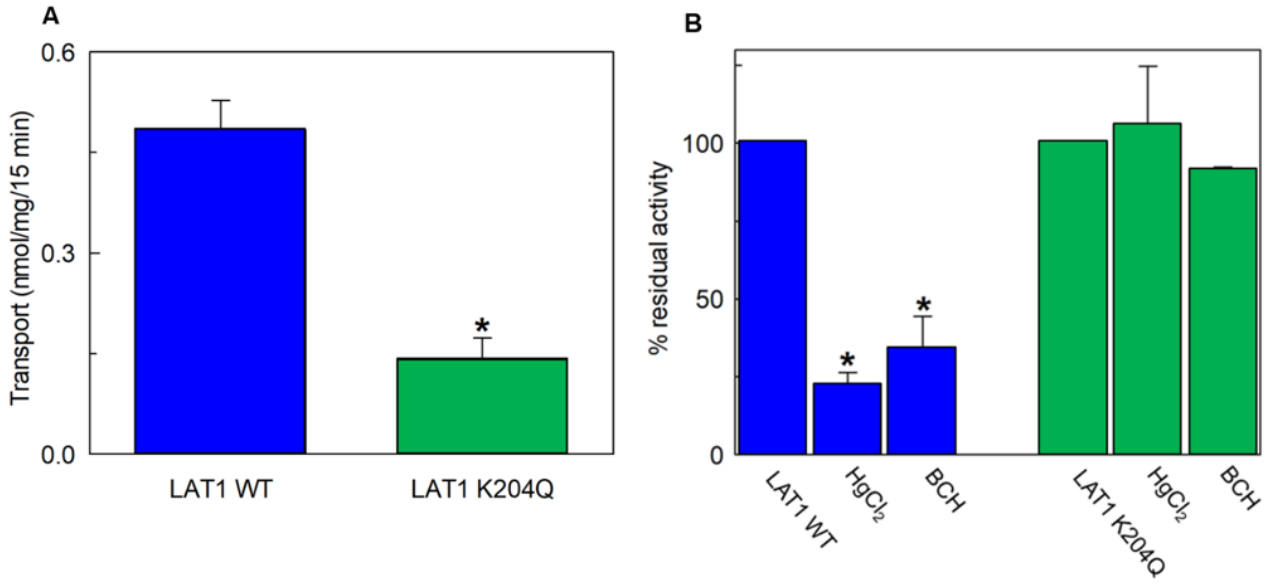

Figure 36 Transport activity of the recombinant hLAT1-WT or hLAT1-K204Q mutant. In (**A**) comparison of the transport activity of hLAT1-WT or hLAT1-K204Q. Transport assay was started adding 5 µM [^{3}H]-histidine to proteoliposomes prepared with 75 µg cholesterol/mg phospholipids *and* containing 10 mM histidine. In (**B**) the effect of HgCl2 and BCH on transport activity of hLAT1-WT or hLAT1-K204Q mutant. Transport assay was started adding 5 µM [^{3}H]-histidine together with 15 µM HgCl2 or 5 mM BCH to proteoliposomes prepared with 75 µg cholesterol/mg phospholipids *and* containing 10 mM histidine. Results are means ± SD of at least three independent experiments. (*) Significantly different from the control (no externally added inhibitor) as estimated by the Student's t-test ($p < 0.05$).

For a serendipity event, it has also been found that this Lys is involved in pH sensitivity. In particular, to evaluate the effect of the pH, the initial mixture of the reconstitution was prepared by adding Hepes Tris at several pHs (Figure 37A). Then the transport activity was measured for the hLAT1-WT and hLAT1-K204Q and it was seen for the first time that hLAT1-WT is pH-dependent, which is in contrast with the previous finding, and in particular, it has a maximum of activity at neutral pH. The mutant showed an inverted pH dependence with respect to the WT at pH 7.0 (Figure 37A). Kinetic analyses were performed for hLAT1-K204Q at pH 7.0 and 6.0 and the Km values measured was of 549 ± 108 µM or 51.4 ± 7.5 µM at pH 6.0 (Figure 37B) or pH 7.0 (Figure 37C), respectively. At pH 6.0 the Km is lower than pH 7.0, but it was still higher than that of the WT protein, confirming the role of Lys 204 in the transport process and in the substrate recognition. These data are in agreement with the location of a Lys residue which is near to the residues belonging to the substrate binding site.

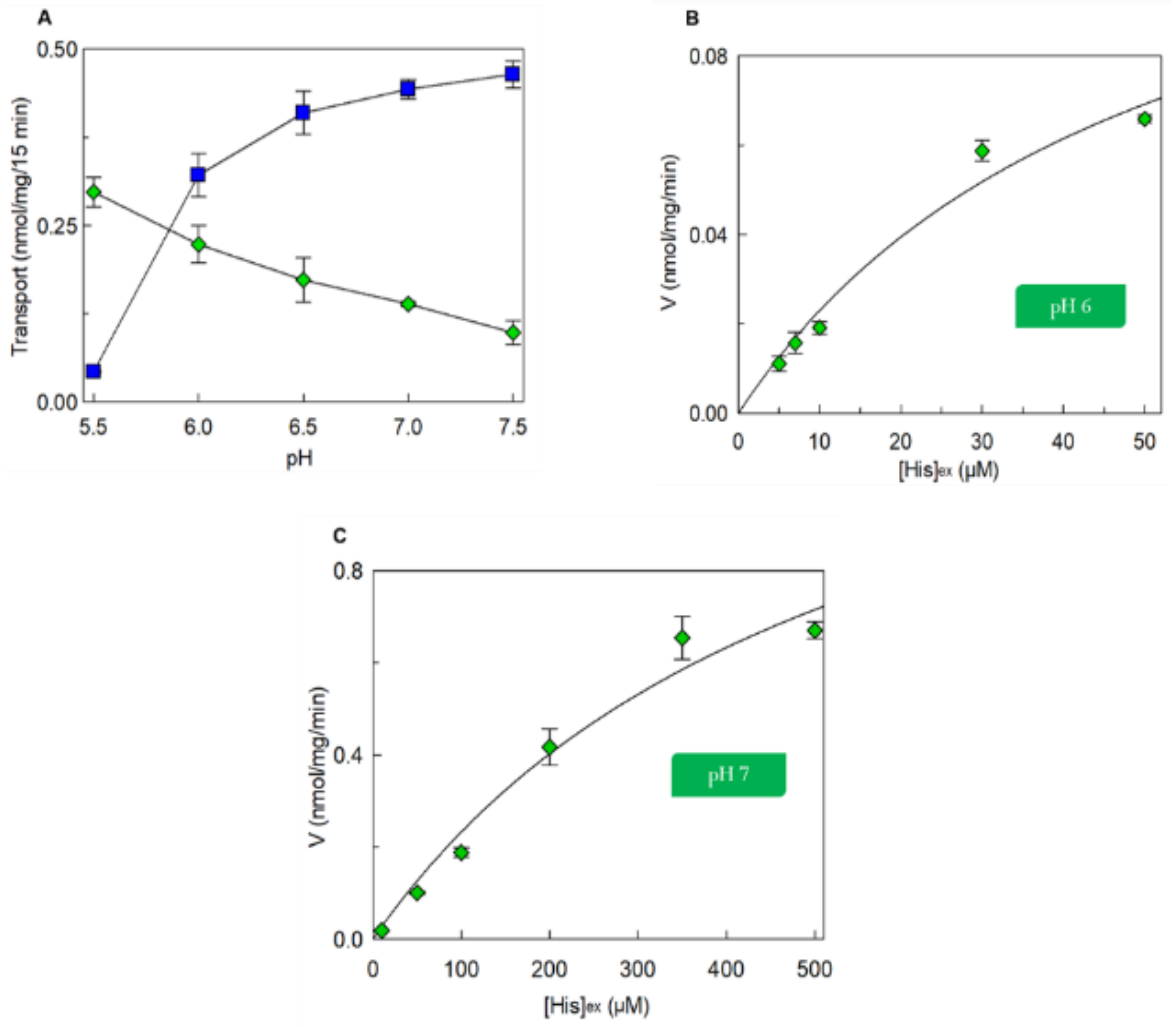

Figure 37 Effect of pH on the transport activity of hLAT1-WT or hLAT1-K204Q mutant. In (**A**), transport rate of LAT1-WT (blue square) and K204Q (green rhombus), was started by adding 5 µM [3H]-histidine to proteoliposomes prepared with 75 µg cholesterol/mg phospholipids and containing 10 mM histidine and 20 mM Hepes Tris at the indicated pH. The pH was equal in both the internal and external sides of proteoliposomes. In (**B** and **C**), the effect of pH on external Km of hLAT1-K204Q mutant. The transport rate was measured by adding [3H]-histidine at the indicated concentrations to proteoliposomes prepared with 75 µg cholesterol/mg phospholipids and containing 10 mM histidine and 20 mM Hepes Tris at pH 6.0 (B) or pH 7.0 (C). Data were plotted according to the Michaelis-Menten equation as transport rate vs histidine concentration. In (**A**, **B** and **C**) results are means ± SD of at least three independent experiments**.**

3.3.5. Effect of the K204Q mutation on ATP and cholesterol dependence.

The effect of cholesterol and ATP was then investigated for hLAT1-K204Q (Figure 38A). The mutant showed a cholesterol dependence which is the same as the WT, indicating that this residue does not affect the cholesterol interaction with LAT1. On the contrary, studying the effect of ATP on the mutant, it has been found that in this case there is a shift of activation, from 4 mM to 8 mM. This data suggested that the substitution of Lys compromised the ATP interaction. (Figure 38B).

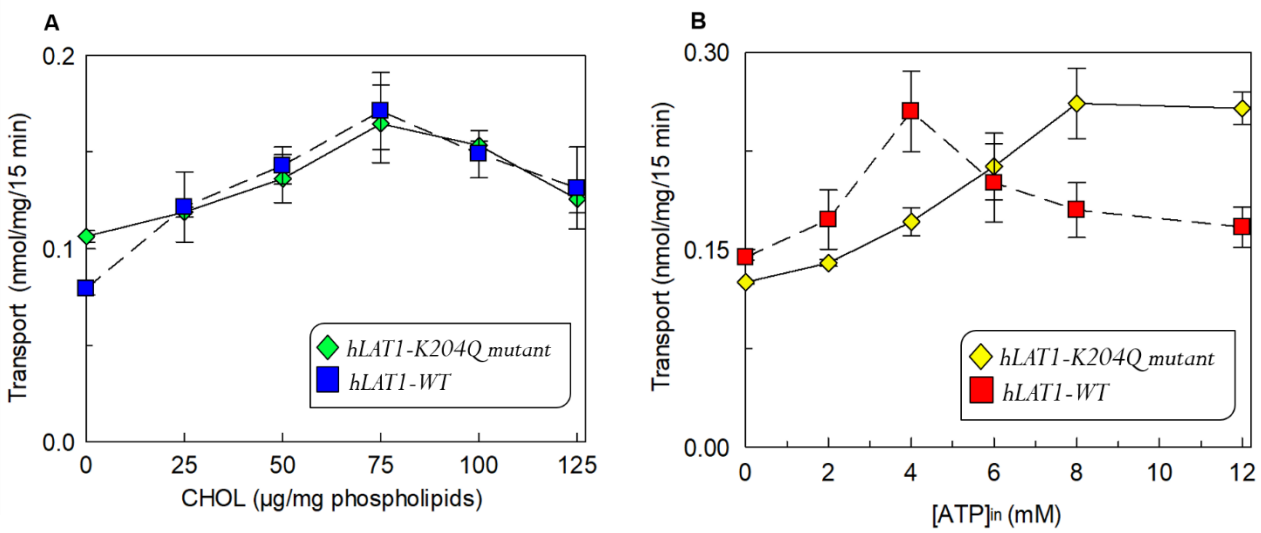

Figure 38 Effect of cholesterol and ATP on the hLAT1-K204Q mutant. In (**A**), transport rate was measured by adding 5 µM [^{3}H]-histidine to proteoliposomes prepared with the indicated amount of cholesterol and containing 10 mM histidine. In (**B**), the effect of internal ATP on transport activity of hLAT1-K204Q mutant. The indicated concentrations of ATP, buffered with 20 mM Hepes Tris pH 7.0, were added in the internal side of proteoliposomes prepared with 75 µg cholesterol/mg phospholipids. Results are means ± SD of at least three independent experiments.

CHAPTER IV

Conclusions

The role of cholesterol in modulating the transport of the mentioned proteins is described in this work. The binding of cholesterol to the transporters seems to stabilize their structure. In particular, the increase of Vmax, without affecting the Km for glutamine in the presence of cholesterol, suggests that cholesterol interaction increases the rate of conformational changes of ASCT2. Cholesterol blind docking to the cryo-EM structure of ASCT2 allowed us to identify six putative cholesterol binding sites, some of which confirmed the cholesterol densities already described in the literature and two of them were found close to a CRAC and a CARC motifs. Putative cholesterol binding sites close to cysteine and tryptophan residues were confirmed using Koshland's reagent and SH-reagents which target tryptophan and cysteine residues. In fact, the presence of cholesterol near these residues could mask and protect them against these compounds. Also in the case of LAT1, an increase of the transport activity in the presence of cholesterol has been observed. Kinetic analysis showed a decrease of internal Km and an increase of Vmax, suggesting a stabilization of the inward conformation. Docking analysis on the cryo-EM structure of LAT1 in an inward facing, showed a cholesterol binding site between the TM 2, 5 and 7. Residues belonging to this site were previously identified by Dickens, on the basis of sequence identity with dDAT. The novel interesting finding in the present work, was the synergistic effect of cholesterol and ATP on the LAT1 transport. Thanks to computational analysis a hydrophilic pocket was identified near the cholesterol binding site, confirming this hypothesis. Therefore, it has been suggested that the interaction of cholesterol with LAT1 stabilizes the inward facing and allows the formation of the ATP binding site. Docking analysis allowed us to identify a lysine in the ATP binding site, Lys 204, which is involved in the interaction with the γ-phosphate of ATP. Interestingly, this Lys is also involved in the binding of substrate and the pH-dependence. About CAT2, the work was mainly focused on the regulation by osmolality and cations, showing an asymmetric dependence on the two sides of the membrane. In particular, a regulation by internal osmolality and external Mg^{2+} was observed. The regulation by cholesterol was also documented for this transporter. In particular, two CRAC motifs were identified on the homology model of CAT2.

Therefore, the three transporters, even though belonging to different organisms share the common feature of being regulated by cholesterol. This is a novel aspect of membrane transporter in general that could be afforded using the strategy of over-expression in a heterologous system and transport studies in the in vitro model of proteoliposome that allows manipulating the membrane composition adding cholesterol. Indeed such a study could not be performed in an intact cell system. The data on transport changes caused by the presence of cholesterol correlated well with the prediction studies performed by bioinformatics. Altogether, the data show that the transporters dealt with are all responsive to cholesterol. The data on the three transporters, in particular, the deeper studies performed on LAT1, allowed us to conclude that the observed effects are due to close interaction of the cholesterol with some domains of the proteins, thus not limited to unspecific effects od the lipid on the membrane fluidity. These novel discoveries are fundamental for understanding the molecular mechanism of transport and regulation as well as for applications to human pathology.

Bibliography

1. Albritton, L. M., J. W. Kim, L. Tseng and J. M. Cunningham (1993). "Envelope-binding domain in the cationic amino acid transporter determines the host range of ecotropic murine retroviruses." J Virol **67**(4): 2091-2096.
2. Arinaminpathy, Y., E. Khurana, D. M. Engelman and M. B. Gerstein (2009). "Computational analysis of membrane proteins: the largest class of drug targets." Drug Discov Today **14**(23-24): 1130-1135.
3. Boddapati, S. V., G. G. D'Souza and V. Weissig (2010). "Liposomes for drug delivery to mitochondria." Methods Mol Biol **605**: 295-303.
4. Bode, B. P. (2001). "Recent molecular advances in mammalian glutamine transport." J Nutr **131**(9 Suppl): 2475S-2485S; discussion 2486S-2477S.
5. Boggio, S. B., J. F. Palatnik, H. W. Heldt and E. M. Valle (2000). "Changes in amino acid composition and nitrogen metabolizing enzymes in ripening fruits of Lycopersicon esculentum Mill." Plant Sci **159**(1): 125-133.
6. Broer, A., N. Brookes, V. Ganapathy, K. S. Dimmer, C. A. Wagner, F. Lang and S. Broer (1999). "The astroglial ASCT2 amino acid transporter as a mediator of glutamine efflux." J Neurochem **73**(5): 2184-2194.
7. Broer, A., C. Wagner, F. Lang and S. Broer (2000). "Neutral amino acid transporter ASCT2 displays substrate-induced Na+ exchange and a substrate-gated anion conductance." Biochem J **346 Pt 3**: 705-710.
8. Broer, S. (2008). "Amino acid transport across mammalian intestinal and renal epithelia." Physiol Rev **88**(1): 249-286.
9. Broer, S. (2014). "The SLC38 family of sodium-amino acid co-transporters." Pflugers Arch **466**(1): 155-172.
10. Broer, S. and A. Broer (2017). "Amino acid homeostasis and signalling in mammalian cells and organisms." Biochem J **474**(12): 1935-1963.
11. Broer, S. and M. Palacin (2011). "The role of amino acid transporters in inherited and acquired diseases." Biochem J **436**(2): 193-211.
12. Casagrande, F., M. Ratera, A. D. Schenk, M. Chami, E. Valencia, J. M. Lopez, D. Torrents, A. Engel, M. Palacin and D. Fotiadis (2008). "Projection structure of a member of the amino acid/polyamine/organocation transporter superfamily." J Biol Chem **283**(48): 33240-33248.
13. Castellano, B. M., A. M. Thelen, O. Moldavski, M. Feltes, R. E. van der Welle, L. Mydock-McGrane, X. Jiang, R. J. van Eijkeren, O. B. Davis, S. M. Louie, R. M. Perera, D. F. Covey, D. K. Nomura, D. S. Ory and R. Zoncu (2017). "Lysosomal cholesterol activates mTORC1 via an SLC38A9-Niemann-Pick C1 signaling complex." Science **355**(6331): 1306-1311.
14. Cesar-Razquin, A., B. Snijder, T. Frappier-Brinton, R. Isserlin, G. Gyimesi, X. Bai, R. A. Reithmeier, D. Hepworth, M. A. Hediger, A. M. Edwards and G. Superti-Furga (2015). "A Call for Systematic Research on Solute Carriers." Cell **162**(3): 478-487.
15. Chillaron, J., R. Roca, A. Valencia, A. Zorzano and M. Palacin (2001). "Heteromeric amino acid transporters: biochemistry, genetics, and physiology." Am J Physiol Renal Physiol **281**(6): F995-1018.
16. Closs, E. I., J. P. Boissel, A. Habermeier and A. Rotmann (2006). "Structure and function of cationic amino acid transporters (CATs)." J Membr Biol **213**(2): 67-77.
17. Closs, E. I., P. Graf, A. Habermeier, J. M. Cunningham and U. Forstermann (1997). "Human cationic amino acid transporters hCAT-1, hCAT-2A, and hCAT-2B: three related carriers with distinct transport properties." Biochemistry **36**(21): 6462-6468.
18. Closs, E. I., A. Simon, N. Vekony and A. Rotmann (2004). "Plasma membrane transporters for arginine." J Nutr **134**(10 Suppl): 2752S-2759S; discussion 2765S-2767S.
19. Cosco, J., T. M. R. Regina, M. Scalise, M. Galluccio and C. Indiveri (2019). "Regulatory Aspects of the Vacuolar CAT2 Arginine Transporter of S. lycopersicum: Role of Osmotic Pressure and Cations." Int J Mol Sci **20**(4).

20. Costa, M., A. Rosell, E. Alvarez-Marimon, A. Zorzano, D. Fotiadis and M. Palacin (2013). "Expression of human heteromeric amino acid transporters in the yeast Pichia pastoris." Protein Expr Purif **87**(1): 35-40.
21. D'Aquila, P., P. Crocco, F. De Rango, C. Indiveri, D. Bellizzi, G. Rose and G. Passarino (2018). "A Genetic Variant of ASCT2 Hampers In Vitro RNA Splicing and Correlates with Human Longevity." Rejuvenation Res **21**(3): 193-199.
22. Danbolt, N. C., J. Storm-Mathisen and B. I. Kanner (1992). "An [Na+ + K+]coupled L-glutamate transporter purified from rat brain is located in glial cell processes." Neuroscience **51**(2): 295-310.
23. del Amo, E. M., A. Urtti and M. Yliperttula (2008). "Pharmacokinetic role of L-type amino acid transporters LAT1 and LAT2." Eur J Pharm Sci **35**(3): 161-174.
24. Di Sansebastiano, G. P., S. Fornaciari, F. Barozzi, G. Piro and L. Arru (2014). "New insights on plant cell elongation: a role for acetylcholine." Int J Mol Sci **15**(3): 4565-4582.
25. Dickens, D., G. N. Chiduza, G. S. Wright, M. Pirmohamed, S. V. Antonyuk and S. S. Hasnain (2017). "Modulation of LAT1 (SLC7A5) transporter activity and stability by membrane cholesterol." Sci Rep **7**: 43580.
26. Duelli, R., B. E. Enerson, D. Z. Gerhart and L. R. Drewes (2000). "Expression of large amino acid transporter LAT1 in rat brain endothelium." J Cereb Blood Flow Metab **20**(11): 1557-1562.
27. Echtay, K. S., M. Bienengraeber, P. Mayinger, S. Heimpel, E. Winkler, D. Druhmann, K. Frischmuth, F. Kamp and S. G. Huang (2018). "Uncoupling proteins: Martin Klingenberg's contributions for 40years." Arch Biochem Biophys **657**: 41-55.
28. Fagerberg, L., K. Jonasson, G. von Heijne, M. Uhlen and L. Berglund (2010). "Prediction of the human membrane proteome." Proteomics **10**(6): 1141-1149.
29. Fantini, J. and F. J. Barrantes (2013). "How cholesterol interacts with membrane proteins: an exploration of cholesterol-binding sites including CRAC, CARC, and tilted domains." Front Physiol **4**: 31.
30. Fantini, J., R. M. Epand and F. J. Barrantes (2019). "Cholesterol-Recognition Motifs in Membrane Proteins." Adv Exp Med Biol **1135**: 3-25.
31. Feral, C. C., N. Nishiya, C. A. Fenczik, H. Stuhlmann, M. Slepak and M. H. Ginsberg (2005). "CD98hc (SLC3A2) mediates integrin signaling." Proc Natl Acad Sci U S A **102**(2): 355-360.
32. Fort, J., L. R. de la Ballina, H. E. Burghardt, C. Ferrer-Costa, J. Turnay, C. Ferrer-Orta, I. Uson, A. Zorzano, J. Fernandez-Recio, M. Orozco, M. A. Lizarbe, I. Fita and M. Palacin (2007). "The structure of human 4F2hc ectodomain provides a model for homodimerization and electrostatic interaction with plasma membrane." J Biol Chem **282**(43): 31444-31452.
33. Fotiadis, D., Y. Kanai and M. Palacin (2013). "The SLC3 and SLC7 families of amino acid transporters." Mol Aspects Med **34**(2-3): 139-158.
34. Fredriksson, R., K. J. Nordstrom, O. Stephansson, M. G. Hagglund and H. B. Schioth (2008). "The solute carrier (SLC) complement of the human genome: phylogenetic classification reveals four major families." FEBS Lett **582**(27): 3811-3816.
35. Frommer, W. B., S. Hummel and J. W. Riesmeier (1993). "Expression cloning in yeast of a cDNA encoding a broad specificity amino acid permease from Arabidopsis thaliana." Proc Natl Acad Sci U S A **90**(13): 5944-5948.
36. Frommer, W. B., S. Hummel, M. Unseld and O. Ninnemann (1995). "Seed and vascular expression of a high-affinity transporter for cationic amino acids in Arabidopsis." Proc Natl Acad Sci U S A **92**(26): 12036-12040.
37. Gabrisko, M. and S. Janecek (2009). "Looking for the ancestry of the heavy-chain subunits of heteromeric amino acid transporters rBAT and 4F2hc within the GH13 alpha-amylase family." FEBS J **276**(24): 7265-7278.
38. Galluccio, M., P. Pingitore, M. Scalise and C. Indiveri (2013). "Cloning, large scale over-expression in E. coli and purification of the components of the human LAT 1 (SLC7A5) amino acid transporter." Protein J **32**(6): 442-448.
39. Garaeva, A. A., G. T. Oostergetel, C. Gati, A. Guskov, C. Paulino and D. J. Slotboom (2018). "Cryo-EM structure of the human neutral amino acid transporter ASCT2." Nat Struct Mol Biol **25**(6): 515-521.

40. Giangregorio, N., A. Tonazzi, L. Console, M. Pistillo, V. Scalera and C. Indiveri (2019). "Tryptophan 224 of the rat mitochondrial carnitine/acylcarnitine carrier is crucial for the antiport mechanism." Biochim Biophys Acta Bioenerg **1860**(9): 708-716.
41. Grewer, C., P. Balani, C. Weidenfeller, T. Bartusel, Z. Tao and T. Rauen (2005). "Individual subunits of the glutamate transporter EAAC1 homotrimer function independently of each other." Biochemistry **44**(35): 11913-11923.
42. Grewer, C., A. Gameiro and T. Rauen (2014). "SLC1 glutamate transporters." Pflugers Arch **466**(1): 3-24.
43. Hammes, U. Z., E. Nielsen, L. A. Honaas, C. G. Taylor and D. P. Schachtman (2006). "AtCAT6, a sink-tissue-localized transporter for essential amino acids in Arabidopsis." Plant J **48**(3): 414-426.
44. Hebert, S. C., D. B. Mount and G. Gamba (2004). "Molecular physiology of cation-coupled Cl- cotransport: the SLC12 family." Pflugers Arch **447**(5): 580-593.
45. Hediger, M. A., B. Clemencon, R. E. Burrier and E. A. Bruford (2013). "The ABCs of membrane transporters in health and disease (SLC series): introduction." Mol Aspects Med **34**(2-3): 95-107.
46. Hsu, L. C., T. J. Chiou, L. Chen and D. R. Bush (1993). "Cloning a plant amino acid transporter by functional complementation of a yeast amino acid transport mutant." Proc Natl Acad Sci U S A **90**(16): 7441-7445.
47. Hyde, R., P. M. Taylor and H. S. Hundal (2003). "Amino acid transporters: roles in amino acid sensing and signalling in animal cells." Biochem J **373**(Pt 1): 1-18.
48. Indiveri, C., L. Palmieri and F. Palmieri (1994). "Kinetic characterization of the reconstituted ornithine carrier from rat liver mitochondria." Biochim Biophys Acta **1188**(3): 293-301.
49. Jack, D. L., I. T. Paulsen and M. H. Saier (2000). "The amino acid/polyamine/organocation (APC) superfamily of transporters specific for amino acids, polyamines and organocations." Microbiology (Reading) **146 (Pt 8)**: 1797-1814.
50. Jaquinod, M., F. Villiers, S. Kieffer-Jaquinod, V. Hugouvieux, C. Bruley, J. Garin and J. Bourguignon (2007). "A proteomics dissection of Arabidopsis thaliana vacuoles isolated from cell culture." Mol Cell Proteomics **6**(3): 394-412.
51. Jungnickel, K. E. J., J. L. Parker and S. Newstead (2018). "Structural basis for amino acid transport by the CAT family of SLC7 transporters." Nat Commun **9**(1): 550.
52. Kageyama, T., M. Nakamura, A. Matsuo, Y. Yamasaki, Y. Takakura, M. Hashida, Y. Kanai, M. Naito, T. Tsuruo, N. Minato and S. Shimohama (2000). "The 4F2hc/LAT1 complex transports L-DOPA across the blood-brain barrier." Brain Res **879**(1-2): 115-121.
53. Kanai, Y., B. Clemencon, A. Simonin, M. Leuenberger, M. Lochner, M. Weisstanner and M. A. Hediger (2013). "The SLC1 high-affinity glutamate and neutral amino acid transporter family." Mol Aspects Med **34**(2-3): 108-120.
54. Kanai, Y. and M. A. Hediger (1992). "Primary structure and functional characterization of a high-affinity glutamate transporter." Nature **360**(6403): 467-471.
55. Kanai, Y. and M. A. Hediger (2003). "The glutamate and neutral amino acid transporter family: physiological and pharmacological implications." Eur J Pharmacol **479**(1-3): 237-247.
56. Kasahara, M. and P. C. Hinkle (1976). "Reconstitution of D-glucose transport catalyzed by a protein fraction from human erythrocytes in sonicated liposomes." Proc Natl Acad Sci U S A **73**(2): 396-400.
57. Kekuda, R., P. D. Prasad, Y. J. Fei, V. Torres-Zamorano, S. Sinha, T. L. Yang-Feng, F. H. Leibach and V. Ganapathy (1996). "Cloning of the sodium-dependent, broad-scope, neutral amino acid transporter Bo from a human placental choriocarcinoma cell line." J Biol Chem **271**(31): 18657-18661.
58. Kim, J. W., E. I. Closs, L. M. Albritton and J. M. Cunningham (1991). "Transport of cationic amino acids by the mouse ecotropic retrovirus receptor." Nature **352**(6337): 725-728.
59. Larriba, S., L. Sumoy, M. D. Ramos, J. Gimenez, X. Estivill, T. Casals and V. Nunes (2001). "ATB(0)/SLC1A5 gene. Fine localisation and exclusion of association with the intestinal phenotype of cystic fibrosis." Eur J Hum Genet **9**(11): 860-866.
60. Laursen, L., K. Severinsen, K. B. Kristensen, X. Periole, M. Overby, H. K. Muller, B. Schiott and S. Sinning (2018). "Cholesterol binding to a conserved site modulates the conformation, pharmacology, and transport kinetics of the human serotonin transporter." J Biol Chem **293**(10): 3510-3523.

61. Lee, Y., P. Wiriyasermkul, C. Jin, L. Quan, R. Ohgaki, S. Okuda, T. Kusakizako, T. Nishizawa, K. Oda, R. Ishitani, T. Yokoyama, T. Nakane, M. Shirouzu, H. Endou, S. Nagamori, Y. Kanai and O. Nureki (2019). "Cryo-EM structure of the human L-type amino acid transporter 1 in complex with glycoprotein CD98hc." Nat Struct Mol Biol **26**(6): 510-517.
62. Lei, H. T., J. Ma, S. Sanchez Martinez and T. Gonen (2018). "Crystal structure of arginine-bound lysosomal transporter SLC38A9 in the cytosol-open state." Nat Struct Mol Biol **25**(6): 522-527.
63. Levine, K. B., E. K. Cloherty, S. Hamill and A. Carruthers (2002). "Molecular determinants of sugar transport regulation by ATP." Biochemistry **41**(42): 12629-12638.
64. Loudon, G. M. and D. E. Koshland, Jr. (1970). "The chemistry of a reporter group: 2-hydroxy-5-nitrobenzyl bromide." J Biol Chem **245**(9): 2247-2254.
65. Magi, S., S. Piccirillo, S. Amoroso and V. Lariccia (2019). "Excitatory Amino Acid Transporters (EAATs): Glutamate Transport and Beyond." Int J Mol Sci **20**(22).
66. Malik, A. R. and T. E. Willnow (2019). "Excitatory Amino Acid Transporters in Physiology and Disorders of the Central Nervous System." Int J Mol Sci **20**(22).
67. Mann, G. E., D. L. Yudilevich and L. Sobrevia (2003). "Regulation of amino acid and glucose transporters in endothelial and smooth muscle cells." Physiol Rev **83**(1): 183-252.
68. Manner, C. K., B. Nicholson and C. L. MacLeod (2003). "CAT2 arginine transporter deficiency significantly reduces iNOS-mediated NO production in astrocytes." J Neurochem **85**(2): 476-482.
69. Milkereit, R., A. Persaud, L. Vanoaica, A. Guetg, F. Verrey and D. Rotin (2015). "LAPTM4b recruits the LAT1-4F2hc Leu transporter to lysosomes and promotes mTORC1 activation." Nat Commun **6**: 7250.
70. Napolitano, L., M. Galluccio, M. Scalise, C. Parravicini, L. Palazzolo, I. Eberini and C. Indiveri (2017). "Novel insights into the transport mechanism of the human amino acid transporter LAT1 (SLC7A5). Probing critical residues for substrate translocation." Biochim Biophys Acta Gen Subj **1861**(4): 727-736.
71. Napolitano, L., M. Scalise, M. Galluccio, L. Pochini, L. M. Albanese and C. Indiveri (2015). "LAT1 is the transport competent unit of the LAT1/CD98 heterodimeric amino acid transporter." Int J Biochem Cell Biol **67**: 25-33.
72. Nelson D.L., C. M. M. (Fourth Edition). Lehninger Principles of Biochemistry.
73. Newman, M. J., D. L. Foster, T. H. Wilson and H. R. Kaback (1981). "Purification and reconstitution of functional lactose carrier from Escherichia coli." J Biol Chem **256**(22): 11804-11808.
74. Nicholson, B., C. K. Manner, J. Kleeman and C. L. MacLeod (2001). "Sustained nitric oxide production in macrophages requires the arginine transporter CAT2." J Biol Chem **276**(19): 15881-15885.
75. Nicholson, B., C. K. Manner and C. L. MacLeod (2002). "Cat2 L-arginine transporter-deficient fibroblasts can sustain nitric oxide production." Nitric Oxide **7**(4): 236-243.
76. O'Donovan, S. M., C. R. Sullivan and R. E. McCullumsmith (2017). "The role of glutamate transporters in the pathophysiology of neuropsychiatric disorders." NPJ Schizophr **3**(1): 32.
77. Ohgaki, R., T. Ohmori, S. Hara, S. Nakagomi, M. Kanai-Azuma, K. Kaneda-Nakashima, S. Okuda, S. Nagamori and Y. Kanai (2017). "Essential Roles of L-Type Amino Acid Transporter 1 in Syncytiotrophoblast Development by Presenting Fusogenic 4F2hc." Mol Cell Biol **37**(11).
78. Ohgimoto, S., N. Tabata, S. Suga, M. Nishio, H. Ohta, M. Tsurudome, H. Komada, M. Kawano, N. Watanabe and Y. Ito (1995). "Molecular characterization of fusion regulatory protein-1 (FRP-1) that induces multinucleated giant cell formation of monocytes and HIV gp160-mediated cell fusion. FRP-1 and 4F2/CD98 are identical molecules." J Immunol **155**(7): 3585-3592.
79. Oppedisano, F., L. Pochini, M. Galluccio, M. Cavarelli and C. Indiveri (2004). "Reconstitution into liposomes of the glutamine/amino acid transporter from renal cell plasma membrane: functional characterization, kinetics and activation by nucleotides." Biochim Biophys Acta **1667**(2): 122-131.
80. Oppedisano, F., L. Pochini, M. Galluccio and C. Indiveri (2007). "The glutamine/amino acid transporter (ASCT2) reconstituted in liposomes: transport mechanism, regulation by ATP and characterization of the glutamine/glutamate antiport." Biochim Biophys Acta **1768**(2): 291-298.
81. Palacin, M. and Y. Kanai (2004). "The ancillary proteins of HATs: SLC3 family of amino acid transporters." Pflugers Arch **447**(5): 490-494.
82. Penmatsa, A., K. H. Wang and E. Gouaux (2013). "X-ray structure of dopamine transporter elucidates antidepressant mechanism." Nature **503**(7474): 85-90.

83. Perkins, C. P., V. Mar, J. R. Shutter, J. del Castillo, D. M. Danilenko, E. S. Medlock, I. L. Ponting, M. Graham, K. L. Stark, Y. Zuo, J. M. Cunningham and R. A. Bosselman (1997). "Anemia and perinatal death result from loss of the murine ecotropic retrovirus receptor mCAT-1." Genes Dev **11**(7): 914-925.
84. Pines, G., N. C. Danbolt, M. Bjoras, Y. Zhang, A. Bendahan, L. Eide, H. Koepsell, J. Storm-Mathisen, E. Seeberg and B. I. Kanner (1992). "Cloning and expression of a rat brain L-glutamate transporter." Nature **360**(6403): 464-467.
85. Pochini, L., G. Pappacoda, M. Galluccio, F. Pastore, M. Scalise and C. Indiveri (2020). "Effect of Cholesterol on the Organic Cation Transporter OCTN1 (SLC22A4)." Int J Mol Sci **21**(3).
86. Pochini, L., M. Scalise, M. Galluccio, G. Pani, K. A. Siminovitch and C. Indiveri (2012). "The human OCTN1 (SLC22A4) reconstituted in liposomes catalyzes acetylcholine transport which is defective in the mutant L503F associated to the Crohn's disease." Biochim Biophys Acta **1818**(3): 559-565.
87. Pochini, L., M. Scalise and C. Indiveri (2015). "Immuno-detection of OCTN1 (SLC22A4) in HeLa cells and characterization of transport function." Int Immunopharmacol **29**(1): 21-26.
88. Poffenberger, M. C. and R. G. Jones (2014). "Amino acids fuel T cell-mediated inflammation." Immunity **40**(5): 635-637.
89. Pramod, A. B., J. Foster, L. Carvelli and L. K. Henry (2013). "SLC6 transporters: structure, function, regulation, disease association and therapeutics." Mol Aspects Med **34**(2-3): 197-219.
90. Prasad, P. D., H. Wang, W. Huang, R. Kekuda, D. P. Rajan, F. H. Leibach and V. Ganapathy (1999). "Human LAT1, a subunit of system L amino acid transporter: molecular cloning and transport function." Biochem Biophys Res Commun **255**(2): 283-288.
91. Rebsamen, M., L. Pochini, T. Stasyk, M. E. de Araujo, M. Galluccio, R. K. Kandasamy, B. Snijder, A. Fauster, E. L. Rudashevskaya, M. Bruckner, S. Scorzoni, P. A. Filipek, K. V. Huber, J. W. Bigenzahn, L. X. Heinz, C. Kraft, K. L. Bennett, C. Indiveri, L. A. Huber and G. Superti-Furga (2015). "SLC38A9 is a component of the lysosomal amino acid sensing machinery that controls mTORC1." Nature **519**(7544): 477-481.
92. Regina, T. M. R., M. Galluccio, M. Scalise, L. Pochini and C. Indiveri (2017). "Bacterial production and reconstitution in proteoliposomes of Solanum lycopersicum CAT2: a transporter of basic amino acids and organic cations." Plant Mol Biol **94**(6): 657-667.
93. Saier, M. H., Jr. (2000). "A functional-phylogenetic classification system for transmembrane solute transporters." Microbiol Mol Biol Rev **64**(2): 354-411.
94. San Martin, R. and L. Sobrevia (2006). "Gestational diabetes and the adenosine/L-arginine/nitric oxide (ALANO) pathway in human umbilical vein endothelium." Placenta **27**(1): 1-10.
95. Savas, B., P. E. Kerr and H. F. Pross (2006). "Lymphokine-activated killer cell susceptibility and adhesion molecule expression of multidrug resistant breast carcinoma." Cancer Cell Int **6**: 24.
96. Scalise, M., M. Galluccio, L. Pochini, J. Cosco, M. Trotta, M. Rebsamen, G. Superti-Furga and C. Indiveri (2019). "Insights into the transport side of the human SLC38A9 transceptor." Biochim Biophys Acta Biomembr **1861**(9): 1558-1567.
97. Scalise, M., L. Pochini, L. Console, M. A. Losso and C. Indiveri (2018). "The Human SLC1A5 (ASCT2) Amino Acid Transporter: From Function to Structure and Role in Cell Biology." Front Cell Dev Biol **6**: 96.
98. Scalise, M., L. Pochini, L. Console, G. Pappacoda, P. Pingitore, K. Hedfalk and C. Indiveri (2018). "Cys Site-Directed Mutagenesis of the Human SLC1A5 (ASCT2) Transporter: Structure/Function Relationships and Crucial Role of Cys467 for Redox Sensing and Glutamine Transport." Int J Mol Sci **19**(3).
99. Scalise, M., L. Pochini, M. Galluccio, L. Console and C. Indiveri (2017). "Glutamine Transport and Mitochondrial Metabolism in Cancer Cell Growth." Front Oncol **7**: 306.
100. Scalise, M., L. Pochini, N. Giangregorio, A. Tonazzi and C. Indiveri (2013). "Proteoliposomes as tool for assaying membrane transporter functions and interactions with xenobiotics." Pharmaceutics **5**(3): 472-497.
101. Scalise, M., L. Pochini, S. Panni, P. Pingitore, K. Hedfalk and C. Indiveri (2014). "Transport mechanism and regulatory properties of the human amino acid transporter ASCT2 (SLC1A5)." Amino Acids **46**(11): 2463-2475.

102. Schlessinger, A., S. W. Yee, A. Sali and K. M. Giacomini (2013). "SLC classification: an update." Clin Pharmacol Ther **94**(1): 19-23.
103. Sille, F. C., R. Thomas, M. T. Smith, L. Conde and C. F. Skibola (2012). "Post-GWAS functional characterization of susceptibility variants for chronic lymphocytic leukemia." PLoS One **7**(1): e29632.
104. Storck, T., S. Schulte, K. Hofmann and W. Stoffel (1992). "Structure, expression, and functional analysis of a Na(+)-dependent glutamate/aspartate transporter from rat brain." Proc Natl Acad Sci U S A **89**(22): 10955-10959.
105. Su, Y. H., W. B. Frommer and U. Ludewig (2004). "Molecular and functional characterization of a family of amino acid transporters from Arabidopsis." Plant Physiol **136**(2): 3104-3113.
106. Takesono, A., J. Moger, S. Farooq, E. Cartwright, I. B. Dawid, S. W. Wilson and T. Kudoh (2012). "Solute carrier family 3 member 2 (Slc3a2) controls yolk syncytial layer (YSL) formation by regulating microtubule networks in the zebrafish embryo." Proc Natl Acad Sci U S A **109**(9): 3371-3376.
107. Tarlungeanu, D. C., E. Deliu, C. P. Dotter, M. Kara, P. C. Janiesch, M. Scalise, M. Galluccio, M. Tesulov, E. Morelli, F. M. Sonmez, K. Bilguvar, R. Ohgaki, Y. Kanai, A. Johansen, S. Esharif, T. Ben-Omran, M. Topcu, A. Schlessinger, C. Indiveri, K. E. Duncan, A. O. Caglayan, M. Gunel, J. G. Gleeson and G. Novarino (2016). "Impaired Amino Acid Transport at the Blood Brain Barrier Is a Cause of Autism Spectrum Disorder." Cell **167**(6): 1481-1494 e1418.
108. Tegeder, M. (2012). "Transporters for amino acids in plant cells: some functions and many unknowns." Curr Opin Plant Biol **15**(3): 315-321.
109. Torres-Zamorano, V., F. H. Leibach and V. Ganapathy (1998). "Sodium-dependent homo- and hetero-exchange of neutral amino acids mediated by the amino acid transporter ATB degree." Biochem Biophys Res Commun **245**(3): 824-829.
110. Utsunomiya-Tate, N., H. Endou and Y. Kanai (1996). "Cloning and functional characterization of a system ASC-like Na+-dependent neutral amino acid transporter." J Biol Chem **271**(25): 14883-14890.
111. Verrey, F., E. I. Closs, C. A. Wagner, M. Palacin, H. Endou and Y. Kanai (2004). "CATs and HATs: the SLC7 family of amino acid transporters." Pflugers Arch **447**(5): 532-542.
112. Verrey, F., D. L. Jack, I. T. Paulsen, M. H. Saier, Jr. and R. Pfeiffer (1999). "New glycoprotein-associated amino acid transporters." J Membr Biol **172**(3): 181-192.
113. Wang, S., Z. Y. Tsun, R. L. Wolfson, K. Shen, G. A. Wyant, M. E. Plovanich, E. D. Yuan, T. D. Jones, L. Chantranupong, W. Comb, T. Wang, L. Bar-Peled, R. Zoncu, C. Straub, C. Kim, J. Park, B. L. Sabatini and D. M. Sabatini (2015). "Metabolism. Lysosomal amino acid transporter SLC38A9 signals arginine sufficiency to mTORC1." Science **347**(6218): 188-194.
114. Wipf, D., U. Ludewig, M. Tegeder, D. Rentsch, W. Koch and W. B. Frommer (2002). "Conservation of amino acid transporters in fungi, plants and animals." Trends Biochem Sci **27**(3): 139-147.
115. Wolf, S., A. Janzen, N. Vekony, U. Martine, D. Strand and E. I. Closs (2002). "Expression of solute carrier 7A4 (SLC7A4) in the plasma membrane is not sufficient to mediate amino acid transport activity." Biochem J **364**(Pt 3): 767-775.
116. Yan, R., Y. Li, Y. Shi, J. Zhou, J. Lei, J. Huang and Q. Zhou (2020). "Cryo-EM structure of the human heteromeric amino acid transporter b(0,+)AT-rBAT." Sci Adv **6**(16): eaay6379.
117. Yan, R., X. Zhao, J. Lei and Q. Zhou (2019). "Structure of the human LAT1-4F2hc heteromeric amino acid transporter complex." Nature **568**(7750): 127-130.
118. Yang, H., M. Krebs, Y. D. Stierhof and U. Ludewig (2014). "Characterization of the putative amino acid transporter genes AtCAT2, 3 &4: the tonoplast localized AtCAT2 regulates soluble leaf amino acids." J Plant Physiol **171**(8): 594-601.
119. Yao, X., J. Nie, R. Bai and X. Sui (2020). "Amino Acid Transporters in Plants: Identification and Function." Plants (Basel) **9**(8).
120. Yoo, H. C., S. J. Park, M. Nam, J. Kang, K. Kim, J. H. Yeo, J. K. Kim, Y. Heo, H. S. Lee, M. Y. Lee, C. W. Lee, J. S. Kang, Y. H. Kim, J. Lee, J. Choi, G. S. Hwang, S. Bang and J. M. Han (2020). "A Variant of SLC1A5 Is a Mitochondrial Glutamine Transporter for Metabolic Reprogramming in Cancer Cells." Cell Metab **31**(2): 267-283 e212.

121. Yu, X., O. Plotnikova, P. D. Bonin, T. A. Subashi, T. J. McLellan, D. Dumlao, Y. Che, Y. Y. Dong, E. P. Carpenter, G. M. West, X. Qiu, J. S. Culp and S. Han (2019). "Cryo-EM structures of the human glutamine transporter SLC1A5 (ASCT2) in the outward-facing conformation." Elife **8**.
122. Zerangue, N. and M. P. Kavanaugh (1996). "ASCT-1 is a neutral amino acid exchanger with chloride channel activity." J Biol Chem **271**(45): 27991-27994.
123. Zhang, Y., Y. Zhang, K. Sun, Z. Meng and L. Chen (2019). "The SLC transporter in nutrient and metabolic sensing, regulation, and drug development." J Mol Cell Biol **11**(1): 1-13.

Publications

International Journal of
Molecular Sciences

MDPI

Article

Regulatory Aspects of the Vacuolar CAT2 Arginine Transporter of *S. lycopersicum*: Role of Osmotic Pressure and Cations

Jessica Cosco [1], Teresa M. R. Regina [1], Mariafrancesca Scalise [1], Michele Galluccio [1] and Cesare Indiveri [1,2,*]

[1] Department DiBEST (Biologia, Ecologia, Scienze della Terra), Unit of Biochemistry and Molecular Biotechnology, University of Calabria, Via P. Bucci 4C, 87036 Arcavacata di Rende, Italy; jessica.cosco@unical.it (J.C.); teresa.regina@unical.it (T.M.R.R.); mariafrancesca.scalise@unical.it (M.S.); michele.galluccio@unical.it (M.G.)

[2] CNR Institute of Biomembranes, Bioenergetics and Molecular Biotechnology, via Amendola 165/A, 70126 Bari, Italy

* Correspondence: cesare.indiveri@unical.it; Tel.: +39-0984-492939

Received: 19 December 2018; Accepted: 15 February 2019; Published: 19 February 2019

Abstract: Many proteins are localized at the vacuolar membrane, but most of them are still poorly described, due to the inaccessibility of this membrane from the extracellular environment. This work focused on the characterization of the CAT2 transporter from *S. lycopersicum* (*Sl*CAT2) that was previously overexpressed in *E. coli* and reconstituted in proteoliposomes for transport assay as [^{3}H]Arg uptake. The orientation of the reconstituted transporter has been attempted and current data support the hypothesis that the protein is inserted in the liposome in the same orientation as in the vacuole. *Sl*CAT2 activity was dependent on the pH, with an optimum at pH 7.5. *Sl*CAT2 transport activity was stimulated by the increase of internal osmolality from 0 to 175 mOsmol while the activity was inhibited by the increase of external osmolality. K^+, Na^+, and Mg^{2+} present on the external side of proteoliposomes at physiological concentrations, inhibited the transport activity; differently, the cations had no effect when included in the internal proteoliposome compartment. This data highlighted an asymmetric regulation of *Sl*CAT2. Cholesteryl hemisuccinate, included in the proteoliposomal membrane, stimulated the *Sl*CAT2 transport activity. The homology model of the protein was built using, as a template, the 3D structure of the amino acid transporter *Gk*ApcT. Putative substrate binding residues and cholesterol binding domains were proposed. Altogether, the described results open new perspectives for studying the response of *Sl*CAT2 and, in general, of plant vacuolar transporters to metabolic and environmental changes.

Keywords: cholesterol; arginine; osmolyte; vacuole; transport; protein expression; CRAC

1. Introduction

The vacuole is the largest organelle in plant cells and it plays several roles. Originally, this organelle was considered mainly responsible for cell turgor; then, it became clear that the vacuole is involved in protein digestions, storage of water, ions, and metabolites as well as toxic compounds [1,2]. Recently, the vacuole received more attention because is involved in plant metabolism, pH homeostasis, stress responses, cell growth and development [2–4], and signal transduction [3,5]. In this frame, many proteins are expected to accomplish these functions [1,3]. In fact, the vacuolar membrane hosts different transporters with specificity towards several classes of molecules. Traffic of amino acids across the vacuolar membrane is crucial for plant cell homeostasis [1,2,6]. However, the characterization of transporters in the vacuolar membrane is not straightforward due to the inaccessibility of

these transporters from the extracellular environment. To overcome this problem, the vacuolar transporter CAT2 from *S. lycopersicum* (*Sl*CAT2) has been recently characterized in the in vitro system of proteoliposomes obtained by reconstituting the recombinant protein over-expressed in *E. coli* [7].

In this experimental model, it was revealed that *Sl*CAT2 is involved in the transport of the cationic amino acids arginine and lysine and of the nonproteogenic amino acid ornithine. The transport is regulated by ATP, which probably binds to an N-terminus domain of the protein [7]. Besides the mentioned amino acids, acetylcholine is also a substrate of *Sl*CAT2. Interestingly, this function might be related to the non-neuronal cholinergic system present also in plants and involved in the regulation of cell elongation, water homeostasis, and photosynthesis [8]. In-line with this, *Sl*CAT2 belongs to the APC family (amino acid polyamine choline) which includes transporters conserved in all living organisms, i.e., from bacteria to humans [9–11].

Despite the importance of membrane transporters for vacuolar homeostasis, the studies of regulatory aspects of these proteins are still at their infancy. One of the factors involved in maintaining the vacuolar homeostasis is the concentration of some cations [12]. In this frame, the V-ATPase, the V-PPase, the aquaporin channel, and the ion exchangers are the most known membrane components, which regulate the intravacuolar concentrations of cations including H^+. The V-ATPase accumulates H^+ inside the vacuolar lumen upon cytosolic ATP hydrolysis with a complex molecular mechanism resembling that of F-type ATPase of mitochondria and chloroplasts [13–16]. The V-PPase is also involved in H^+ uptake into the vacuole but uses the energy deriving from PPi hydrolysis in the cytosol [13,14,17,18]. The constant activity of these proteins allows the maintenance of a ΔpH, that can reach two to three units, and a $\Delta\Psi$ of 30 mV positive inside [13,14]. The aquaporins, referred to as TIPs (tonoplast intrinsic proteins), are responsible for the traffic of water and other small molecules in vacuole to balance the osmotic pressure and to respond to salt stress [14,19,20]. Na^+ is the main player in salt stress regulation; its concentration in cytosol normally ranges from 20 to 50 mM. Under conditions of high salinity, the vacuolar concentration of Na^+ can exceed 10 times the cytosolic one [21,22]. K^+ represents one of the most important nutrients for cell growth and development being the cofactor of several enzymes [1,21,23,24]. It is also involved in turgor-driven processes such as stomatal movements and cell growth by distention [13,25]. For these reasons, the vacuolar concentration of K^+ can vary from 20 to 200 mM, while the cytosolic concentration is kept quite constant, roughly 100 mM [22,26].

Nitrogen is a limiting factor for plant growth and development [13]. The major source of nitrogen is represented by ammonia (NH_4^+/NH_3) and urea. The equilibrium between NH_4^+ and NH_3 depends on the cytosolic pH. Since the vacuolar pH is more acidic than the cytosolic one, NH_4^+ is the prevailing vacuolar form and its concentration in vacuole is 100-fold higher than in cytosol [13].

Among divalent cations, Mg^{2+} and Ca^{2+} are the most abundant in plant cells. Mg^{2+} is involved in several processes such as conformational stabilization of macromolecules, chlorophyll synthesis, enzyme activation, and osmotic regulation together with K^+. In-line with these regulatory features, a high level of Mg^{2+} or its deficit in the soil could be destructive for plant life [27]. Therefore, vacuoles play an essential role also in the Mg^{2+} homeostasis, being able to accumulate Mg^{2+} up 80 mM [28], while in the cytosol the Mg^{2+} concentration is approximately 0.2–0.4 mM [1].

As in animal cells, Ca^{2+} plays the role of second messenger in plants and is responsible for the activation of several signaling pathways. As an example, Ca^{2+} is involved in stomatal movements: stomatal closure is linked to abscisic acid stimulation caused by the opening of vacuolar Ca^{2+} channels with the consequent increase in cytosolic Ca^{2+} concentration [29]. Ca^{2+} is also important to neutralize vacuolar anions to strengthen cell walls for responding to stress [30].

The cytosolic Ca^{2+} concentration is ~200 nM, while the vacuolar concentration is three orders of magnitude higher. Therefore, an energy-dependent process is required to accumulate Ca^{2+} within the vacuole. Indeed, a primary energized Ca^{2+}-ATPase and a secondary energized Ca^{2+} exchanger mediate the process [13,29,31].

From the depicted scenario, it is evident that the described ion distribution may play some role in the regulation of transporters working in the vacuolar membrane [32].

Therefore, the present study sought to define some regulatory properties of *Sl*CAT2, among which the response to cations. In order to correlate the role of this protein to tomato physiology, the experiments have been performed taking into consideration the physiological composition of intra- and extraluminal milieu. Indeed, tomato crop is very relevant for both nutrition and biotechnology purposes and, therefore, the knowledge of tomato biology is an up-to-date field of investigation.

2. Results

2.1. Orientation of the SlCAT2 Reconstituted in Proteoliposomes

To assess the orientation of the *Sl*CAT2 transporter in the proteoliposomal membrane, a method based on side-specific targeting was employed [33]. In particular, an antibody against the 6His-tag has been used exploiting the location of the 6His-tag at the C-terminus of the recombinant protein. The interaction between the antibody and the 6-His tag of the protein should create a steric hindrance impairing the transport activity, as previously observed in the case of other transporters [33,34]. After the reconstitution procedure, the C-terminus portion of the protein may be exposed towards the internal or the external side of the proteoliposomes. To discriminate between the two possibilities, *Sl*CAT2 was incubated with the anti-His antibody before or after the insertion into the proteoliposomal membrane. In the first case, the antibody can reach both sides (internal or external) of the recombinant protein. In the second case, the antibody can bind only to the protein side exposed towards the extraliposomal compartment. After incubating the anti-His in the two different conditions, the transport activity has been measured as [^{3}H]Arg uptake in proteoliposomes [7]. Transport inhibition was observed upon incubation of the antibody with the protein before the insertion in the membrane, while no significant effect could be observed upon addition of the antibody to the external side (Figure 1A). The addition of anti-His antibody to the external side of proteoliposomes prepared with protein pretreated with anti-His antibody did not further increase the inhibitory effect (Figure 1A). In parallel samples, an anti-actin antibody was added to the protein before reconstitution, as control; in this case, no effect was observed indicating that, indeed, the inhibition was specifically due to the targeting of the 6His-tag sequence located at the C-terminus of the recombinant *Sl*CAT2. The same experiment was performed using liposomes, i.e., without reconstituted protein, and no effect by addition of any antibody was measured (light gray bar in Figure 1A). It has to be stressed that the [^{3}H]Arg accumulated in the control liposomes (with no reconstituted protein) was always less than 30% with respect to that taken up by proteoliposomes. This data clearly indicates that the 6His-tag is exposed towards the internal side of the protein inserted in the proteoliposomal membrane. The actual presence of *Sl*CAT2 in the membrane was tested by separating proteoliposomes deriving from experiment in Figure 1A by size exclusion chromatography and applying the samples on SDS-PAGE and WB analysis after extraction by detergent (Figure 1B). As shown by the figure, the reconstituted protein was ~30% with respect to the protein added to the reconstitution mixture in all the analyzed conditions.

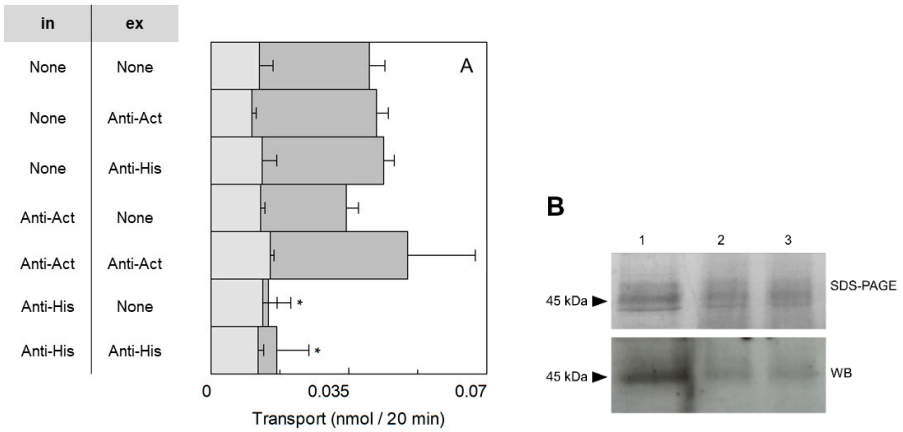

Figure 1. Sidedness of the reconstituted *Solanum lycopersicum* CAT2 (*Sl*CAT2) in proteoliposomes. (**A**) *Sl*CAT2 was purified and reconstituted in proteoliposomes as described in Section 4.4. The purified protein was preincubated or not, for 30 min under rotatory shaker at room temperature, with 6 µg of anti-His or anti-Actin antibody, as indicated in the table (in; intraliposomal compartment). Transport was measured in 20 min, as described in Section 4.5, by adding 100 µM [^{3}H]Arg to proteoliposomes containing 200 mM sucrose and 15 mM ATP at pH 7.5. In the external compartment, 0.6 µg of anti-His or anti-Actin were added or not, as indicated in the table (ex; extraliposomal compartment). The transport in proteoliposomes (dark gray bars) and in liposomes (light gray bars) is measured as nmol of radioactive substrate taken up in 20 min. Results are the means ± SD from three experiments. (*), significantly different from the control (none) for $p < 0.05$ as calculated from 1-way ANOVA test. (**B**) Sodium dodecyl sulfate polyacrylamide gel electrophoresis (SDS-PAGE) of 0.15 µg purified *Sl*CAT2 (lane 1) and the corresponding protein volume of *Sl*CAT2 reconstituted in proteoliposomes not preincubated with antibody (lane 2), after preincubation with anti-His antibody (lane 3). Proteoliposomes were purified by size-exclusion chromatography as described in Section 4.5 prior to SDS-PAGE run.

2.2. Regulation of the SlCAT2 Transport Activity by pH and Osmolality

The activities of the plant transporters *At*CAT1, *At*CAT5, and *At*CAT6 which share 26.8%, 25%, and 26.3% of identity with *Sl*CAT2, respectively, are dependent on pH [9]. Therefore, the transport activity of *Sl*CAT2 was evaluated at a pH ranging from pH 5.0 to pH 8.5. As shown in Figure 2A, the pH dependence of the [^{3}H]Arg uptake showed a bell-shaped behavior with an optimum at pH 7.5. The effect of a pH gradient artificially created at the two sides of the proteoliposomes was also tested. A small but significant increase of transport activity was found in the presence of a pH gradient acidic inside ($pH\ 5.5_{in}/pH7.5_{out}$) with respect to the condition of equal internal and external pH 7.5 (Figure 2B).

To evaluate also the possible influence of osmolality on the activity of *Sl*CAT2, sucrose was used as an osmolyte. The effect was studied by changing the concentration of sucrose in the intraliposomal compartment (Figure 3A). In this condition, the [^{3}H]Arg uptake increased approximately three times when the intraliposomal osmolality was in the range of 50 to 175 mOsmol, reaching a plateau up to 225 mOsmol. To evaluate the side-specificity of such a regulation, the same experiment was also conducted as dependence on the external osmolality (Figure 3B). Differently from the internal hyperosmolality, the increase in external osmolality caused a reduction of [^{3}H]Arg uptake to about 45% of the control at 50 mM sucrose, i.e., 0.51 ± 0.18 with respect to the control 0.93 ± 0.2 nmol/(mg × min); this reduction did not change by further increasing the external osmolality.

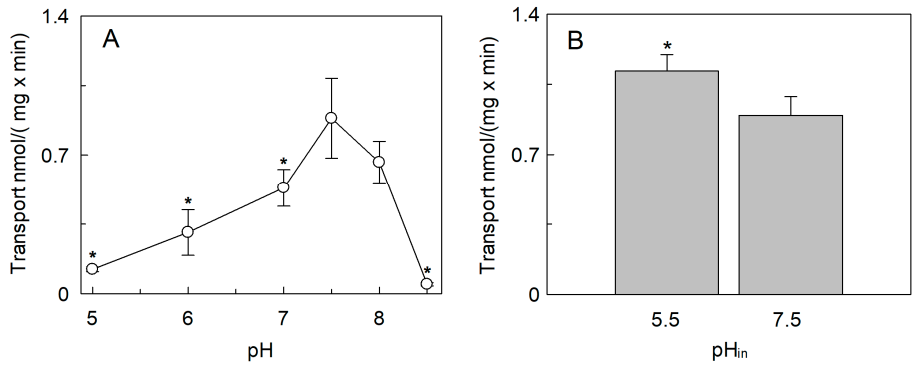

Figure 2. Effect of pH on the transport activity of SlCAT2 in proteoliposomes. *Sl*CAT2 was purified and reconstituted in proteoliposomes as described in Section 4.4. (**A**) Transport rate (nmol/(mg × min)) was measured in 10 min, as described in Section 4.5, by adding 100 μM [^{3}H]Arg to proteoliposomes containing 200 mM sucrose and 15 mM ATP. The pH was kept equal in both the internal and external site of proteoliposomes. (**B**) To generate the pH gradient, transport was measured in 10 min, as described in Section 4.5, by adding 100 μM [^{3}H]Arg (pH 7.5) to proteoliposomes prepared using the buffer at pH 7.5 or pH 5.5, as indicated (pH_{in}) and containing 200 mM sucrose and 15 mM ATP. Results are the means ± SD from three experiments. (*), Significantly different, from the control at pH_{in} 7.5, for $p < 0.05$ as calculated from the Student's *t*-test analysis.

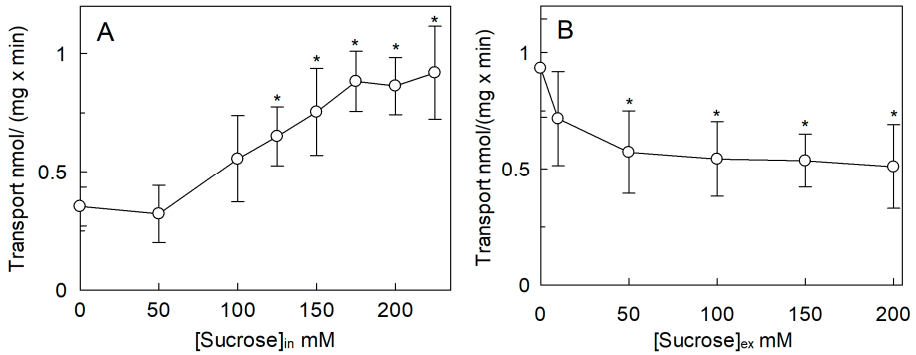

Figure 3. Effect of osmotic pressure on the transport activity of *Sl*CAT2 in proteoliposomes. *Sl*CAT2 was purified and reconstituted in proteoliposomes as described in Section 4.4. (**A**) Transport rate (nmol/(mg × min)) was measured in 10 min, as described in Section 4.5, by adding 100 μM [^{3}H]Arg to proteoliposomes containing indicated concentrations of sucrose and 15 mM ATP, at pH 7.5. (**B**) Transport rate was measured in 10 min, as described in Section 4.5, by adding 100 μM [^{3}H]Arg together with indicated concentrations of sucrose to proteoliposomes containing 200 mM sucrose and 15 mM ATP, at pH 7.5. Results are the means ± SD from three experiments. (*), Significantly different from the control (without sucrose in both (**A**) and (**B**)) for $p < 0.05$ as calculated from Student's *t*-test analysis.

2.3. Effect of Cations on the SlCAT2 Transport Activity

The [^{3}H]Arg uptake was measured in the presence of KCl, NaCl, NH_4Cl, $CaCl_2$, or $MgCl_2$ added to the external proteoliposome compartment (Figure 4). The cation concentrations were kept close to their physiological concentrations in cytosol [21,22,24,26,28,29]. The [^{3}H]Arg uptake was inhibited by external KCl. The effect of KCl was compared to that of K-gluconate to discriminate the possible influence by Cl^- from that of K^+; no difference between the two K^+ salts was observed indicating that the inhibition was specifically due to K^+. Na^+ and NH_4^+ caused an inhibition similar to that of K^+, i.e., ~40% with respect to 40 mM sucrose used as the control of osmolality. Notably, sucrose per se, when used at 40 mM, caused a reduction of transport activity with respect to the condition without sucrose, in-line with the results of Figure 3B. Among divalent cations, Mg^{2+} exerted an inhibition of 33%, while Ca^{2+} did not exert a significant effect with respect to sucrose used as control of osmolality. It has to be stressed that no difference of activity was observed in the presence of 1.2 mM sucrose

with respect to control without sucrose (see Figure 3B). Dose–response analyses were performed for those cations, which exerted a stronger inhibition on the extraliposomal (cytosolic) side of the protein (Figure 5). From these experiments an IC_{50} value of 10.9 ± 0.8 mM, 11.3 ± 1.2 mM, 5.7 ± 1.49 mM, or 0.42 ± 0.18 mM was derived for Na^+ (Figure 5A), K^+ (Figure 5B), NH_4^+ (Figure 5C), or Mg^{2+} (Figure 5D), respectively.

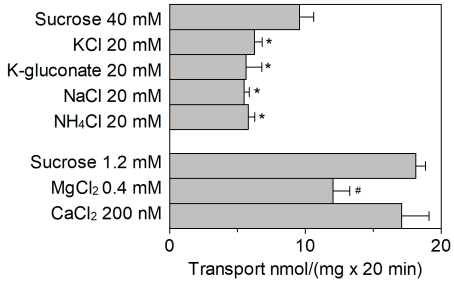

Figure 4. Effect of extraliposomal cations on the transport activity of *Sl*CAT2. *Sl*CAT2 was purified and reconstituted in proteoliposomes as described in Section 4.4. Transport was measured in 20 min, as described in Section 4.5, by adding 100 μM [^{3}H]Arg together with the indicated compounds to proteoliposomes containing 200 mM sucrose and 15 mM ATP, at pH 7.5. Concentrations were chosen according to the average concentrations of cations in the cytosol. Results are the means ± SD from four experiments. (*), significantly different from the control (sucrose 40 mM) for $p < 0.05$ as calculated from 1Way ANOVA test. (#), significantly different from the control (sucrose 1.2 mM) for $p < 0.05$ as calculated from 1-way ANOVA test.

The sidedness of *Sl*CAT2 transport was further investigated by testing the effect of ATP on the extraliposomal side (Figure 6). Differently from the internal side, ATP inhibited *Sl*CAT2-mediated [^{3}H]Arg uptake when used at concentrations within the same range of those activating the transport from the intraliposomal compartment [7], indicating that the activation by ATP is side-specific. However, the effect of ATP, used as $(Na^+)_2$ salt, is partially due to the inhibition by Na^+ (Figure 5A) and osmolality (Figure 3B). Since the cytosolic concentration of free-ATP is in the micromolar range [35] the observed inhibition might not be physiologically relevant.

The effect of cations in the internal compartment was also evaluated (Figure 7). In this case, activation of the transporter by both K^+ and Na^+ was observed, with respect to the condition without osmolytes. The extent of activation, however, corresponded to that of the isoosmolar concentration of sucrose (Figure 7), indicating that the activation was due to an osmotic effect (see also Figure 3A). Ca^{2+} and NH_4^+ did not exert any significant effect as in the case of K^+ and Na^+. On the contrary, Mg^{2+} had a strong inhibitory effect. Therefore, a dose–response analysis of the Mg^{2+} inhibition from the internal side was performed (Figure 8A) and an IC_{50} value of 23.0 ± 9.9 mM was derived, which is two orders of magnitude higher than that measured on the external side (Figure 5D). As previously described, *Sl*CAT2 activity is stimulated by intraliposomal ATP [7], that is present inside the proteoliposomes in all the experiments. Therefore, the effect of Mg^{2+} could be due to the known interaction with ATP. In order to dissect the effect of the sole Mg^{2+}, transport was also assayed in the absence of internal ATP (Figure 8B). The inhibition of *Sl*CAT2 by Mg^{2+} virtually disappeared when ATP was omitted, confirming the above mentioned hypothesis (Figure 8B). This result definitively demonstrated that Mg^{2+}, as the other cations, does not exert any direct effect on *Sl*CAT2 from the internal (luminal) side. For the sake of clarity, it has to be stressed that in absence of ATP, the transport activity of *Sl*CAT2 is much lower than that measured in the presence of ATP, explaining the higher scattering observed in the transport measurements (Figure 8B) across different experiments. *Sl*CAT2 catalyzes arginine efflux as well [7]. Then, the effect of Mg^{2+} on the external side was also tested on the [^{3}H]Arg efflux measured from preloaded proteoliposomes in the presence or absence of external Mg^{2+}. Interestingly, the presence of the cation in the external compartment had no, or only a slight, effect on the [^{3}H]Arg efflux (Figure 9).

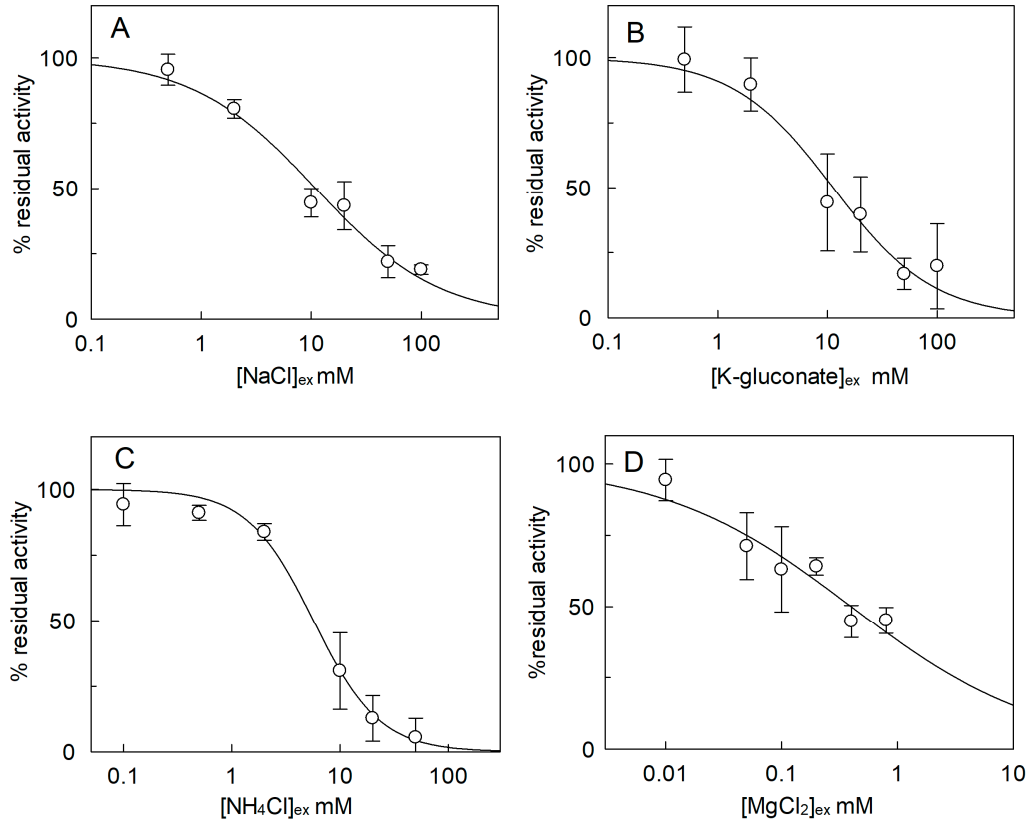

Figure 5. Dose–response curve for the inhibition of *Sl*CAT2 by external cations. *Sl*CAT2 was purified and reconstituted in proteoliposomes as described in Section 4.4. Transport was measured in 20 min, as described in Section 4.5, by adding 100 μM [^{3}H]Arg together with the indicated concentrations of NaCl (**A**), K-gluconate (**B**), NH_4Cl (**C**), or $MgCl_2$ (**D**) to proteoliposomes containing 200 mM sucrose and 15 mM ATP, at pH 7.5. Transport activity was calculated as the percent of residual activity with respect to condition without any addition (in absence of indicated compounds). Results are the means ± SD from three experiments.

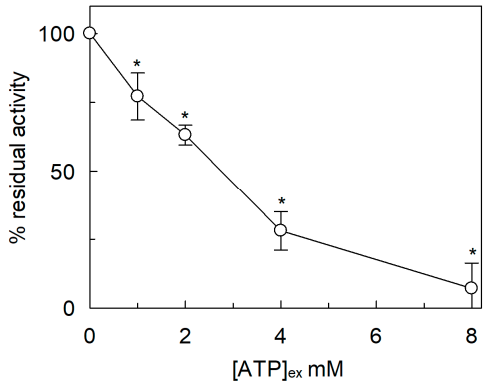

Figure 6. Effect of ATP(Na^+)$_2$ salt on the transport activity of *Sl*CAT2 in proteoliposomes. *Sl*CAT2 was purified and reconstituted in proteoliposomes as described in Section 4.4. Transport was measured in 20 min, as described in Section 4.5, by adding 100 μM [^{3}H]Arg together with the indicated concentrations of ATP to proteoliposomes containing 200 mM sucrose and 15 mM ATP, at pH 7.5. Transport activity was calculated as the percent of residual activity with respect to condition without any addition (in absence of external ATP). Results are the means ± SD from three experiments. (*), Significantly different, from the control (without ATP in the extraliposomal compartment) for $p < 0.05$ as calculated from Student's *t*-test analysis.

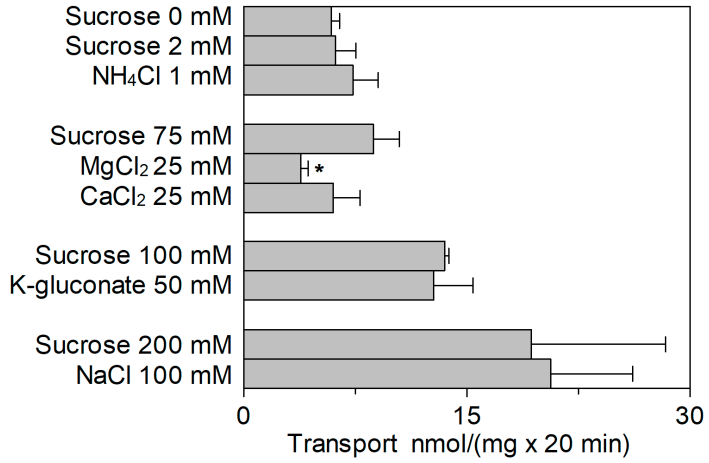

Figure 7. Effect of intraliposomal cations on the transport activity of *Sl*CAT2. *Sl*CAT2 was purified and reconstituted in proteoliposomes as described in Section 4.4. Transport was measured in 20 min, as described in Section 4.5, by adding 100 μM [^{3}H]Arg to proteoliposomes containing indicated concentrations of sucrose or cations and 15 mM ATP, at pH 7.5. Concentrations were chosen according to the average concentrations of cations in the vacuolar lumen. Results are the means ± SD from four experiments. (*), Significantly different from the control (isoosmotic concentration of sucrose for each category of cations) for $p < 0.05$ as calculated from 1-way ANOVA test.

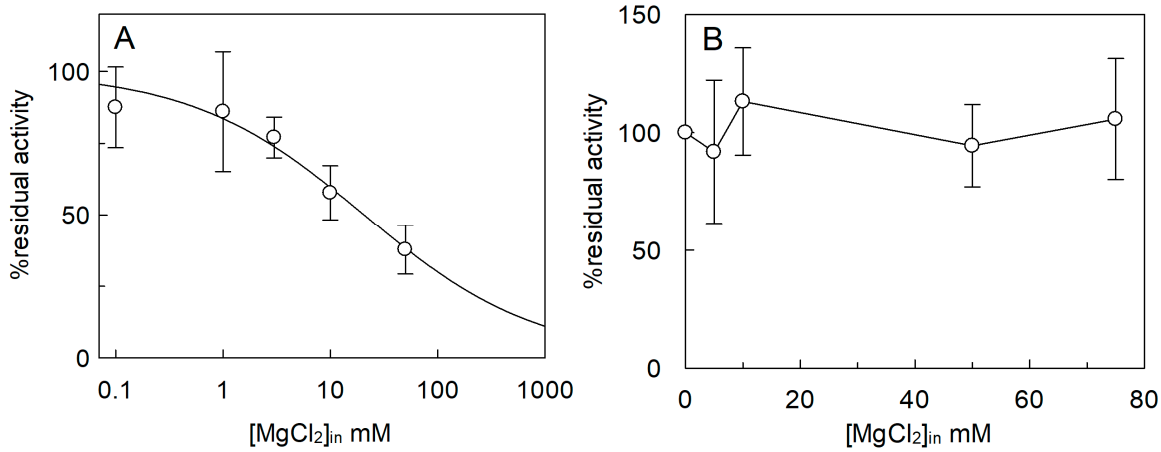

Figure 8. Effect of intraliposomal Mg^{2+} on the transport activity of *Sl*CAT2. *Sl*CAT2 was purified and reconstituted in proteoliposomes as described in Section 4.4. (**A**) Dose–response curve for the inhibition of Mg^{2+} in the presence of intraliposomal ATP. Transport was measured in 20 min, as described in Section 4.5, by adding 100 μM [^{3}H]Arg to proteoliposomes containing the indicated concentrations of Mg^{2+}, 200 mM sucrose, and 15 mM ATP at pH 7.5. (**B**) Analysis of the inhibition of Mg^{2+} in the absence of intraliposomal ATP. Transport was measured in 20 min, as described in Section 4.5, by adding 100 μM [^{3}H]Arg to proteoliposomes containing the indicated concentrations of Mg^{2+} and 200 mM sucrose. Transport activity was calculated as the percent of residual activity with respect to condition without any addition (in absence of intraliposomal Mg^{2+}). Results are the means ± SD from three experiments.

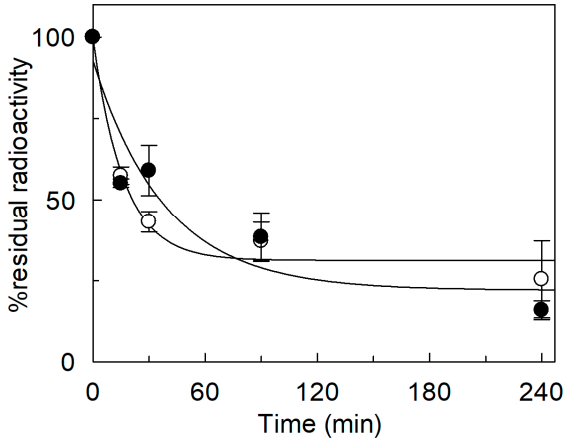

Figure 9. Efflux from proteoliposomes reconstituted with *Sl*CAT2. *Sl*CAT2 was purified and reconstituted in proteoliposomes as described in Section 4.4. Arginine efflux was measured at the indicated time, as described in Section 4.5. Internal residual radioactivity was measured as percent with respect to control (time 0), in the absence (open circle) or in the presence (closed circle) of 0.45 mM Mg^{2+} in the extraliposomal compartment. Data are plotted using the single exponential equation with offset as described in Section 4.5. Results are the means ± SD from three experiments.

2.4. Effect of Cholesterol on the SlCAT2 Transport Activity

The vacuole membrane contains 30% sterols [36]. Since cholesterol was found to be important in the interaction and in the stabilization of several membrane proteins, we have exploited the suitability of the proteoliposome model in changing the lipid composition. Cholesteryl hemisuccinate (CHS), a commercial form of cholesterol with a relatively higher water solubility than cholesterol and widely used in this kind of applications [37–40], was included in the proteoliposomal membrane. The transport activity of *Sl*CAT2 was measured in the presence of two different amounts of CHS. Interestingly, the [^{3}H]Arg uptake was stimulated by increasing amounts of CHS up to 30% in the presence of 1 mg of CHS corresponding to 10% of total lipid composition (Figure 10).

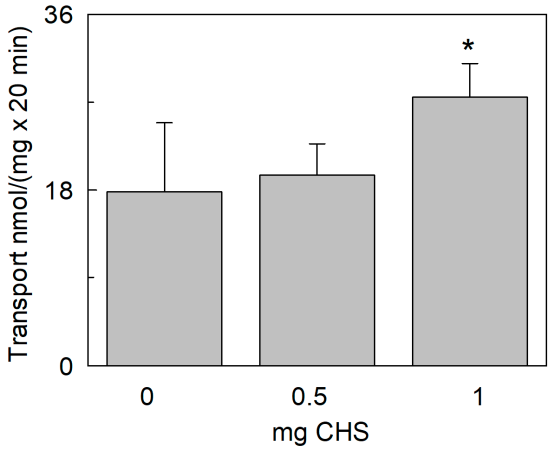

Figure 10. Effect of cholesteryl hemisuccinate (CHS) on the transport activity of *Sl*CAT2. *Sl*CAT2 was purified and reconstituted in proteoliposomes as described in Section 4.4. Transport was measured in 20 min, as described in Section 4.5, by adding 100 μM [^{3}H]Arg to proteoliposomes containing 200 mM sucrose and 15 mM ATP at pH 7.5. Proteoliposomes are prepared without CHS or with 0.5 mg or 1 mg CHS in 1 mL of proteoliposomes as described in Section 4.6. Results are the means ± SD from four experiments. (*), significantly different from the control (condition with no addition of CHS) for $p < 0.05$ as calculated from Student's *t*-test analysis.

2.5. Homology Model

As previously reported, *Sl*CAT2 has 14 putative transmembrane segments and it should be oriented, in the vacuolar membrane, with N- and C-termini exposed towards the internal side [7,9] in agreement with the data shown in Figure 1. The three-dimensional structure of any CAT member is not solved, yet. The transporter shares 27% identity (Figure 11) with the prokaryotic transporter *Gk*ApcT (*G. kaustophilus*) responsible for proton-coupled amino acid transport across the plasma membrane [41]. Therefore, to gain some information on *Sl*CAT2 fold, the homology model was constructed on the basis of the crystal structure of *Gk*ApcT (Figure 12A). As shown by the Ramachandran plot (Figure 12B), the obtained structure was suitable, although it lacks two transmembrane domains (TM 11 and TM 12). In particular, 84.8% or 93.9% of all residues were in favored or in allowed regions, respectively, as derived by MolProbity software [42]. In this structure, it was possible to identify the typical APC superfamily fold, with transmembrane α-helices TM1-TM5 (orange) linked to α-helices TM6-TM10 (blue) by a pseudo-two-fold symmetry axis (Figure 12A). The binding of arginine could be predicted on the basis of the position of the amino acid substrate in *Gk*ApcT. Phe263 (Figure 12C) is homologous of Phe231 that is responsible for substrate gating in *Gk*ApcT. Interestingly, this residue is also conserved in the human histidine transporter LAT1 (Phe 252) which belongs to the same APC superfamily [43].

```
SlCAT2    MGFVGDGSCSSSGGDKGGCFIGGMKSLVRRKQVDSANSKSSSTSGSSHQLAKALTIPHLI   60
GkApcT    -----------------------MNLFRKKPIQLLMKES---GAKGASLRKELGAFDLT   33
                                  .*.*:* ::   .:*   .... .* * *   .*

SlCAT2    TIGVGSTIGAGVYILVGTVAREHSGPALTISFLIAGIAAALSAFCYAELASRCPSAGSAY  120
GkApcT    MLGIGAIIGTGIFVLTGVAAAEHAGPALVLSFILSGLACVFAALCYAEFASTVPVSGSAY   93
           :*:*: **:*:::*.*..* **:****.:**:::*:*.:::*:****:**  * :****

SlCAT2    HYSYICVGEGVAWLIGWALVLEYTIGGSAVARGISPNLAMLF-GSPDSLPSFLARHTIPG  179
GkApcT    TYSYATFGELIAWILGWDLILEYGVASSAVAVGWSGYFQGLLSGFGIELPKALTSAYDPA  153
           ***  .** :**::** *:*** :..**** * *  :  *: *   .**. *:    *.

SlCAT2    LNITVDPCAAILVFLVTGLLCVGIKESTVVQGFVTSVNVCVMAFVIIAGGYLGYKAGWPG  239
GkApcT    KGTFIDLPAIIIVLFITFLLNLGAKKSARFNAVIVAIKVAVVLLFLAVGVWYVKPENWT-  212
           .  :*  * *:*:::* ** :* *:*: .:..:.:::*.*: :.: .* :     .*

SlCAT2    YELPVGYFPYGVDGMLAGASTVFFAYIGFDSVASTAEEVKNPQRDLPMGIGFALSICCSL  299
GkApcT    -----PFMPYGFSGVATGAATVFFAYIGFDAVSTAAEEVRNPQRDMPIGIIVSLLVCTLL  267
                ::***..*: :**:**********:*:::****:*****:*:** .:* :*  *

SlCAT2    YMLVSAVIVGLVPYYAMDPDTPISSAFASHGINWAAYIITIGACTSLCSTLMGSIMPQPR  359
GkApcT    YIAVSLVLTGIVPYEQLNVKNPVAFALNYIHQDWVAGFISLGAIAGITTVLLVMMYGQTR  327
           *: ** *:.*:***  :: ..*:: *:     :*.* :*::** :.: :.*:  :  * *

SlCAT2    ILMAMARDGLLPSFFSDVNKRTQVPIKGTIATGLLSGTLAFFMNVEQLSGMVSVGTLLAF  419
GkApcT    LFYAISRDGLLPKVFARISPTRQVPYVNTWLTGAAVAVFAGIIPLNKLAELTNIGTLFAF  387
           :: *::******..*: :.   ***  .*  **   ..:* :: :::*: :..:***:**

SlCAT2    TMVAISVLILRYVPPDEVPVPSSYQEAIDSVRLRRSSCSSSSDMDVEKTKIPAVTSGDST  479
GkApcT    ITVSIGVLVLRKTQ-----------------------------------------------  401
            *:*.**:** .

SlCAT2    PLLGEISVGHPLAEKAAAKLSYLVSQRRKVAGCTILFICIGVCIVTSAASIVNLSNPARY  539
GkApcT    -------------------------------------------------------------  401

SlCAT2    ALSGIGGLLLISGLIILTCIDQDDARHSFGHTGGFTCPFVPLLPIACILINVYLLINLGG  599
GkApcT    ---------------------------PDLKRAFRVPFVPVVPILAVLFCGYLVLQLPA  433
                                    . . .*  ****::** .:*:  **:::* .

SlCAT2    ETWARVSIWLVIGTCIYALYGRTHSSLKTAVYVPSTHVDEIYETSAISLAC 650
GkApcT    MTWIGFVSWLLIGLVIYFIYGRKHSELNEMARTEEKAG------------ 471
           **  .  **:**  ** :***.**.*:  . . ..
```

Figure 11. The sequences of *Sl*CAT2 and *Gk*ApcT were aligned using the software Clustal Omega as described in Section 4.7.

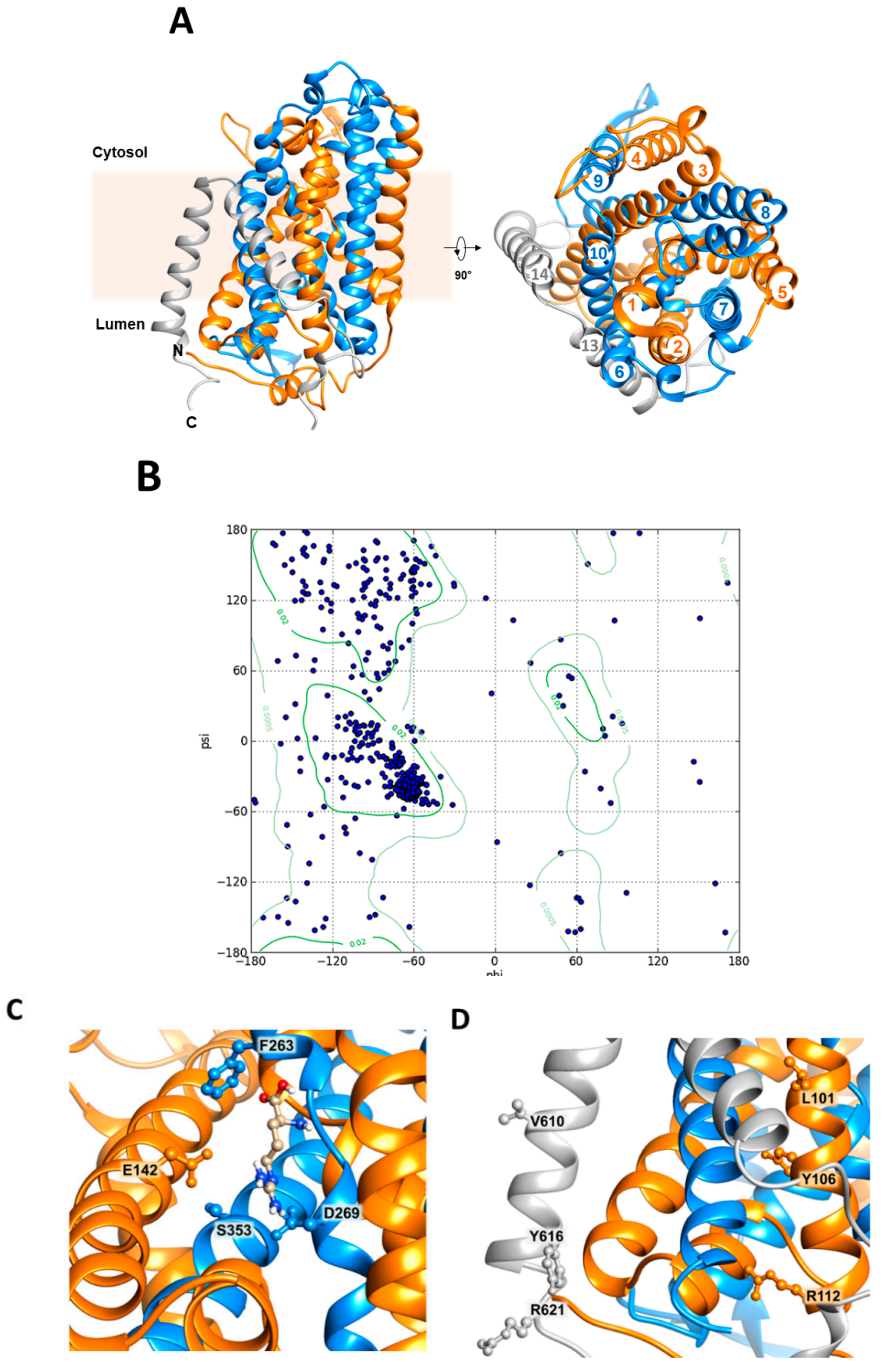

Figure 12. Homology structural model of *Sl*CAT2. The three-dimensional model is built, as described in Section 4.7, using the *Gk*ApcT atomic coordinates (5OQT) as a template. The α-helices are colored in orange or in blue to identify the pseudo two-fold symmetry axis of LeuT-fold. The α-helices which are not part of LeuT fold are colored in gray. The model is designed using the Chimera 1.13.1 software. (**A**) The protein is inserted in the membrane with the N- and C-termini in the luminal space (left-front view); on the right, the model is rotated by 90 °C showing the top view and α-helices are numbered. (**B**) Ramachandran plot of the model in A with residues in favored (smaller gate) and allowed (larger gate) regions. The residues are depicted as blue circles. (**C**) Molecular docking of arginine in the putative binding site of *Sl*CAT2; residues putatively responsible for arginine binding and gating (S353, D269, and F263) together with the residue putatively responsible for proton coordination (E142) are indicated in the ball and stick representation. (**D**) Residues of CRAC motifs responsible for cholesterol binding are highlighted in TM 2 (orange α-helix) and TM 14 (gray α-helix) in the ball and stick representation; numbering of α-helices corresponds to that of Figure 12A.

3. Discussion

The majority of the studies on plant transporters has been conducted so far, on *A. thaliana*, whose genome has been sequenced revealing the existence of 14 APC genes. However, studying *S. lycopersicum* transporters might be in some instances, even more interesting due to the applications of tomato in biotechnology. Arginine is the highest affinity substrate of *Sl*CAT2, as previously shown using the recombinant protein reconstituted into proteoliposomes [7]. Noteworthy, a relatively high concentration of arginine into the vacuole has been measured [44]. The importance of this amino acid for plants mainly resides in its high nitrogen content and in its involvement in polyamines and nitric oxide (NO) synthesis, which is important during fruit development [44].

On the basis of the data here presented, the *Sl*CAT2 inserts asymmetrically into the proteoliposomal membrane (Figures 1 and 12) allowing both arginine uptake and efflux. The asymmetric insertion is further confirmed by the side-specific regulation observed for both osmolyte and cations, which exert opposite effects at the two sides of the membrane. The side-specific regulation of *Sl*CAT2 suggests that the protein is inserted in the proteoliposomal membrane with an orientation that may correspond to that in the native membrane of vacuoles (right-side-out). This is consistent with the detergent removal reconstitution procedure that forms proteoliposomes with a relatively small radius. This physical property forces the orientation of the membrane proteins as shown for several transporters from either plasma membrane or intracellular organelles [45–49]. Notably, the percentage of reconstituted *Sl*CAT2 is ~30%, in-line with previous literature data demonstrating that the average of reconstitution efficiency is in the range of 10 to 30% [50,51]. We cannot absolutely exclude that the orientation of the transporter in proteoliposomes could be the opposite of the native membrane, even though this would not fit with the data on regulation. In fact, it is well known that the intravacuolar osmolality can undergo wide oscillations in normal conditions. In good agreement with this physiological phenomenon, also the activity of the *Sl*CAT2 is modulated only by the increase of intraliposomal, i.e., intravacuolar, osmolality. This may ensure a fast response of the transporter to osmotic changes in vivo [52–54]. On the contrary, increased external (cytosolic) osmolality has an opposite effect with a slight inhibition occurring in conditions of high osmotic imbalance, which may not be physiological [54].

The side-specific effect of ions is in favor of a right-side-out orientation, too. In fact, in the external compartment, i.e., cytosolic, besides a plausible sucrose-similar osmotic effect, an additional effect by cations, superimpose the osmotic one. On the contrary, in the intraliposomal side, i.e., vacuolar lumen, the effects of ions are negligible. Noteworthy, the response of the protein to ions is coherent with their cytosolic/luminal concentrations being in favor of a largely right-side-out orientation of the protein. In the frame of regulation by cations, Mg^{2+} revealed to be particularly interesting: this divalent cation does not exert direct effects on the transporter when present in the internal side. The apparent inhibition observed is due to the formation of an Mg-ATP complex which reduces the concentration of free ATP, necessary for *Sl*CAT2 full activity [7]. At this stage, we cannot assess with certainty whether or not the ATP sequestering effect in the vacuolar lumen, may be physiologically relevant. Differently from the luminal side, Mg^{2+} inhibits the transporter from the cytosolic (extraliposomal) side even at low concentration. However, this effect is observed on the arginine uptake while there is no transinhibition on the arginine efflux. Therefore, it can be hypothesized that the regulation by Mg^{2+} affects arginine storage, not its release from vacuoles. The asymmetric effect of Mg^{2+} further supports the side-specific (right-side-out) orientation of the transporter. Possible physiological regulators could induce arginine remobilization from the vacuole under specific physiopathological conditions. Some clues can also derive from bioinformatics by analyzing the 3D homology model built in the present work (Figure 12). As an example, Glu115 involved in proton binding on the internal side in *Gk*ApcT may suggest that the corresponding homologous Glu142 of *Sl*CAT2 might be involved in the binding of a proton in *Sl*CAT2, as well (Figure 12C). At this stage, it cannot be ascertained if a proton moves across the membrane or only binds to a regulatory site. Counter-translocation of a proton may compensate for the movement of the positive charge of arginine. Alternatively, a proton might only bind and be released from the protein allowing some conformational changes which facilitate arginine transport as shown

for other transporters [55]. The physical interaction between the transporter *Gk*ApcT and cholesterol has been proposed to mediate the connection of the transporter with another bacterial protein with a single membrane-spanning domain [41]; interestingly, the molecule of cholesterol could interact with *Sl*CAT2 at transmembrane domains 2 and 14. In this region, in fact, we identified two possible cholesterol binding sites on the basis of the algorithm of CRAC motif (L/V)-$X_{1–5}$-(Y)-$X_{1–5}$-(K/R) (Figure 12D) [41,56]. However, additional site-directed mutagenesis and structural and topological studies are required to deal with these aspects, including the definitive assessment of the orientation of the transporter in the artificial and native membranes. Finally, the function of arginine uptake or efflux and its diverse modulation may be linked also to a more complex phenomenon, i.e., intracellular amino acid sensing, whose study in the plant is yet underdeveloped, as recently pointed out [32]. Amino acid sensing is, in fact, a well-described phenomenon in animals and yeast where availability of these molecules is responsible for modulation of mTOR and GCN2 pathways involved in cell growth, development, and metabolism regulation [57]. In particular, amino acid transporters of the plasma membrane as well as of intracellular organelles may be considered a "transceptor", i.e., low capacity transporter with a receptor function able to transmit the availability of a specific nutrient for sensing machinery [48,57]. In this scenario, arginine is one of the amino acids known to play a role in the mentioned signaling function in cells via mTOR pathway modulation [58]. Therefore, the results here presented suggest that *Sl*CAT2 may be also involved in sensing pathways via mobilization of arginine from vacuoles.

In conclusion, the proteoliposome experimental model allowed us to characterize the transport mediated by *Sl*CAT2. Some information on osmotic as well as salt regulation of *Sl*CAT2 were gained by exploiting the suitability of proteoliposomes in handling and precisely manipulating the experimental conditions in the internal and external compartments. Even though the experiments were conducted exquisitely in vitro, this work highlights one of the few examples of the influence of cations and osmolytes at physiological concentrations on the activity of a plant transporter. To uncover the structural basis of these regulatory responses, future work using bioinformatics coupled to site-directed mutagenesis will be carried out.

4. Materials and Methods

4.1. Materials

E. coli Rosetta(DE3)pLysS cells were from Novagen (Rome, Italy); ECL plus, Hybond ECL membranes were from GE Healthcare; L-[^{3}H]Arg was from Perkin Elmer (Waltham, MA, USA); conjugated anti-His6 antibody, TX-100, Amberlite XAD-4, egg yolk phospholipids (3-sn-phosphatidylcholine from egg yolk), Sephadex G-75, His-Select resin, L-Arg and all the other reagents were from Sigma-Aldrich (Saint Louis, MO, USA).

4.2. Protein Production

Heterologous expression of SlCAT2 E. coli Rosetta(DE3)pLysS cells (Novagen) were transformed with pET21-SlCAT2 (pET21 from Novagen and SlCAT2 amplified and cloned in Indiveri's lab) as previously described [7]. In brief, *E. coli* Rosetta(DE3)pLysS cells carrying the pET21-SlCAT2-6His were preinoculated in LB medium, supplemented with same concentrations of ampicillin and chloramphenicol, and grown overnight at 37 °C under rotatory stirring (300 rpm). After overnight growth, the saturated inoculum was diluted 1:10 in the same LB medium supplemented with the same concentrations of ampicillin and chloramphenicol. Then, at an OD of ~0.8 measured at 600 nm, 0.4 mM isopropyl-β-D-thiogalactopyranoside (IPTG) was added to induce protein synthesis. After 4 h of growth at a temperature of 28 °C, cells were harvested by centrifugation at 3000× *g* for 15 min at 4 °C. The bacterial pellets were resuspended in a buffer containing 20 mM Hepes Tris pH 7.5 and 300 mM NaCl supplemented with protease inhibitor cocktail. Thus, cells were lysate by mild sonication at 4 °C (10 min in pulses of 1 s sonication, 1 s intermission) with a Vibracell VCX-130 sonifier (SONICS). The soluble and the insoluble fractions were separated by centrifugation at 12,000× *g* for 5 min at 4 °C. The proteins of the cell lysates were analyzed by 12% SDS-PAGE.

4.3. Protein Purification

The protein was purified as previously described [7] with some modifications: in brief, the insoluble fraction was treated with 10 mM DTE, 3.2 M urea, 0.8% Sarkosyl, 200 mM NaCl, 20 mM Tris, and HCl pH 8.0 and centrifuged at 12,000× *g* for 10 min at 4 °C. One milliliter of the solubilized lysate was applied onto a column filled with His-select Ni-Chelating affinity gel (0.5 cm diameter, 3 cm height) preconditioned with 8 mL of a buffer containing 0.1% Sarkosyl, 200 mM NaCl, 10% glycerol, and 20 mM Tris HCl pH 8.0. The elution profile: 5 mL of a wash buffer containing 20 mM Tris HCl pH 8.0, 10% glycerol, 200 mM NaCl, 0.1% DDM, and 5 mM DTE; then, the protein was eluted with 3 mL of the same buffer containing 10 mM imidazole and 3 mL of the same buffer containing 50 mM imidazole; fractions of 1 mL were collected. The third fraction of protein eluted with 10 mM imidazole and the first and the second fraction of 50 mM imidazole were pulled together for subsequent desalting using PD-10 column using the desalting buffer composed of 20 mM Tris HCl pH 8.0, 0.1% DDM, 10% glycerol, and 5 mM DTE. The desalted protein was then used for reconstitution in proteoliposomes as described in the following paragraph. Protein concentration was estimated by the Chemidoc imaging system to calculate the *Sl*CAT2 specific activity as previously described [59].

4.4. Reconstitution of the SlCAT2 Transporter into Liposomes

The desalted *Sl*CAT2 was reconstituted by removing the detergent from mixed micelles containing detergent, protein, and phospholipids by incubation with Amberlite XAD-4 in a batch-wise procedure, as previously described [60]. The composition of the initial mixture used for reconstitution (except when differently indicated) was 400 µL of the purified protein (6 µg protein in 0.1% DDM), 80 µL of 10 % TX-100, 120 µL of 10% egg yolk phospholipids in the form of sonicated liposomes prepared as previously described [61], 15 mM ATP, and 10 mM Tris Hepes pH 7.5 (except where differently indicated) in a final volume of 700 µL. After vortexing, this mixture was incubated with 0.5 g Amberlite XAD-4 under rotatory stirring (1200 rpm) at 23 °C for 40 min in a batchwise procedure as previously pointed out [62].

4.5. Transport Measurements

Five-hundred-and-fifty microliters of proteoliposomes were passed through a Sephadex G-75 column (0.7 cm diameter × 15 cm height) preequilibrated with 10 mM Tris Hepes pH 7.5. From these columns, 550 µL of proteoliposomes were collected and divided into aliquots (samples) of 100 µL. Transport was started by adding 100 µM of [^{3}H]Arg to the proteoliposome samples. The pH gradient experiments were performed reconstituting protein in liposome with 10 mM Tris Hepes pH 5.5. After incubation with Amberlite XAD 4 resin, 550 µL of proteoliposomes were passed through a Sephadex G-75 column preequilibrated with 0.5 mM Tris Hepes pH 5.5. Transport was started by adding 100 µM [^{3}H]Arg buffered with 10 mM Tris Hepes at the different pH as indicated in the figure legend.

The changes in external/internal osmolality were performed by adding in the extraliposomal/intraliposomal compartment appropriate concentrations of sucrose as indicated in the figure legend.

Transport reaction was stopped by adding 5 mM Pyridoxal Phosphate (PLP); according to the stop inhibitor method, the same inhibitor was added at time zero to control samples (blank) [63]. The initial rate was measured in 10 min, i.e., in the linear range of time courses as previously described [7]. The PLP insensitive radioactivity associated with the control samples (blank) was less than 30% with respect to the PLP-sensitive arginine transport.

For efflux measurements, proteoliposomes containing 15 mM ATP were preloaded by incubation with 100 µM [^{3}H]Arg (1 µCi/mL) for 90 min [64]. External compounds were removed by another passage through Sephadex G-75 and efflux was measured as indicated in the figure legend. In both uptake and efflux, transport was stopped by passing 100 µL of each sample through a Sephadex G-75 column (0.6 cm diameter × 8 cm height) in order to separate the external from the internal radioactivity. Samples were eluted with 1 mL 50 mM NaCl and collected in 4 mL of scintillation mixture, vortexed and counted.

The experimental values were corrected by subtracting the respective controls. Specific activity was calculated and expressed as nmol/mg at a given time of measurement or as nmol/(mg × min) in the case of initial rate measurement. For calculation of initial rate, transport was measured in 10 min, i.e., within the initial linear part of the uptake. Grafit 5.0.13 software (Erithacus Software, West Sussex, UK) was used to derive IC_{50} values in inhibition assays and to measure transport rate by first-order rate equation and by a single exponential decay with offset.

4.6. Other Methods

CHS was solubilized in 20 mM Tris HCl pH 8.0 and 5% TX-100 by two sonication cycles of 2 min (no pulse, 40 W) with a Vibracell VCX-130 sonifier (SONICS, Newtown, CT, USA) as previously suggested [65]. Solubilized CHS was added to liposome preparation under rotatory stirring (1200 rpm) at 23 °C for 30 min. Electrophoresis was conducted using 12% SDS-PAGE and the resulting gel was stained using standard silver staining procedure.

4.7. Homology Modeling and Docking Analysis

The crystal structure of *Gk*ApcT (5OQT) was used as a template to build the homology structural model of *Sl*CAT2 [41]. The amino acid sequence of *Sl*CAT2 and *Gk*ApcT were aligned through the Clustal Omega [66]. The alignment was used to run the program Swiss Model [67]. On the basis of the binding site of *Gk*ApcT, the position of Arg was determined using the software ArgusLab (M.A. Thompson, ArgusLab 4.0.1, Planaria Software LLC, Seattle, WA, USA).

4.8. Statistical Analysis

Results were analyzed by nonparametric Student's *t*-test or 1-way ANOVA test as appropriate as described in figure legends.

Author Contributions: J.C. and C.I. conceived, designed the experiments, and analyzed the data; T.M.R.R. and M.G. performed protein production in *E. coli*; J.C. performed protein purification, proteoliposome functional assays, and bioinformatics; M.S. performed proteoliposomes functional assays, designed some experiments, and analyzed the data; J.C., M.S., and C.I. wrote the paper. C.I. supervised the work.

Funding: This work was supported by the Ministry of Instruction University and Research (MIUR)-Italy, by a grant from PON-Ricerca e competitività 2007–2013 (PON project 01_00937) to C.I.

Conflicts of Interest: The authors declare no conflicts of interest. The funding sponsor had no role in the design of the study, in the collection, analyses, or interpretation of the data, in the writing of the manuscript and in the decision to publish the results.

Abbreviations

APC	Amino acid Polyamine Choline
*Sl*CAT2	*Solanum lycopersicum* CAT2
*Gk*ApcT	*Geobacillus kaustophilus* ApcT
CAT	Cationic Amino acid Transporter
CRAC	Cholesterol Recognition/interaction Amino acid Consensus sequence
TX-100	Triton X-100
DTE	DiThioErythritol
CHS	Cholesteryl HemiSuccinate
DDM	n-Dodecyl-β-D-Maltoside

References

1. Martinoia, E.; Meyer, S.; De Angeli, A.; Nagy, R. Vacuolar transporters in their physiological context. *Annu. Rev. Plant Biol.* **2012**, *63*, 183–213. [CrossRef] [PubMed]
2. Etxeberria, E.; Pozueta-Romero, J.; Gonzalez, P. In and out of the plant storage vacuole. *Plant Sci.* **2012**, *190*, 52–61. [CrossRef] [PubMed]

3. Carter, C.; Pan, S.; Zouhar, J.; Avila, E.L.; Girke, T.; Raikhel, N.V. The vegetative vacuole proteome of Arabidopsis thaliana reveals predicted and unexpected proteins. *Plant Cell* **2004**, *16*, 3285–3303. [CrossRef] [PubMed]
4. Schumacher, K. pH in the plant endomembrane system-an import and export business. *Curr. Opin. Plant Biol.* **2014**, *22*, 71–76. [CrossRef] [PubMed]
5. Gao, C.; Zhao, Q.; Jiang, L. Vacuoles protect plants from high magnesium stress. *Proc. Natl. Acad. Sci. USA* **2015**, *112*, 2931–2932. [CrossRef] [PubMed]
6. Hildebrandt, T.M.; Nunes Nesi, A.; Araujo, W.L.; Braun, H.P. Amino Acid Catabolism in Plants. *Mol. Plant* **2015**, *8*, 1563–1579. [CrossRef]
7. Regina, T.M.R.; Galluccio, M.; Scalise, M.; Pochini, L.; Indiveri, C. Bacterial production and reconstitution in proteoliposomes of Solanum lycopersicum CAT2: A transporter of basic amino acids and organic cations. *Plant Mol. Biol.* **2017**, *94*, 657–667. [CrossRef]
8. Wessler, I.; Kirkpatrick, C.J. Acetylcholine beyond neurons: The non-neuronal cholinergic system in humans. *Br. J. Pharm.* **2008**, *154*, 1558–1571. [CrossRef]
9. Su, Y.H.; Frommer, W.B.; Ludewig, U. Molecular and functional characterization of a family of amino acid transporters from Arabidopsis. *Plant Physiol.* **2004**, *136*, 3104–3113. [CrossRef]
10. Yang, H.; Krebs, M.; Stierhof, Y.D.; Ludewig, U. Characterization of the putative amino acid transporter genes AtCAT2, 3 &4: The tonoplast localized AtCAT2 regulates soluble leaf amino acids. *J. Plant Physiol.* **2014**, *171*, 594–601. [CrossRef]
11. Rentsch, D.; Schmidt, S.; Tegeder, M. Transporters for uptake and allocation of organic nitrogen compounds in plants. *FEBS Lett.* **2007**, *581*, 2281–2289. [CrossRef] [PubMed]
12. Demidchik, V.; Maathuis, F.J. Physiological roles of nonselective cation channels in plants: From salt stress to signalling and development. *New Phytol.* **2007**, *175*, 387–404. [CrossRef] [PubMed]
13. Martinoia, E.; Maeshima, M.; Neuhaus, H.E. Vacuolar transporters and their essential role in plant metabolism. *J. Exp. Bot.* **2007**, *58*, 83–102. [CrossRef] [PubMed]
14. Maeshima, M. TONOPLAST TRANSPORTERS: Organization and Function. *Annu. Rev. Plant Physiol. Plant Mol. Biol.* **2001**, *52*, 469–497. [CrossRef] [PubMed]
15. Kluge, C.; Golldack, D.; Dietz, K.J. Subunit D of the vacuolar H+-ATPase of Arabidopsis thaliana. *Biochim. Biophys. Acta* **1999**, *1419*, 105–110. [CrossRef]
16. Schumacher, K.; Krebs, M. The V-ATPase: Small cargo, large effects. *Curr. Opin. Plant Biol.* **2010**, *13*, 724–730. [CrossRef] [PubMed]
17. Gaxiola, R.A.; Palmgren, M.G.; Schumacher, K. Plant proton pumps. *FEBS Lett.* **2007**, *581*, 2204–2214. [CrossRef]
18. Maeshima, M. Vacuolar H(+)-pyrophosphatase. *Biochim. Biophys. Acta* **2000**, *1465*, 37–51. [CrossRef]
19. Kapilan, R.; Vaziri, M.; Zwiazek, J.J. Regulation of aquaporins in plants under stress. *Biol. Res.* **2018**, *51*, 4. [CrossRef]
20. Maurel, C.; Verdoucq, L.; Luu, D.T.; Santoni, V. Plant aquaporins: Membrane channels with multiple integrated functions. *Annu. Rev. Plant Biol.* **2008**, *59*, 595–624. [CrossRef]
21. Volkov, V. Salinity tolerance in plants. Quantitative approach to ion transport starting from halophytes and stepping to genetic and protein engineering for manipulating ion fluxes. *Front. Plant Sci.* **2015**, *6*, 873. [CrossRef] [PubMed]
22. Conde, A.; Chaves, M.M.; Geros, H. Membrane transport, sensing and signalling in plant adaptation to environmental stress. *Plant Cell Physiol.* **2011**, *52*, 1583–1602. [CrossRef] [PubMed]
23. Benito, B.; Haro, R.; Amtmann, A.; Cuin, T.A.; Dreyer, I. The twins K^+ and Na^+ in plants. *J. Plant Physiol.* **2014**, *171*, 723–731. [CrossRef] [PubMed]
24. Adams, E.; Shin, R. Transport, signaling, and homeostasis of potassium and sodium in plants. *J. Integr. Plant Biol.* **2014**, *56*, 231–249. [CrossRef] [PubMed]
25. Trankner, M.; Tavakol, E.; Jakli, B. Functioning of potassium and magnesium in photosynthesis, photosynthate translocation and photoprotection. *Physiol. Plant.* **2018**. [CrossRef] [PubMed]
26. Ashley, M.K.; Grant, M.; Grabov, A. Plant responses to potassium deficiencies: A role for potassium transport proteins. *J. Exp. Bot.* **2006**, *57*, 425–436. [CrossRef] [PubMed]
27. Tang, R.J.; Luan, S. Regulation of calcium and magnesium homeostasis in plants: From transporters to signaling network. *Curr. Opin. Plant Biol.* **2017**, *39*, 97–105. [CrossRef]

28. Hermans, C.; Conn, S.J.; Chen, J.; Xiao, Q.; Verbruggen, N. An update on magnesium homeostasis mechanisms in plants. *Metallomics* **2013**, *5*, 1170–1183. [CrossRef]
29. Schonknecht, G. Calcium Signals from the Vacuole. *Plants* **2013**, *2*, 589–614. [CrossRef]
30. White, P.J.; Broadley, M.R. Calcium in plants. *Ann. Bot.* **2003**, *92*, 487–511. [CrossRef]
31. Pittman, J.K. Vacuolar Ca(2+) uptake. *Cell Calcium* **2011**, *50*, 139–146. [CrossRef] [PubMed]
32. Dinkeloo, K.; Boyd, S.; Pilot, G. Update on amino acid transporter functions and on possible amino acid sensing mechanisms in plants. *Semin. Cell Dev. Biol.* **2018**, *74*, 105–113. [CrossRef] [PubMed]
33. Scalise, M.; Pochini, L.; Panni, S.; Pingitore, P.; Hedfalk, K.; Indiveri, C. Transport mechanism and regulatory properties of the human amino acid transporter ASCT2 (SLC1A5). *Amino Acids* **2014**, *46*, 2463–2475. [CrossRef] [PubMed]
34. Pochini, L.; Scalise, M.; Indiveri, C. Immuno-detection of OCTN1 (SLC22A4) in HeLa cells and characterization of transport function. *Int. Immunopharm.* **2015**, *29*, 21–26. [CrossRef] [PubMed]
35. Gout, E.; Rebeille, F.; Douce, R.; Bligny, R. Interplay of Mg^{2+}, ADP, and ATP in the cytosol and mitochondria: Unravelling the role of Mg^{2+} in cell respiration. *Proc. Natl. Acad. Sci. USA* **2014**, *111*, E4560–E4567. [CrossRef] [PubMed]
36. Zhang, C.; Hicks, G.R.; Raikhel, N.V. Molecular Composition of Plant Vacuoles: Important but Less Understood Regulations and Roles of Tonoplast Lipids. *Plants* **2015**, *4*, 320–333. [CrossRef] [PubMed]
37. Dickens, D.; Chiduza, G.N.; Wright, G.S.; Pirmohamed, M.; Antonyuk, S.V.; Hasnain, S.S. Modulation of LAT1 (SLC7A5) transporter activity and stability by membrane cholesterol. *Sci. Rep.* **2017**, *7*, 43580. [CrossRef]
38. Zeppelin, T.; Ladefoged, L.K.; Sinning, S.; Periole, X.; Schiott, B. A direct interaction of cholesterol with the dopamine transporter prevents its out-to-inward transition. *PLoS Comput. Biol.* **2018**, *14*, e1005907. [CrossRef]
39. Navratna, V.; Tosh, D.K.; Jacobson, K.A.; Gouaux, E. Thermostabilization and purification of the human dopamine transporter (hDAT) in an inhibitor and allosteric ligand bound conformation. *PLoS ONE* **2018**, *13*, e0200085. [CrossRef]
40. Meury, M.; Costa, M.; Harder, D.; Stauffer, M.; Jeckelmann, J.M.; Bruhlmann, B.; Rosell, A.; Ilgu, H.; Kovar, K.; Palacin, M.; et al. Detergent-induced stabilization and improved 3D map of the human heteromeric amino acid transporter 4F2hc-LAT2. *PLoS ONE* **2014**, *9*, e109882. [CrossRef]
41. Jungnickel, K.E.J.; Parker, J.L.; Newstead, S. Structural basis for amino acid transport by the CAT family of SLC7 transporters. *Nat. Commun.* **2018**, *9*, 550. [CrossRef] [PubMed]
42. Chen, V.B.; Arendall, W.B., 3rd; Headd, J.J.; Keedy, D.A.; Immormino, R.M.; Kapral, G.J.; Murray, L.W.; Richardson, J.S.; Richardson, D.C. MolProbity: All-atom structure validation for macromolecular crystallography. *Acta Crystallogr. D Biol. Crystallogr.* **2010**, *66*, 12–21. [CrossRef] [PubMed]
43. Napolitano, L.; Galluccio, M.; Scalise, M.; Parravicini, C.; Palazzolo, L.; Eberini, I.; Indiveri, C. Novel insights into the transport mechanism of the human amino acid transporter LAT1 (SLC7A5). Probing critical residues for substrate translocation. *Biochim. Biophys. Acta* **2017**, *1861*, 727–736. [CrossRef] [PubMed]
44. Winter, G.; Todd, C.D.; Trovato, M.; Forlani, G.; Funck, D. Physiological implications of arginine metabolism in plants. *Front. Plant Sci.* **2015**, *6*, 534. [CrossRef] [PubMed]
45. Klingenberg, M.; Winkler, E. The reconstituted isolated uncoupling protein is a membrane potential driven H^+ translocator. *EMBO J.* **1985**, *4*, 3087–3092. [CrossRef] [PubMed]
46. Spagnoletta, A.; De Palma, A.; Prezioso, G.; Scalera, V. A micro-batchwise technique method for rapid reconstitution of functionally active mitochondrial ADP/ATP carrier from Jerusalem artichoke (*Helianthus tuberosus* L.) tubers. *J. Biochem. Biophys. Methods* **2008**, *70*, 954–957. [CrossRef]
47. Rigaud, J.L.; Levy, D. Reconstitution of membrane proteins into liposomes. *Methods Enzymol.* **2003**, *372*, 65–86. [CrossRef] [PubMed]
48. Rebsamen, M.; Pochini, L.; Stasyk, T.; de Araujo, M.E.; Galluccio, M.; Kandasamy, R.K.; Snijder, B.; Fauster, A.; Rudashevskaya, E.L.; Bruckner, M.; et al. SLC38A9 is a component of the lysosomal amino acid sensing machinery that controls mTORC1. *Nature* **2015**, *519*, 477–481. [CrossRef] [PubMed]
49. Wang, S.; Tsun, Z.Y.; Wolfson, R.L.; Shen, K.; Wyant, G.A.; Plovanich, M.E.; Yuan, E.D.; Jones, T.D.; Chantranupong, L.; Comb, W.; et al. Metabolism. Lysosomal amino acid transporter SLC38A9 signals arginine sufficiency to mTORC1. *Science* **2015**, *347*, 188–194. [CrossRef] [PubMed]
50. Fiermonte, G.; Dolce, V.; Palmieri, F. Expression in Escherichia coli, functional characterization, and tissue distribution of isoforms A and B of the phosphate carrier from bovine mitochondria. *J. Biol. Chem.* **1998**, *273*, 22782–22787. [CrossRef] [PubMed]

51. Stipani, V.; Cappello, A.R.; Daddabbo, L.; Natuzzi, D.; Miniero, D.V.; Stipani, I.; Palmieri, F. The mitochondrial oxoglutarate carrier: Cysteine-scanning mutagenesis of transmembrane domain IV and sensitivity of Cys mutants to sulfhydryl reagents. *Biochemistry* **2001**, *40*, 15805–15810. [CrossRef] [PubMed]
52. Suprasanna, P.; Nikalje, G.C.; Rai, A.N. Osmolyte Accumulation and Implications in Plant Abiotic Stress Tolerance. In *Osmolytes and Plants Acclimation to Changing Environment: Emerging Omics Technologies*; Iqbal, N., Nazar, R.A., Khan, N., Eds.; Springer: New Delhi, India, 2016; pp. 1–12.
53. Wang, L.; Li, X.R.; Lian, H.; Ni, D.A.; He, Y.K.; Chen, X.Y.; Ruan, Y.L. Evidence that high activity of vacuolar invertase is required for cotton fiber and Arabidopsis root elongation through osmotic dependent and independent pathways, respectively. *Plant Physiol.* **2010**, *154*, 744–756. [CrossRef] [PubMed]
54. Zhang, H.; Zhao, F.G.; Tang, R.J.; Yu, Y.; Song, J.; Wang, Y.; Li, L.; Luan, S. Two tonoplast MATE proteins function as turgor-regulating chloride channels in Arabidopsis. *Proc. Natl. Acad. Sci. USA* **2017**, *114*, E2036–E2045. [CrossRef] [PubMed]
55. Jin, X.; Shao, Y.; Bai, Q.; Xue, W.; Liu, H.; Yao, X. Insights into conformational regulation of PfMATE transporter from Pyrococcus furiosus induced by alternating protonation state of Asp41 residue: A molecular dynamics simulation study. *Biochim. Biophys. Acta* **2016**, *1860*, 1173–1180. [CrossRef]
56. Fantini, J.; Barrantes, F.J. How cholesterol interacts with membrane proteins: An exploration of cholesterol-binding sites including CRAC, CARC, and tilted domains. *Front. Physiol.* **2013**, *4*, 31. [CrossRef]
57. Efeyan, A.; Comb, W.C.; Sabatini, D.M. Nutrient-sensing mechanisms and pathways. *Nature* **2015**, *517*, 302–310. [CrossRef] [PubMed]
58. Wang, Y.P.; Lei, Q.Y. Metabolite sensing and signaling in cell metabolism. *Signal Transduct. Target. Ther.* **2018**, *3*, 30. [CrossRef]
59. Torchetti, E.M.; Bonomi, F.; Galluccio, M.; Gianazza, E.; Giancaspero, T.A.; Iametti, S.; Indiveri, C.; Barile, M. Human FAD synthase (isoform 2): A component of the machinery that delivers FAD to apo-flavoproteins. *FEBS J.* **2011**, *278*, 4434–4449. [CrossRef]
60. Napolitano, L.; Scalise, M.; Galluccio, M.; Pochini, L.; Albanese, L.M.; Indiveri, C. LAT1 is the transport competent unit of the LAT1/CD98 heterodimeric amino acid transporter. *Int. J. Biochem. Cell Biol.* **2015**, *67*, 25–33. [CrossRef]
61. Indiveri, C.; Prezioso, G.; Dierks, T.; Kramer, R.; Palmieri, F. Kinetic characterization of the reconstituted dicarboxylate carrier from mitochondria: A four-binding-site sequential transport system. *Biochim. Biophys. Acta* **1993**, *1143*, 310–318. [CrossRef]
62. Galluccio, M.; Pochini, L.; Peta, V.; Ianni, M.; Scalise, M.; Indiveri, C. Functional and molecular effects of mercury compounds on the human OCTN1 cation transporter: C50 and C136 are the targets for potent inhibition. *Toxicol. Sci.* **2015**, *144*, 105–113. [CrossRef] [PubMed]
63. Giangregorio, N.; Tonazzi, A.; Console, L.; Indiveri, C. Post-translational modification by acetylation regulates the mitochondrial carnitine/acylcarnitine transport protein. *Mol. Cell. Biochem.* **2017**, *426*, 65–73. [CrossRef] [PubMed]
64. Giangregorio, N.; Console, L.; Tonazzi, A.; Palmieri, F.; Indiveri, C. Identification of amino acid residues underlying the antiport mechanism of the mitochondrial carnitine/acylcarnitine carrier by site-directed mutagenesis and chemical labeling. *Biochemistry* **2014**, *53*, 6924–6933. [CrossRef] [PubMed]
65. Hanson, M.A.; Cherezov, V.; Griffith, M.T.; Roth, C.B.; Jaakola, V.P.; Chien, E.Y.; Velasquez, J.; Kuhn, P.; Stevens, R.C. A specific cholesterol binding site is established by the 2.8 A structure of the human beta2-adrenergic receptor. *Structure* **2008**, *16*, 897–905. [CrossRef] [PubMed]
66. Sievers, F.; Wilm, A.; Dineen, D.; Gibson, T.J.; Karplus, K.; Li, W.; Lopez, R.; McWilliam, H.; Remmert, M.; Soding, J.; et al. Fast, scalable generation of high-quality protein multiple sequence alignments using Clustal Omega. *Mol. Syst. Biol.* **2011**, *7*, 539. [CrossRef] [PubMed]
67. Arnold, K.; Bordoli, L.; Kopp, J.; Schwede, T. The SWISS-MODEL workspace: A web-based environment for protein structure homology modeling. *Bioinformatics* **2006**, *22*, 195–201. [CrossRef] [PubMed]

BBA - Biomembranes 1861 (2019) 1558–1567

Contents lists available at ScienceDirect

BBA - Biomembranes

journal homepage: www.elsevier.com/locate/bbamem

Insights into the transport side of the human SLC38A9 transceptor

Mariafrancesca Scalise[a], Michele Galluccio[a], Lorena Pochini[a], Jessica Cosco[a], Miriam Trotta[a], Manuele Rebsamen[b], Giulio Superti-Furga[b,c], Cesare Indiveri[a,d,*]

[a] Department DiBEST (Biologia, Ecologia, Scienze della Terra) Unit of Biochemistry and Molecular Biotechnology, University of Calabria, Via P. Bucci 4C, 87036 Arcavacata di Rende, Italy
[b] CeMM Research Center for Molecular Medicine of the Austrian Academy of Sciences, 1090 Vienna, Austria
[c] Center for Physiology and Pharmacology, Medical University of Vienna, 1090 Vienna, Austria
[d] CNR Institute of Biomembranes, Bioenergetics and Molecular Biotechnology, via Amendola 165/A, 70126 Bari, Italy

ARTICLE INFO

Keywords:
mTOR
Proteoliposomes
Cholesterol
Glutamine
Transceptor
hSLC38A9

ABSTRACT

The lysosomal amino acid transporter SLC38A9 is referred to as transceptor, i.e. a transporter with a receptor function. The protein is responsible for coupling amino acid transport across the lysosomal membrane according to the substrate availability to mTORC1 signal transduction. This process allows cells to sense amino acid level responding to growth stimuli in physiological and pathological conditions triggering mTOR regulation. The main substrates underlying this function are glutamine and arginine. The functional and kinetic characterization of glutamine and arginine transport was performed using human SLC38A9 produced in *E. coli*, purified by affinity chromatography and reconstituted in liposomes. A cooperative behaviour for the wild type protein was revealed for both the substrates. A novel Na^+ binding site, namely T453, was described by combined approaches of bioinformatics, site-directed mutagenesis and transport assay. Stimulation by cholesterol of glutamine and arginine transport was observed. The biological function of SLC38A9 relies on the interaction between its N-terminus and components of the mTOR complex; a deletion mutant of the N-terminus tail was produced and transport of glutamine was assayed revealing that this portion does not play any role in the intrinsic transport function of the human SLC38A9. Different features for glutamine and arginine transport were revealed: human SLC38A9 is competent for glutamine efflux, while that of arginine is negligible. In line with these results, imposed ΔpH stimulated glutamine, not arginine transport. Arginine plays, on the contrary, a modulatory function and is able to stimulate glutamine efflux. Interestingly, reciprocal inhibition experiments also supported by bioinformatics, suggested that glutamine and arginine may bind to different sites in the human SLC38A9 transporter.

1. Introduction

The amino acid transceptor SLC38A9 belongs to the SLC38 cluster of the Major Facilitator Superfamily (MFS). The SLC38 group includes eleven members some of which have been functionally characterized in cell systems [1,2]. Historically, these transporters were known as SNATs and classified in systems A and N, according to different transport modes and substrate specificity. In particular, System A includes those transporters that are specific for small amino acids whose prototype is alanine, are inhibited by MeAIB and work in a Na^+-dependent uniport mode. Instead, System N includes transporters specific for glutamine, histidine and asparagine with a transport mode dependent on both Na^+ and H^+ [1]. Some of the SLC38 family members are still orphan transporters. Recently, the human SLC38A9 (hSLC38A9) has been deorphanized, revealing its crucial role in amino acid-dependent mTORC1 activation at the lysosomal membrane. Owing to the intracellular localization, the transport function of hSLC38A9 has been investigated in proteoliposomes [3,4]. It was produced by recombinant biotechnology in *E. coli*, purified by Ni^{2+} affinity chromatography and inserted in the proteoliposome membrane in a right-side-out orientation with respect to its natural location. In this system, some biochemical information in terms of substrate specificity was provided with

Abbreviations: MeAIB, 2-Methylaminoisobutyric acid; mTORC1, mammalian target of rapamycin complex 1; $C_{12}E_8$, Octaethylene Glycol Monododecyl Ether; CHS, Cholesteryl HemiSuccinate; NEM, N-EthylMaleimide; MTSEA, 2-aminoethyl methanethiosulfonate hydrobromide; PLP, pyridoxal phosphate; drSLC38A9, *Danio rerio* SLC38A9, hSLC38A9, human SLC38A9

* Corresponding author at: Department DiBEST (Biologia, Ecologia, Scienze della Terra) Unit of Biochemistry and Molecular Biotechnology, University of Calabria, Via P. Bucci 4C, 87036 Arcavacata di Rende, Italy.
E-mail address: cesare.indiveri@unical.it (C. Indiveri).

https://doi.org/10.1016/j.bbamem.2019.07.006
Received 18 January 2019; Received in revised form 17 May 2019; Accepted 3 July 2019
Available online 08 July 2019

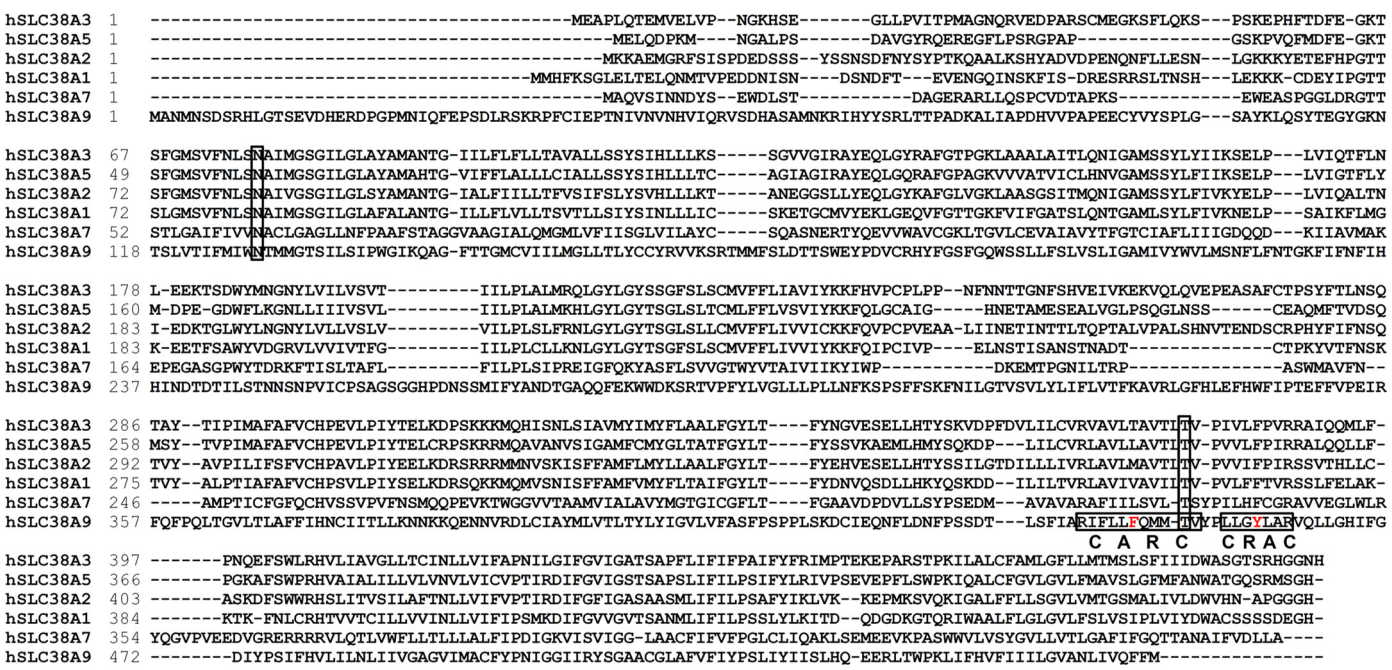

Fig. 1. Alignment of the Na^+-dependent members of the human SLC38A family. All the members with the exception of SLC38A9 (due to the presence of N-terminus long tail boxed in grey) were aligned with ClustalX2 software to create a scaffold. The hSLC38A9 sequence was aligned to the scaffold by the same software and the alignment was manually adjusted. Amino acids involved in sodium binding and in forming CRAC and CARC motifs are boxed in black; residues F449 and Y460, responsible for cholesterol binding, are in red.

glutamine as a main substrate and transport activity also observed for arginine [3]. Some regulatory aspects were also shown: the transport is dependent on intraliposomal sodium that, according to the lysosome/cytosol gradient, stimulates the transport from the internal side. Multiple alignment with the glutamine/sodium co-transporters SLC38A1, A2, A3, A5 and A7 identified the residue N128 as a putative sodium binding site in hSLC38A9 [5]. Indeed, the N128A mutant showed impaired sodium-dependent transport with respect to the WT protein [3]. In a parallel study, the role of hSLC38A9 in mTORC1 activation has been described and the protein has been over-expressed in human cells, purified and inserted in the proteoliposomes in a right-side-out orientation, as well; in this study, arginine was revealed as a low-affinity substrate [4]. The double role of transporting amino acids and interacting with other proteins for mTORC1 activation deserved the classification of SLC38A9 as a transceptor [3,4]. Larger attention was addressed, so far, to the receptor role of this protein that displays a larger molecular mass than the other SLC38 members, due to the presence of an extra-membrane N-terminus tail of more than one hundred amino acids long (Fig. 1). This tail enabled hSLC38A9 to act as an activator of mTORC1 via binding to the Rag GTPase-Ragulator complex [3]. The complex is responsible for the regulation of key cell functions ranging from metabolism to cell growth and proliferation [6,7]. The mechanism of mTORC1 activation via hSLC38A9 requires the efflux of specific amino acids from lysosomes which triggers conformational changes at the level of the N-terminus tail and the consequent contact with mTORC1. Furthermore, positive regulation of receptor function by cholesterol present in the lysosomal membrane was revealed in line with the presence of two consensus motifs for cholesterol binding in the hSLC38A9 primary structure [8]. More recently, it was demonstrated that in the presence of amino acids, hSLC38A9 acts as a guanine exchange factor (GEF) for RAGA [9]. Notwithstanding the information concerning the receptor role of hSLC38A9, the transport function is still underneath. In this respect, the capacity for leucine transport induced by intra-lysosomal arginine has been recently shown [10]. The three-dimensional structure of SLC38A9 from *D. rerio*, that shares 61.9% identity with the human one, was recently solved and the residues responsible for arginine binding were shown, even though this structure lacks of 185 amino acids [11]. In order to shed light on the transport features of hSLC38A9, the kinetics of transported substrates and some regulatory aspects have been approached in this work. Moreover, some feasible structural clues have been predicted combining the experimental data with the homology model, obtained on the basis of the *D. rerio* SLC38A9 structure [11].

2. Materials and methods

2.1. Materials

Pico-Fluor Plus, L-Arginine [^{3}H] and L-Glutamine [3,4-^{3}H(N)] were from PerkinElmer; ECL plus, Hybond ECL membranes from GE Healthcare; pET vectors, RosettaGami2 and RosettaGami2(DE3)pLysS strains from Novagen; restriction endonucleases, other cloning reagents from Fermentas; Lemo21(DE3)pLysS from New England Biolabs; optimized hSLC38A9 cDNA from GenScript. Protease inhibitor cocktail, Monoclonal Anti-polyHistidine-Peroxidase antibody produced in mouse, $C_{12}E_8$, Amberlite XAD-4, egg yolk phospholipids (3-sn-phosphatidylcholine from egg yolk), Sephadex G-75, cholesteryl hemisuccinate, L-Gln and L-Arg were from Sigma–Aldrich; all of the other common reagents were of analytical grade.

2.2. Cloning of hSLC38A9 WT and mutants

The cDNA coding for the full length and Δ111-hSLC38A9 proteins were amplified by PCR reaction starting from wild type full length construct cloned into pH6EX3 expression vector [3] and sub-cloned into the pET16b plasmid in order to add a 10 His tag at the N-terminus of the proteins. T453A, F449I and Y460I mutants were obtained by PCR overlap extension method as previously described [3]. All the primers used for cloning and mutagenesis are reported in Table 1.

2.3. Expression of hSLC38A9 WT and mutants

The recombinant plasmid pH6EX3-6His-hSLC38A9 obtained as described in [3] was used to transform *E. coli* RosettaGami2 strain. The

Table 1
Forward and Reverse primers for performing mutagenesis of hSLC38A9 cDNA.

	Forward primer	Reverse primer
T453A mutation	ctgtttcagatgatggcagtttatccgctgctg	cagcagcggataaactgccatcatctgaaacag
F449I mutation	cgtatcttcctgctgattcagatgatgacggttt	aaaccgtcatcatctgaatcagcaggaagatacg
Y460I mutation	tatccgctgctgggtattctggcgcgcgtccaa	ttggacgcgcgccagaatacccagcagcggata
pH6EX3-Δ111-hSLC38A9	cgcggatccgaaggctacggcaagaacacctctctg	acgcgtcgacttacataaagaattgaacgatcaga
pET-16b-Δ111-hSLC38A9	gggaattccatatggaaggctacggcaagaacacctctctg	cgcggatccttacataaagaattgaacgatcagat
pET-16b-WT-hSLC38A9	gggaattccatatggcgaacatgaactccgaca	cgcggatccttacataaagaattgaacgatcagat

selection was performed on LB-agar added with 100 μg/ml ampicillin, 34 μg/ml chloramphenicol and 12.5 μg/ml tetracycline. One colony was inoculated overnight in LB broth with the same antibiotics and the day after the culture was diluted 1:20 in fresh LB broth. When the culture reached an optical density of about 0.8–1 at 600 nm wavelength, 1 mM IPTG was added to induce protein expression and cells were grown at 28 °C for 4 h. Cells were resuspended and sonified as previously described [12]. The protein patterns of the cell lysate fractions were analysed by SDS-PAGE and western blotting. The recombinant constructs pET16b-10His-hSLC38A9, or pET16b-10His-hSLC38A9 T453A, pET16b-10His-hSLC38A9 F449I, pET16b-10His-hSLC38A9 Y460I or pET16b-10His- Δ111-hSLC38A9 were used to transform *E. coli* RosettaGami2(DE3)pLysS strain. The selection was conducted as described above. One colony was picked and cultured overnight in LB broth added with 100 μg/ml ampicillin, 34 μg/ml chloramphenicol and 12.5 μg/ml tetracycline. The day after the culture was diluted 1:20 in fresh LB broth containing the same antibiotics. When the optical density of the culture measured at 600 nm of wavelength reached 0.8–1 the protein synthesis was induced by 0.4 mM of IPTG and the cells were grown at 28 °C for up to 4 h. Cells were treated as described above and protein expression was verified by SDS-PAGE and western blotting.

2.4. Western blotting analysis

To verify protein expression, samples of bacterial lysates were analysed on SDS-PAGE 12% and transferred onto the nitrocellulose membrane. Western blot analysis has been performed using anti-His antibody 1:10000 (Sigma) incubated 1 h in 3% BSA under shaking at room temperature and revealed by Electrochemiluminescence (ECL) assay.

2.5. Purification of hSLC38A9 WT and mutants

The purification procedure was performed using the Akta Start system. The insoluble cell fraction (about 1.5 mg proteins) from cells expressing hSLC38A9 WT or mutants, was washed with 100 mM TrisHCl pH 8.0 and resuspended in 10 mM DTE, 3.2 M urea, 0.5% sarkosyl, 200 mM NaCl, 10% glycerol, 20 mM TrisHCl pH 8.0 and centrifuged at 12,000*g* for 10 min at 4 °C. The supernatant (of about 1.5 ml) was applied on a His-Trap HP column (5 ml Ni-Sepharose) equilibrated with 10 ml buffer (20 mM Tris HCl pH 8.0, 10% glycerol, 200 mM NaCl, 0.1% sarkosyl). Ten ml of buffer (20 mM Tris HCl pH 8, 10% glycerol, 200 mM NaCl, 0.05% n-Dodecyl β-D-maltoside and 3 mM DTE) was used to wash column while the protein was eluted using 15 ml of the same buffer plus 500 mM imidazole. Fractions of 1 ml were collected and protein was present in the fractions 8–9.

2.6. Reconstitution of the hSLC38A9 in proteoliposomes

The purified hSLC38A9 WT or mutants were reconstituted by removing the detergent in a batch-wise procedure previously pointed out for another human membrane transporter [13]. The reconstitution mixture, except where differently specified, was prepared adding: 400 μl of protein (about 2 μg protein), 80 μl of 10% $C_{12}E_8$, 120 μl of 10% egg yolk phospholipids (w/v) prepared as previously described [14], 20 mM Hepes Tris pH 6.8, except when differently indicated, in a final volume of 700 μl. After vortexing, the mixture was incubated with 0.5 g of Amberlite XAD-4 for 90 min at 23 °C under rotatory stirring at 1200 rpm as previously described [3].

2.7. Transport measurements

After detergent removal, 600 μl of proteoliposomes was passed through a Sephadex G-75 column (0.7 cm diameter × 15 cm height) pre-equilibrated with 20 mM Hepes Tris pH 6.8. Transport (uptake) measurement was started adding 100 μM [^{3}H]glutamine or [^{3}H]arginine to 100 μl proteoliposomes aliquots. For efflux measurements, aliquots of the same pool of proteoliposomes passed through a Sephadex G75 column (0.7 cm diameter × 15 cm height) pre-equilibrated with 20 mM Hepes Tris pH 6.8 (except where differently indicated) were incubated with external 100 μM [^{3}H]glutamine or [^{3}H]arginine (0.5 μCi/nmol) for 120 min. After loading, proteoliposomes were passed again through a Sephadex G75 column (0.7 cm diameter × 15 cm height) pre-equilibrated with 20 mM Hepes Tris pH 6.8, for removing the residual external (not taken up) radioactivity. The time course of [^{3}H]glutamine or [^{3}H]arginine efflux was then measured. Both uptake and efflux assays were carried out at 25 °C; transport was stopped by applying each sample on a Sephadex G75 column (0.6 × 8 cm) to separate the external from the internal radioactivity. Proteoliposomes eluted with 1 ml 50 mM NaCl were collected in scintillation cocktail for counting. The experimental values were analysed by subtracting to each sample the respective controls (blank) according to the stop inhibitor method [15]. In this procedure, the stop inhibitor $HgCl_2$ is added at time zero to proteoliposomes (blank) together with the radiolabelled substrate(s). The initial rate of transport was measured by stopping the reaction after 20 min, i.e., within the initial linear range of [^{3}H]glutamine or [^{3}H]arginine uptake into the proteoliposomes. Grafit 5.0.13 software was used to measure transport rate by first-order rate equation calculated as k × transport at equilibrium, to derive kinetic parameters using Michaelis-Menten and Hill equations and to measure IC_{50} values from dose-response analysis. The amount of reconstituted recombinant protein was estimated as previously described [3].

2.8. Homology modelling and docking of hSLC38A9 transporter

The homology structural model of the hSLC38A9 was built using the interactive mode on the SWISS-MODEL Workspace available at https://swissmodel.expasy.org/interactive. The structure of *D. rerio* SLC38A9 transporter (PDB 6C08) [11] was used as a template. The ligands (Arg and Gln) were downloaded from PubChem Database (https://pubchem.ncbi.nlm.nih.gov/#) and converted to PDB file format by using Openbabel software [16]. The ligands were prepared using ADT [17]. Gasteiger charge was assigned to the ligands that were saved in PDBQT format. AutoDock Vina was used for molecular docking studies [18]. The grid box size was set at 32, 32, and 36 Å for x, y, and z, respectively. The spacing between the grid points was 1.0 Å. The grid centre was set at −49.505, 37.334, and 63.076 Å for x, y, and z, respectively.

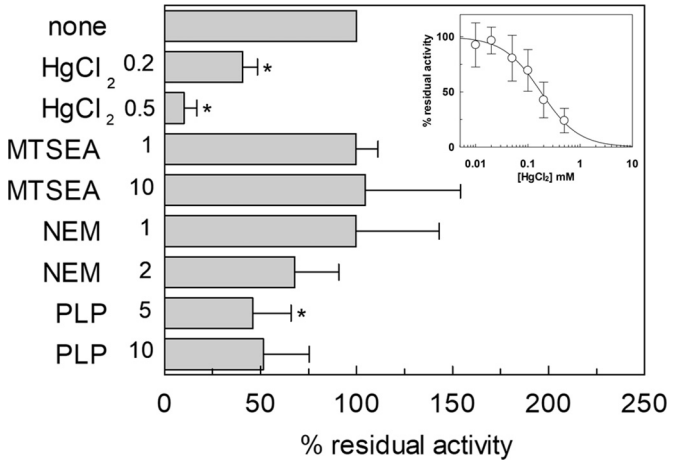

Fig. 2. Effect of inhibitors on hSLC38A9 transport activity. The reconstitution was performed as described in Materials and Methods. Transport was started by adding 100 μM [^{3}H]glutamine at time zero to proteoliposomes in the presence of $HgCl_2$ (0.2 and 0.5 mM), MTSEA (1 and 10 mM), NEM (1 and 2 mM), PLP (5 and 10 mM). The transport reaction was stopped after 30 min, as described in Materials and Methods. Transport activity was calculated as the percent of residual activity with respect to condition without any addition. In the inset, dose-response analysis for the inhibition of hSLC38A9-WT by $HgCl_2$. Transport was measured adding 100 μM [^{3}H]glutamine to proteoliposomes in the presence of indicated concentrations of $HgCl_2$. Transport activity was calculated as the percent of residual activity with respect to condition without any addition. Results are means ± SD of three different experiments. *significantly different from sample prepared without any addition (control) ex as estimated by Student's *t*-test ($P < 0.05$).

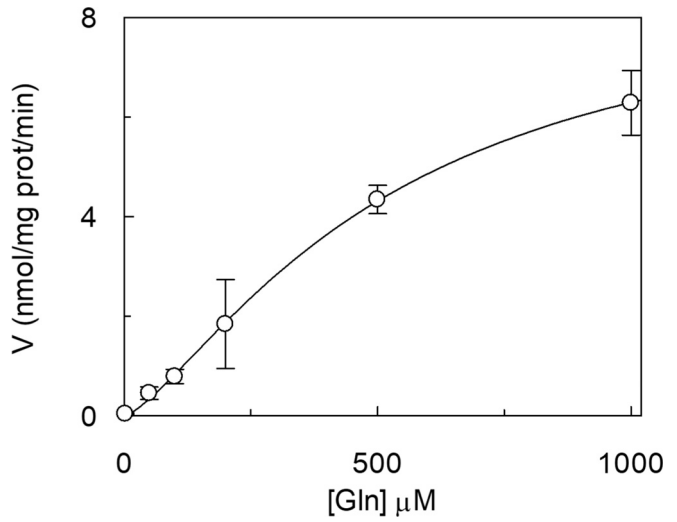

Fig. 3. Kinetics of hSLC38A9 glutamine transport. The reconstitution was performed as described in Materials and Methods. Transport was started by adding indicated concentrations of [^{3}H]glutamine at time zero to proteoliposomes and stopped after 20 min. Initial rates of transport are plotted vs glutamine concentration using non-linear fit Hill equation to evaluate external Km and cooperativity index. Results are means ± SD of three different experiments.

2.9. Other methods

Cholesteryl hemisuccinate (CHS) was solubilized in 20 mM Tris HCl pH 8.0 and 5% $C_{12}E_8$ by two sonication cycles of 2 min (no pulse, 40 W) with a Vibracell VCX-130 sonifier (SONICS) as previously suggested [19]. Solubilized CHS was added to liposome preparation under rotatory stirring (1200 rpm) at 23 °C for 30 min prior reconstitution to reach concentration of 75μg/ml.

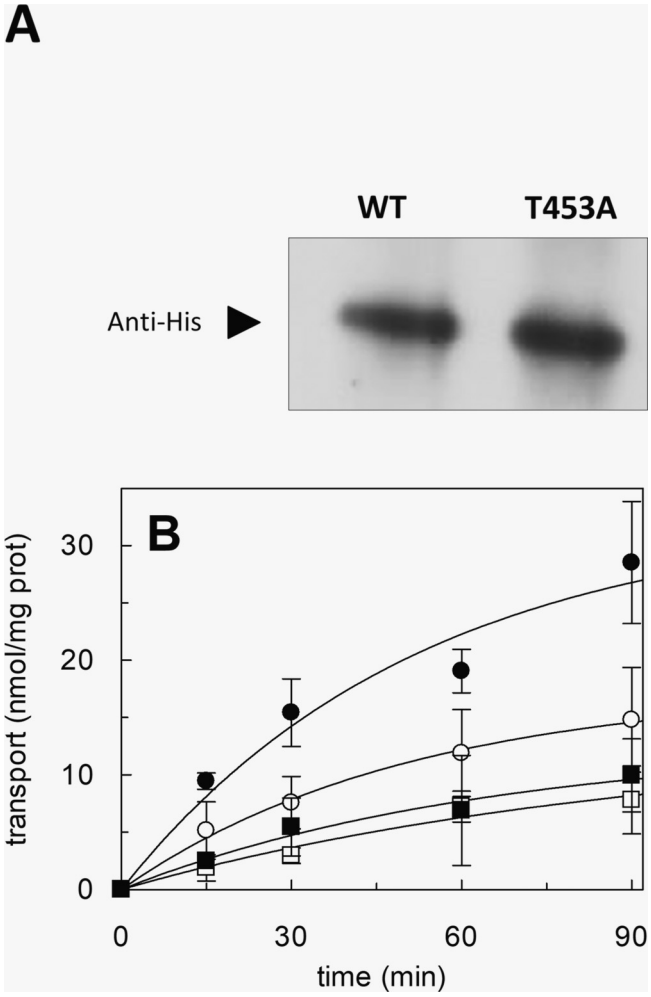

Fig. 4. Functional characterization of hSLC38A9-T453A mutant. (A) Western blotting analysis of purified WT and T453A mutant using anti-His antibody. (B) Time course analysis of WT and T453A mutant. The reconstitution was performed as described in Materials and Methods. Transport was started by adding 100 μM [^{3}H]glutamine at time zero and stopped at indicated times to proteoliposomes reconstituted with WT (○,●) or T453A (□, ■) purified in the presence of 50 mM NaCl (○,□) or 200 mM NaCl (●, ■). Data are plotted using first order rate equation. Results are means ± SD of three different experiments.

3. Results

3.1. Inhibition and kinetic characterization of WT hSLC38A9

The inhibition of transport activity mediated by the hSLC38A9 has been investigated in proteoliposomes reconstituted with the recombinant protein produced in *E. coli*. Different reagents have been tested on [^{3}H]glutamine uptake in proteoliposomes as shown in Fig. 2. The SH reagents NEM, MTSEA and $HgCl_2$ have been used exploiting the presence of 12 cysteine residues in the structure of hSLC38A9. The hydrophilic MTSEA failed to inhibit transport, while $HgCl_2$ strongly inhibited glutamine uptake, with an IC_{50} value of 176 ± 30 μM (inset of Fig. 2). The membrane-permeable NEM was a poor inhibitor with 40% inhibition at 2 mM. The lysine reagent PLP also inhibited hSLC38A9-mediated transport (8. 2). Based on the described data, the mercury compound, which exhibited a higher efficiency of inhibition, was used in the following experiments as stop-inhibitor for kinetic measurements. The dependence of transport rate on the external glutamine concentration (Fig. 3) shows a cooperative behaviour with a $K_{0.5}$ of 518 ± 58 μM, a positive cooperativity index (Hill coefficient) of 1.4 ± 0.079 and a V_{max} of 8.8 ± 0.57 nmol · mg prot^{-1} · min^{-1}.

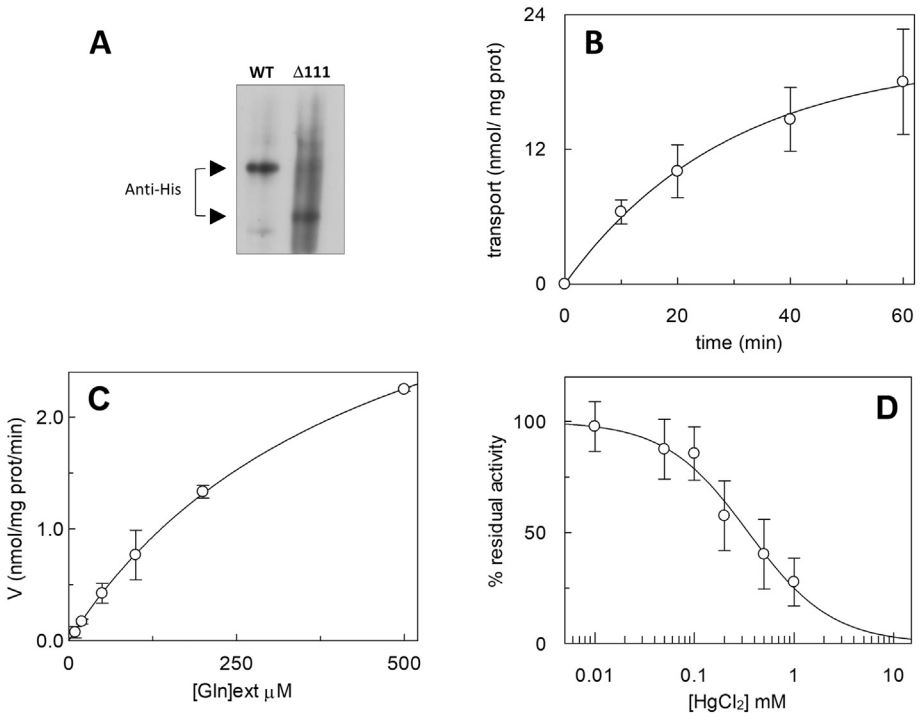

Fig. 5. Functional characterization of hSLC38A9-Δ111 mutant. (A) Western blotting analysis of purified WT and Δ111 mutant using anti-His antibody as described in Materials and Methods. (B) Time course analysis of WT and Δ111. The reconstitution was performed as described in Materials and Methods. Transport was started by adding 100 μM [^{3}H]glutamine at time zero and stopped at indicated times to proteoliposomes reconstituted with Δ111 (○). (C) Kinetics of Δ111 transport. Transport was started by adding indicated concentrations of [^{3}H]glutamine at time zero and stopped after 20 min. Initial rates of transport are plotted vs glutamine concentration using non-linear fit Michaelis Menten equation to evaluate external Km. (D) Dose-response analysis for the inhibition of hSLC38A9-Δ111 mutant reconstituted in proteoliposomes by $HgCl_2$. Transport was measured adding 100 μM [^{3}H]glutamine to proteoliposomes in the presence of indicated concentrations of $HgCl_2$. Transport activity was calculated as the percent of residual activity with respect to condition without any addition. Results are means ± SD of three different experiments.

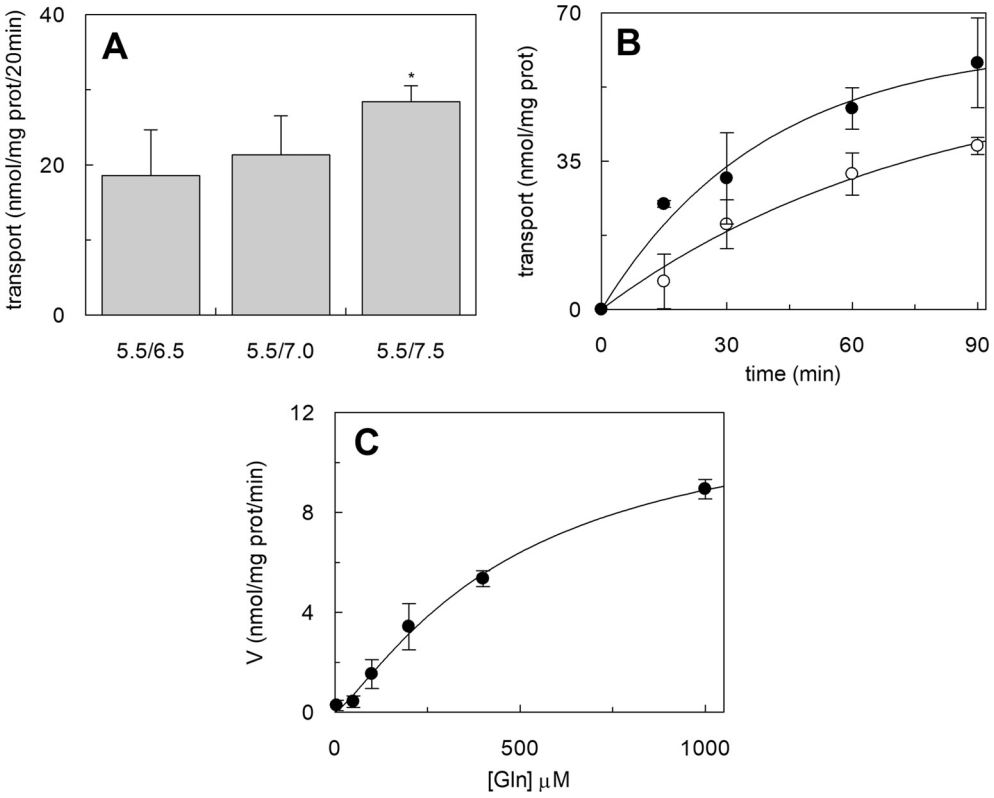

Fig. 6. Regulation of glutamine transport mediated by WT hSLC38A9 reconstituted in proteoliposomes. The reconstitution was performed as described in Materials and Methods. (A) Transport was started by adding 100 μM [^{3}H]glutamine at time zero to proteoliposomes reconstituted with buffers at the indicated internal/external pH. Transport was stopped after 20 min. (B) Transport was started adding 100 μM [^{3}H] glutamine at time zero and stopped at indicated times to proteoliposomes prepared in the absence (○) or presence (●) of cholesteryl hemisuccinate. (C) Kinetics of glutamine transport in the presence of cholesteryl hemisuccinate. Transport was started by adding indicated concentrations of [^{3}H] glutamine at time zero to proteoliposomes and stopped after 20 min. Initial rates of transport are plotted vs glutamine concentration using non-linear fit Hill equation to evaluate external Km and cooperativity index. In (A), *significantly different from sample prepared without any addition (control) ex as estimated by Student's *t*-test ($P < 0.05$). Results are means ± SD of three different experiments.

3.2. Identification and characterization of the putative Na^+ binding site

As stated in the introduction, the effect of Na^+ in stimulating glutamine transport by human SLC38A9 was previously demonstrated and a Na^+ binding residue was identified [3]. The alignment of Fig. 1 highlights the presence of another putative residue participating in the Na^+ binding, i.e. the T453 in line with previous results [5,20]. Thus, the site-directed mutant T453A was constructed and the corresponding recombinant protein was produced in *E. coli* and purified for functional assay as described in Materials and Methods section (Fig. 4A). To evaluate the response to Na^+, both WT and T453A were reconstituted in proteoliposomes containing 50 or 200 mM NaCl in the internal compartment. As shown in Fig. 4B, the WT transporter exhibited a higher transport activity in the presence of internal 200 mM NaCl with respect to the condition of 50 mM internal NaCl, in agreement with previous data [3]. The T453A mutant showed nearly no stimulation by

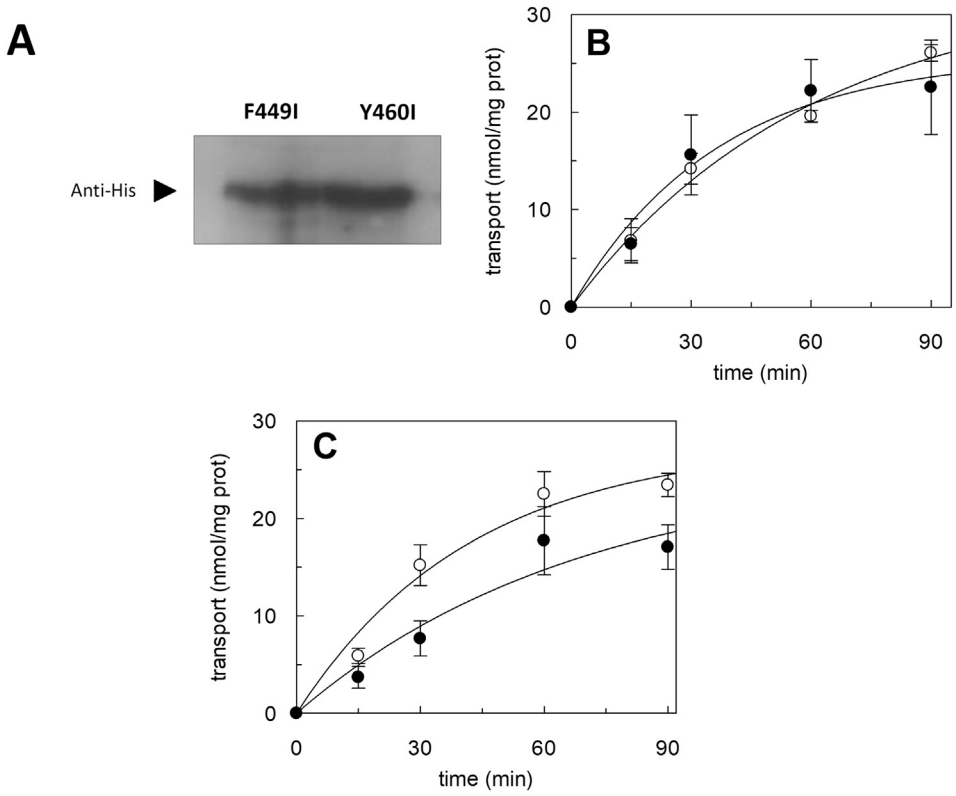

Fig. 7. Functional characterization of hSLC38A9-F449I and Y460I mutants. (A) Western blotting analysis of F449I and Y460I mutants using anti-His antibody. Time course analysis of F449I (B) and Y460I (C) mutants. The reconstitution was performed as described in Materials and Methods. Transport was started by adding 100 μM [^{3}H]glutamine at time zero and stopped at indicated times to proteoliposomes prepared in the absence (○) or presence (●) of cholesteryl hemisuccinate. Data are plotted using first order rate equation. Results are means ± SD of three different experiments.

increasing the concentration of intraliposomal NaCl, demonstrating that, indeed, T453 is involved in the interaction with Na^+, as well. Noteworthy, from time course analysis the measurement of initial transport rate revealed that intraliposomal Na^+ was able to double the rate of WT, leaving unaltered that of T453A (Fig. 4B). It has to be stressed that if Na^+ was omitted from the purification buffer, the transport protein was nearly inactive both in the case of the WT and the mutant.

3.3. Characterization of Δ111 mutant

The hSLC38A9 protein has an N-terminus tail (Fig. 1) responsible for interaction with the mTORC1 complex [3,5]. To ascertain whether this protein moiety plays any role in the intrinsic transport function, a truncated protein, lacking of the first 111 amino acids, was produced in *E. coli* and purified for functional assay as described in Materials and Methods section (Fig. 5A). This deletion mutant mediated uptake of glutamine with an activity comparable to that of WT indicating that the N-terminus portion does not affect its intrinsic transport properties (Fig. 5B and see Fig. 4B). To further confirm this analysis, kinetics was also studied. Interestingly, the data points obtained studying the dependence of the transport rate on the glutamine concentration, fitted a Michaelis Menten equation, thus corresponding to a non-cooperative behaviour. The external Km for glutamine, derived from this experiment was 455 ± 18 μM, which is similar to the $K_{0.5}$ of WT (Fig. 5C). The same results applied to the inhibition exerted by $HgCl_2$ (Fig. 5D); in this case, IC_{50} value of 348 ± 120 μM was measured.

3.4. Effect of pH and cholesterol on glutamine uptake

The SLC38A9 is localized in the lysosomal membrane where a gradient of pH is maintained thanks to the activity of V-ATPase [21]. Thus, the effect of pH on glutamine transport mediated by hSLC38A9 was investigated. The uptake of glutamine in proteoliposomes was stimulated in the presence of a pH gradient of about 2.0 units (pH 5.5. inside/pH 7.5 outside; Fig. 6A). This corresponds to the physiological condition in which the pH in the internal lysosomal compartment is acidic [22]. This conclusion can be drawn on the basis of the right-side-out orientation of the transporter that is inserted in the proteoliposomes as in the native membrane [3]. Cholesterol is an essential component of the lysosomal membrane and mTORC1 regulates the synthesis of fatty acids and sterols [23]. It has been previously shown that hSLC38A9 is required for mTORC1 activation by cholesterol [8]. Indeed, hSLC38A9 harbours in its primary structure a CARC motif followed by CRAC a motif, which are acknowledged cholesterol-binding sequences (Fig. 1) [8]. Thus, cholesterol, in the form of Cholesteryl HemiSuccinate (CHS), was added to the liposomal membrane and its effect on glutamine transport was evaluated. As shown in Fig. 6B, the transport was stimulated with respect to the control, without added CHS. The effect of cholesterol was evaluated in terms of kinetics as reported in Fig. 6C: in line with data reported in the time course, only Vmax is increased by roughly 35% (12.4 ± 1.9 nmol · mg prot^{-1} · min^{-1}) while no variations of $K_{0.5}$ (476 ± 144 μM) and Hill coefficient (1,3 ± 0.2) were observed. The key residues, i.e. F449 and Y460, in CARC and CRAC motifs (Fig. 1), were substituted by isoleucine and the mutant proteins were over-expressed in *E. coli* and purified (Fig. 7A). The effect of cholesterol on the glutamine transport activity of reconstituted proteins was evaluated (Fig. 7B and C): no stimulation was observed for the two mutants, confirming that F449 and Y460 are involved in the interaction with cholesterol.

3.5. Transport of arginine mediated by hSLC38A9

It was previously demonstrated that hSLC38A9 is also able to mediate arginine transport [3,4,10]. Arginine uptake could be measured in proteoliposomes with an efficiency comparable to that of glutamine; however, differently from glutamine, arginine uptake showed a scarce sensitivity to ΔpH (Fig. 8A). Kinetics was conducted and, similarly to glutamine kinetics, a cooperative behaviour was observed with a Km of 2.7 ± 0.83 mM and a Hill coefficient of

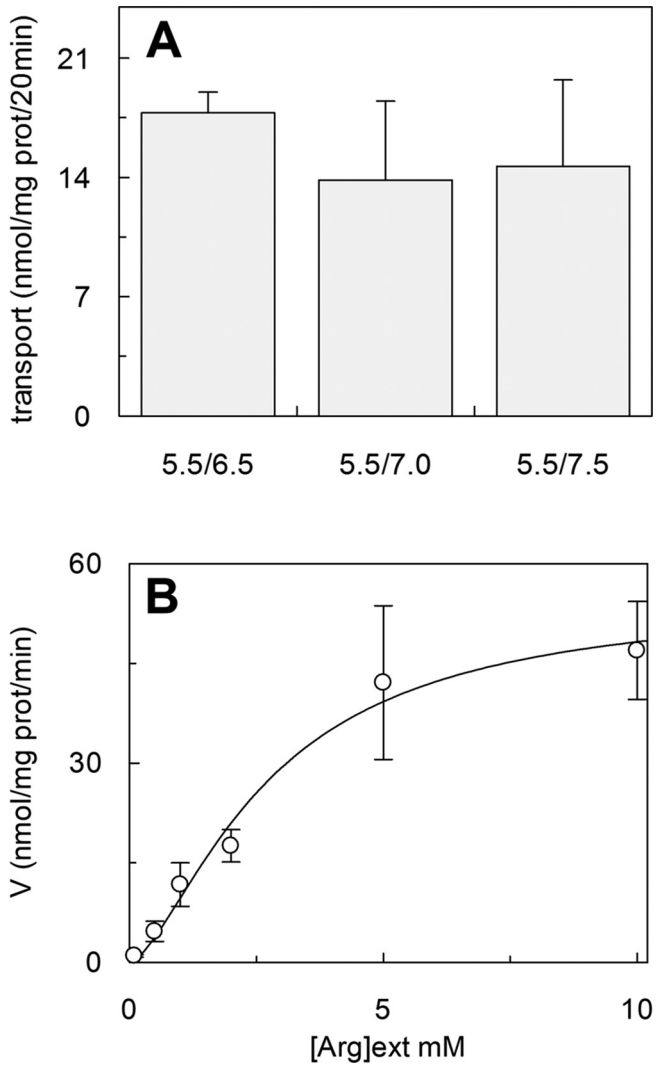

Fig. 8. Regulation of arginine transport mediated by WT hSLC38A9 reconstituted in proteoliposomes. The reconstitution was performed as described in Materials and Methods. (A) Transport was started by adding 100 μM [^{3}H]arginine at time zero to proteoliposomes reconstituted with buffers at the indicated internal/external pH. Transport was stopped after 20 min. (B) Kinetics of arginine transport. Transport was started by adding indicated concentrations of [^{3}H]arginine at time zero and stopped after 20 min. Initial rates of transport are plotted vs arginine concentration using non-linear fit Hill equation to evaluate external Km and cooperativity index. Results are means ± SD of three different experiments.

1.5 ± 0.38 (Fig. 8B). The measured $K_{0.5}$ value for arginine is higher than that for glutamine correlating with previous reports highlighting that arginine is a lower affinity substrate [4,10]. Effect of cholesterol was also evaluated on arginine transport and, as shown in Fig. 9, the presence of cholesterol stimulates arginine uptake, as well. According to the physiological function of SLC38A9 in vivo, this transporter may mediate efflux of amino acids across the lysosomal membrane [10]. Thus, the efflux of both glutamine and arginine was measured (Fig. 10A). Interestingly, a different behaviour was observed between the two substrates: while hSLC38A9 efficiently mediates glutamine efflux, the arginine efflux was poor. These results suggested that different mechanisms of transport might occur for the two amino acids. The biological significance of amino acids efflux has been suggested to rely on the presence of arginine in the lysosomal compartment. Therefore, glutamine efflux was measured in the presence of arginine in the intraliposomal (intralysosomal) compartment (Fig. 10B); in this condition, the efflux of glutamine was stimulated. The reciprocal inhibition

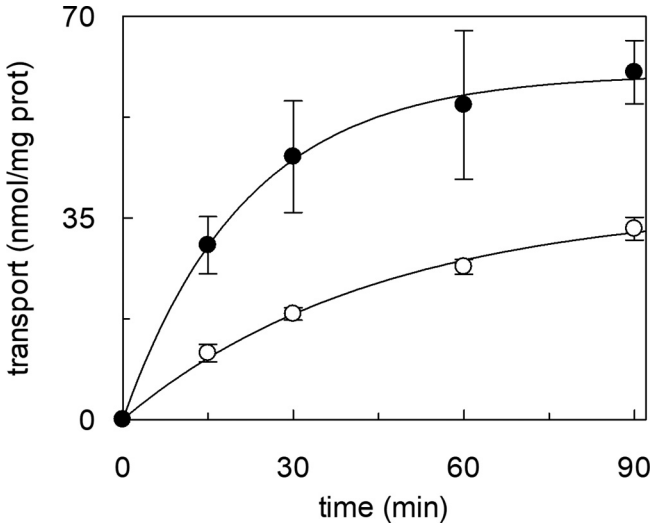

Fig. 9. Effect of cholesterol on arginine transport by WT hSLC38A9 reconstituted in proteoliposomes. The reconstitution was performed as described in Materials and Methods. Transport was started adding 100 μM [^{3}H]arginine at time zero and stopped at indicated times to proteoliposomes prepared in the absence (○) or presence (●) of cholesteryl hemisuccinate. Results are means ± SD of three different experiments.

of glutamine and arginine transport was evaluated (Fig. 11A and B). Interestingly, arginine did not inhibit glutamine uptake up to 10 mM concentration (Fig. 11A) while glutamine, at high concentration, is able to cause inhibition of arginine transport (Fig. 11B).

3.6. Homology modelling of hSLC38A9 and docking of substrates

As stated in the introduction, the 3D structure of drSLC38A9 that shares 61.9% identity with hSLC38A9, has been recently solved [11]. Therefore, the homology model of hSLC38A9 has been built on the basis of drSLC38A9 (PDB 6C08) as shown in Fig. 12. The structure of drSLC38A9 lacks of 185 out of 549 amino acids corresponding to about 28% of the human amino acid sequence. The two substrates, arginine and glutamine (Fig. 12), have been positioned in the homology model. Interestingly, the two amino acids bind to regions that do not perfectly overlap. This result may suggest the existence of two alternative binding sites of hSLC38A9 presumably with different affinities in line with kinetics and lack of reciprocal inhibition data.

4. Discussion

The localization of hSLC38A9 in the intracellular lysosomal membrane and its interaction with many other proteins hampered the possibility of studying the transport role in intact cells. Therefore, the most suitable strategy to dissect the transport function of hSLC38A9 was the reconstitution of the recombinant protein into proteoliposomes. In this experimental model, the sole hSLC38A9 protein is inserted into the membrane in the absence of interactors and with the same orientation as in the lysosomal membrane, previously demonstrated by combining western-blotting with protease cleavage analysis [3]. In line with these premises, the available information on transport features of hSLC38A9 derives from studies conducted in proteoliposomes [3,4,10]. Therefore, it was extremely interesting to better characterize the transport mediated by this protein. In this work, we dealt with inhibition studies, the kinetics of glutamine and arginine, direct assay of efflux activity and some regulatory aspects. Glutamine transport revealed to be blockable by the mercurial agent $HgCl_2$. The inhibition correlates well with the presence of at least one cysteine residue (C375) of the protein close to the predicted glutamine binding site (Fig. 12B). However, it is likely that other cysteine residues are also involved in the inhibition since the

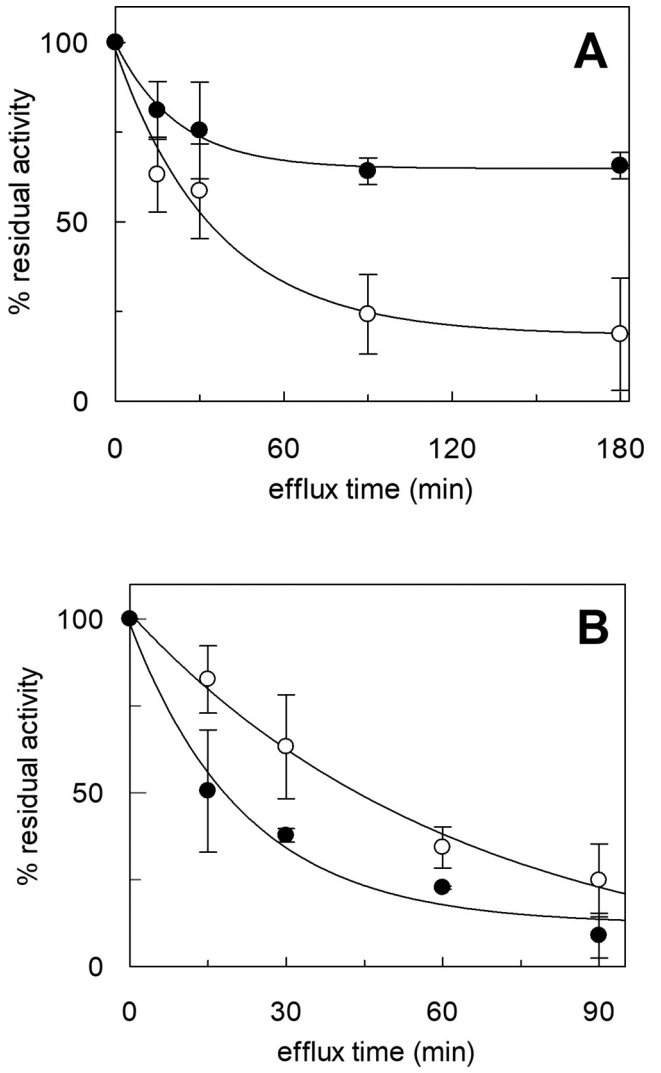

Fig. 10. Efflux of arginine and glutamine by WT hSLC38A9 reconstituted in proteoliposomes. The reconstitution was performed as described in Materials and Methods. (A) Efflux of [^{3}H]arginine (●) or [^{3}H]glutamine (○) from proteoliposomes reconstituted with hSLC38A9. (B) Efflux of [^{3}H]glutamine in the absence (○) or presence (●) of 0.2 mM intraliposomal arginine. In (A) and (B) the efflux is measured as described in Materials and Methods at indicated times. Data are calculated as the percent of residual activity with respect to the control sample (efflux time zero). Results are means ± SD of three different experiments.

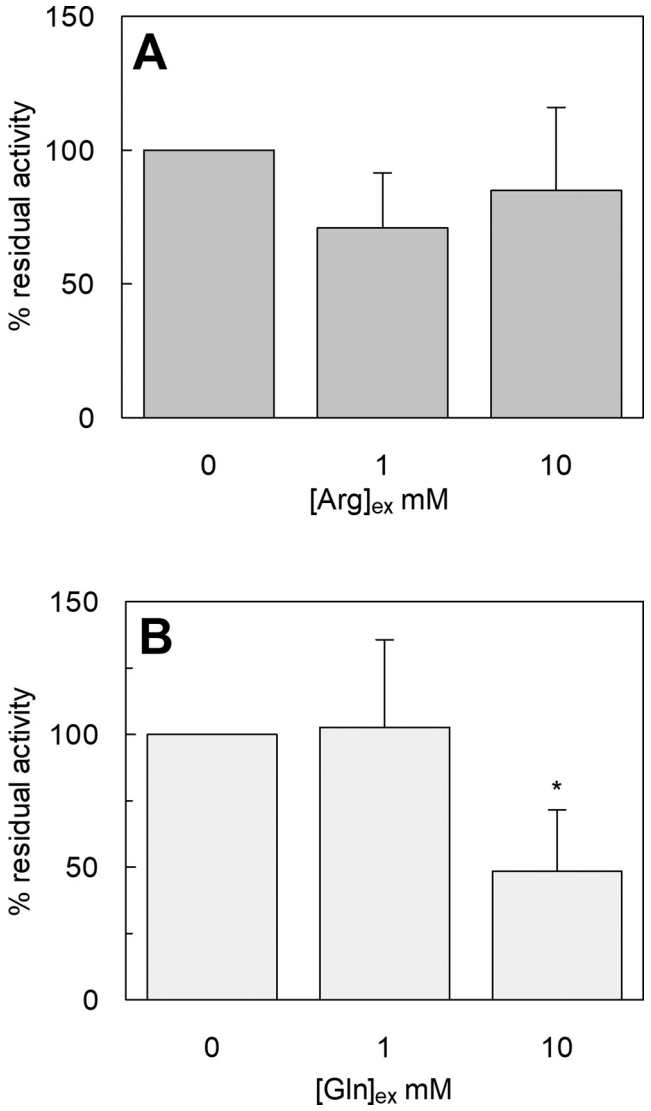

Fig. 11. Inhibition experiments on WT hSLC38A9 reconstituted in proteoliposomes. (A) Reciprocal inhibition of glutamine transport. Transport was started by adding 100 μM of [^{3}H]glutamine at time zero in the presence of 1 mM or 10 mM of unlabelled arginine. (B) Reciprocal inhibition of arginine transport. Transport was started by adding 100 μM of [^{3}H]arginine at time zero in the presence of 1 mM or 10 mM of unlabelled glutamine. In (A) and (B) transport was stopped after 30 min. Data are calculated as the percent of residual activity with respect to sample without any addition. Results are means ± SD of three different experiments. *significantly different from the control sample (without any addition) as estimated by Student's t-test ($P < 0.05$).

protein possesses 12 cysteine residues. Indeed, the mutant Δ111, which lacks of 2 out of the 12 cysteines, shows a lower affinity for $HgCl_2$ with respect to the WT protein. The alkylating reagent NEM is much less effective in inhibiting glutamine transport. This could be ascribed to a scarce and/or slow reactivity of the cysteine(s) towards alkylation with respect to the formation of the metal-sulfur bond. The strong and fast inhibition exerted by $HgCl_2$ was exploited to efficiently stop the transport for kinetic measurements. This gives the advantage of improving the kinetic resolution compared to the previous studies in which transport was stopped by radioactive substrate removal [3,4,10] which is not as fast as the inhibitor stop procedure [24,25]. The hSLC38A9 catalyzes glutamine uptake and efflux, according to previous findings [3]. The external Km for glutamine was measured for the first time and the obtained value is in the range of the physiological concentrations of this amino acid in the cytoplasm (up to 0.8 mM), thus indicating that the transporter can potentially catalyze the flux of glutamine in the two directions. Interestingly, the catalytic constant is 0.5 min^{-1}, which is lower than that of other transporters [26,27]. However, for most transporters, only the Vmax is available, not the kcat. The Vmax of hSLC38A9 is also lower than that measured for other purified and reconstituted transporters [28,29]. It is not possible to compare the Vmax (kcat) data with transporters assayed in intact cells since the calculation of their specific activity is influenced by the presence of other proteins. Taken together our data supports the role of hSLC38A9 in mediating sensing rather than the abundant flux of amino acids, that is probably performed by other high capacity transporters [30]. Differently from glutamine, the Km for arginine is in the millimolar range, similar to that previously reported for the same substrate [10]. Even though the Vmax for arginine is higher than that for glutamine, the data indicates that arginine uptake in vivo is unlike since the average concentration of arginine in cells is much lower than the Km of the hSLC38A9 for this substrate [31]. At difference with

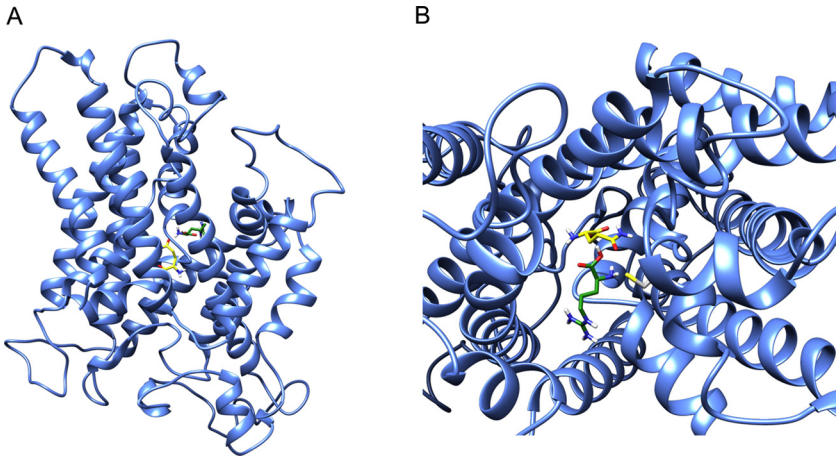

Fig. 12. Homology structural model of the hSLC38A9 transporter. Side view (A) and top view (B) of the hSLC38A9 homology model. Arginine depicted in green or glutamine depicted in yellow is positioned in the binding center. (B) C375 as a hypothetical mercurial binding residue is highlighted in stick.

glutamine, our direct measurements show that the transporter catalyzes a scarce, if any, efflux of arginine. Thus, the efflux of arginine is unlikely to occur in vivo reinforcing the idea of an involvement of arginine in regulating the transport of other essential amino acids by hSLC38A9 [10]. On the contrary, arginine was shown to stimulate the efflux of glutamine demonstrating the hypothesis that arginine plays a modulatory function from the internal side of the protein that corresponds to the intralysosomal compartment. Furthermore, the different kinetics of glutamine and arginine also correlates with the absence of inhibitory effect of arginine on the transport of glutamine, while, some inhibition of glutamine on arginine transport is observed at glutamine concentration higher than the Km of hSLC38A9 for arginine. These results could be interpreted in light of the prediction of different binding sites for arginine and glutamine (Fig. 12). In this respect, hSLC38A9 reflects some transport features of SLC38A7, in which arginine was not able to inhibit glutamine uptake [32]. This finding also correlates with homology modelling and docking showing that the predicted site of glutamine is different from that of arginine, positioned according to the previous data on drSLC38A9 [11]. As already mentioned, an important aspect of hSLC38A9 biology is its dual function as transporter and receptor for sensing nutrient sufficiency to regulate the mTORC1 pathway that relies on the presence of the N-terminus tail [3,4]. Interestingly, the glutamine uptake in proteoliposomes is fully active in the deletion mutant (Δ111); this finding confirms that the N-terminus tail plays its role in interacting with mTORC1 rather than in the intrinsic transport activity of the hSLC38A9, as previously suggested [3]. This is in line with the recent finding showing that the N-terminus tail is not required for uptake of arginine and leucine [10,11,33]. However, an interesting novelty is the different kinetic behaviour between the deletion mutant (Δ111) and the wild type hSLC38A9. While the Km values are similar, the Δ111 mutant loses cooperativity suggesting that the N-terminus tail has some role in transport regulation, probably conserved across evolution [11,33]. In this respect, a complex model in which the N-terminus tail acts as a plug regulated by arginine availability has been proposed for drSLC38A9 [33]. Interestingly, the presence of alternative binding sites is common also to other transporters, i.e. LeuT, SERT, DAT and B^0AT1 [10,29,34,35], which have two distinct binding sites, one for the transported molecule and another for a modulatory molecule.

Glutamine, but not arginine uptake, is stimulated by internal acidic pH, i.e. under conditions mimicking the physiological context. This finding is again in agreement with a lower, if any, contribution of hSLC38A9 in transporting arginine. Internal sodium, close to the intralysosomal level, stimulates glutamine uptake, as previously shown [3]. The interaction of sodium with the protein is mediated by, at least, two residues as demonstrated by the loss of sodium stimulation in site-directed mutants. The first residue, N128, has been previously identified [3]. The second, T453, was described in this work. Both residues are homologues to those conserved in the SLC38 family (Fig. 1). The mutation at T453 residue only slightly impairs the glutamine uptake but abolishes the responsiveness to intraliposomal, i.e. intralysosomal, Na^+ mediated by hSLC38A9 suggesting a modulatory function of Na^+ rather than a direct involvement in the transport cycle. This finding smooths the distinction of hSLC38A9 as belonging to system A or N as already described for the other lysosomal transporter, i.e. SLC38A7 specific for both glutamine and asparagine [30]. This correlates with the much lower identity among A9 and the other SLC38 members (Fig. 1). Another regulatory property, that is the effect of cholesterol, was investigated; in the recent years, in fact, modulation by cholesterol has been reported for other transporters, even though the studies are still not completed and effects are not always the same in the different proteins [36–38]. The use of cholesterol-like lipids has been also employed to dissect the precise effect of cholesterol; however, also in this case, studies are still at infancy. In line with the presence of CRAC and CARC motifs in the structure of hSLC38A9, the addition of cholesterol to the proteoliposomes stimulates the uptake of glutamine and arginine demonstrating that, besides the effect on mTOR regulation [8], cholesterol has also a direct effect on the intrinsic transport activity affecting the Vmax but not the Km of hSLC38A9 for glutamine. The mutation of two key residues for CARC and CRAC motif abolished cholesterol effect, confirming that the molecule binds to these regions, as previously proposed [8]. Therefore, it can be concluded that the modulatory effect of cholesterol on the receptor function of hSLC38A9 is exerted through to the activation of its transport function.

5. Conclusions

In this work, we improved the molecular knowledge of the transport function of hSLC38A9 by using the recombinant protein produced in *E. coli*, site-directed mutagenesis and transport assay in proteoliposomes. As previously proposed, we have assessed that hSLC38A9 is a low-capacity transporter confirming that its transport function is important for mediating the local flux of small amount of amino acids compatible with a sensing role, for activating mTORC1 to the lysosomal membrane. The transport activity is modulated by cholesterol potentially explaining the previously described action of this lipid on the activation of mTORC1. Altogether, the results described in this work support the classification of hSLC38A9 as a transceptor, i.e. a transporter with a receptor function, crucial for mTOR activation. Due to this role, hSLC38A9 is considered a potential target for several human diseases. Therefore, the knowledge of the regulatory aspects related to its transport function may give additional clues, which may be relevant to human health.

Transparency document

The Transparency document associated with this article can be found, in online version.

Acknowledgements

This work was supported by grant from Italian MIUR, Ministero dell'Istruzione, dell'Università e della Ricerca [PON01_00937 to C.I.], the Austrian Academy of Sciences (G.S.-F.) and the European Research Council (ERC AdG 695214 G.S.-F, M.R).

References

[1] S. Broer, The SLC38 family of sodium-amino acid co-transporters, Pflugers Arch. - Eur. J. Physiol. 466 (2014) 155–172.
[2] H.B. Schioth, S. Roshanbin, M.G. Hagglund, R. Fredriksson, Evolutionary origin of amino acid transporter families SLC32, SLC36 and SLC38 and physiological, pathological and therapeutic aspects, Mol. Asp. Med. 34 (2013) 571–585.
[3] M. Rebsamen, L. Pochini, T. Stasyk, M.E. de Araujo, M. Galluccio, R.K. Kandasamy, B. Snijder, A. Fauster, E.L. Rudashevskaya, M. Bruckner, S. Scorzoni, P.A. Filipek, K.V. Huber, J.W. Bigenzahn, L.X. Heinz, C. Kraft, K.L. Bennett, C. Indiveri, L.A. Huber, G. Superti-Furga, SLC38A9 is a component of the lysosomal amino acid sensing machinery that controls mTORC1, Nature 519 (2015) 477–481.
[4] S. Wang, Z.Y. Tsun, R.L. Wolfson, K. Shen, G.A. Wyant, M.E. Plovanich, E.D. Yuan, T.D. Jones, L. Chantranupong, W. Comb, T. Wang, L. Bar-Peled, R. Zoncu, C. Straub, C. Kim, J. Park, B.L. Sabatini, D.M. Sabatini, Metabolism. Lysosomal amino acid transporter SLC38A9 signals arginine sufficiency to mTORC1, Science 347 (2015) 188–194.
[5] Z. Zhang, A. Gameiro, C. Grewer, Highly conserved asparagine 82 controls the interaction of Na+ with the sodium-coupled neutral amino acid transporter SNAT2, J. Biol. Chem. 283 (2008) 12284–12292.
[6] R.L. Wolfson, D.M. Sabatini, The Dawn of the age of amino acid sensors for the mTORC1 pathway, Cell Metab. 26 (2017) 301–309.
[7] R.A. Saxton, D.M. Sabatini, mTOR signaling in growth, metabolism, and disease, Cell 168 (2017) 960–976.
[8] B.M. Castellano, A.M. Thelen, O. Moldavski, M. Feltes, R.E. van der Welle, L. Mydock-McGrane, X. Jiang, R.J. van Eijkeren, O.B. Davis, S.M. Louie, R.M. Perera, D.F. Covey, D.K. Nomura, D.S. Ory, R. Zoncu, Lysosomal cholesterol activates mTORC1 via an SLC38A9-Niemann-pick C1 signaling complex, Science 355 (2017) 1306–1311.
[9] K. Shen, D.M. Sabatini, Ragulator and SLC38A9 activate the Rag GTPases through noncanonical GEF mechanisms, Proc. Natl. Acad. Sci. U. S. A. 115 (2018) 9545–9550.
[10] G.A. Wyant, M. Abu-Remaileh, R.L. Wolfson, W.W. Chen, E. Freinkman, L.V. Danai, M.G. Vander Heiden, D.M. Sabatini, mTORC1 activator SLC38A9 is required to efflux essential amino acids from lysosomes and use protein as a nutrient, Cell 171 (2017) 642–654 (e612).
[11] H.T. Lei, J. Ma, S. Sanchez Martinez, T. Gonen, Crystal structure of arginine-bound lysosomal transporter SLC38A9 in the cytosol-open state, Nat. Struct. Mol. Biol. 25 (2018) 522–527.
[12] M. Galluccio, L. Pochini, L. Amelio, R. Accardi, M. Tommasino, C. Indiveri, Over-expression in E. coli and purification of the human OCTN1 transport protein, Protein Expr. Purif. 68 (2009) 215–220.
[13] M. Galluccio, L. Pochini, V. Peta, M. Ianni, M. Scalise, C. Indiveri, Functional and molecular effects of mercury compounds on the human OCTN1 cation transporter: C50 and C136 are the targets for potent inhibition, Toxicol. Sci. 144 (2015) 105–113.
[14] C. Indiveri, G. Prezioso, T. Dierks, R. Kramer, F. Palmieri, Kinetic characterization of the reconstituted dicarboxylate carrier from mitochondria: a four-binding-site sequential transport system, Biochim. Biophys. Acta 1143 (1993) 310–318.
[15] N. Giangregorio, A. Tonazzi, L. Console, C. Indiveri, Post-translational modification by acetylation regulates the mitochondrial carnitine/acylcarnitine transport protein, Mol. Cell. Biochem. 426 (2017) 65–73.
[16] N.M. O'Boyle, M. Banck, C.A. James, C. Morley, T. Vandermeersch, G.R. Hutchison, Open babel: an open chemical toolbox, J. Cheminform. 3 (2011) 33.
[17] G.M. Morris, R. Huey, W. Lindstrom, M.F. Sanner, R.K. Belew, D.S. Goodsell, A.J. Olson, AutoDock4 and AutoDockTools4: automated docking with selective receptor flexibility, J. Comput. Chem. 30 (2009) 2785–2791.
[18] O. Trott, A.J. Olson, AutoDock Vina: improving the speed and accuracy of docking with a new scoring function, efficient optimization, and multithreading, J. Comput. Chem. 31 (2010) 455–461.
[19] M.A. Hanson, V. Cherezov, M.T. Griffith, C.B. Roth, V.P. Jaakola, E.Y. Chien, J. Velasquez, P. Kuhn, R.C. Stevens, A specific cholesterol binding site is established by the 2.8 A structure of the human beta2-adrenergic receptor, Structure 16 (2008) 897–905.
[20] Z. Zhang, T. Albers, H.L. Fiumera, A. Gameiro, C. Grewer, A conserved Na(+) binding site of the sodium-coupled neutral amino acid transporter 2 (SNAT2), J. Biol. Chem. 284 (2009) 25314–25323.
[21] R. Zoncu, L. Bar-Peled, A. Efeyan, S. Wang, Y. Sancak, D.M. Sabatini, mTORC1 senses lysosomal amino acids through an inside-out mechanism that requires the vacuolar H(+)-ATPase, Science 334 (2011) 678–683.
[22] M.E. Finbow, M.A. Harrison, The vacuolar H+-ATPase: a universal proton pump of eukaryotes, Biochem. J. 324 (Pt 3) (1997) 697–712.
[23] A. Efeyan, W.C. Comb, D.M. Sabatini, Nutrient-sensing mechanisms and pathways, Nature 517 (2015) 302–310.
[24] F. Palmieri, M. Klingenberg, Direct methods for measuring metabolite transport and distribution in mitochondria, Methods Enzymol. 56 (1979) 279–301.
[25] N. Giangregorio, F. Palmieri, C. Indiveri, Glutathione controls the redox state of the mitochondrial carnitine/acylcarnitine carrier Cys residues by glutathionylation, Biochim. Biophys. Acta 1830 (2013) 5299–5304.
[26] C. Indiveri, A. Tonazzi, G. Prezioso, F. Palmieri, Kinetic characterization of the reconstituted carnitine carrier from rat liver mitochondria, Biochim. Biophys. Acta 1065 (1991) 231–238.
[27] C. Indiveri, L. Palmieri, F. Palmieri, Kinetic characterization of the reconstituted ornithine carrier from rat liver mitochondria, Biochim. Biophys. Acta 1188 (1994) 293–301.
[28] L. Pochini, M. Scalise, M. Galluccio, G. Pani, K.A. Siminovitch, C. Indiveri, The human OCTN1 (SLC22A4) reconstituted in liposomes catalyzes acetylcholine transport which is defective in the mutant L503F associated to the Crohn's disease, Biochim. Biophys. Acta 1818 (2012) 559–565.
[29] L. Pochini, A. Seidita, C. Sensi, M. Scalise, I. Eberini, C. Indiveri, Nimesulide binding site in the B0AT1 (SLC6A19) amino acid transporter. Mechanism of inhibition revealed by proteoliposome transport assay and molecular modelling, Biochem. Pharmacol. 89 (2014) 422–430.
[30] Q. Verdon, M. Boonen, C. Ribes, M. Jadot, B. Gasnier, C. Sagne, SNAT7 is the primary lysosomal glutamine exporter required for extracellular protein-dependent growth of cancer cells, Proc. Natl. Acad. Sci. U. S. A. 114 (2017) E3602–E3611.
[31] L.A. Cynober, Plasma amino acid levels with a note on membrane transport: characteristics, regulation, and metabolic significance, Nutrition 18 (2002) 761–766.
[32] M.G. Hagglund, S. Sreedharan, V.C. Nilsson, J.H. Shaik, I.M. Almkvist, S. Backlin, O. Wrange, R. Fredriksson, Identification of SLC38A7 (SNAT7) protein as a glutamine transporter expressed in neurons, J. Biol. Chem. 286 (2011) 20500–20511.
[33] J.L. Ma, HT; Gonen, T., A conformational change in the N terminus of SLC38A9 signals mTORC1 activation, bioRxiv, (2018).
[34] H.A. Neubauer, C.G. Hansen, O. Wiborg, Dissection of an allosteric mechanism on the serotonin transporter: a cross-species study, Mol. Pharmacol. 69 (2006) 1242–1250.
[35] S.K. Singh, A. Yamashita, E. Gouaux, Antidepressant binding site in a bacterial homologue of neurotransmitter transporters, Nature 448 (2007) 952–956.
[36] D. Dickens, G.N. Chiduza, G.S. Wright, M. Pirmohamed, S.V. Antonyuk, S.S. Hasnain, Modulation of LAT1 (SLC7A5) transporter activity and stability by membrane cholesterol, Sci. Rep. 7 (2017) 43580.
[37] A. Penmatsa, K.H. Wang, E. Gouaux, X-ray structure of dopamine transporter elucidates antidepressant mechanism, Nature 503 (2013) 85–90.
[38] L. Laursen, K. Severinsen, K.B. Kristensen, X. Periole, M. Overby, H.K. Muller, B. Schiott, S. Sinning, Cholesterol binding to a conserved site modulates the conformation, pharmacology, and transport kinetics of the human serotonin transporter, J. Biol. Chem. 293 (2018) 3510–3523.

frontiers in Molecular Biosciences

ORIGINAL RESEARCH
published: 23 October 2019
doi: 10.3389/fmolb.2019.00110

Interaction of Cholesterol With the Human SLC1A5 (ASCT2): Insights Into Structure/Function Relationships

*Mariafrancesca Scalise, Lorena Pochini, Jessica Cosco, Emma Aloe, Tiziano Mazza, Lara Console, Antonella Esposito and Cesare Indiveri**

Unit of Biochemistry and Molecular Biotechnology, Department DiBEST (Biologia, Ecologia, Scienze della Terra), University of Calabria, Cosenza, Italy

The human SLC1A5 commonly known as ASCT2 is a sodium-dependent neutral amino acid antiporter involved in transmembrane traffic of glutamine that is exchanged through the cell membrane with smaller amino acids such as serine or threonine. Due to the strong overexpression in human cancers, ASCT2 is widely studied for its relevance to human health. Of special interest are the aspects related to the regulation of its function. The role of cholesterol as a modulator of the transport activity has been studied using a combined strategy of computational and experimental approaches. The effect of cholesterol on the Na^+_{ex}-[^{3}H]glutamine$_{ex}$/glutamine$_{in}$ antiport in proteoliposomes has been evaluated by adding cholesteryl hemisuccinate. A strong stimulation of transport activity was observed in the presence of 75 μg cholesteryl hemisuccinate per mg total lipids. The presence of cholesterol did not influence the proteoliposome volume, in a wide range of tested concentration, excluding that the stimulation could be due to effects on the vesicles. cholesteryl hemisuccinate, indeed, improved the incorporation of the protein into the phospholipid bilayer to some extent and increased about three times the V_{max} of transport without affecting the K_m for glutamine. Docking of cholesterol into the hASCT2 trimer was performed. Six poses were obtained some of which overlapped the hypothetical cholesterol molecules observed in the available 3D structures. Additional poses were docked close to CARC/CRAC motifs (Cholesterol Recognition/interaction Amino acid Consensus sequence). To test the direct binding of cholesterol to the protein, a strategy based on the specific targeting of tryptophan and cysteine residues located in the neighborhood of cholesterol poses was employed. On the one hand, cholesterol binding was impaired by modification of tryptophan residues by the Koshland's reagent. On the other hand, the presence of cholesterol impaired the interaction of thiol reagents with the protein. Altogether, these results confirmed that cholesterol molecules interacted with the protein in correspondence of the poses predicted by the docking analysis.

Keywords: membrane transport, proteoliposomes, SLC, cholesterol, chemical targeting, mercury, cysteine, tryptophan

OPEN ACCESS

Edited by:
Graça Soveral,
University of Lisbon, Portugal

Reviewed by:
Ildikò Szabò,
University of Padova, Italy
Christof Grewer,
Binghamton University, United States

****Correspondence:***
Cesare Indiveri
cesare.indiveri@unical.it

Specialty section:
This article was submitted to Cellular Biochemistry, a section of the journal Frontiers in Molecular Biosciences

Received: *02 August 2019*
Accepted: *07 October 2019*
Published: *23 October 2019*

Citation:
Scalise M, Pochini L, Cosco J, Aloe E, Mazza T, Console L, Esposito A and Indiveri C (2019) Interaction of Cholesterol With the Human SLC1A5 (ASCT2): Insights Into Structure/Function Relationships. Front. Mol. Biosci. 6:110. doi: 10.3389/fmolb.2019.00110

INTRODUCTION

The human ASCT2 transporter is one of the seven members of the SLC1 family (SLC1A5) and represents one of the most studied proteins among the SLC members being considered a hot spot topic for either biochemical interest and pharmacological applications (Kanai et al., 2013; Scalise et al., 2019). ASCT2 shows a broad tissue expression. The first pioneering studies on the mice and human isoforms, conducted in intact cells, showed that this transporter has a preference toward neutral amino acids (Kekuda et al., 1996; Utsunomiya-Tate et al., 1996; Torres-Zamorano et al., 1998; McGivan and Bungard, 2007) and displays a peculiar transport mode: an antiport of neutral amino acids coupled to co-transport of Na^+ from the external to the internal side of the cell membrane. Soon after, the rat transporter (Oppedisano et al., 2004, 2007) was studied employing the proteoliposome technology that allows investigating a single protein inserted in an artificial membrane with the same orientation as in the native cell membrane (Scalise et al., 2017a). These studies confirmed most of the characteristics described in intact cells. The human protein has been then obtained by overexpression in *Pichia pastoris* and purification by affinity chromatography (Pingitore et al., 2013). Novel features of the human ASCT2 have been revealed thanks to the proteoliposome tool (Scalise et al., 2014). Functional asymmetry of the transporter has been described: the ASCT2 revealed to be competent for the bidirectional transport of glutamine, asparagine, threonine, and serine while alanine can be only inwardly transported. Kinetic asymmetry has been also demonstrated with external affinities toward substrates in the micromolar range and internal affinities in the millimolar range. These parameters correlate with the extra and intracellular concentrations of the amino acids (Cynober, 2002; Pingitore et al., 2013; Scalise et al., 2014). Interestingly, cysteine, i.e., one of the amino acids underlying the acronym ASC(Cysteine)T2, has been shown to be a modulator of the transporter but not a substrate (Scalise et al., 2015) explaining overlooked old data (Utsunomiya-Tate et al., 1996). This peculiar regulation mode, together with the discovered responsiveness to GSH, H_2S, and NO suggested that ASCT2 could be a redox sensor in physiological and pathological conditions. This was confirmed by site-directed mutagenesis identifying key residues for the redox sensing (Scalise et al., 2018b). An interesting and controversial aspect is the electrical nature of the transport reaction that has been solved in the proteoliposome model by specifically setting the experimental conditions close to the physiological milieu: the ASCT2 mediated Na^+ dependent antiport is electrogenic involving at least one Na^+ ion per transport cycle (Scalise et al., 2014). Combining *in vivo* and *in vitro* approaches, novel aspects of ASCT2 biology have been revealed. ASCT2 contains PDZ binding domain allowing for interaction with PDZK1, a well-known scaffold protein which takes contact with several plasma membrane transporters and regulates either activity and/or stability of the interactors (Dephoure et al., 2008). Furthermore, the molecular determinants for trafficking to the plasma membrane, i.e., glycosyl residues linked to asparagine 163 and 212, have been characterized. Glycosylation is required for both routing the transporter to the definitive location and for stabilizing the protein while it is not needed for intrinsic transport function (Console et al., 2015). From the findings obtained in different experimental systems, it can be deduced that the main physiological role of ASCT2 consists in mediating cell uptake of glutamine and balancing the amino acid pools in several tissues. ASCT2 has been also reported to be involved in the glutamine/glutamate cycle between astrocytes and neurons allowing for both the recycle of glutamate from the synaptic cleft in astrocytes and its re-synthesis in neurons (Broer et al., 1999; Leke and Schousboe, 2016). However, it has to be stressed that the enormous interest in ASCT2 derives from the well-acknowledged involvement in cancer development and growth. Indeed, ASCT2 is overexpressed in virtually all human cancers so far analyzed thus making this transporter a valuable target for novel drugs (Bhutia and Ganapathy, 2016; Scalise et al., 2017b; Schulte et al., 2018). Few molecules revealed to be potent inhibitors of ASCT2 and one of these, i.e., V-9302, has been tested in cell culture, tumor xenograft, and mice model for cancers (Schulte et al., 2018), even though the specificity of V-9302 is still controversial (Broer et al., 2018). The hASCT2 overexpression can find an explanation on at least two molecular events. At first, on the metabolic point of view, over-expression of hASCT2 provides cancer cells with glutamine, one of the major nutrients for cells under high proliferative state, in exchange with other amino acids such as serine deriving from glucose metabolism (Scalise et al., 2017b). At second, the glutamine taken up by hASCT2 may play also a role in cell signaling, for cell growth and development, due to the regulation of mTOR pathway with the sensing of amino acids availability in cells (Chantranupong et al., 2015; Rebsamen et al., 2015). Deciphering other regulatory properties and structure/function relationships of ASCT2 is thus of primary interest. In this respect, very recently cholesterol revealed to be important for several plasma membrane transporters function and stability (Penmatsa et al., 2013; Coleman et al., 2016; Dickens et al., 2017; Garcia et al., 2019). The presence of protein-bound cholesterol, in the form of Cholesteryl HemiSuccinate (CHEMS), has been hypothesized in the Cryo-EM structures of the hASCT2 trimer in both inward and outward-facing conformations (Garaeva et al., 2018; Yu et al., 2019). In the present study, we sought to investigate the relationships among cholesterol interacting with ASCT2 and modulation of its transport activity.

Abbreviations: SLC, SoLute Carrier; GSH, Reduced Glutathione; H_2S Hydrogen Sulfide; NO, Nitric Oxide; mTOR, mammalian Target of Rapamicyn; CHEMS, Cholesteryl HemiSuccinate; β-MCD, Methyl-beta-CycloDextrin; Cryo-EM, Cryo Electron Microscopy; $C_{12}E_8$, Octaethylene glycol monododecyl ether; YPDS, Yeast Extract Peptone Dextrose Sorbitol; BMGY, Buffered Glycerol-complex Medium; BMMY, Buffered Methanol-complex Medium; DTE, DiThioErythritol; NEM, N-ethylmaleimide; BSA, Bovine Serum Albumin; CRAC, Cholesterol Recognition/interaction Amino acid Consensus sequence.

MATERIALS AND METHODS

Materials

The *P. pastoris* wild type strain (X-33), the pPICZB vector, zeocin, Ni-NTA agarose resin were from Invitrogen; anti-rabbit IgG HRP conjugate from Cell Signaling; PD-10 columns, ECL

plus, Hybond ECL membranes were from GE Healthcare; L-[^{3}H]Glutamine was from Perkin Elmer; anti-ASCT2 (rabbit) was from Millipore; conjugated anti-His antibody, $C_{12}E_8$, Cholesteryl hemisuccinate, Amberlite XAD-4, egg yolk phospholipids (3-sn-phosphatidylcholine from egg yolk), Sephadex G-75, L-glutamine, methyl-β-cyclodextrin (MβCD) and all the other reagents were from Sigma-Aldrich.

Recombinant Production of hASCT2 WT and Mutants

To obtain the recombinant hASCT2-6His proteins, 10 μg of pPICZB-ASCT2-6His WT or mutant constructs were linearized with PmeI and used to transform *P. pastoris* wild type strain X-33 by electroporation (Oberg et al., 2011). Putative multi-copy recombinants were selected using YPDS plates containing 2,000 μg/ml zeocin and analyzed after 3 days as previously described (Scalise et al., 2018b). For large scale protein production, transformed *P. pastoris* cells were inoculated in BMGY medium and grown at 30°C under rotatory stirring. To over-express hASCT2 WT and mutants, *P. pastoris* cells were centrifuged to remove the BMGY medium and resuspended at final OD of 1 in 250 mL BMMY medium added with 0.5% of methanol and placed in a 2 L conical flask. The growth in methanol was performed at 30°C under rotatory stirring, for 3 days adding fresh methanol every 24 h. To isolate the membrane fraction, 30 g of *P. pastoris* cells were resuspended in 300 ml of a buffer containing 50 mM Tris HCl pH 7.4, 150 mM NaCl, 6 mM β-mercaptoethanol, and 0.5 mM PMSF and disrupted using a bead beater (BioSpec Product). The chamber of the bead beater was loaded with the cell suspension mixed with glass beads (0.5 mm). After 5 min, almost 90% of the cell wall was destructed. The cell suspension was centrifuged in a JA30.50 rotor at 108,000 g for 30 min and the supernatant containing membrane and cytosolic fractions was collected. The supernatant was centrifuged in a JA30.50 rotor at 108,000 g for 90 min. The resulting membrane pellet was washed with urea buffer (5 mM Tris HCl pH 7.4, 2 mM EDTA, 2 mM EGTA, and 4 M urea) and then centrifuged as above described. The pellet containing the washed membrane fraction was resuspended at a final concentration of about 300 mg/ml in a buffer containing 25 mM Tris HCl pH 7.4, 250 mM NaCl, 6 mM β-mercaptoethanol and, 10% glycerol and homogenized using a potter homogenizer. Aliquots of 3 mL of the membrane fraction were stored at −80°C before solubilization.

Solubilization and Purification of hASCT2 WT and Mutants

For a large-scale solubilization and purification of WT hASCT2 protein and mutants, about 1.5 g of washed membranes (400 mg/mL) were solubilized using a buffer containing 25 mM Tris HCl pH 7.4, 250 mM NaCl, 6 mM β-mercaptoethanol, 1 mM L-glutamine, 10% glycerol, and 2% $C_{12}E_8$ (w/w) by rotatory stirring for 3 h at 4°C. Then, centrifugation at 18,000 g for 45 min was performed and the supernatant was recovered for purification. The supernatant was applied to 2 mL Ni-nitrilotriacetic acid (NTA) agarose resin pre-equilibrated with the equilibration buffer (20 mM Tris HCl pH 7.4, 300 mM NaCl, 10% glycerol, 6 mM β-mercaptoethanol, 0.03% $C_{12}E_8$, 1 mM L-glutamine, and 50 mM imidazole). The resin, after supernatant application, was incubated over night with gentle agitation at 4°C to allow specific binding of recombinant hASCT2 to the NiNTA resin. After incubation, the Ni-NTA resin was packed into a column and washed with 30 mL of the equilibration buffer. Then, 10 mL of the elution buffer (20 mM Tris HCl pH 7.4, 30 0mM NaCl, 10% glycerol, 6 mM β-mercaptoethanol, 0.03% $C_{12}E_8$, 1 mM L-glutamine, and 500 mM imidazole) were added. Fractions containing purified protein were pooled to 2.5 mL and desalted on a PD-10 desalting column pre-equilibrated with desalting buffer (20 mM Tris HCl pH 7.4, 100 mM NaCl, 10% glycerol, 6 mM β-mercaptoethanol, 0.03% $C_{12}E_8$, and 1 mM L-glutamine), from which 3.5 mL were collected.

Preparation of Cholesteryl Hemisuccinate

Cholesteryl HemiSuccinate (CHEMS) was prepared in 5% $C_{12}E_8$, to reach the final concentration required in the initial reconstitution mixture (see section Reconstitution of the hASCT2 WT and mutants into liposomes) and 20 mM Tris HCl pH 8.0. The solubilization was performed by two sonication cycles of 2 min (no pulse, 40 W) with a Vibracell VCX-130 sonifier as previously suggested (Hanson et al., 2008). The solubilized CHEMS was centrifuged for 5 min at 10,000 g and the supernatant was added to sonicated liposomes for 30 min under rotatory stirring (1,200 rpm) at 23°C before reconstitution.

Protein Treatments With NEM and Koshland's Reagent

The purified WT or mutants hASCT2 were incubated with 0.5 mM NEM during the transport assay below described. In the case of the Koshland's reagent (Giangregorio et al., 2019), the purified WT hASCT2 was incubated with 0.5 mM of the reagent under rotatory stirring (1,200 rpm) at 23°C for 15 min before reconstitution.

Reconstitution of the hASCT2 WT and Mutants Into Liposomes

The purified WT hASCT2 protein and mutants were reconstituted by removing the detergent using the batch-wise method in which mixed micelles of detergent, protein and phospholipids were incubated with 0.5 g Amberlite XAD-4 resin under rotatory stirring (1,200 rpm) at room temperature (23°C) for 40 min (Scalise et al., 2018a). The composition of the initial reconstitution mixture was: 50 μL of the purified WT protein or mutants (5 μg protein), 5 μL of 0.3 M EDTA, 340 μL of the mixture containing 100 μL of 10% egg yolk phospholipids (w/v) in the form of sonicated liposomes (Tonazzi et al., 2015) and 240 μL of 5% $C_{12}E_8$ or CHEMS as specified in the figure legends, 10 mM L-glutamine (except were differently indicated in the figure legend), 20 mM Hepes Tris pH 7.0 in a final volume of 700 μL. All the operations were performed at room temperature.

Transport Measurements

To remove the external compounds prior functional uptake experiments, 600 μL of proteoliposomes was passed through a

Sephadex G-75 column (0.7 cm diameter × 15 cm height) pre-equilibrated with 20 mM Hepes Tris pH 7.0 and sucrose at an appropriate concentration to balance the internal osmolarity. Uptake experiment was started by adding 50 μM [^{3}H]glutamine and 50 mM Na-gluconate to 100 μL proteoliposomes, at 25°C. Transport reaction was stopped by adding 100 μM $HgCl_2$; according to the inhibitor stop method, the same inhibitor was added at time zero to control samples (blanks) (Palmieri and Klingenberg, 1979). At the end of the transport, 100 μL of proteoliposomes was passed through a Sephadex G-75 column (0.6 cm diameter × 8 cm height) to separate the external from the internal liposomal radioactivity. Then, proteoliposomes were eluted with 1 mL 50 mM NaCl and collected in 3 mL of scintillation mixture, vortexed and counted. The experimental values were analyzed by subtracting to each sample the respective control (blank); the initial rate of transport was measured by stopping the reaction after 15 min, i.e., within the initial linear range of [^{3}H]glutamine uptake into the proteoliposomes. Grafit 5.0.13 software was used to calculate kinetic parameters, to derive percent of residual activity values in inhibition assays and to measure transport rate by first-order rate equation.

Cell Culture, Methyl-β-Cyclodextrin Treatment, and Transport Assay

HeLa cells were maintained in Dulbecco's Modified Eagle Medium (DMEM) supplemented with 10% (v/v) Fetal Bovine Serum (FBS), 1 mM glutamine and 1 mM sodium pyruvate under standard conditions, i.e., 37°C in a humidified incubator and a 5% CO_2 atmosphere. Prior of methyl-β-cyclodextrin experiments, cells were plated on 12-well plates and treatment was performed when cells reached 70% confluence. Treatment with 10 mM methyl-β-cyclodextrin was performed for 60 min in the incubator in serum free medium (Dickens et al., 2017) and then, transport assay was performed as previously described (Console et al., 2015). In brief, cells were rinsed twice with warm transport buffer prepared with 20 mM TrisHCl pH 7.4, 10 mM BCH, and 10 mM MeAIB. Radiolabeled 10 μM [^{3}H]glutamine was added together with 100 mM NaCl and the transport reaction was terminated after 60 s by discarding the uptake buffer and rinsing the cells three times with the same ice-cold transport buffer (500 μL per well per rinse). Cells from each well were solubilized in 500 μL of 1% TX-100 solution. Cell extracts were counted for radioactivity (400 μL). The remaining 100 μL in each well were used for protein concentration assay. Na^+-dependent glutamine transport was evaluated by subtracting the transport values from those deriving from transport conducted in the absence of Na^+.

Cross-Link Reaction of hASCT2

The HeLa cells were plated on 10 cm^2 dishes an treatment was performed when cells reached 70% confluence. Then, cells were treated with 0.75% formaldehyde for 10 min shaking at room temperature; the reaction was stopped using 125 mM glycine prepared in PBS for 5 min shaking at room temperature. Then, cells were collected and washed with PBS. Cells pellet were stored at −20°C. The purified WT hASCT2 protein, incubated in the absence or the presence of 0.75 mg CHEMS prepared as above described, was used for the cross-link reaction with formaldehyde diluted in 20 mM Tris HCl pH 9.0. The protein in both conditions was treated with increasing concentrations of the cross-linker for 2 min at 23°C, as detailed in the figure legends. The reaction was stopped adding cold 1.25 M glycine solubilized in PBS. Samples were prepared using loading dye with 10% SDS and heated for 5 min at 65°C. Samples were analyzed by SDS—PAGE followed by western blotting as described below.

Internal Volume Measurement

The internal volume of proteoliposomes prepared with different amount of cholesterol was calculated using the colorimetric phosphate method as previously described (Indiveri et al., 1994). In brief, different proteoliposome samples were prepared including, in the reconstitution mixture, 50 mM dipotassium phosphate (K_2HPO_4). After elution from Sephadex G75, buffered without phosphate, 100 μL of sample were used for the colorimetric reaction with 150 μL of 10% SDS and 700 μL of solution R (prepared with 10 mM hexammonium heptamolybdate 4-hydrate, 0.3 mM of H_2SO_4, and 0.1 mM $FeSO_4$). After incubating samples in the dark for 30 min, the absorbance was measured using spectrophotometer analysis (wavelength = 578 nm). Internal volume in μL was derived from nmol of phosphate included in liposomes.

Molecular Docking Approach

To identify cholesterol binding sites in ASCT2 transporter (PDB: 6GCT), molecular docking was performed using Autodock 4.2 (Forli et al., 2016). At first, a blind docking was made, generating a grid which covered the whole trimer. The size of the grid box was set to 114 × 114 × 114 Å (x, y, and z). The optimized ligand molecule was docked into refined ASCT2. The best conformation space of the ligand was searched employing the Lamarckian Genetic Algorithm. Default parameters were used and 20 different conformers were generated for cholesterol molecule. Other six refined docking simulations were then carried out for accurate results. For each docking, a grid box with reduced size and space between gridpoints was generated in a specific area. For each docking process, the number of generation was reduced to 10 conformers. The best final pose was chosen giving priority to the lowest binding-energy conformation. As a further docking proof, a blind docking calculation was also performed with Achilles Blind Docking Server (https://bio-hpc.ucam.edu/achilles/) (Sanchez-Linares et al., 2012). Molecular graphics and visualization of the amino acids involved in the interaction with cholesterol were performed with the UCSF Chimera 1.13.1 software (Pettersen et al., 2004) (Resource for Biocomputing, Visualization, and Informatics, University of California, San Francisco, CA, USA).

Other Methods

The amount of purified recombinant hASCT2 WT and mutants was estimated from Coomassie blue-stained 12% SDS–PAGE gels by using the Chemidoc imaging system equipped with Quantity One software (Bio-Rad) as previously described (Torchetti et al., 2011). The cross-linked samples were analyzed

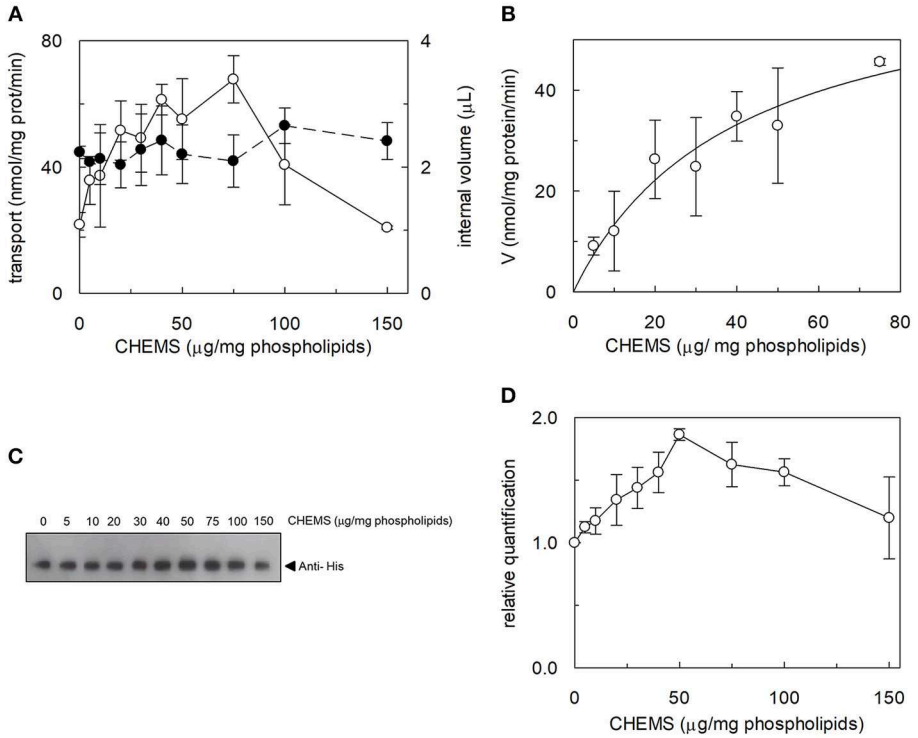

FIGURE 1 | Effect of cholesterol on hASCT2 reconstitution in proteoliposomes. **(A)** Purified WT hASCT2 was reconstituted in proteoliposomes prepared with the indicated amounts of CHEMS per mg phospholipids as described in Materials and Methods. Transport assay was started adding 50 μM of [^{3}H]glutamine and 50 mM Na-Gluconate to proteoliposomes containing 10 mM glutamine. Transport was measured in 20 min, i.e., within the initial linear part of the time course. Transport rate was expressed as nmol/mg prot/min (○, left y-axis). In the right y-axis, the internal volume of proteoliposomes used for the transport assay was calculated as described in Materials and Methods (•). **(B)** Experimental data obtained from experiments shown in **(A)** were analyzed subtracting each value corresponding to a specific CHEMS amount to the condition in which CHEMS was not present in the reconstitution mixture. Data were then plotted using non-linear Michaelis- Menten equation as described in Materials and Methods excluding data of high CHEMS amount, i.e., 100 and 150 μg/mg phospholipids, because out of the plot range. **(C)** Samples (a volume corresponding to 1% of the total reconstitution mixture) derived from **(A)** were subjected to SDS-PAGE and western blotting analysis, as described in Materials and Methods, for evaluating the incorporation of hASCT2 into proteoliposomes prepared with the indicated amount of CHEMS. Recombinant protein, harboring a 6His tag at the C-terminus, was detected using anti-His antibody. **(D)** Relative quantification of band intensity from western blotting of **(C)**. In **(A,B)** data are means ± SD of three independent experiments. In **(C)**, a representative image of three different experiments; in **(D)** data are means ± SD of three different western blotting analysis.

on 8% SDS-PAGE. For Western Blot analysis, hASCT2 was immuno-detected incubating membrane with conjugated anti-His antibody 1:10,000 in 3% BSA for 1 h at room temperature or with anti-hASCT2 (1:1,000) incubated overnight in 3% BSA under shaking at 4°C and then 1 h at room temperature with secondary antibody anti-rabbi (1: 5,000) in 1% BSA. The reaction was detected by Electro Chemi Luminescence (ECL) assay in the darkroom.

RESULTS

Effect of Cholesterol on the hASCT2 Reconstitution and Function

The effect of cholesterol on the transport function of ASCT2 was studied using the proteoliposome experimental model which allows modifying the lipid composition of the membrane. Cholesterol, in the form of cholesteryl hemisuccinate (CHEMS), was added to the lipid/detergent mixture before the formation of proteoliposomes, as described in Materials and Methods. As shown in **Figure 1A**, cholesterol strongly stimulated the transport activity of hASCT2 measured as sodium-dependent glutamine antiport (Na^+_{ex}-[^{3}H]glutamine$_{ex}$/glutamine$_{in}$). Maximal stimulation was observed at a cholesterol concentration of 75 μg/mg total lipids corresponding to 7.5% cholesterol which falls within the physiological cholesterol concentration in cells (Litvinov et al., 2018); at higher concentrations, the activity dramatically decreased. To investigate whether the increase of [^{3}H]glutamine accumulation could simply be due to an increase in the internal space of proteoliposomes caused by the inclusion of cholesterol, the internal volume was measured. Nearly no variations were observed at the various concentration of cholesterol, with respect to the control, indicating that cholesterol does not affect the internal proteoliposome volume (**Figure 1A**). Thus, the stimulation may be caused by an effect of cholesterol in improving the protein insertion into the membrane and/or the kinetics. The hyperbolic trend of the data up to 75 μg/mg total lipids (**Figure 1B**) observable after subtracting the control value (absence of cholesterol), correlates with a saturation process which is typical of protein-ligand interactions. A further increase in cholesterol concentration

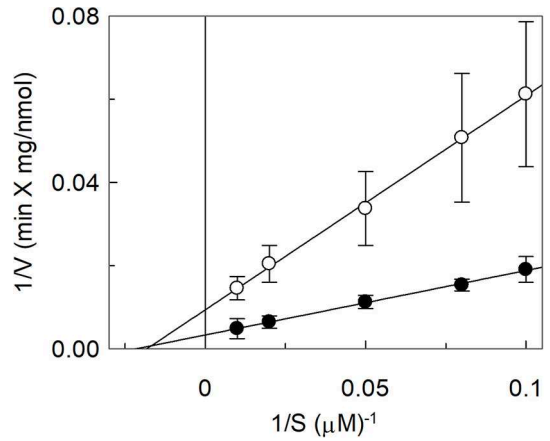

FIGURE 2 | Effect of cholesterol on kinetics of hASCT2 reconstituted in proteoliposomes. Purified hASCT2 was reconstituted in proteoliposomes prepared without CHEMS (○) or with 75 μg/mg phospholipids CHEMS (•) as described in Materials and Methods. Transport was started by adding indicated concentrations of [^{3}H]glutamine and 50 mM Na-Gluconate to proteoliposomes containing 10 mM glutamine. Transport was stopped after 15 min and analysis of the data was performed according to linear Lineweaver–Burk plot as reciprocal transport rate vs. reciprocal glutamine concentration. Data are means ± SD of three independent experiments.

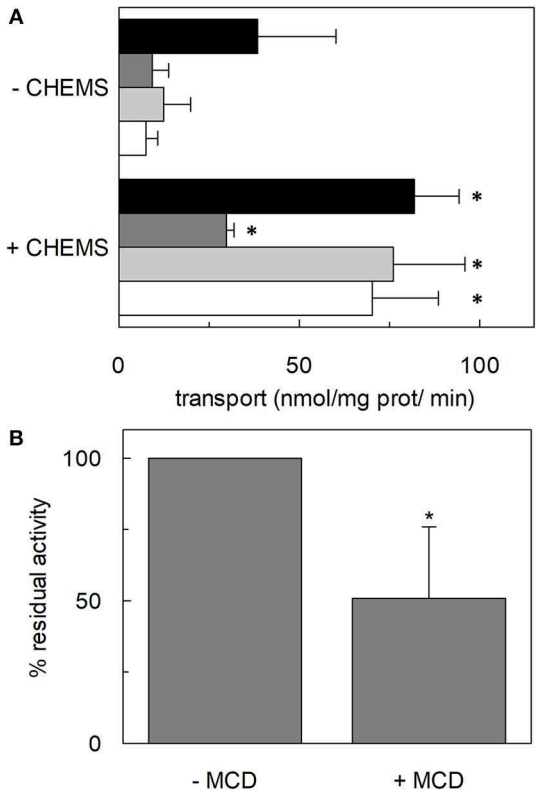

FIGURE 3 | Effect of cholesterol on transport activity mediated by hASCT2. In **(A)**, purified hASCT2 was reconstituted in proteoliposomes prepared without CHEMS or with 75 μg/mg phospholipids CHEMS as indicated and described in Materials and Methods. Transport assay was started adding 50 μM of [^{3}H]glutamine and 50 mM Na-Gluconate to proteoliposomes containing 10 mM glutamine (black bar) or asparagine (dark gray bar) or threonine (light gray bar) or serine (white bar). Initial transport rates were calculated as k x limit (nmol/mg prot/min) from the first-order rate equation used to plot the time course data. Data are means ± SD of three independent experiments. In **(B)**, HeLa cells were treated with 10 mM methyl-β-cyclodextrin (MCD) as described in Materials and Methods. Transport was started adding 10 μM [^{3}H]glutamine in the presence or in the absence of 100 mM NaCl. Transport activity was calculated as the percent of residual activity with respect to the control condition (without MCD in the transport assay). *Significantly different from the control sample (proteoliposomes prepared without CHEMS in **A** or without MCD in **B**) as estimated by Student's t-test ($P < 0.05$).

impaired the transport function. To gain further insights into the mechanism of stimulation of the transport activity, the amount of protein incorporated into proteoliposomes at increasing cholesterol concentrations was detected (**Figure 1C**). As shown by the Western blot, protein incorporation increased by increasing the cholesterol concentration with a maximum at 50 μg/mg total lipids of cholesterol. Thus, the increase in reconstituted protein amount did not exactly follow the increase in transport activity (**Figure 1D**), as indicated by the low correlation coefficient of 0.78 calculated for the two sets of data. Taken together, these results showed that the effect on reconstitution of hASCT2 into proteoliposomes is not the sole responsible for transport stimulation. To gain further insights into these aspects, kinetics was studied in the absence or presence of cholesterol (**Figure 2**). The K_m for glutamine was not substantially changed in the absence or presence of cholesterol while the V_{max} increased about three times (113 ± 26.6 nmol · mg $^{-1}$ · min^{-1} and 370 ± 79.3 nmol · mg $^{-1}$ · min^{-1} in the absence or the presence of cholesterol, respectively). Furthermore, to evaluate the effect of cholesterol in the transport cycles resembling those occurring in physiological conditions, the heterologous exchanges Na^+-[^{3}H]glutamine$_{ex}$/asparagine$_{in}$, Na^+-[^{3}H]glutamine$_{ex}$/threonine$_{in}$, or Na^+-[^{3}H]glutamine$_{ex}$/serine$_{in}$, were measured (**Figure 3A**). Interestingly, the addition of cholesterol was much more effective on the heterologous antiport of [^{3}H]glutamine$_{ex}$/serine$_{in}$ and [^{3}H]glutamine$_{ex}$/threonine$_{in}$ (six and nine times stimulation, respectively) than on the homologous antiport (two times stimulation) or the heterologous [^{3}H]glutamine$_{ex}$/asparagine$_{in}$ antiport (three times stimulation). The effect of cholesterol was shown also in intact HeLa cells treated with methyl-β-cyclodextrin, which is a known cholesterol depleting reagent (Dickens et al., 2017). In line with results obtained in proteoliposomes the Na^+-dependent glutamine transport was impaired upon cholesterol deprivation (**Figure 3B**).

Docking of Cholesterol to the 3D Structure of hASCT2

To shed new lights on the molecular mechanisms underlying effects of cholesterol on the transport activity of ASCT2 and in agreement with the data of **Figure 1**, direct binding of cholesterol to the protein was hypothesized. This correlated well with previous structural data that showed electron density areas in the 3D structure of the hASCT2 trimer (Garaeva

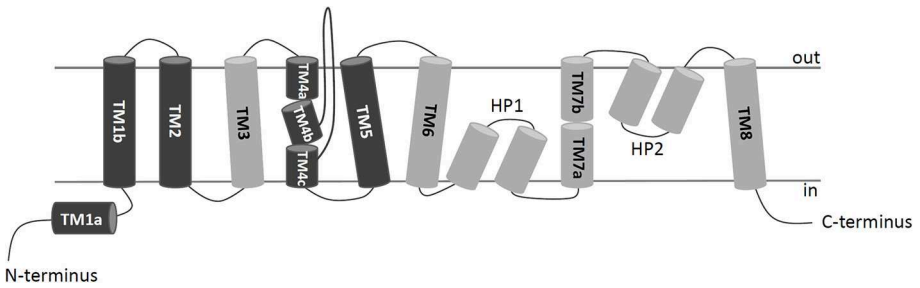

FIGURE 4 | 2D schematic representation of a protomer organization. TransMembrane domains (TMs) of hASCT2 are depicted in dark gray (scaffold domain) or light gray (transport domain); HP1 and HP2 hairpins connect TM6-8; loops between TMs are indicated in lines. N- and C-termini of the protein face to the intracellular space delimited by the membrane.

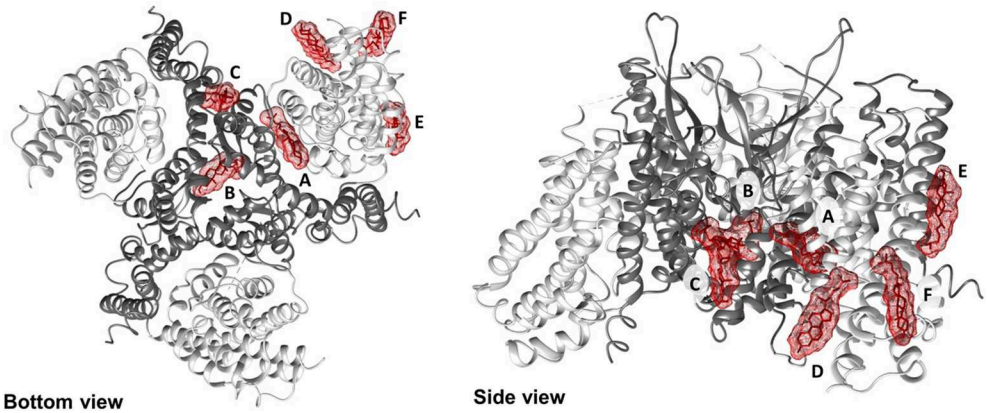

FIGURE 5 | Docking of cholesterol molecules with hASCT2. Bottom view (left) and side view (right) of the trimeric hASCT2 (PDB: 6GCT). Cholesterol molecules, indicated by letters A, B, C, D, E, and F are depicted as red sticks with mesh surface interacting with the scaffold domain (TMs 1,2,4,5 in dark gray ribbon) and with the transport domain (TMs 3,6,7,8, HP1 and HP2 in the light gray ribbon) of a protomer. The numbering of TMs corresponds to those described in **Figure 4**. Dotted gray lines indicate missing residues in the 3D structure (PDB: 6GCT). The structure was visualized using Chimera 1.13.1 software.

et al., 2018; Yu et al., 2019). To predict the possible sites of interaction, docking of cholesterol into the hASCT2 trimer was performed. As shown in **Figures 4–6**, at least six sites were predicted. Some of these poses, i.e., those indicated by A, B, C, and D well overlap the electron density areas in the recently published 3D structures (Garaeva et al., 2018; Yu et al., 2019). Interestingly, two additional poses, indicated by the letters E and F, resulted from the docking. Noteworthy, the mentioned poses E and F were docked close to CARC (pose E, TM6) and CRAC (pose F, TM6) motifs that are well-acknowledged binding sites for cholesterol. CRAC is an acronym standing for Cholesterol Recognition/interaction Amino acid Consensus sequence, while CARC is considered as an inverted CRAC domain (Fantini and Barrantes, 2013; Fantini et al., 2019). Moreover, pose D (TM3), also present in the 3D structure, is docked close to a R-W-L domain that is considered a simil-CARC/CRAC domain (Fantini and Barrantes, 2013). To prove that indeed cholesterol binds to the protein, a strategy based on the specific targeting of residues located in the neighborhood of cholesterol molecules was employed. According to this approach, we sought to evaluate the possible prevention of chemical targeting by the cholesterol added to the proteoliposomes.

Targeting Tryptophan Residues by the Koshland's Reagent

The Koshland's reagent was employed due to its acknowledged specific reactivity toward tryptophan residues at pH 7.0. In particular, the reaction triggers a chemical modification of the indole ring of the tryptophan side chain (Loudon and Koshland, 1970). The purified WT hASCT2 was treated with Koshland's reagent as described in Materials and Methods in the presence or the absence of cholesterol (**Figure 7**). The treatment of the protein with the reagent had nearly no effect in the absence of cholesterol indicating that the modification of such residues does not influence the protein activity, i.e., tryptophan residues are not crucial for transport function. The reagent, on the contrary, prevented the stimulation exerted by cholesterol by roughly 30%, indicating that tryptophan residues might be critical for the interaction with cholesterol thus confirming the predicted location of cholesterol in the vicinity of those residues (poses letters C, D, and E; see related **Figure 6**).

Targeting Cysteine Residues With SH-Reagents

Following the same experimental setup, changes of the reactivity toward SH reagents was also investigated considering that the poses B and E are predicted to be in the vicinity of cysteine residues. Previous work showed that hASCT2 transport activity is stimulated by DTE that reduces thiol residues of cysteines (Scalise et al., 2018b); interestingly, in the presence of cholesterol, the stimulation by DTE was nearly abolished (**Figure 8A**). Interestingly, the addition of DTE had no effect on transport measured in HeLa cells (not shown) where the ASCT2 should have an optimal cholesterol milieu. To further investigate this issue, the transporter was treated with SH reagents previously shown to interact with the protein, causing transport inhibition. The treatment of WT hASCT2 with $HgCl_2$ was performed using proteoliposomes prepared in the presence or absence of cholesterol; as expected, $HgCl_2$ exerted strong transport inhibition (**Figure 8B**); interestingly, the presence of cholesterol protected from the inhibition. A similar experiment was performed with the SH alkylating reagent NEM and, also, in this case, significant protection by cholesterol was observed (**Figure 8B**). These results indicated that some cysteine residues of the hASCT2 are masked by one or more bound cholesterol molecules (**Figures 6B,E**). The availability in our laboratory of some cysteine mutants (Scalise et al., 2018b), together with the previous finding that C467 is the major target of SH reagents, allowed us to map the presence of the new predicted cholesterol pose E (**Figure 6E**) facing to the C467 residue. Therefore, the extent of inhibition by $HgCl_2$ was evaluated on three mutants, i.e., C308A, C309A, and C467A reconstituted in proteoliposomes prepared in the absence or in the presence of cholesterol (**Figure 9A**). The data showed that the protection of $HgCl_2$ binding and inhibition by cholesterol in the mutants was different with respect to the WT. The protection index was calculated as the ratio between residual activity in the presence and in the absence of cholesterol (dotted boxes in the **Figure 9A**) confirming that protection observed in the WT was lost or much smoothed in the three mutants indicating that a cholesterol molecule may mask one or more of the three cysteine residues. Furthermore, the same experiment was conducted using the C110A mutant (**Figure 9A**) since this residue lies in the neighborhood of the cholesterol pose B which corresponded to an electron density area in the previously published 3D structure (**Figure 6B**). Also, in this case, protection was observed. However, differently from C308A, C309A, and C467A data, the protection index was more similar to that of the WT. This may indicate that either the cysteine is targeted by $HgCl_2$ without consequences for the transport activity, or that this cysteine residue is not easily accessible to the provided reagent given its location in the core of the scaffold domain of the homotrimer (**Figure 4**). Therefore, the alkylating reagent NEM was employed on the C308A, C309A, C467A, and C110A mutants (**Figure 9B**). Interestingly, the observed results were very similar to those obtained with $HgCl_2$ even if the extent of inhibition and, hence, of protection by cholesterol were less strong than those observed using $HgCl_2$.

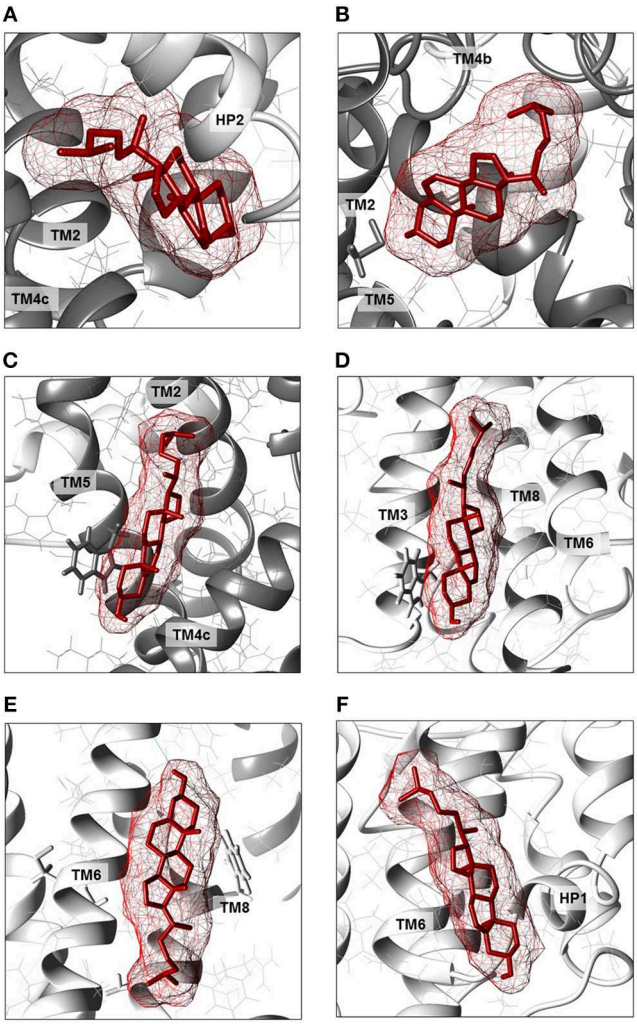

FIGURE 6 | Enlargements of cholesterol poses. Cholesterol molecules are depicted as red sticks with mesh surface facing to residues of neighboring helices in scaffold domain (dark gray ribbon) or transport domain (light gray ribbon). **(A)** Cholesterol facing to TMs 2, 4c (scaffold domain) and HP2 (transport domain) of a protomer. **(B)** Cholesterol facing to TMs 2, 4b and 5 (scaffold domain) of two protomers; in gray stick, residue C110. **(C)** Cholesterol facing to TM4c (scaffold domain) of a protomer and TM2 and TM5 (scaffold domain) of the adjacent protomer; in gray stick, residue W272. **(D)** Cholesterol facing to TMs 3, 6 and 8 (transport domain) of a protomer; in gray stick, residue W130. **(E)** Cholesterol facing to TM6 (transport domain) including CARC motif and TM8 (transport domain); in gray stick, residues C308 and C309 (TM6) and W461 and C467 (TM8). **(F)** Cholesterol facing to TM6 (transport domain) including CRAC motif and HP1 (transport domain) of a protomer. Except those indicated in gray stick, all residues are indicated as gray wire. The structure was visualized using Chimera 1.13.1 software.

Effect of Cholesterol on the Homotrimer Formation of hASCT2

The 3D structure of ASCT2, as well as the previous homology models obtained on the GltPh and on the hEAAT1 (Yernool et al., 2004; Canul-Tec et al., 2017), share a trimeric organization (Garaeva et al., 2018; Scalise et al., 2018b; Yu et al., 2019). This oligomeric form is very probably the functional one as

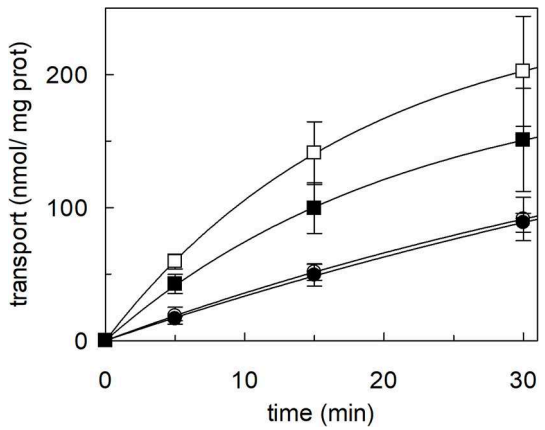

FIGURE 7 | Effect of Koshland's reagent on cholesterol stimulation of hASCT2 reconstituted in proteoliposomes. Purified hASCT2 was incubated (•, ■) or not (○, □) with 0.5 mM Koshland's reagent prior reconstitution. After treatment with the Koshland's reagent, the protein was reconstituted in proteoliposomes prepared without CHEMS (○, •) or with 75 μg/mg phospholipids CHEMS (□, ■) as described in Materials and Methods. Transport assay was started adding 50 μM of [^{3}H]glutamine and 50 mM Na-Gluconate to proteoliposomes containing 10 mM glutamine. Transport was stopped as described in Materials and Methods at the indicated time points. Values were plotted according to the first-order rate equation. Data are means ± SD of three independent experiments.

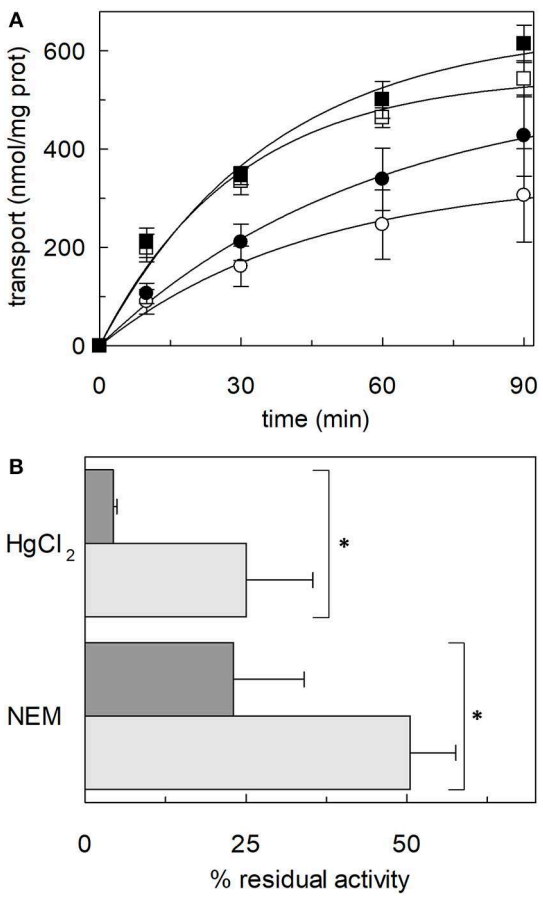

FIGURE 8 | Effect of SH reagents on the transport activity of hASCT2 reconstituted in proteoliposomes. **(A)** Effect of DTE. Purified hASCT2 was reconstituted in proteoliposomes prepared without CHEMS (○, •) or with 75 μg/mg phospholipids CHEMS (□, ■) as described in Materials and Methods. Transport was started by adding 50 μM [^{3}H]glutamine and 50 mM Na-Gluconate in the absence (○, □) or the presence (•, ■) of 10 mM DTE, to proteoliposomes containing 10 mM glutamine. Transport was stopped as described in Materials and Methods at the indicated time points. Values were plotted according to the first-order rate equation. **(B)** Effect of $HgCl_2$ and NEM. Purified hASCT2 was reconstituted in proteoliposomes prepared without CHEMS (dark gray bars) or with 75 μg/mg phospholipids CHEMS (light gray bars) as described in Materials and Methods. Transport was started by adding 50 μM [^{3}H]glutamine and 50 mM Na-Gluconate, in the presence of 20 μM $HgCl_2$ or 0.5 mM NEM, to proteoliposomes containing 10 mM glutamine. Transport was measured in 20 min. Transport activity was calculated as the percent of residual activity with respect to the control condition (without any addition in the transport assay). *Significantly different from the control sample (proteoliposomes prepared without CHEMS) as estimated by Student's *t*-test ($P < 0.05$). In **(A,B)** data are means ± SD of three independent experiments.

it was indicated by previous kinetic and functional studies (Pingitore et al., 2013; Scalise et al., 2014). To address this issue, a cross-linking approach was employed in intact cells using formaldehyde (Sutherland et al., 2008). The experiment showed that in HeLa cells ASCT2 is mostly assembled in a trimeric form (**Figure 10A**). The effect of cholesterol on the trimeric form of hASCT2 was further evaluated using the recombinant purified protein in a cross-linking reaction conducted by adding cholesterol to the protein. The western blot analysis suggested that the presence of cholesterol facilitated the formation of ASCT2 trimer with respect to the samples with no added cholesterol (**Figure 10B**) as indicated by both the decrease of the monomer band and the increase of the band at a triplicate apparent molecular mass.

DISCUSSION

Interaction Between Cholesterol and Membrane Proteins

In the recent years, the studies on SLCs received more and more attention for either physiological and pathological aspects given their well-acknowledged role in mediating traffic of nutrients, catabolites, drugs, and xenobiotics across cell membranes and within cells across intracellular compartments. Besides function and kinetics, characterization of regulatory properties of membrane transporters represents a novel and promising field of investigation that is still *in nuce* (Cesar-Razquin et al., 2015). In this scenario, a very important issue is the influence that the lipid milieu can exert on transporter function. Among membrane lipids, cholesterol is of special interest since besides influencing physical properties of membranes (Yang et al., 2016; Fantini et al., 2019), it mediates the interaction between the transmembrane domains of proteins and the membrane interior thereby modulating protein function (Fantini and Barrantes, 2013). Noteworthy, over the years, some protein motifs have been described which are responsible for cholesterol binding: the best known are the CRAC and CARC (inverted CRAC) motifs (Li and Papadopoulos, 1998).

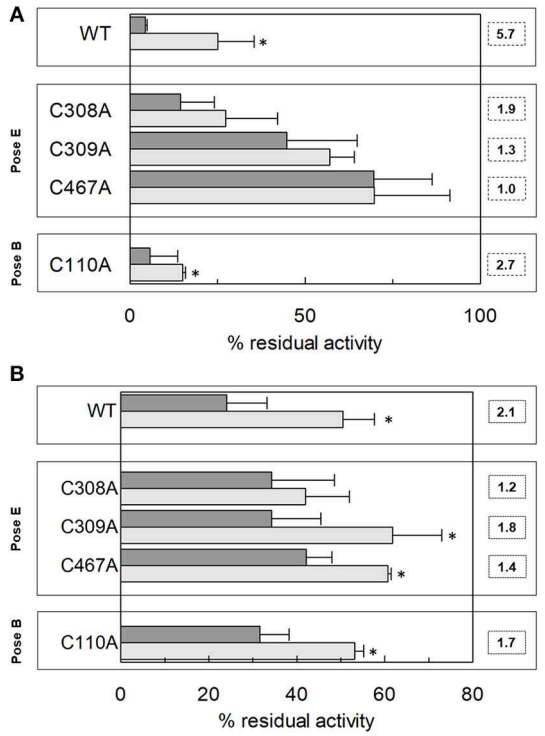

FIGURE 9 | Effect of $HgCl_2$ and NEM on transport activity of hASCT2 WT and Cys mutants reconstituted in proteoliposomes. Effect of $HgCl_2$ **(A)** or NEM **(B)**. Purified hASCT2 WT, C308A, C309, C467A or C110A was reconstituted in proteoliposomes prepared without CHEMS (dark gray bars) or with 75 μg/mg phospholipids CHEMS (light gray bars) as described in Materials and Methods. Transport was started by adding 50 μM [^{3}H]glutamine and 50 mM Na-Gluconate in the presence of 20 μM $HgCl_2$ **(A)** or 0.5 mM NEM **(B)**, to proteoliposomes containing 10 mM glutamine. Transport was measured in 20 min. The boxes grouped the residues corresponding to the indicated poses (see **Figure 6**). Dotted boxes indicated the protection index calculated as the ratio between residual activity in the presence of CHEMS and the residual activity in the absence of CHEMS. Transport activity was calculated as the percent of residual activity with respect to the control condition (without any addition in the transport assay). *Significantly different from the control sample (proteoliposomes prepared without CHEMS) as estimated by Student's *t*-test ($P < 0.05$). Data are means ± SD of three independent experiments.

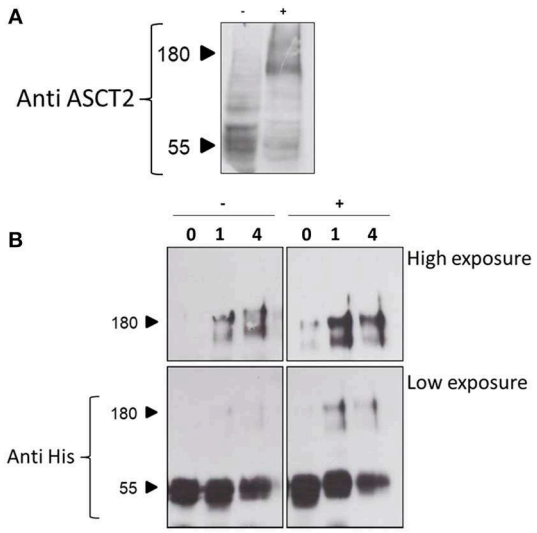

FIGURE 10 | Cross-linking analysis of hASCT2. In **(A)**, immunoblot analysis of protein extracted from HeLa cells treated with 0.75% formaldehyde as described in Materials and Methods. Samples (50 μg total lysate) were subjected to SDS-PAGE and immunoblot with anti-hASCT2 (1:1,000); (–), control without formaldehyde; (+), sample treated with formaldehyde. In **(B)**, immunoblot analysis of purified hASCT2 treated with 1 or 4% formaldehyde as described in Materials and Methods. Samples were subjected to SDS-PAGE and immunoblot with anti-hASCT2 (1:1,000).

Binding of cholesterol to transmembrane domains may also occur at motifs not completely overlapping CARC and CRAC (Fantini and Barrantes, 2013). This scenario has been depicted for different eukaryotic membrane transporters; interestingly, the first report dealing with cholesterol effects on a eukaryotic membrane transporter has been published in the 1970s. In this work, it has been shown that the activity and also the affinity of a glucose transporter is modulated by sterols (Komor et al., 1974). Later on, the effect of cholesterol has been also evaluated on the Na^+ pump in human blood cells (Giraud et al., 1976) and also on ion channels (Brini et al., 2017). Recently, other studies have been conducted and more refined results have been obtained thanks to the resolution of 3D structures such as in the case of DAT from *Drosophila melanogaster* (Penmatsa et al., 2013), hSERT (Coleman et al., 2016), hLAT1 (Yan et al., 2019).

Combination of Computational Analysis and Chemical Targeting Approaches

In the current work, a combined strategy of experimental and computational approaches has been used for describing the effects of cholesterol bound to the hASCT2. It is worth noting that docking of cholesterol is particularly challenged by its hydrophobic nature and, hence, experimental validation is useful to confirm the predictions (Listowski et al., 2015). The employed strategy allowed us to compare the transport function and kinetics under conditions of absence (or low content) with the increased cholesterol content. The range of used cholesterol concentrations does not affect the size of proteoliposomes and, hence, the observed effects are due to direct interaction with the protein. The presence of saturable sites for cholesterol on hASCT2 has been suggested by the hyperbolic dependence of transport activity on cholesterol concentrations. This has been further confirmed by the activity impairment at higher cholesterol concentrations (**Figure 1**). The results correlate with the presence of multiple cholesterol sites on each protein monomer as observed in the case of the nicotinic receptor (Baier et al., 2011). Interestingly, cholesterol did not change the K_m for glutamine, while strongly affected the initial transport rate (**Figures 2**, **3**). This finding indicates that the structure and/or the binding properties of the active site do not vary, while cholesterol probably influences the rate of conformational changes that are at the basis of the elevator mechanism of transport. Indeed, four out of six poses are on the transport domain: three cholesterol molecules face toward the lipid bilayer, one faces

toward the scaffold domain. Cholesterol may play a major role in mediating the interaction with the phospholipid bilayer favoring the sliding of the elevator. This finding can be relevant in terms of the biological function of ASCT2 favoring an increase of glutamine uptake when cells undergo high proliferation (Scalise et al., 2018a). In this condition, glutamine is exchanged with smaller amino acids such as serine allowing the net uptake of at least one carbon atom used in the truncated form of TCA for energy production from glutamine carbon skeleton (Scalise et al., 2017b). Interestingly, the reaction $serine_{in}/glutamine_{ex}$ was stimulated by cholesteryl hemisuccinate more than the other hetero-exchanges (**Figure 3A**). This indicates that cholesterol may exert a specific modulation of serine binding to the internal site, increasing the rate of conformational changes underlying the transport reaction. Indeed, allosteric sites for lipid binding have been recently described in the ASCT2 structure (Garaeva et al., 2019). Therefore, it can be speculated that cholesterol may act as another key regulation point of hASCT2 transport activity and/or stability in the plasma membrane, required in both physiological and pathological conditions. Interestingly, cholesterol membrane content is modulated in cancer cells (Garcia-Bermudez et al., 2019). It is worth noting that docking performed with cholesteryl hemisuccinate or cholesterol perfectly overlapped (not shown) in line with the observation that cholesteryl hemisuccinate and cholesterol show similar properties in cell membranes and the interaction with proteins. Indeed, cholesteryl hemisuccinate is virtually always used for studying protein-cholesterol interaction (Kulig et al., 2015).

Identification of Cholesterol Poses on ASCT2 Transport Protein

Interestingly, the pose shown in **Figure 6C** occupies a site which overlaps the allosteric site described in SLC1A3 as the binding site of the inhibitor $UCPH_{101}$ (Canul-Tec et al., 2017). In addition, the pose shown in **Figure 6D** is included in a non-canonical cholesterol binding motif very close to another key regulatory point of hASCT2, that is the PDZ binding domain; interestingly, cholesterol has been shown to regulate also the interactions between PDZ binding domain and scaffold proteins (Sheng et al., 2012). Furthermore, the protection by cholesterol on the SH reagents $HgCl_2$ and NEM is prevented in the case of cysteine mutants C308 and C309 which lie on the CARC motif of the pose E. When looking at the C467A mutant the protection by cholesterol was not measurable. This may indicate that in the WT protein, cholesterol that binds in the vicinity of C308 and C309 residues, can reduce the inhibition by $HgCl_2$ caused by binding of the reagent to C467. When this cysteine residue is missing, also protection by cholesterol is less evident. It is important to note that C467 is one of the residues responsible for substrate recognition in hASCT2 but cholesterol does not affect the K_m for glutamine. Indeed cholesterol does not enter the substrate-binding site (pose E) but is peripherally located and exposed toward the residues C308, C309. This location, therefore, only influences the environment involved in the reagent reaction with C467. Cholesterol molecules are also predicted and described in the 3D structure (Yu et al., 2019) to interact with the scaffold domain. Thus, besides the effect on the function of hASCT2, cholesterol may play also a role in the stabilization of the trimer. Indeed, the two poses interacting with the scaffold domain (**Figures 6B,C**), take contact with two different subunits. The cross-linking experiment on the recombinant protein confirms the hypothesis. The trimer formation is, indeed, required for the proper functionality of the protein which is almost exclusively present in a trimeric form in the plasma membrane (**Figure 10A**). In conclusion, the suggested physical interaction of cholesterol with hASCT2 has been confirmed at the functional level by employing biochemical and bioinformatics approach. Further work is in the course to better define the molecular determinants of such interactions and to identify other potential sites.

DATA AVAILABILITY STATEMENT

The datasets generated for this study are available on request to the corresponding author.

AUTHOR CONTRIBUTIONS

MS and CI conceived, designed the experiments, and analyzed the data. MS and JC performed proteoliposome functional assays. EA performed docking analysis. LP prepared yeast constructs and optimized yeast cell growth. TM, AE, and LC performed yeast cell growth for protein over-expression and purification. MS, JC, and CI wrote the paper. CI supervised the work.

FUNDING

This work was in part supported by PRIN (Progetti di Ricerca di Interesse Nazionale) project n. 2017PAB8EM to CI, and in part by PON (Programma Operativo Nazionale) Project No. 01_00937 to CI. Both projects are granted by MIUR (Ministry of Education, University and Research)-Italy.

REFERENCES

Baier, C. J., Fantini, J., and Barrantes, F. J. (2011). Disclosure of cholesterol recognition motifs in transmembrane domains of the human nicotinic acetylcholine receptor. *Sci. Rep.* 1:69. doi: 10.1038/srep00069

Bhutia, Y. D., and Ganapathy, V. (2016). Glutamine transporters in mammalian cells and their functions in physiology and cancer. *Biochim. Biophys. Acta* 1863, 2531–2539. doi: 10.1016/j.bbamcr.2015.12.017

Brini, M., Leanza, L., and Szabo, I. (2017). Lipid-mediated modulation of intracellular ion channels and redox state: physiopathological implications. *Antioxid. Redox Signal.* 28. doi: 10.1089/ars.2017.7215

Broer, A., Brookes, N., Ganapathy, V., Dimmer, K. S., Wagner, C. A., Lang, F., et al. (1999). The astroglial ASCT2 amino acid transporter as a mediator of glutamine efflux. *J. Neurochem.* 73, 2184–2194. doi: 10.1046/j.1471-4159.1999.02184.x

Broer, A., Fairweather, S., and Broer, S. (2018). Disruption of amino acid homeostasis by novel ASCT2 inhibitors involves multiple targets. *Front. Pharmacol.* 9:785. doi: 10.3389/fphar.2018.00785

Canul-Tec, J. C., Assal, R., Cirri, E., Legrand, P., Brier, S., Chamot-Rooke, J., et al. (2017). Structure and allosteric inhibition of excitatory amino acid transporter 1. *Nature* 544, 446–451. doi: 10.1038/nature22064

Cesar-Razquin, A., Snijder, B., Frappier-Brinton, T., Isserlin, R., Gyimesi, G., Bai, X., et al. (2015). A call for systematic research on solute carriers. *Cell* 162, 478–487. doi: 10.1016/j.cell.2015.07.022

Chantranupong, L., Wolfson, R. L., and Sabatini, D. M. (2015). Nutrient-sensing mechanisms across evolution. *Cell* 161, 67–83. doi: 10.1016/j.cell.2015.02.041

Coleman, J. A., Green, E. M., and Gouaux, E. (2016). X-ray structures and mechanism of the human serotonin transporter. *Nature* 532, 334–339. doi: 10.1038/nature17629

Console, L., Scalise, M., Tarmakova, Z., Coe, I. R., and Indiveri, C. (2015). N-linked glycosylation of human SLC1A5 (ASCT2) transporter is critical for trafficking to membrane. *Biochim. Biophys. Acta* 1853, 1636–1645. doi: 10.1016/j.bbamcr.2015.03.017

Cynober, L. A. (2002). Plasma amino acid levels with a note on membrane transport: characteristics, regulation, and metabolic significance. *Nutrition* 18, 761–766. doi: 10.1016/S0899-9007(02)00780-3

Dephoure, N., Zhou, C., Villen, J., Beausoleil, S. A., Bakalarski, C. E., Elledge, S. J., et al. (2008). A quantitative atlas of mitotic phosphorylation. *Proc. Natl. Acad. Sci. U.S.A.* 105, 10762–10767. doi: 10.1073/pnas.0805139105

Dickens, D., Chiduza, G. N., Wright, G. S., Pirmohamed, M., Antonyuk, S. V., and Hasnain, S. S. (2017). Modulation of LAT1 (SLC7A5) transporter activity and stability by membrane cholesterol. *Sci. Rep.* 7:43580. doi: 10.1038/srep43580

Fantini, J., and Barrantes, F. J. (2013). How cholesterol interacts with membrane proteins: an exploration of cholesterol-binding sites including CRAC, CARC, and tilted domains. *Front. Physiol.* 4:31. doi: 10.3389/fphys.2013.00031

Fantini, J., Epand, R. M., and Barrantes, F. J. (2019). Cholesterol-recognition motifs in membrane proteins. *Adv. Exp. Med. Biol.* 1135, 3–25. doi: 10.1007/978-3-030-14265-0_1

Forli, S., Huey, R., Pique, M. E., Sanner, M. F., Goodsell, D. S., and Olson, A. J. (2016). Computational protein-ligand docking and virtual drug screening with the AutoDock suite. *Nat. Protoc.* 11, 905–919. doi: 10.1038/nprot.2016.051

Garaeva, A. A., Guskov, A., Slotboom, D. J., and Paulino, C. (2019). A one-gate elevator mechanism for the human neutral amino acid transporter ASCT2. *Nat. Commun.* 10:3427. doi: 10.1038/s41467-019-11363-x

Garaeva, A. A., Oostergetel, G. T., Gati, C., Guskov, A., Paulino, C., and Slotboom, D. J. (2018). Cryo-EM structure of the human neutral amino acid transporter ASCT2. *Nat. Struct. Mol. Biol.* 25, 515–521. doi: 10.1038/s41594-018-0076-y

Garcia, A., Lev, B., Hossain, K. R., Gorman, A., Diaz, D., Pham, T. H. N., et al. (2019). Cholesterol depletion inhibits Na(+),K(+)-ATPase activity in a near-native membrane environment. *J. Biol. Chem.* 294, 5956–5969. doi: 10.1074/jbc.RA118.006223

Garcia-Bermudez, J., Baudrier, L., Bayraktar, E. C., Shen, Y., La, K., Guarecuco, R., et al. (2019). Squalene accumulation in cholesterol auxotrophic lymphomas prevents oxidative cell death. *Nature* 567, 118–122. doi: 10.1038/s41586-019-0945-5

Giangregorio, N., Tonazzi, A., Console, L., Pistillo, M., Scalera, V., and Indiveri, C. (2019). Tryptophan 224 of the rat mitochondrial carnitine/acylcarnitine carrier is crucial for the antiport mechanism. *Biochim. Biophys. Acta Bioenerg.* 1860, 708–716. doi: 10.1016/j.bbabio.2019.07.006

Giraud, F., Claret, M., and Garay, R. (1976). Interactions of cholesterol with the Na pump in red blood cells. *Nature* 264, 646–648. doi: 10.1038/264646a0

Hanson, M. A., Cherezov, V., Griffith, M. T., Roth, C. B., Jaakola, V. P., Chien, E. Y., et al. (2008). A specific cholesterol binding site is established by the 2.8 A structure of the human beta2-adrenergic receptor. *Structure* 16, 897–905. doi: 10.1016/j.str.2008.05.001

Indiveri, C., Palmieri, L., and Palmieri, F. (1994). Kinetic characterization of the reconstituted ornithine carrier from rat liver mitochondria. *Biochim. Biophys. Acta* 1188, 293–301. doi: 10.1016/0005-2728(94)90048-5

Kanai, Y., Clemencon, B., Simonin, A., Leuenberger, M., Lochner, M., Weisstanner, M., et al. (2013). The SLC1 high-affinity glutamate and neutral amino acid transporter family. *Mol. Aspects Med.* 34, 108–120. doi: 10.1016/j.mam.2013.01.001

Kekuda, R., Prasad, P. D., Fei, Y. J., Torres-Zamorano, V., Sinha, S., Yang-Feng, T. L., et al. (1996). Cloning of the sodium-dependent, broad-scope, neutral amino acid transporter Bo from a human placental choriocarcinoma cell line. *J. Biol. Chem.* 271, 18657–18661. doi: 10.1074/jbc.271.31.18657

Komor, B., Komor, E., and Tanner, W. (1974). Transformation of a strictly coupled active transport system into a facilitated diffusion system by nystatin. *J. Membr. Biol.* 17, 231–238. doi: 10.1007/BF01870184

Kulig, W., Jurkiewicz, P., Olzynska, A., Tynkkynen, J., Javanainen, M., Manna, M., et al. (2015). Experimental determination and computational interpretation of biophysical properties of lipid bilayers enriched by cholesteryl hemisuccinate. *Biochim. Biophys. Acta* 1848, 422–432. doi: 10.1016/j.bbamem.2014.10.032

Leke, R., and Schousboe, A. (2016). The glutamine transporters and their role in the glutamate/GABA-glutamine cycle. *Adv. Neurobiol.* 13, 223–257. doi: 10.1007/978-3-319-45096-4_8

Li, H., and Papadopoulos, V. (1998). Peripheral-type benzodiazepine receptor function in cholesterol transport. Identification of a putative cholesterol recognition/interaction amino acid sequence and consensus pattern. *Endocrinology* 139, 4991–4997. doi: 10.1210/endo.139.12.6390

Listowski, M. A., Leluk, J., Kraszewski, S., and Sikorski, A. F. (2015). Cholesterol interaction with the MAGUK protein family member, MPP1, via CRAC and CRAC-like motifs: an in silico docking analysis. *PLoS ONE* 10:e0133141. doi: 10.1371/journal.pone.0133141

Litvinov, D. Y., Savushkin, E. V., and Dergunov, A. D. (2018). Intracellular and plasma membrane events in cholesterol transport and homeostasis. *J. Lipids* 2018:3965054. doi: 10.1155/2018/3965054

Loudon, G. M., and Koshland, D. E. Jr. (1970). The chemistry of a reporter group: 2-hydroxy-5-nitrobenzyl bromide. *J. Biol. Chem.* 245, 2247–2254.

McGivan, J. D., and Bungard, C. I. (2007). The transport of glutamine into mammalian cells. *Front. Biosci.* 12, 874–882. doi: 10.2741/2109

Oberg, F., Sjohamn, J., Conner, M. T., Bill, R. M., and Hedfalk, K. (2011). Improving recombinant eukaryotic membrane protein yields in Pichia pastoris: the importance of codon optimization and clone selection. *Mol. Membr. Biol.* 28, 398–411. doi: 10.3109/09687688.2011.602219

Oppedisano, F., Pochini, L., Galluccio, M., Cavarelli, M., and Indiveri, C. (2004). Reconstitution into liposomes of the glutamine/amino acid transporter from renal cell plasma membrane: functional characterization, kinetics and activation by nucleotides. *Biochim. Biophys. Acta* 1667, 122–131. doi: 10.1016/j.bbamem.2004.09.007

Oppedisano, F., Pochini, L., Galluccio, M., and Indiveri, C. (2007). The glutamine/amino acid transporter (ASCT2) reconstituted in liposomes: transport mechanism, regulation by ATP and characterization of the glutamine/glutamate antiport. *Biochim. Biophys. Acta* 1768, 291–298. doi: 10.1016/j.bbamem.2006.09.002

Palmieri, F., and Klingenberg, M. (1979). Direct methods for measuring metabolite transport and distribution in mitochondria. *Meth. Enzymol.* 56, 279–301. doi: 10.1016/0076-6879(79)56029-7

Penmatsa, A., Wang, K. H., and Gouaux, E. (2013). X-ray structure of dopamine transporter elucidates antidepressant mechanism. *Nature* 503, 85–90. doi: 10.1038/nature12533

Pettersen, E. F., Goddard, T. D., Huang, C. C., Couch, G. S., Greenblatt, D. M., Meng, E. C., et al. (2004). UCSF Chimera–a visualization system for exploratory research and analysis. *J. Comput. Chem.* 25, 1605–1612. doi: 10.1002/jcc.20084

Pingitore, P., Pochini, L., Scalise, M., Galluccio, M., Hedfalk, K., and Indiveri, C. (2013). Large scale production of the active human ASCT2 (SLC1A5) transporter in Pichia pastoris–functional and kinetic asymmetry revealed in proteoliposomes. *Biochim. Biophys. Acta* 1828, 2238–2246. doi: 10.1016/j.bbamem.2013.05.034

Rebsamen, M., Pochini, L., Stasyk, T., de Araujo, M. E., Galluccio, M., Kandasamy, R. K., et al. (2015). SLC38A9 is a component of the lysosomal amino acid sensing machinery that controls mTORC1. *Nature* 519, 477–481. doi: 10.1038/nature14107

Sanchez-Linares, I., Perez-Sanchez, H., Cecilia, J. M., and Garcia, J. M. (2012). High-throughput parallel blind virtual screening using BINDSURF. *BMC Bioinformatics* 13(Suppl. 14):S13. doi: 10.1186/1471-2105-13-S14-S13

Scalise, M., Console, L., Galluccio, M., Pochini, L., Tonazzi, A., Giangregorio, N., et al. (2019). Exploiting cysteine residues of SLC membrane transporters as targets for drugs. *SLAS Discov.* 24, 867–881. doi: 10.1177/2472555219856601

Scalise, M., Galluccio, M., Pochini, L., Console, L., Barile, M., Giangregorio, N., et al. (2017a). Studying interactions of drugs with cell membrane nutrient transporters: new frontiers of proteoliposome nanotechnology. *Curr. Pharm. Des.* 23, 3871–3883. doi: 10.2174/1381612823666170616083705

Scalise, M., Pochini, L., Console, L., Losso, M. A., and Indiveri, C. (2018a). The human SLC1A5 (ASCT2) amino acid transporter: from function to structure and role in cell biology. *Front. Cell Dev. Biol.* 6:96. doi: 10.3389/fcell.2018.00096

Scalise, M., Pochini, L., Console, L., Pappacoda, G., Pingitore, P., Hedfalk, K., et al. (2018b). Cys site-directed mutagenesis of the human SLC1A5 (ASCT2) transporter: structure/function relationships and crucial role of Cys467 for redox sensing and glutamine transport. *Int. J. Mol. Sci.* 19:E648. doi: 10.3390/ijms19030648

Scalise, M., Pochini, L., Galluccio, M., Console, L., and Indiveri, C. (2017b). Glutamine transport and mitochondrial metabolism in cancer cell growth. *Front. Oncol.* 7:306. doi: 10.3389/fonc.2017.00306

Scalise, M., Pochini, L., Panni, S., Pingitore, P., Hedfalk, K., and Indiveri, C. (2014). Transport mechanism and regulatory properties of the human amino acid transporter ASCT2 (SLC1A5). *Amino Acids* 46, 2463–2475. doi: 10.1007/s00726-014-1808-x

Scalise, M., Pochini, L., Pingitore, P., Hedfalk, K., and Indiveri, C. (2015). Cysteine is not a substrate but a specific modulator of human ASCT2 (SLC1A5) transporter. *FEBS Lett.* 589, 3617–3623. doi: 10.1016/j.febslet.2015.10.011

Schulte, M. L., Fu, A., Zhao, P., Li, J., Geng, L., Smith, S. T., et al. (2018). Pharmacological blockade of ASCT2-dependent glutamine transport leads to antitumor efficacy in preclinical models. *Nat. Med.* 24, 194–202. doi: 10.1038/nm.4464

Sheng, R., Chen, Y., Yung Gee, H., Stec, E., Melowic, H. R., Blatner, N. R., et al. (2012). Cholesterol modulates cell signaling and protein networking by specifically interacting with PDZ domain-containing scaffold proteins. *Nat. Commun.* 3:1249. doi: 10.1038/ncomms2221

Sutherland, B. W., Toews, J., and Kast, J. (2008). Utility of formaldehyde cross-linking and mass spectrometry in the study of protein-protein interactions. *J. Mass Spectrom.* 43, 699–715. doi: 10.1002/jms.1415

Tonazzi, A., Giangregorio, N., Console, L., Scalise, M., La Russa, D., Notaristefano, C., et al. (2015). Mitochondrial carnitine/acylcarnitine transporter, a novel target of mercury toxicity. *Chem. Res. Toxicol.* 28, 1015–1022. doi: 10.1021/acs.chemrestox.5b00050

Torchetti, E. M., Bonomi, F., Galluccio, M., Gianazza, E., Giancaspero, T. A., Iametti, S., et al. (2011). Human FAD synthase (isoform 2): a component of the machinery that delivers FAD to apo-flavoproteins. *FEBS J.* 278, 4434–4449. doi: 10.1111/j.1742-4658.2011.08368.x

Torres-Zamorano, V., Leibach, F. H., and Ganapathy, V. (1998). Sodium-dependent homo- and hetero-exchange of neutral amino acids mediated by the amino acid transporter ATB degree. *Biochem. Biophys. Res. Commun.* 245, 824–829. doi: 10.1006/bbrc.1998.8434

Utsunomiya-Tate, N., Endou, H., and Kanai, Y. (1996). Cloning and functional characterization of a system ASC-like Na+-dependent neutral amino acid transporter. *J. Biol. Chem.* 271, 14883–14890. doi: 10.1074/jbc.271.25.14883

Yan, R., Zhao, X., Lei, J., and Zhou, Q. (2019). Structure of the human LAT1-4F2hc heteromeric amino acid transporter complex. *Nature* 568, 127–130. doi: 10.1038/s41586-019-1011-z

Yang, S. T., Kreutzberger, A. J. B., Lee, J., Kiessling, V., and Tamm, L. K. (2016). The role of cholesterol in membrane fusion. *Chem. Phys. Lipids* 199, 136–143. doi: 10.1016/j.chemphyslip.2016.05.003

Yernool, D., Boudker, O., Jin, Y., and Gouaux, E. (2004). Structure of a glutamate transporter homologue from *Pyrococcus horikoshii*. *Nature* 431, 811–818. doi: 10.1038/nature03018

Yu, X., Plotnikova, O., Bonin, P. D., Subashi, T. A., McLellan, T. J., Dumlao, D., et al. (2019). Structural basis for the transport mechanism of the human glutamine transporter SLC1A5 (ASCT2). *bioRxiv*, 622563. doi: 10.1101/622563

Conflict of Interest: The authors declare that the research was conducted in the absence of any commercial or financial relationships that could be construed as a potential conflict of interest.

frontiers in Cell and Developmental Biology

ORIGINAL RESEARCH
published: 08 July 2020
doi: 10.3389/fcell.2020.00603

The Human SLC1A5 Neutral Amino Acid Transporter Catalyzes a pH-Dependent Glutamate/Glutamine Antiport, as Well

Mariafrancesca Scalise[1†], Tiziano Mazza[1†], Gilda Pappacoda[1], Lorena Pochini[1], Jessica Cosco[1], Filomena Rovella[1] and Cesare Indiveri[1,2]*

[1] Department DiBEST (Biologia, Ecologia, Scienze della Terra), Unit of Biochemistry and Molecular Biotechnology, University of Calabria, Arcavacata, Italy, [2] CNR Institute of Biomembranes, Bioenergetics and Molecular Biotechnologies (IBIOM), Bari, Italy

OPEN ACCESS

Edited by:
Graça Soveral,
University of Lisbon, Portugal

Reviewed by:
Stefan Broer,
Australian National University, Australia
Piero Pingitore,
University of Gothenburg, Sweden
Christof Grewer,
Binghamton University, United States

***Correspondence:**
Cesare Indiveri
cesare.indiveri@unical.it

[†] These authors have contributed equally to this work

Specialty section:
This article was submitted to Cellular Biochemistry, a section of the journal Frontiers in Cell and Developmental Biology

Received: 17 May 2020
Accepted: 19 June 2020
Published: 08 July 2020

Citation:
Scalise M, Mazza T, Pappacoda G, Pochini L, Cosco J, Rovella F and Indiveri C (2020) The Human SLC1A5 Neutral Amino Acid Transporter Catalyzes a pH-Dependent Glutamate/Glutamine Antiport, as Well. Front. Cell Dev. Biol. 8:603. doi: 10.3389/fcell.2020.00603

ASCT2 is a neutral amino acid transporter, which catalyzes a sodium-dependent obligatory antiport among glutamine and other neutral amino acids. The human ASCT2 over-expressed in *Pichia pastoris* and reconstituted in proteoliposomes has been employed for identifying alternative substrates of the transporter. The experimental data highlighted that hASCT2 also catalyzes a sodium-dependent antiport of glutamate with glutamine. This unconventional antiport shows a preferred sidedness: glutamate is inwardly transported in exchange for glutamine transported in the counter direction. The orientation of the transport protein in proteoliposomes is the same as in the cell membrane; then, the observed sidedness corresponds to the transport of glutamate from the extracellular to the intracellular compartment. The competitive inhibition exerted by glutamate on the glutamine transport together with the docking analysis indicates that the glutamate binding site is the same as that of glutamine. The affinity for glutamate is lower than that for neutral amino acids, while the transport rate is comparable to that measured for the asparagine/glutamine antiport. Differently from the neutral amino acid antiport that is insensitive to pH, the glutamate/glutamine antiport is pH-dependent with optimal activity at acidic pH on the external (extracellular) side. The stimulation of glutamate transport by a pH gradient suggests the occurrence of a proton flux coupled to the glutamate transport. The proton transport has been detected by a spectrofluorometric method. The rate of proton transport correlates well with the rate of glutamate transport indicating a 1:1 stoichiometry H^+: glutamate. The glutamate/glutamine antiport is also active in intact HeLa cells. On a physiological point of view, the described antiport could have relevance in some districts in which a glutamate/glutamine cycling is necessary, such as in placenta.

Keywords: amino acid, SLC, glutamine, glutamate, membrane, transport, proteoliposome

Abbreviations: BBB, Blood Brain Barrier; BMGY, Buffered Glycerol-complex Medium; BMMY, Buffered Methanol-complex Medium; $C_{12}E_8$, Octaethylene glycol monododecyl ether; CNS, Central Nervous System; CryoEM, CryoElectron Microscopy; DEPC; diethyl pyrocarbonate; DMEM, Dulbecco's Modified Eagle Medium; DTE, DiThioErythritol; SLC, SoLute Carrier; YPDS, Yeast Extract Peptone Dextrose Sorbitol.

INTRODUCTION

The fifth member of the SLC1 family, ASCT2 (SLC1A5), attracted the attention of the membrane transport scientific community in the last years for its link with the metabolic rewiring occurring in cancer cells. The increased efforts in studying this transporter revealed novel physiological roles in the regulation of the amino acid homeostasis (Scalise et al., 2018a; Freidman et al., 2020) and brought to the resolution of the 3D structure (Garaeva et al., 2018). Since its first isolation in mice and human cells, ASCT2 was described as a sodium-dependent obligatory antiporter of neutral amino acids with specificity toward Ala, Ser, and Cys as indicated by the acronym ASCT2. Soon after its basic functional characterization, glutamine revealed to be the preferred substrate of the protein. This data was obtained in studies conducted in intact cell systems as well as in proteoliposomes using the murine and the human isoforms of ASCT2 either in native form or obtained by over-production in *P. pastoris* (Utsunomiya-Tate et al., 1996; Torres-Zamorano et al., 1998; Oppedisano et al., 2007; Pingitore et al., 2013). Interestingly, the availability of the recombinant hASCT2 together with its reconstitution in proteoliposomes allowed solving some controversies around this protein. As an example, it was demonstrated that the antiport of neutral amino acids, coupled to the movement of at least one sodium ion, is electrogenic in contrast with the previous believing describing an electroneutral exchange of amino acids and sodium. The intracellular sodium is an allosteric regulator of the hASCT2 transport function (Scalise et al., 2014). The kinetics of transport reaction obeys to a random simultaneous mechanism in which the three substrates do not influence the affinity of the transporter toward each other. A trimeric assembly of hASCT2 was proposed by cross-linking experiments. In this quaternary structure, the monomers work independently from each other (Scalise et al., 2014). Later on, the 3D structure of ASCT2 was solved by CryoEM employing the protein over-produced in *P. pastoris* (Pingitore et al., 2013; Garaeva et al., 2018, 2019), confirmed that the protein is organized as a trimer in the plasma membrane. The high affinity of hASCT2 toward glutamine underlies its role in cancer (Bhutia et al., 2015; Scalise et al., 2018a). Indeed, cancer cells are glutamine addicted and require a great supply of this amino acid to sustain their high proliferation rate both in terms of biomass and energy production. Interestingly, ASCT2 is overexpressed in virtually all human cancers, thus, it is not a surprise that this protein became a hot target for drug design (Bhutia et al., 2015; Scalise et al., 2018a). Therefore, one of the most attractive topics around hASCT2 is defining the molecular determinants for the substrate specificity. Understanding this basic aspect is, indeed, fundamental in either physiological studies and pharmacological applications. In this respect, it was recently described that cysteine is not a substrate of ASCT2 but acts as an allosteric regulator driving a glutamine efflux in intact cells as well as in proteoliposomes (Scalise et al., 2015). Then, data on the substrate-binding site were obtained by site-directed mutagenesis (Scalise et al., 2018a), which correlated well with the 3D structure (Garaeva et al., 2018, 2019). Soon after, the modulation of the transport function by cholesterol was described by structure/function relationship studies (Scalise et al., 2019). Again, this last finding correlated well with structural data obtained by CryoEM (Yu et al., 2019). In the frame of substrate specificity, previous results showed that some transporters of the SLC1 family, as well as their bacterial homologs, can be forced to switch the specificity from neutral amino acids to acidic ones (glutamate or aspartate) or vice versa, by mutating some specific residues (Scopelliti et al., 2013, 2018; Canul-Tec et al., 2017). Noteworthy, besides these artificial mutations, the very first report on mice ASCT2 showed Na^+ and pH-dependent transport of glutamate with a Km in the millimolar range, indicating a lower affinity compared to that of neutral amino acids (Utsunomiya-Tate et al., 1996; Broer et al., 1999). Then, it was shown that glutamate triggered the glutamine efflux in rat astrocytes but without a definitive molecular explanation (Deitmer and Rose, 1996; Broer and Brookes, 2001). The rat ASCT2 reconstituted in liposomes catalyzed a glutamine/glutamate antiport even though at a lower efficiency in comparison to that of neutral amino acids (Oppedisano et al., 2007) correlating with the data collected in intact cells. No data on direct glutamate transport by the human isoform of ASCT2 was available so far, then, we have further dealt with the issue of substrate "adaptation" by investigating the capacity of the hASCT2 to transport glutamate and aspartate. Indeed, we here demonstrated that the wild type hASCT2 can mediate a Na^+ dependent $aspartate_{ex}$-$glutamate_{ex}$/$glutamine_{in}$ antiport without any artificial modification of its primary structure. This novel aspect represents a step forward in the understanding of the actual physiological role of hASCT2 with potential outcomes also in pharmaceutical applications.

MATERIALS AND METHODS

Materials

The *P. pastoris* wild type strain (X-33), the pPICZB vector, zeocin, Ni-NTA agarose resin were from Invitrogen; PD-10 columns were from GE Healthcare; L-[^{3}H]Glutamine and L-[^{3}H]glutamic acid were from Perkin Elmer; $C_{12}E_8$ was from TCI Europe; Cholesterol, Amberlite XAD-4, egg yolk phospholipids (3-sn-phosphatidylcholine from egg yolk), Sephadex G-75, L-glutamine, L-glutamic acid monosodium salt, DEPC, valinomycin, nigericin, pyranine (8-Hydroxypyrene-1,3,6-trisulfonic acid trisodium salt) and all the other reagents were from Sigma-Aldrich.

Recombinant Production of hASCT2-6His

To produce the recombinant hASCT2-6His protein a previously pointed out approach was employed (Pingitore et al., 2013). In brief: 10 μg of pPICZB-ASCT2-6His WT construct was linearized with *Pme*I. The linearized plasmid was used to transform *P. pastoris* wild type strain X-33 by electroporation (Oberg et al., 2011). Prior large scale protein production, transformed *P. pastoris* cells were selected using YPDS plates containing 2,000 μg/ml zeocin; then, cells were inoculated in BMGY medium (Buffered glycerol-complex medium) and grown at 30°C under rotatory stirring (Scalise et al., 2018b). Then, the

BMGY medium was removed by centrifuging *P. pastoris* cells which were resuspended at final OD of 1 in 250 ml BMMY medium (Buffered complex methanol medium) containing 0.5% methanol. The cells were placed in a 2 L conical flask and grown in the same medium at 30°C under rotatory stirring, for 3 days. Fresh methanol was added every 24 h. The *P. pastoris* membrane fraction was prepared using, as starting material, 30-40 g of cells resuspended in 300 ml of a buffer composed by 50 mM Tris–HCl pH 7.4, 150 mM NaCl, 2 mM β-mercaptoethanol and 0.5 mM PMSF. The cell suspension was loaded in the chamber of a bead beater (BioSpec Product) for disruption using glass beads (0.5 mm) for 5 min cycle reaching 90% of cell disruption. Then, the broken cell suspension was centrifuged in a JA10 rotor at 10,000 g for 30 min at 4°C. The collected supernatant, containing membrane and cytosolic fractions, was subjected to centrifugation in a JA30.50 rotor at 45,000 g for 90 min at 4°C. The resulting pellet containing membrane fraction was washed with a buffer composed by 5 mM Tris–HCl pH 7.4, 2 mM EDTA, 2 mM EGTA and 4 M urea, followed by another centrifugation cycle as above described. The washed membrane fraction was resuspended in a buffer composed by 25 mM Tris–HCl pH 7.4, 250 mM NaCl, 2 mM β-mercaptoethanol and 10% glycerol to reach a concentration of about 400 mg/ml. The membranes were homogenized with a potter and 3 mL aliquots were stored at −80°C before solubilization.

Solubilization and Purification of hASCT2-6His

The purification of hASCT2-6His was performed starting from about 1.2 g of washed membranes (400 mg/ml) that were solubilized in a buffer composed by 25 mM Tris–HCl pH 7.4, 250 mM NaCl, 6 mM β-mercaptoethanol, 1 mM L-glutamine, 10% glycerol and 2% $C_{12}E_8$ (w/w). The solubilization was performed under rotatory stirring for 3 h at 4°C followed by centrifugation at 18,000 × *g* for 45 min. The supernatant was applied to 2 ml Ni-nitrilotriacetic acid (NTA) agarose resin pre-equilibrated with a buffer containing 20 mM Tris–HCl pH 7.4, 300 mM NaCl, 10% glycerol, 6 mM β-mercaptoethanol, 0.03% $C_{12}E_8$, 1 mM L-glutamine and 50 mM imidazole and incubated over-night, with gentle agitation, at 4°C. Then, the Ni-NTA resin was packed by gravity into a glass-column and washed with 30 ml of the same buffer above described. Elution of protein was, then, performed using 10 ml of a buffer containing 20 mM Tris–HCl pH 7.4, 300 mM NaCl, 10% glycerol, 6 mM β-mercaptoethanol, 0.03% $C_{12}E_8$, 1 mM L-glutamine and 500 mM imidazole. 2.5 ml of purified protein were pooled and desalted on a PD-10 column from which 3.5 ml were collected. The column was pre-equilibrated and eluted with a buffer composed by 20 mM Tris–HCl pH 7.4, 100 mM NaCl, 10% glycerol, 6 mM β-mercaptoethanol, 0.03% $C_{12}E_8$ and 1 mM L-glutamine.

Inclusion of Cholesterol in Liposome Preparation

7.5 mg of cholesterol were added to 100 mg of egg yolk phospholipids and solubilized with 1 mL of chloroform obtaining a completely clear solution. After short incubation under rotatory stirring (30°C 5 min 1200 rpm) open tube is dried O.N. at room temperature. The dried lipid film was resuspended in 1 mL water (10% final concentration) and unilamellar liposomes were formed by two sonication cycles of 1 min (1 pulse ON and 1 pulse OFF, 40 W) with a Vibracell VCX-130 sonifier as previously suggested (Hanson et al., 2008).

Reconstitution of the hASCT2-6His Into Liposomes

The purified hASCT2 was reconstituted by detergent removal in a batch-wise procedure. Mixed micelles of detergent, protein and phospholipids were incubated with 0.5 g Amberlite XAD-4 resin under rotatory stirring (1,200 rpm) at 23°C for 40 min as previously described (Scalise et al., 2019). The composition of the reconstitution was: 50 μl of the purified hASCT2 (5 μg protein), 2 mM EDTA, 220 μl of a mixture composed by 100 μl of 10% (w/v) egg yolk phospholipids (with or without included cholesterol as described in section 2.4) in the form of sonicated liposomes and 120 μl of 10% $C_{12}E_8$, 10 mM L-glutamine (or other amino acids as specified in the figure legend), 20 mM Hepes Tris pH 6.0 (or different pH as specified in the figure legend) and 10 mM NaCl (deriving from the purified protein and EDTA) in a final volume of 700 μl. All the operations were performed at room temperature.

Transport Measurements

To remove the external compounds, 600 μL of proteoliposomes was passed through a sephadex G-75 column (0.7 cm diameter × 15 cm height) pre-equilibrated with a buffer composed by 20 mM Hepes Tris pH 6.0 and sucrose to balance the internal osmolarity. Uptake experiments were started in a 100 μl proteoliposomes sample by adding 50 μM [^{3}H]glutamine or 500 μM [^{3}H]glutamic acid (or other radiolabeled substrates as indicated in the figure legends) together with 50 mM Na-gluconate to, at 25°C. The transport reaction was stopped at the indicated times using 100 μM $HgCl_2$. The control sample, blank, was prepared by adding the same inhibitor at time zero according to the inhibitor stop method (Palmieri and Klingenberg, 1979). At the end of the transport, 100 μL of proteoliposomes was passed through a sephadex G-75 column (0.6 cm diameter × 8 cm height) buffered with 50 mM NaCl to separate the external from the internal radioactivity. Then, proteoliposomes were eluted with 1 ml 50 mM NaCl and added with 3 ml of scintillation mixture, vortexed and counted. The experimental values were analyzed by subtracting to each sample the respective blank; the initial rate of transport was measured by stopping the reaction after 15 min, i.e., within the initial linear range of radiolabeled substrate uptake into the proteoliposomes.

Spectrofluorometric Assays

The intraliposomal pH changes were monitored by measuring the fluorescence emission of pyranine included inside the proteoliposomes. Reconstitution mixture was performed as described in section 2.4 with some modifications: 25 μg purified

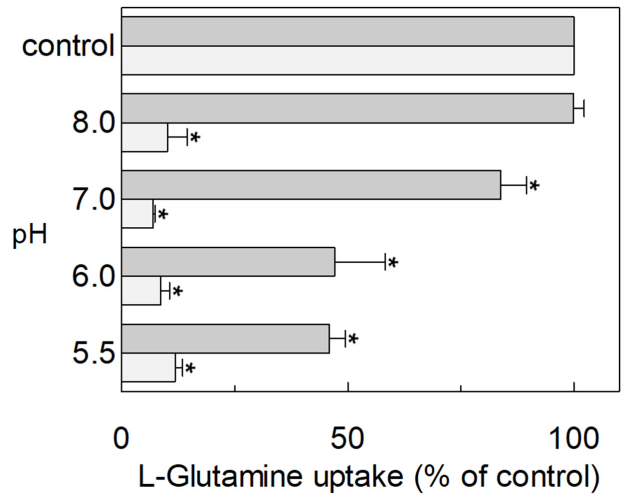

FIGURE 1 | Effect of glutamate and alanine on the glutamine transport by hASCT2 reconstituted in proteoliposomes. Purified hASCT2 was reconstituted in proteoliposomes prepared at the indicated pH and containing 10 mM glutamine, as described in materials and methods. The transport assay was started by adding 50 μM [^{3}H]glutamine, buffered at the indicated pH, in the presence of 50 mM Na-gluconate and 1 mM glutamate (gray bar) or 1 mM alanine (light gray bar). The transport was measured in 15 min according to the stop inhibitor method. The transport was indicated as % [^{3}H]glutamine uptake with respect to the condition with no addition (control). Results are means ± S.D. from three independent experiments. *Significantly different from the control as estimated by Student's *t*-test ($P < 0.05$).

protein was used for the reconstitution mixture and 0.1 mM pyranine at pH 7.0 was included in proteoliposomes. After reconstitution, 600 μL of proteoliposomes was passed through a sephadex G-75 column, pre-equilibrated with 20 mM Hepes Tris pH 7.0 and 10 mM sucrose, except where differently indicated. Then, 150 μL proteoliposomes were diluted in 3 ml of the same buffer containing 100 mM Na-gluconate, except where differently indicated. In the blank sample, 10 μM $HgCl_2$ was added according to the stop inhibitor method above described. To start the transport assay, 5 mM glutamate buffered at pH 7.0, except where differently indicated, was added to induce $glutamine_{in}/glutamate_{ex}$ antiport; the uptake of protons was measured as a reduction of pyranine fluorescence included in proteoliposomes. The measurement was performed in the fluorescence spectrometer (LS55) from Perkin Elmer under rotatory stirring. The fluorescence was measured following time drive acquisition protocol with λ excitation = 450 nm and λ emission = 520 nm (slit 5/5) according to manufacturer instructions of pyranine. Calibration of the internal fluorescence changes vs. pH inside the proteoliposomes has been performed by reconstituting proteoliposomes with different pH buffers (from pH 6.0 to pH 7.5). Then, the fluorescence of internal pyranine was measured as function of the internal pH finding a linear correlation. The calibration was used to report the data of **Figure 9B** as nmol of protons transported inside proteoliposomes with glutamate and to calculate the stoichiometry of proton uptake vs. glutamate uptake.

Sequence Alignment and Molecular Docking Approach

Multiple sequence alignment of SLC1 members was performed using Clustal Omega, after downloading amino acid sequences from UniProt. Docking analysis was performed using AutoDock Vina v.1.1.2 (Trott and Olson, 2010). The grid box was generated on the binding site, on the basis of glutamine coordination, and its size was set to 40 × 40 × 40 Å (x, y, and z) with spacing 0.375. Glutamate was downloaded from PubChem in sdf format. The ligand was prepared using LigPrep (Schrödinger, 2020a) within Schrödinger-Maestro v.12.4 (Schrödinger, 2020b). Default parameters were applied, except for the pH range since the ligand was prepared at two pH, 2.0 ± 0.5 and 7.0 ± 0.5, to have two different protonation states. Glutamate, with two different protonation states, was docked into refined ASCT2 (PDB ID: 6GCT, chain A). Lamarckian Genetic Algorithm was employed to search for the best conformation space of the ligand. Default parameters were used and 20 different conformations of glutamic acid were generated. The pose with the lowest binding energy conformation was chosen. Molecular visualization was performed with the UCSF Chimera v.1.14 software (Pettersen et al., 2004) (Resource for Biocomputing, Visualization, and Informatics, University of California, San Francisco, CA, United States).

Cell Culture and Transport Assay in Intact Cells

HeLa cells were maintained in Dulbecco's Modified Eagle Medium (DMEM) supplemented with 10% (v/v) fetal bovine serum (FBS), 1 mM sodium pyruvate and 4 mM glutamine. The cells were grown in a humidified incubator in a 5% CO2 atmosphere at 37°C. Cells for the transport assay were seeded into a 12 well dish up to 80% confluence. After 24 h, the medium was removed and the cells were washed twice with warm transport medium containing 20 mM Tris–HCl pH 7.4, 130 mM NaCl, 10 mM BCH, 10 mM MeAIB and 100 μM nimesulide. For efflux experiments, cells were allowed to take in 10 μM [^{3}H]glutamine up to 10 min. Thus, uptake buffer was removed and cells were rinsed two times with 0.5 mL per well of ice-cold transport buffer containing 20 mM Tris–HCl pH 7.4; [^{3}H]glutamine efflux was measured in 0.5 mL of transport buffer containing 130 mM NaCl and 20 mM Tris–HCl pH 7.0 or pH 6.0 as indicated in the figure legends in the presence of 10 mM different substrates. The efflux was measured within 1 min and cells from each well were solubilized in 500 μl of 1% TX-100 solution. Intracellular radioactivity was measured by adding 3 mL of Scintillation Cocktail to 400 μl of cell extract.

Other Methods

To generate imposed membrane potential, valinomycin (0.75 μg/mg of phospholipid) was added to proteoliposomes prepared with intraliposomal 50 mM K-gluconate. Proteoliposomes were passed through sephadex-G75 and, then, treated with valinomycin for 30 sec before transport

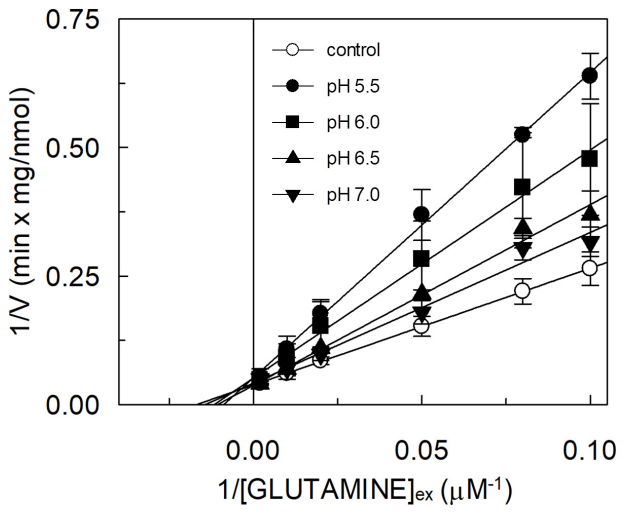

FIGURE 2 | Effect of glutamate on the kinetics of glutamine transport by hASCT2 reconstituted in proteoliposomes. Purified hASCT2 was reconstituted in proteoliposomes prepared at the indicated pH and containing 10 mM glutamine, as described in materials and methods. The transport was started by adding indicated concentrations of [^{3}H]glutamine and 50 mM Na-gluconate to proteoliposomes in the presence of 5 mM glutamate buffered at different pH: pH 5.5 (●), pH 6.0(■), pH 6.5 (▲), pH 7.0 (▼). The control condition (○) represents a mean of [^{3}H]glutamine measurements at the different pH (5.5, 6.0, 6.5, and 7.0) being Km for glutamine not affected by pH variations. The transport was measured in 15 min according to the stop inhibitor method. Data were plotted according to linear Lineweaver–Burk equation as reciprocal transport rate vs. reciprocal glutamine concentration. Results are means ± SD from three independent experiments.

measurement to allow potassium diffusion downhill its concentration gradient. To generate an artificial pH gradient (ΔpH), nigericin (0.15 μg/mg phospholipid) was added to proteoliposomes in the presence of an inwardly directed K^+ gradient. Proteoliposomes were passed through sephadex-G75 and, then, treated with nigericin for 30 sec before transport measurement to allow potassium/proton exchange. For DEPC treatment, proteoliposomes were incubated after passage through sephadex G-75 column with 5 mM DEPC solution for 5 min under rotatory stirring (1,200 rpm) at 23°C prior transport measurement. Stock solutions of valinomycin, nigericin and DEPC in ethanol were prepared daily, and intermediate dilutions of this reagent into buffer were prepared immediately before use. The amount of purified recombinant hASCT2 WT was estimated from Coomassie blue-stained 12% SDS–PAGE gels by using the ChemiDoc imaging system equipped with Quantity One software (Bio-Rad) as previously described (Giancaspero et al., 2015).

Data Analysis

Results are expressed as means ± SD. GraFit 5.0.13 software was used to calculate kinetic parameters, to derive per cent of residual activity values in inhibition assays and to measure transport rate by first-order rate equation. The statistical significance of experimental data was assessed by Student's test for $p < 0.05$ as specified in the figure legends.

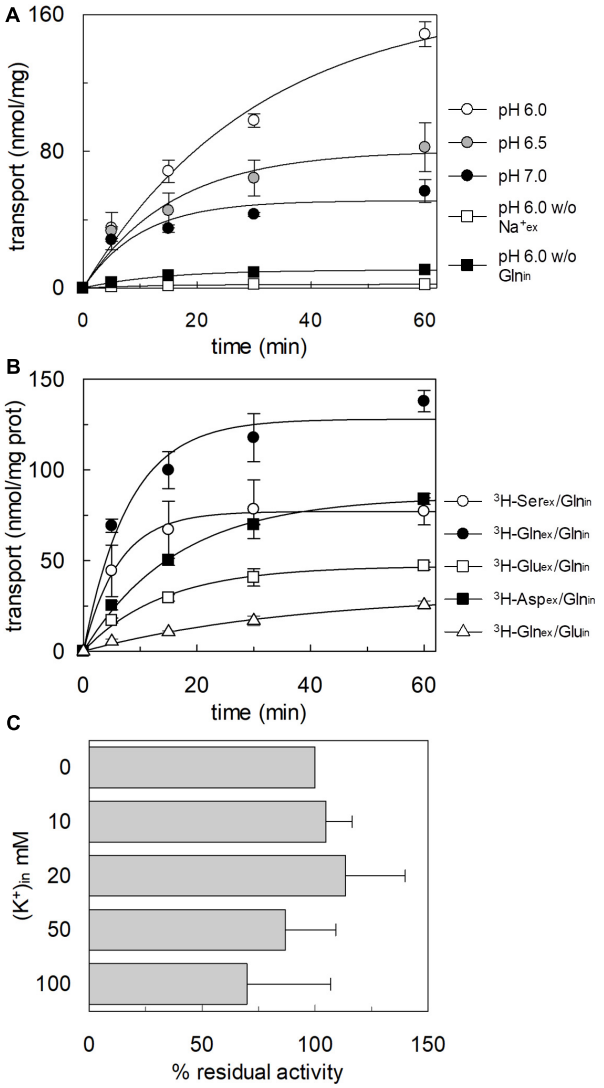

FIGURE 3 | Functional characterization of glutamate transport by hASCT2 reconstituted in proteoliposomes. Purified hASCT2 was reconstituted in proteoliposomes as described in materials and methods. In **(A)**, Uptake of [^{3}H]glutamate. The transport was started by adding 500 μM of [^{3}H]glutamate in the absence (■) or the presence (○,■,●,●) of 50 mM Na-gluconate to proteoliposomes containing (○,■,●,●) or not (□) 10 mM glutamine. Proteoliposomes and radiolabeled substrate were prepared at pH 6 (○,■,□), pH 6.5 (●), or pH 7(●). In **(B)**, Uptake of [^{3}H]serine, [^{3}H]asparagine, [^{3}H]glutamine, and [^{3}H]glutamate. The transport was started by adding 50 μM [^{3}H]serine$_{ex}$ (○) or [^{3}H]asparagine (■) or [^{3}H]glutamine (●,△) or 500 μM [^{3}H] glutamate (□) together with 50 mM Na-gluconate to proteoliposomes containing 10 mM glutamine (○, ●, □, ■) or 10 mM glutamate (△). In **(A,B)**, the transport was measured at the indicated times according to the stop inhibitor method. Data were plotted according to the first-order rate equation. In **(C)**, Dependence on internal K^+ of the [^{3}H]glutamate transport. Indicated concentrations of K-gluconate were added together with 10 mM glutamine in the intraliposomal compartment. The transport assay was started by adding 500 μM of [^{3}H]glutamate together with 50 mM Na-gluconate. The transport was measured in 60 min according to the stop inhibitor method. The values were expressed as percent residual activity with respect to the control condition that is no K^+ in (0 mM K^+). Results are means ± SD from three independent experiments. No significant difference from the control was observed as estimated by Student's *t*-test ($P < 0.05$).

RESULTS

Effect of Glutamate on the Glutamine Transport by hASCT2 Reconstituted in Proteoliposomes

The hASCT2 was reconstituted in proteoliposomes and the transport was assayed as Na^+-[^{3}H]glutamine$_{ex}$/glutamine$_{in}$ antiport. The effect of glutamate added to the proteoliposomes was tested on the transport function. As shown in **Figure 1**, glutamate inhibits the glutamine antiport in a pH-dependent fashion; the extent of inhibition varied substantially being maximal, around 50%, at acidic pH and very low or null at pH 7.0 and pH 8.0, respectively. The pH-dependent effect was specific for glutamate: indeed, when alanine was added to the proteoliposomes at the same concentration of glutamate, the inhibition ranged from 80 to 90%, being nearly pH-independent. As expected, the extent of inhibition by alanine was stronger than that by glutamate, given the higher affinity of ASCT2 toward alanine (Zander et al., 2013; Scalise et al., 2014). To characterize the inhibition, kinetic experiments were conducted (**Figure 2**). The dependence of the transport rate on glutamine concentration was measured in the presence of 5 mM glutamate at different pH values from pH 5.5 to pH 7.0. The pattern depicted in **Figure 2** is typical of competitive inhibition, suggesting that glutamate binds to the glutamine binding site and, hence, it could be a potential substrate of the transporter.

Transport of Glutamate by hASCT2 Reconstituted in Proteoliposomes

To confirm that hASCT2 could mediate the glutamate transport, the [^{3}H]glutamate uptake in proteoliposomes containing internal glutamine, in the presence of external sodium, was measured. As shown by the figure, the reconstituted transporter is indeed able to mediate the uptake of [^{3}H]glutamate as a function of time (**Figure 3A**). In line with the results from **Figure 2**, the uptake of [^{3}H]glutamate is dependent on pH with an optimum at pH 6.0. According to the peculiar three-substrate reaction of hASCT2, the transport of [^{3}H]glutamate requires both internal glutamine and external sodium. Indeed, the uptake was not measurable in the absence of the internal substrate or external sodium. To compare the efficiency of the Na^+[^{3}H]glutamate$_{ex}$/glutamine$_{in}$ antiport with that of other neutral amino acids, the antiport of [^{3}H]serine or [^{3}H]asparagine in exchange for internal glutamine was measured (**Figure 3B**). The transport rate of [^{3}H]glutamate$_{ex}$/glutamine$_{in}$ antiport is only four or two times lower than that of [^{3}H]serine$_{ex}$/glutamine$_{in}$ or [^{3}H]asparagine$_{ex}$/glutamine$_{in}$, respectively. Interestingly, the reverse reaction, i.e., [^{3}H]glutamine$_{ex}$/glutamate$_{in}$ was the least stimulated suggesting that glutamate is preferentially transported from the external to the internal side of cells, in line with the feature of the glutamine/glutamate cycle (Leke and Schousboe, 2016). The activity of glutamate transporters belonging to the SLC1 family is dependent on intracellular potassium; then, increasing concentrations of intraliposomal (intracellular) potassium were tested on the [^{3}H]glutamate uptake via hASCT2 (**Figure 3C**). None or negligible effect was measured on hASCT2 transport activity. Moreover, the electric nature of the Na^+ [^{3}H]glutamate$_{ex}$/glutamine$_{in}$ antiport was investigated imposing a K^+ diffusion membrane potential in the presence of valinomycin, as previously described for the Na^+ [^{3}H]glutamine$_{ex}$/glutamine$_{in}$ antiport (Pingitore et al., 2013; Scalise et al., 2014). This triggered a slight stimulation of the Na^+[^{3}H]glutamate$_{ex}$/glutamine$_{in}$ transport (**Figure 4A**). In line with the electrical nature of the vectorial reaction, the homoexchange Na^+[^{3}H]glutamate$_{ex}$/glutamate$_{in}$ (**Figure 4B**) is more stimulated than the heteroexchange Na^+[^{3}H]glutamate$_{ex}$/glutamine$_{in}$ (**Figure 4C**). However, the homoexchange (Glu$_{ex}$/Glu$_{in}$) is less efficient than the heteroexchange (Glu$_{ex}$/Gln$_{in}$) in line with the results obtained from the experiments reported in **Figure 3B**.

Kinetics of Glutamate Transport by hASCT2 Reconstituted in Proteoliposomes

The kinetic analysis of the [^{3}H]glutamate$_{ex}$/glutamine$_{in}$ antiport was performed as the dependence of the transport rate on glutamate concentration at different pH conditions (**Figure 5A**). The collected data showed that the Km was virtually not affected by the pH, while the Vmax doubled at pH 6.0 with respect to pH 7.0. Km values in the millimolar range were obtained at the different pH values: 4.8 $\pm$ 1.9 mM, 5.3 $\pm$ 1.4 mM and 3.9 $\pm$ 1.5 mM at pH 6.0, pH 6.5, and pH 7.0, respectively. The data reported in **Figure 5A** were re-plotted against proton concentration to evaluate the affinity of the hASCT2 toward proton at different glutamate concentrations, reported in **Figure 5B**. Interestingly, the Km toward proton was only slightly affected by the glutamate concentrations in a range from 0.5 to 5 mM, being around a proton concentration corresponding to pH 7.0. On the contrary, Vmax increased by increasing glutamate concentration. It is worthy of note that the range of pH used in these experiments is above the pKa of the side chain carboxylic group of glutamate; in these conditions, the majority (from 98.3% at pH 6.0 to 99.8% at pH 7.0) of glutamate is in a dissociated form, suggesting that the proton should not be bound to glutamate during the transport process.

Involvement of Proton in the Transport of Glutamate by hASCT2 in Proteoliposomes

The transport of glutamate via the high-affinity glutamate transporters of the SLC1 family occurs together with the movement of a proton across the plasma membrane (Zerangue and Kavanaugh, 1996). Therefore, the possible involvement of proton in the transport of glutamate via hASCT2 was investigated. According to the results described in **Figure 5**, two hypotheses could explain the collected data: (i) the proton is transported along a different pathway than that of glutamate; (ii) the proton binds to a transporter site, facilitating the glutamate transport, but is not transported itself. To discriminate between the two possibilities, we employed different approaches. At first, the [^{3}H]glutamate$_{ex}$/glutamine$_{in}$ antiport was measured in the presence of a ΔpH (**Figure 6**). In particular, the

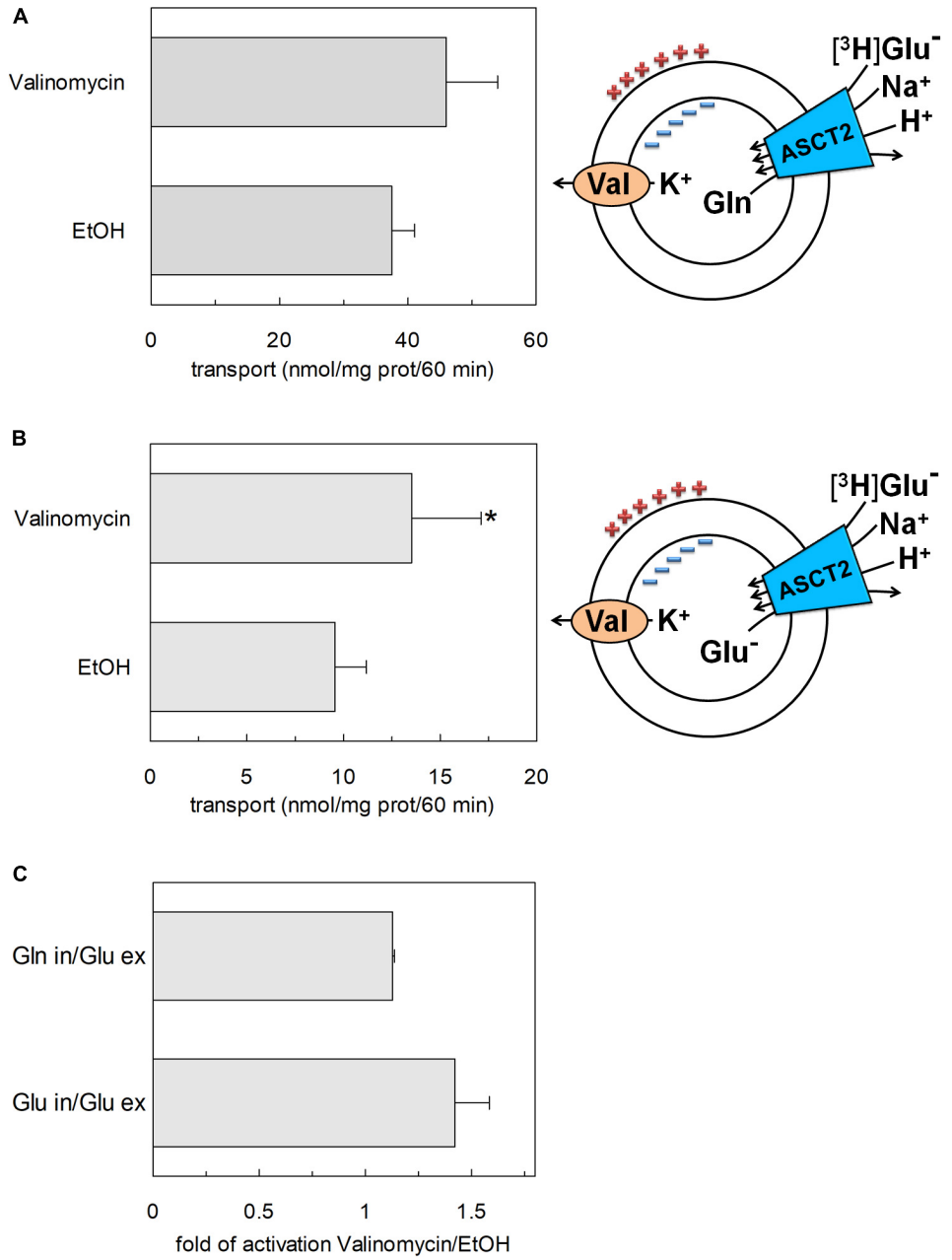

FIGURE 4 | Effect of imposed membrane potential on glutamate transport by hASCT2 reconstituted in proteoliposomes. Purified hASCT2 was reconstituted in proteoliposomes as described in materials and methods. After sephadex-G75 chromatography, proteoliposomes were treated with valinomycin (0.75 μg/mg phospholipid) to impose the artificial membrane potential. The vehicle of valinomycin, ethanol (EtOH) was used as control of valinomycin treatment. The transport assay was started adding 500 μM of [^{3}H]glutamate together with 50 mM Na-gluconate to proteoliposomes containing 10 mM glutamine **(A)** or glutamate **(B)** and 50 mM K-gluconate. The transport was measured in 60 min according to the stop inhibitor method. The transport rate was expressed as nmol/mg in 60 min. In **(A,B)** sketch of the experimental set up (proteoliposomes); Val: valinomycin. In **(C)**, data from **(A,B)** were used to calculate the fold of activation valinomycin/ethanol. Results are means ± SD from four independent experiments. *Significantly different from the control sample (EtOH) as estimated by Student's *t*-test ($P < 0.05$).

transport of [^{3}H]glutamate in proteoliposomes was stimulated by a pH gradient pH 6.0_{ex}/pH 7.0_{in} if compared to the conditions with no gradient, i.e., pH 7.0_{ex}/pH 7.0_{in} or pH 6.0_{ex}/pH 6.0_{in} (**Figure 6A**). This feature was specific for the glutamate transport; indeed, when the same experiment was conducted using [^{3}H]glutamine, the transport in the presence of the pH gradient was less active than the control condition at pH 7.0_{ex}/pH 7.0_{in}, i.e., the optimal transport condition for the glutamine antiport (**Figure 6B**). To confirm the observed effect on the Na^+[^{3}H]glutamate$_{ex}$/glutamine$_{in}$, a pH gradient was

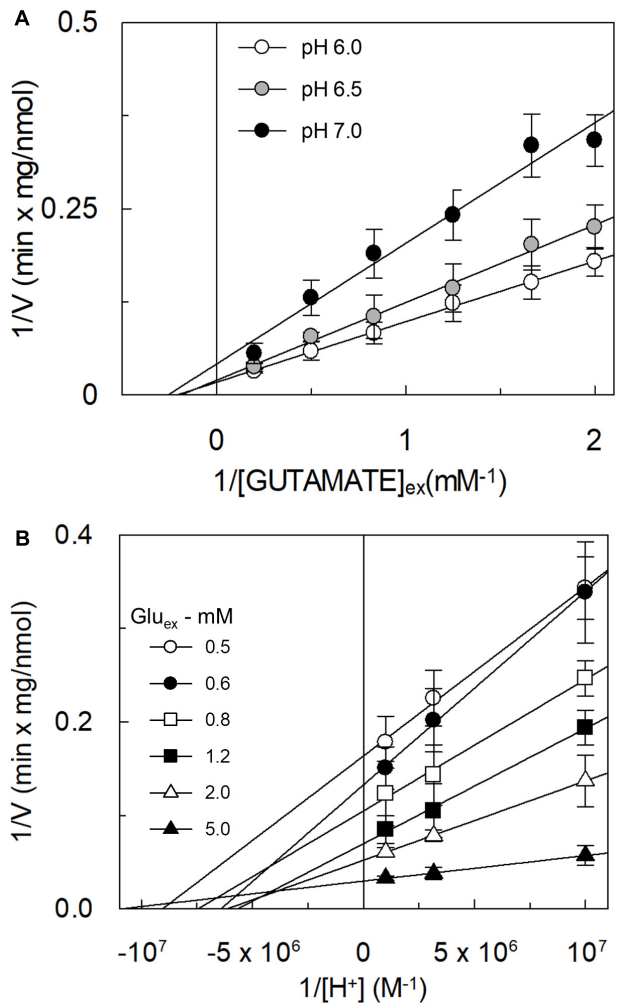

FIGURE 5 | Effect of pH on the kinetics of glutamate transport by hASCT2 reconstituted in proteoliposomes. Purified hASCT2 was reconstituted in proteoliposomes prepared at the indicated pH and containing 10 mM glutamine, as described in materials and methods. In **(A)**, the transport was started by adding indicated concentrations of [^{3}H]glutamate and 50 mM Na-gluconate to proteoliposomes buffered at different pH: pH 6.0 (○), pH 6.5 (●), and pH 7 (●). The transport was measured in 15 min according to the stop inhibitor method. Data were plotted according to linear Lineweaver–Burk equation as reciprocal transport rate vs. reciprocal glutamate concentration. In **(B)**, data from **Figure 5A** were replotted according to Lineweaver-Burk equation as reciprocal transport rate vs. reciprocal proton concentration, performed at different glutamate concentration: 0.5 mM (○), 0.6 mM (●), 0.8 mM (□), 1.2 mM (■), 2 mM (△), and 5 mM (▲). The derived pKa values were as follows: 7.0 ± 0.2, 6.8 ± 0.2, 6.9 ± 0.2, 6.8 ± 0.2, 6.8 ± 0.2, 7.0 ± 0.2 at 0.5, 0.6, 0.8, 1.2, 2, and 5 mM glutamate, respectively. Results are means ± SD from five independent experiments.

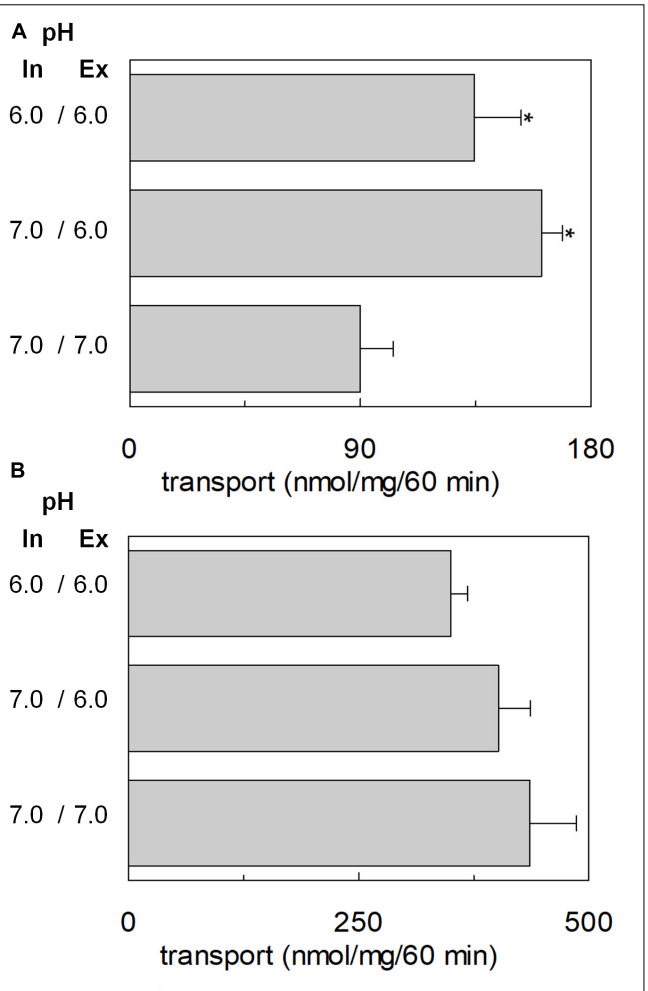

FIGURE 6 | Effect of ΔpH on glutamate transport by hASCT2 reconstituted in proteoliposomes. Purified hASCT2 was reconstituted in proteoliposomes as described in materials and methods, buffered at the indicated intraliposomal pH (in). The transport assay was started by adding 50 mM Na-gluconate and 500 μM of [^{3}H]glutamate **(A)** or 50 μM of [^{3}H]glutamine **(B)** prepared at the indicated pH (ex). The transport was measured in 60 min according to the stop inhibitor method. The transport rate was expressed as nmol/mg in 60 min. Results are means ± SD from three independent experiments. *Significantly different from the control sample (pH $7.0_{in}/7.0_{ex}$) as estimated by Student's *t*-test ($P < 0.05$).

generated by using nigericin, an ionophore able to mediate the exchange of K^+ with H^+ (sketch in **Figure 7A**). In this condition, an inwardly directed pH gradient was generated and an increased [^{3}H]glutamate uptake was observed in comparison to the control, i.e., no nigericin (**Figure 7A**). The extent of activation is about 75% at the initial transport rate, as derived from the time-course analysis. In good agreement with this data, when the same experiment was conducted without K^+ in the extraliposomal compartment, no stimulation was observed (**Figure 7B**).

Transport of Proton by hASCT2 in Proteoliposomes

To achieve the final proof of proton movement across the membrane, an alternative strategy was employed based on spectrofluorometric measurement using the pH-sensitive dye pyranine whose fluorescence emission increases with the pH (Giuliano and Gillies, 1987; Indiveri et al., 1994). Therefore, pyranine was included in the intraliposomal compartment (see Materials and methods) and the uptake of protons was measured

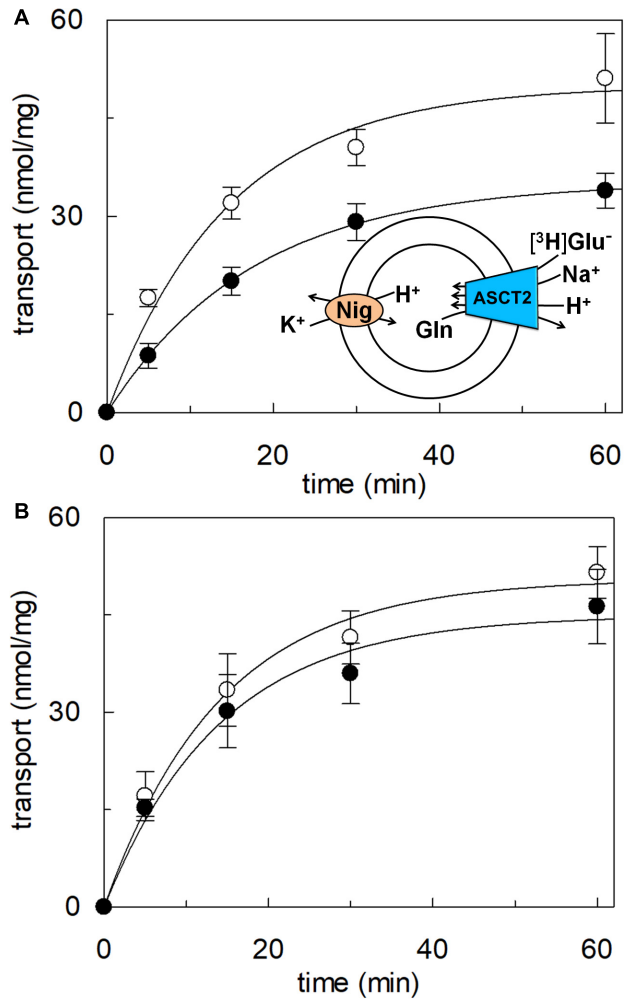

FIGURE 7 | Effect of imposed membrane proton gradient on glutamate transport by hASCT2 reconstituted in proteoliposomes. Purified hASCT2 was reconstituted in proteoliposomes as described in materials and methods. After sephadex-G75 chromatography, proteoliposomes were treated with nigericin (0.12 μg/mg phospholipid) (○) to impose the artificial membrane proton gradient. The vehicle of nigericin, ethanol (●) was used as control of nigericin treatment. The transport assay was started adding 500 μM of [^{3}H]glutamate together with 20 mM Na-gluconate and 30 mM K-gluconate to proteoliposomes containing 10 mM glutamine **(A)**. In **(B)**, the transport was performed in the absence of external K-gluconate, as control. In the figure, sketch of the experimental set up (proteoliposomes); Nig: nigericin. The transport was measured at the indicated times according to the stop inhibitor method. Data were plotted according to the first-order rate equation. Results are means ± SD from four independent experiments.

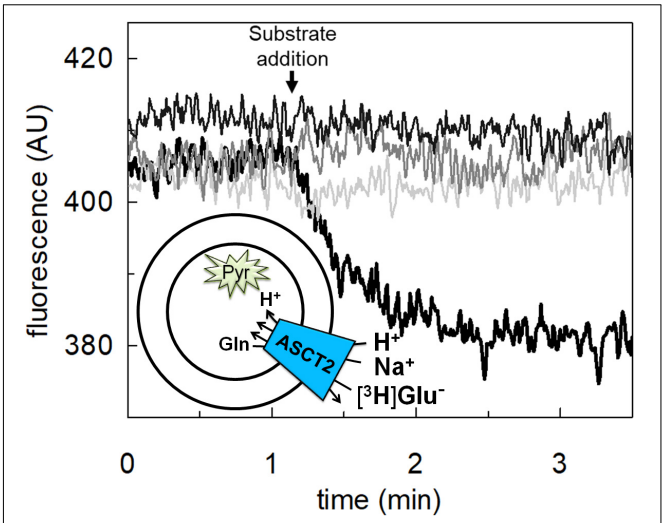

FIGURE 8 | Transport of proton by hASCT2 reconstituted in proteoliposomes. Purified hASCT2 was reconstituted in proteoliposomes containing 10 mM glutamine and 0.1 mM pyranine as described in materials and methods. The fluorescence measurement was started by adding 150 μL proteoliposomes to the transport buffer (up to 3 mL final volume) composed by Hepes Tris 20 mM pH 7 and 100 mM Na-gluconate. After ∼1 min, as indicated by the arrow, 5 mM glutamate (thick black line) or 1 mM glutamine (gray line) was added to the sample and fluorescence change was recorded. As a control, the same measurement was performed in the absence of Na-gluconate (black line); in the blank sample, 10 μM $HgCl_2$ was added at time 0 to the transport buffer (light-gray line). In the figure, sketch of the experimental set up (proteoliposomes); Pyr: pyranine. The fluorescence signal is indicated as arbitrary units (AU). Results are representative of three independent experiments.

in the presence of glutamate or glutamine externally added (**Figure 8**). As shown in the figure, the addition of glutamate caused a time-dependent decrease of the fluorescence, in line with the uptake of protons coupled to that of glutamate. As a control, the addition of glutamine did not induce any fluorescence changes, i.e., protons were not taken up during the glutamine/glutamine antiport reaction. According to the sodium dependence of glutamate transport, proton movement was not detected when sodium was not included in the transport buffer. Finally, the proton uptake, i.e., fluorescence decrease, was abolished by the addition of the inhibitor, $HgCl_2$ (**Figure 8**). The dependence on pH was also evaluated in the spectrofluorometric assay (**Figure 9**); the decrease of fluorescence, i.e., the increase of proton concentration in the intraliposomal compartment, is indeed pH-dependent (**Figure 9A**). The maximal fluorescence decrease is observed at pH 6.5. To quantify the extent of proton transport, the data from **Figure 9A** was used to calculate the nmol of proton taken up in proteoliposomes at different pH values (**Figure 9B**). The uptake of protons in terms of specific transport, i.e., nmol/mg protein taken up, was in the same order of magnitude of that measured for glutamate under similar experimental conditions (**Figure 5A**), being in favor of a 1:1 stoichiometry for H^+:Glu^- transport. The hASCT2 harbors in its primary structure four histidine residues; therefore, we argued that at least one of them could be involved in the proton transport. Then, DEPC was employed for spectrofluorometric measurements performed at pH 6.5 (**Figure 10**). Interestingly, the decrease of fluorescence, i.e., the proton flux toward the intraliposomal compartment, was reduced in the presence of 10 mM DEPC.

Docking of Glutamate to hASCT2

The binding site for neutral amino acids on hASCT2 was previously identified by a site-directed mutagenesis approach

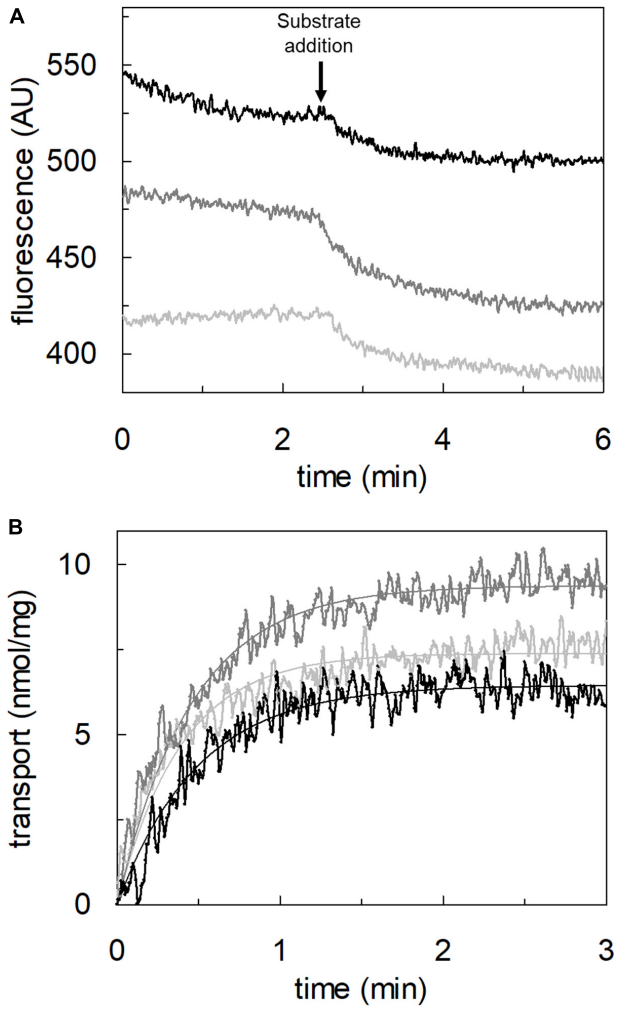

FIGURE 9 | Effect of pH on proton transport by hASCT2 reconstituted in proteoliposomes. Purified hASCT2 was reconstituted in proteoliposomes buffered at pH 7.0, containing 10 mM glutamine and 0.1 mM pyranine, as described in materials and methods. In **(A)**, the fluorescence measurement was started by adding 150 μL proteoliposomes to the transport buffer (up to 3 mL final volume) composed by 100 mM Na-gluconate and Hepes Tris 20 mM at pH 6.0 (light gray) or pH 6.5 (gray) or pH 7.0 (black). After ∼2 min, as indicated by the arrow, 5 mM buffered glutamate was added to the sample and fluorescence change was recorded. The fluorescence signal is indicated as arbitrary units (AU). In **(B)**, data from **(A)** were converted in nmol of transported proton measured as nmol/mg; the calculation was performed after calibrating the fluorescence signal assuming a linear relationship between fluorescence decrease and proton uptake (Gibrat and Grignon, 2003). Data were plotted according to a first-order rate equation. Results are representative of three independent experiments.

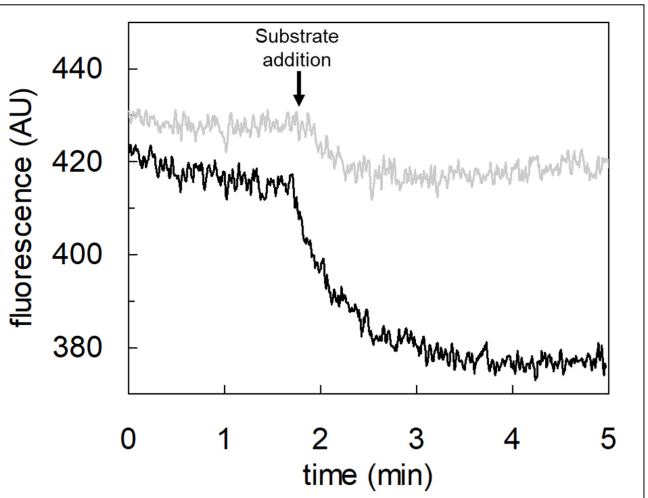

FIGURE 10 | Effect of DEPC on the proton transport by hASCT2 reconstituted in proteoliposomes. Purified hASCT2 was reconstituted in proteoliposomes buffered at pH 7.0, containing 10 mM glutamine and 0.1 mM pyranine, as described in materials and methods. After reconstitution, proteoliposomes were incubated with 10 mM DEPC (gray line) or ethanol (black line) for 5 min at 23°C and, then were subjected to sephadex-G75 chromatography. The fluorescence measurement was started by adding 150 μL proteoliposomes to transport buffer (up to 3 mL final volume) composed by 100 mM Na-gluconate and Hepes Tris 20 mM at pH 7.0. After ∼2 min as indicated by the arrow, 5 mM glutamate was added to the sample and fluorescence was recorded. The fluorescence signal is indicated as arbitrary units (AU). Results are representative of three independent experiments.

(Scalise et al., 2018a) and then confirmed by the recently obtained 3D structure (Garaeva et al., 2018, 2019; Yu et al., 2019). The competitive inhibition data reported in **Figure 2**, suggested that also glutamate binds to the substrate-binding site of hASCT2. To further support this biochemical finding, we performed docking analysis on the available 3D structure of hASCT2 in the inward open conformation (PDB 6GCT) (**Figures 11A,B**). Glutamate, both in the protonated (**Figure 11A**) and deprotonated (**Figure 11B**) state, positioned similarly to glutamine (**Figure 11C**), docked as a control (**Figure 11C**). Interestingly, docked glutamate did not directly interact with Cys467 but with the residues of the hASCT2 substrate-binding site conserved among the SLC1 family members (**Figure 11D**).

Transport of Aspartate by hASCT2 Reconstituted in Proteoliposomes

The high-affinity glutamate transporters of the SLC1 family can mediate the flux of aspartate as well. Therefore, the inhibition of the [^{3}H]glutamate transport by aspartate added to the extraliposomal compartment was evaluated; indeed, aspartate inhibited the hASCT2 mediated glutamate transport (**Figure 12A**). Then, we evaluated the direct transport of [^{3}H]aspartate via hASCT2 reconstituted in proteoliposomes; interestingly, as it is shown in **Figure 12B**, the transport of aspartate was lower than that of glutamate in line with the lack of complete inhibition of glutamate transport (**Figure 12A**).

Glutamine Efflux Induced by Glutamate via hASCT2 in Intact Cells and Proteoliposomes

The ability of glutamate to induce efflux of glutamine was investigated in both proteoliposomes and intact cells (**Figure 13**). In line with the data from **Figure 3**, glutamate was able to induce the efflux of [^{3}H]glutamine from preloaded proteoliposomes (**Figure 13A**). As shown by the figure, externally added glutamate

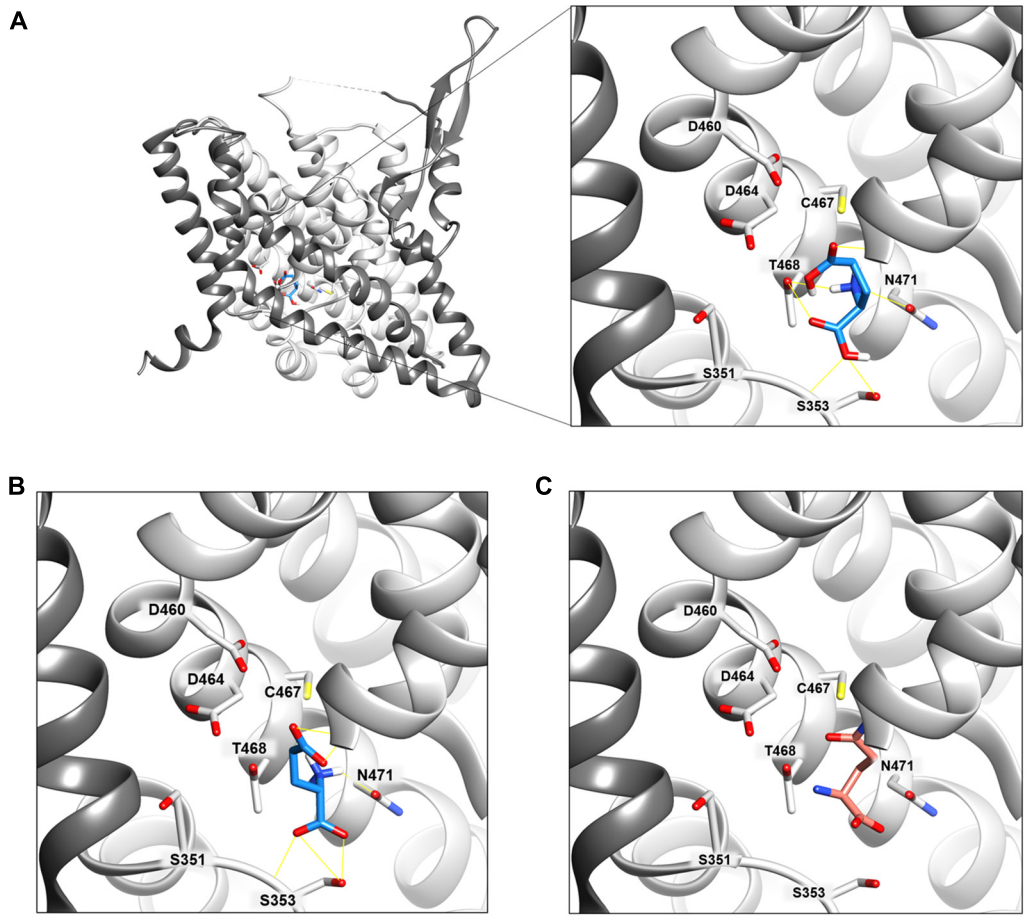

D

```
SLC1A4      LGHVIHGGIVLPLIYFVFTRKNPFRFLLGLLAPFATAFATCSSSATLPSMMKCIEENNGV   362
SLC1A5      LGHAIHGLLVLPLIYFLFTRKNPYRFLWGIVTPLATAFGTSSSSATLPLMMKCVEENNGV   370
SLC1A2      IGLIIHGGIFLPLIYFVVTRKNPFSFFAGIFQAWITALGTASSAGTLPVTFRCLEENLGI   381
SLC1A1      TGLAIHSIVILPLIYFIVVRKNPFRFAMGMAQALLTALMISSSSATLPVTFRCAEENNQV   350
SLC1A7      CGLVLHGLFILPLLYFFITKKNPIVFIRGILQALLIALATSSSSATLPITFKCLLENNHI   361
SLC1A3      VGLLIHAVIVLPLLYFLVTRKNPWVFIGGLLQALITALGTSSSSATLPITFKCLEENNGV   382
SLC1A6      VGLFLHAGIVLPLIYFLVTHRNPFPFIGGMLQALITAMGTSSSSATLPITFRCLEEGLGV   407
                 *  :*. ..***:**...::**  *  *:      *:  .**:.***  ::*  *.  :

SLC1A4      DKRISRFILPIGATVNMDGAAIFQCVAAVFIAQLNNVELNAGQIFTILVTATASSVGAAG   422
SLC1A5      AKHISRFILPIGATVNMDGAALFQCVAAVFIAQLSQQSLDFVKIITILVTATASSVGAAG   430
SLC1A2      DKRVTRFVLPVGATINMDGTALYEAVAAIFIAQMNGVVLDGGQIVTVSLTATLASVGAAS   441
SLC1A1      DKRITRFVLPVGATINMDGTALYEAVAAVFIAQLNDLDLGIGQIITISITATSASIGAAG   410
SLC1A7      DRRIARFVLPVGATINMDGTALYEAVAAIFIAQVNNYELDFGQIITISITATAASIGAAG   421
SLC1A3      DKRVTRFVLPVGATINMDGTALYEALAAIFIAQVNNFELNFGQIITISITATAASIGAAG   442
SLC1A6      DRRITRFVLPVGATVNMDGTALYEALAAIFIAQVNNYELNLGQITTISITATAASVGAAG   467
                 ::::**:**:***:****:*::::**:****:.   *.  :* *: :*** :*:***.

SLC1A4      VPAGGVLTIAIILEAIGLPTHDLPLILAVDWIVDRTTTVVNVEGDALGAGILHHLNQKAT   482
SLC1A5      IPAGGVLTLAIILEAVNLPVDHISLILAVDWLVDRSCTVLNVEGDALGAGLLQNYVDRTE   490
SLC1A2      IPSAGLVTMLLILTAVGLPTEDISLLVAVDWLLDRMRTSVNVVGDSFGAGIVYHLSKSEL   501
SLC1A1      VPQAGLVTMVIVLSAVGLPAEDVTLIIAVDWLLDRFRTMVNVLGDAFGTGIVEKLSKKEL   470
SLC1A7      IPQAGLVTMVIVLTSVGLPTDDITLIIAVDWALDRFRTMINVLGDALAAGIMAHICRKDF   481
SLC1A3      IPQAGLVTMVIVLTSVGLPTDDITLIIAVDWFLDRLRTTTNVLGDSLGAGIVEHLSRHEL   502
SLC1A6      IPQAGLVTMVIVLTSVGLPTEDITLIIAVDWFLDRLRTMTNVLGDSIGAAVIEHLSQREL   527
            :* .*::*: ::* ::.**...: *::**** :**  *  ** **::.:.:: :
```

FIGURE 11 | Sequence alignment and docking analysis of the hASCT2 binding site. In **(A,B)**, Molecular docking of glutamic acid in the binding site of ASCT2. The crystal structure of ASCT2 in the inward open conformation has been used (PDB ID: 6GCT). To simplify the visualization, only the Chain A without Cholesterol was represented as light gray ribbon, with the scaffold domain in dim gray, using Chimera v.1.14. In **(A)**, a zoom of protonated glutamate docking in the binding site. The ligand was represented as dodger blue stick and amino acids belonging to the binding site as a stick and labeled using Chimera v.1.14. Glutamate in the protonated state was prepared at a pH range of 2.0 ± 0.5 using Schrödinger-Maestro v.12.4 and docking was performed using AutoDock Vina v.1.1.2 as described in materials and methods. This pose has a docking score of −6.0 and it makes hydrogen bonds with G435, T468, N471, and S353. In **(B)**, a zoom of deprotonated glutamate docking in the binding site. The ligand was represented as dodger blue sticks and amino acids belonging to the binding site are represented as a stick and

(Continued)

FIGURE 11 | labeled using Chimera v.1.14. Glutamate in the deprotonated state was prepared at a pH range of 7.0 ± 0.5 using Schrödinger-Maestro v.12.4 and docking was performed using AutoDock Vina v.1.1.2 as described in Methods. The best pose has a docking score of −6.1 and it makes interaction with G430, G434, G435, N471, and S353. In **(C)** visualization of the glutamine binding site. Glutamine is represented as salmon sticks and the amino acids belonging to the binding site are represented as a stick and labeled using Chimera v.1.14. In **(D)**, Multiple sequence alignment of SLC1 members. To simplify, the multiple alignment is represented from L311 to E490 referring to SLC1A5 (boxed in light blue). Residues belonging to the binding site (A390, S351, S353, D460, D464, C467, N471 in SLC1A5) are highlighted with a red box.

caused a reduction of intraliposomal radioactivity of about 65% at pH 6.0. As controls, glutamine or buffer alone was externally added: 85% or 0% efflux was detected, respectively. The data confirmed that hASCT2 could mediate the antiport of glutamate$_{ex}$/[^{3}H]glutamine$_{in}$, even though at a lower extent with respect to glutamine$_{ex}$/[^{3}H]glutamine$_{in}$. In line with the ability of hASCT2 to mediate also aspartate transport, a similar extent of efflux was observed adding aspartate in the place of glutamate. In good agreement with the uptake of radiolabeled glutamate, the described phenomenon is also pH-dependent; indeed, the addition of glutamate or aspartate buffered at pH 7.0, caused a lower efflux compared to that measured at pH 6.0. As a control, in the case of glutamine, nearly no difference was observed at the different pH values. A similar experiment was performed in intact HeLa cells, which are known to express ASCT2 and have been previously used for studying ASCT2 transport (Torres-Zamorano et al., 1998; Scalise et al., 2014, 2019). Also in this case, glutamate and aspartate evoked a glutamine efflux of about 50% and 25%, respectively, in comparison to the control. Glutamine, as expected, induced a greater efflux, reaching about 60%. Collectively, the data from intact cells and proteoliposomes confirmed the ability of glutamate to induce glutamine efflux in line with the glutamine/glutamate cycle (Leke and Schousboe, 2016).

DISCUSSION

Transport of Glutamate via hASCT2

In this work, different assays have been employed to shed light on the substrate specificity of hASCT2; this represents a vintage but very relevant issue in the understanding of hASCT2 biology in both physiological and pathological conditions with potential outcomes in pharmacology. In line with very early but disregarded observations on mice and rat ASCT2 (Utsunomiya-Tate et al., 1996; Broer et al., 1999; Oppedisano et al., 2007), the capacity of the hASCT2 to mediate a Na^+ and H^+ dependent glutamate$_{ex}$/glutamine$_{in}$ antiport emerged. The rate of this reaction is comparable to the well-assessed antiport of neutral amino acids (**Figure 3B**). As a matter of fact, the substrate-binding site of wild type hASCT2 can accept glutamate and, at a lower extent, aspartate (**Figure 12**). The critical variation, with respect to the conventional hASCT2 transport mode, is the requirement for acidic pH that suggests the involvement of protons in the transport mechanism, reminiscent of the other glutamate transporters belonging to the SLC1 family, i.e., the EAAT members. Based on the kinetic data on WT hASCT2, it can be assumed that the transported form of glutamate is the anionic one (**Figure 5**); this is in line with the observation that the Km values toward glutamate do not change when varying the pH of the transport assay, reflecting the concentration of glutamate in the anionic form. It is then expected that the proton *flux* occurs through an independent transport path, even though at this stage, we cannot completely exclude that the proton might be transported together with glutamate.

Transport of Proton via hASCT2

The availability of recombinant hASCT2 reconstituted in proteoliposomes allowed to directly measure the proton movement by fluorescence changes induced by the glutamate transport. This approach represents a methodological novelty in the study of the transporter; the advancement was made feasible thanks to the improvement of the functional protein fraction following the discovery that cholesterol facilitates the formation of the trimeric functional assembly of the protein (Garaeva et al., 2018, 2019; Scalise et al., 2019). These achievements resulted in a substantial increase in the active space of proteoliposomes and, hence, of the volume available for the fluorescence detection by pyranine (Indiveri et al., 1994). The results collected by the spectrofluorometric assays correlated well with the transport assay of glutamate by radioactivity. The stoichiometry of transport is in favor of an overall Na^+ dependent transport reaction of $1H^+$:$1Glu^-$ in exchange for internal glutamine. From the kinetic data reported in **Figure 5**, a further biochemical conclusion can be drawn: the pH dependence of glutamate transport, that is maximal at pH 6.0, is in line with the Km toward proton calculated as a proton concentration corresponding to pH 7.0 (**Figure 5B**). Indeed, when measuring glutamate transport at pH 6.0, the proton concentration is 10 times above the Km, i.e., close to saturation, correlating well with the doubling of the Vmax of glutamate transport from pH 7.0 to pH 6.0. In line with the proposed charge movement, valinomycin imposed membrane potential positively affects the glutamate transport via hASCT2. In good agreement with the hypothesis that glutamate is transported in the anionic form, the stimulation by the imposed membrane potential is amplified when the glutamate$^-_{ex}$/glutamate$^-_{in}$ antiport is measured: the homologous glutamate/glutamate antiport, *per se*, is indeed electroneutral with consequent net inward movement of two positive charges deriving from sodium and proton. In the case of glutamate$^-_{ex}$/glutamine$_{in}$ exchange, the negative charge of glutamate compensates one of the co-transported positive charges. It has to be stressed that the charge movement accounts only partially in the overall driving force of transport, that mainly derives by the antiport component and the sodium gradient (Scalise et al., 2014) similarly to

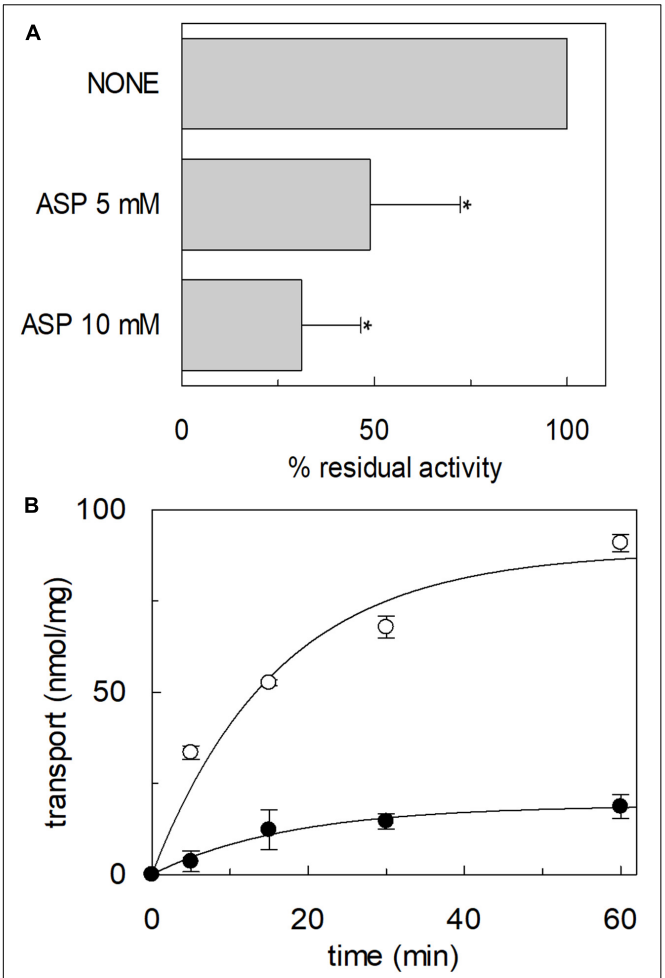

FIGURE 12 | Interaction of hASCT2 reconstituted in proteoliposomes with aspartate. Purified hASCT2 was reconstituted in proteoliposomes containing 10 mM glutamine as described in materials and methods. In **(A)**, inhibition by aspartate of the glutamate transport by ASCT2 reconstituted in proteoliposomes. The transport assay was started by adding 500 μM [^{3}H]glutamate together with 50 mM Na-gluconate to proteoliposomes in the presence of indicated concentrations of aspartate. The transport was measured in 60 min according to the stop inhibitor method. The transport was indicated as % residual activity with respect to the condition with no external addition (none). Results are means ± SD from four independent experiments. *Significantly different from the control sample (none) as estimated by Student's *t*-test ($P < 0.05$). In **(B)**, uptake of glutamate and aspartate by ASCT2 in proteoliposomes. The transport assay was started by adding 500 μM [^{3}H]glutamate (○) or 500 μM [^{3}H]aspartate (●) together with 50 mM Na-gluconate to proteoliposomes. The transport was stopped at the indicated times according to the stop inhibitor method. Data were plotted with the first-order rate equation. Results are means ± SD from three independent experiments.

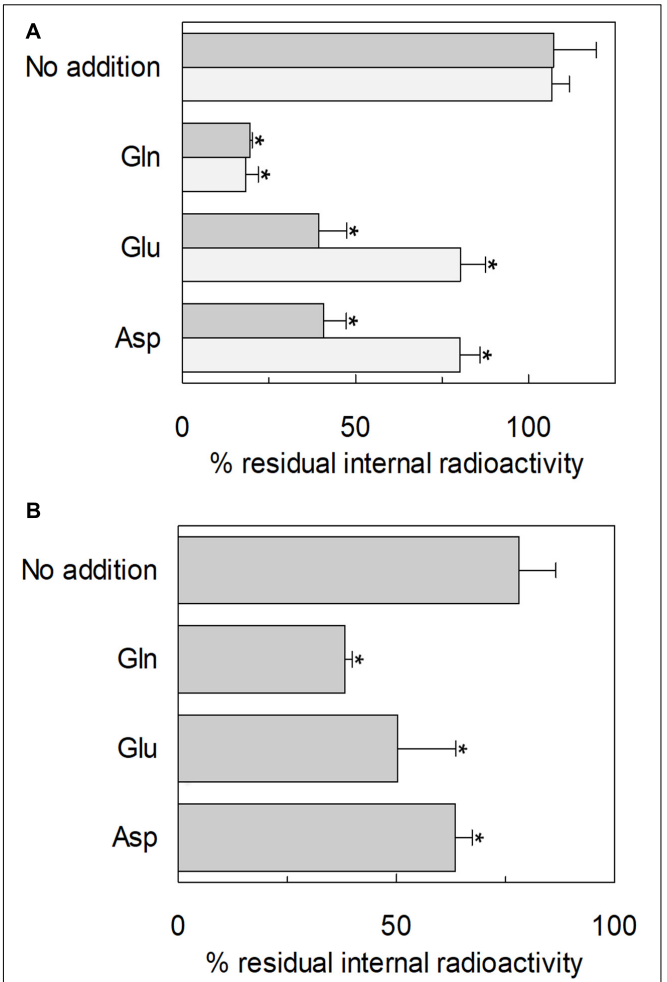

FIGURE 13 | Efflux of glutamine through hASCT2. In **(A)** [^{3}H]glutamine efflux from proteoliposomes. Purified hASCT2 was reconstituted in proteoliposomes containing 10 mM glutamine as described in materials and methods. The accumulation of radiolabeled glutamine was started by adding 50 μM [^{3}H]glutamine in the presence of 50 mM Na-gluconate. After 60 min uptake, the [^{3}H]glutamine efflux was started in different conditions: no addition (control), the addition of 10 mM of glutamate or aspartate or 1 mM glutamine to the transport buffer in the presence of 50 mM Na-gluconate. The efflux was measured in 60 min using substrates buffered at pH 7.0 (light gray) or pH 6.0 (dark gray). In **(B)**, Efflux of [^{3}H]glutamine from HeLa intact cells. Cells were cultured as described in materials and methods; uptake was performed in 10 min adding 10 μM [^{3}H]glutamine in the presence of 20 mM Tris–HCl pH 7.0 and 130 mM NaCl as described in materials and methods. The efflux was measured in 1 min in the presence of different conditions: no addition (control), the addition of 10 mM of glutamate or aspartate or 1 mM glutamine to the transport buffer constituted by 20 mM Tris–HCl pH 6.0 and 130 mM NaCl. Results are means ± SD from four independent experiments. *Significantly different from the control sample (no addition) as estimated by Student's *t*-test ($P < 0.05$).

what previously observed for the rat ASCT2 (Zander et al., 2013). The electrogenic nature of the glutamate$_{ex}$/glutamine$_{in}$ antiport is in agreement with the role of allosteric regulation by internal Na^+, similar to that described in the case of the neutral amino acid antiport (Scalise et al., 2014). Noteworthy, when measuring the glutamine$_{ex}$/glutamate$_{in}$ antiport, the transport activity was lower if compared to the *vice versa* reaction (**Figure 3B**); besides the affinity issue, this can be explained by the electrogenicity of the hASCT2 mediated transport. Indeed, the exit of a net negative charge due to glutamate$^-$ movement, would create a charge unbalance positive inside which counteracts the movement of Na^+ and H^+, from the external environment.

Transport of Acidic Amino Acids Within the SLC1 Family

Interestingly and differently from the high-affinity glutamate transporters of the SLC1 family, the glutamate transport via hASCT2 does not require internal potassium. This is in good agreement with data collected in the pre-3D structure era, in which a residue of glutamate of EAAT2 (previously known as GLT-1), namely E404, was identified as responsible for the EAAT-specific potassium stimulation; indeed, ASCTs does not harbor a glutamate residue in the corresponding position but a neutral glutamine residue (Kavanaugh et al., 1997; Grewer et al., 2003). Still in agreement with our data, the EAAT2-E404Q mutant is not sensitive to intracellular potassium (Grewer et al., 2003). The layout of hASCT2 binding site able to coordinate both neutral and negatively charged amino acids is a distinctive trait of hASCT2 with respect to the other members of SLC1 family (**Figure 11**). Over the years, several mutations have been generated on ASCT1 and EAATs to switch substrate specificity of these proteins. In the case of hASCT2, the presence of C467 seems to increase the range of acceptable substrates depending on the pH. This may find a possible explanation in the size of the cysteine side chain. Indeed, in old papers, it was already highlighted that cysteine, smaller than arginine of EAATs and smaller than threonine of ASCT1, creates a larger niche to accommodate substrates (Bendahan et al., 2000). Later on, the 3D structure of hASCT2 showed the presence of a narrow space, between scaffold and transport domain, that forms a larger space directed to the intracellular side; this feature is peculiar of hASCT2 (Freidman et al., 2020). Furthermore, recent work showed that, even if lysine is not recognized as a substrate of hASCT2, small amino acids, modified to have basic side chains, can be translocated by hASCT2 and rASCT2 (Ndaru et al., 2020). Also in this case, the basic amino acid substrates do not interact with C467. The interaction of protons with the high-affinity glutamate transporters has been investigated in the very early studies conducted on EAAT2. The key residues H326, and a stretch constituted by D398, E404 and D470, were identified by site-directed mutagenesis. Interestingly, these amino acids are conserved in all the EAATs (Pines et al., 1995) and a similar mechanism was described for the proton dependent lac permease (Sahin-Toth and Kaback, 2001). Interestingly, in hASCT2, three out of the four mentioned residues are conserved, suggesting that they could be part of the proton path in the protein. Investigations are in the course for identifying the transport path of protons and glutamate in hASCT2.

Glutamate and Aspartate Transport in Physiological and Pathological Conditions

Besides the mere biochemical feasibility of the exchange of external glutamate or aspartate with internal glutamine, this vectorial reaction is plausible to take place also in the actual physiological context, as suggested by the experiments conducted on intact cells (**Figure 13B**). Indeed, the presence of ASCT2 in the placenta may account for the glutamate/glutamine cycle between placenta and fetus to sustain the metabolic requirement (Vaughn et al., 1995; Torres-Zamorano et al., 1998; Day et al., 2013). A similar role may be suggested for ASCT2 in the glutamate/glutamine cycle between neurons and astrocytes to sustain the activity of EAATs, i.e., the major players in the glutamate reuptake from the synaptic cleft to avoid glutamate excitotoxicity (Leke and Schousboe, 2016). It has to be noted that in synaptic cleft the transient concentration of glutamate may reach 100-200 mM (Meldrum, 2000; Gras et al., 2006), that is much higher than the Km of ASCT2 for glutamate. However, given the major role played by EAATs and the relatively low expression of ASCT2 in the adult brain, it can be speculated that the role of ASCT2 in the reuptake of glutamate in the brain may become relevant in pathological conditions characterized by transient pH changes, such as in hypoxia (Deitmer and Rose, 1996). Besides the transport of glutamate, a physiological explanation of recognizing negatively charged amino acids by hASCT2, relies on the transport of aspartate across the BBB, as previously suggested in mice to maintain the homeostasis of excitatory amino acids in the brain (Tetsuka et al., 2003). A glutamate/glutamine cycle has been proposed also in activated macrophages in CNS following HIV infection, as a neuroprotective mechanism (Gras et al., 2006). Recently, a glutamate/glutamine cycle has been suggested to occur between cancer and stromal cells to sustain the metabolic changes (Lyssiotis and Kimmelman, 2017; Bott et al., 2019). Interestingly, a pH-dependent glutamate uptake was described in the intestine, where luminal pH is acidic. This glutamate transport was attribute to the ASC transporter by competitive inhibition studies (Munck and Munck, 1999; Munck et al., 2000). From the described scenario, it can be speculated that the substrate specificity of ASCT2 may change according to the tissues in which the protein is expressed following also developmental stage and/or post-translational modifications that may refine the preference toward one or more amino acids. Furthermore, the possibility of mediating the uptake of glutamate and aspartate further enlarges the significance of ASCT2 overexpression in the context of cancer metabolic rewiring; as an example, aspartate is required for nucleotide biosynthesis and glutamate is required for redox balance in cancer initiation and progression (Lieu et al., 2020). Taken together, the novelties on substrate specificity here presented further points out that ASCT2 is one of the key players for the metabolism of highly proliferative cells. Furthermore, the identification of other substrates, rather than neutral amino acids, may have also a relevance in providing new clues for pharmacological research. Indeed, ASCT2 is considered an eminent druggable target and the design of drugs able to specifically interact with this protein is subjected to its improved biochemical characterization.

DATA AVAILABILITY STATEMENT

The raw data supporting the conclusions of this article will be made available by the authors, without undue reservation, to any qualified researcher.

AUTHOR CONTRIBUTIONS

MS and CI conceived, designed the experiments, and analyzed the data. MS and TM performed the proteoliposome functional assays. JC and FR performed the docking analysis. LP and TM prepared the yeast constructs and optimized yeast cell growth. GP performed the yeast cell growth for protein over-expression and purification. MS, TM, and CI wrote the manuscript. CI supervised the entire work. All authors contributed to the article and approved the submitted version.

FUNDING

This work was supported by PRIN (Progetti di Ricerca di Interesse Nazionale) project no. 2017PAB8EM to CI granted by MIUR (Ministry of Education, University and Research) – Italy.

REFERENCES

Bendahan, A., Armon, A., Madani, N., Kavanaugh, M. P., and Kanner, B. I. (2000). Arginine 447 plays a pivotal role in substrate interactions in a neuronal glutamate transporter. *J. Biol. Chem.* 275, 37436–37442. doi: 10.1074/jbc.m006536200

Bhutia, Y. D., Babu, E., Ramachandran, S., and Ganapathy, V. (2015). Amino Acid transporters in cancer and their relevance to "glutamine addiction": novel targets for the design of a new class of anticancer drugs. *Cancer Res.* 75, 1782–1788. doi: 10.1158/0008-5472.can-14-3745

Bott, A. J., Maimouni, S., and Zong, W. X. (2019). The pleiotropic effects of glutamine metabolism in Cancer. *Cancers (Basel)* 11:770. doi: 10.3390/cancers11060770

Broer, A., Brookes, N., Ganapathy, V., Dimmer, K. S., Wagner, C. A., Lang, F., et al. (1999). The astroglial ASCT2 amino acid transporter as a mediator of glutamine efflux. *J. Neurochem.* 73, 2184–2194. doi: 10.1046/j.1471-4159.1999.02184.x

Broer, S., and Brookes, N. (2001). Transfer of glutamine between astrocytes and neurons. *J. Neurochem.* 77, 705–719. doi: 10.1046/j.1471-4159.2001.00322.x

Canul-Tec, J. C., Assal, R., Cirri, E., Legrand, P., Brier, S., Chamot-Rooke, J., et al. (2017). Structure and allosteric inhibition of excitatory amino acid transporter 1. *Nature* 544, 446–451. doi: 10.1038/nature22064

Day, P. E., Cleal, J. K., Lofthouse, E. M., Goss, V., Koster, G., Postle, A., et al. (2013). Partitioning of glutamine synthesised by the isolated perfused human placenta between the maternal and fetal circulations. *Placenta* 34, 1223–1231. doi: 10.1016/j.placenta.2013.10.003

Deitmer, J. W., and Rose, C. R. (1996). pH regulation and proton signalling by glial cells. *Prog. Neurobiol.* 48, 73–103. doi: 10.1016/0301-0082(95)00039-9

Freidman, N., Chen, I., Wu, Q., Briot, C., Holst, J., Font, J., et al. (2020). amino acid transporters and exchangers from the SLC1A family: structure, mechanism and roles in physiology and Cancer. *Neurochem. Res.* 45, 1268–1286. doi: 10.1007/s11064-019-02934-x

Garaeva, A. A., Guskov, A., Slotboom, D. J., and Paulino, C. (2019). A one-gate elevator mechanism for the human neutral amino acid transporter ASCT2. *Nat. Commun.* 10:3427.

Garaeva, A. A., Oostergetel, G. T., Gati, C., Guskov, A., Paulino, C., and Slotboom, D. J. (2018). Cryo-EM structure of the human neutral amino acid transporter ASCT2. *Nat. Struct. Mol. Biol.* 25, 515–521. doi: 10.1038/s41594-018-0076-y

Giancaspero, T. A., Colella, M., Brizio, C., Difonzo, G., Fiorino, G. M., Leone, P., et al. (2015). Remaining challenges in cellular flavin cofactor homeostasis and flavoprotein biogenesis. *Front. Chem.* 3:30. doi: 10.3389/fchem.2015.00030

Gibrat, R., and Grignon, C. (2003). Liposomes with multiple fluorophores for measurement of ionic fluxes, selectivity, and membrane potential. *Methods Enzymol.* 372, 166–186. doi: 10.1016/s0076-6879(03)72010-2

Giuliano, K. A., and Gillies, R. J. (1987). Determination of intracellular pH of BALB/c-3T3 cells using the fluorescence of pyranine. *Anal. Biochem.* 167, 362–371. doi: 10.1016/0003-2697(87)90178-3

Gras, G., Porcheray, F., Samah, B., and Leone, C. (2006). The glutamate-glutamine cycle as an inducible, protective face of macrophage activation. *J. Leukoc Biol.* 80, 1067–1075. doi: 10.1189/jlb.0306153

Grewer, C., Watzke, N., Rauen, T., and Bicho, A. (2003). Is the glutamate residue Glu-373 the proton acceptor of the excitatory amino acid carrier 1? *J. Biol. Chem.* 278, 2585–2592. doi: 10.1074/jbc.m207956200

Hanson, M. A., Cherezov, V., Griffith, M. T., Roth, C. B., Jaakola, V. P., Chien, E. Y., et al. (2008). A specific cholesterol binding site is established by the 2.8 A structure of the human beta2-adrenergic receptor. *Structure* 16, 897–905. doi: 10.1016/j.str.2008.05.001

Indiveri, C., Palmieri, L., and Palmieri, F. (1994). Kinetic characterization of the reconstituted ornithine carrier from rat liver mitochondria. *Biochim. Biophys. Acta* 1188, 293–301. doi: 10.1016/0005-2728(94)90048-5

Kavanaugh, M. P., Bendahan, A., Zerangue, N., Zhang, Y., and Kanner, B. I. (1997). Mutation of an amino acid residue influencing potassium coupling in the glutamate transporter GLT-1 induces obligate exchange. *J. Biol. Chem.* 272, 1703–1708. doi: 10.1074/jbc.272.3.1703

Leke, R., and Schousboe, A. (2016). The glutamine transporters and their role in the glutamate/GABA-glutamine cycle. *Adv. Neurobiol.* 13, 223–257. doi: 10.1007/978-3-319-45096-4_8

Lieu, E. L., Nguyen, T., Rhyne, S., and Kim, J. (2020). Amino acids in cancer. *Exp. Mol. Med.* 52, 15–30.

Lyssiotis, C. A., and Kimmelman, A. C. (2017). Metabolic interactions in the tumor microenvironment. *Trends Cell Biol.* 27, 863–875. doi: 10.1016/j.tcb.2017.06.003

Meldrum, B. S. (2000). Glutamate as a neurotransmitter in the brain: review of physiology and pathology. *J. Nutr.* 130, 1007S–1015S. doi: 10.1093/jn/130.4.1007s

Munck, B. G., and Munck, L. K. (1999). Effects of pH changes on systems ASC and B in rabbit ileum. *Am. J. Physiol.* 276, G173–G184.

Munck, L. K., Grondahl, M. L., Thorboll, J. E., Skadhauge, E., and Munck, B. G. (2000). Transport of neutral, cationic and anionic amino acids by systems B, b(o,+), X(AG), and ASC in swine small intestine. *Comp. Biochem. Physiol. A Mol. Integr. Physiol.* 126, 527–537. doi: 10.1016/s1095-6433(00)00227-0

Ndaru, E., Garibsingh, R. A., Zielewicz, L., Schlessinger, A., and Grewer, C. (2020). Interaction of the neutral amino acid transporter ASCT2 with basic amino acids. *Biochem. J.* 477, 1443–1457. doi: 10.1042/bcj20190859

Oberg, F., Sjohamn, J., Conner, M. T., Bill, R. M., and Hedfalk, K. (2011). Improving recombinant eukaryotic membrane protein yields in Pichia pastoris: the importance of codon optimization and clone selection. *Mol. Membr. Biol.* 28, 398–411. doi: 10.3109/09687688.2011.602219

Oppedisano, F., Pochini, L., Galluccio, M., and Indiveri, C. (2007). The glutamine/amino acid transporter (ASCT2) reconstituted in liposomes: electrical nature of the glutamine/glutamate antiport. *Ital. J. Biochem.* 56, 275–278.

Palmieri, F., and Klingenberg, M. (1979). Direct methods for measuring metabolite transport and distribution in mitochondria. *Methods Enzymol.* 56, 279–301. doi: 10.1016/0076-6879(79)56029-7

Pettersen, E. F., Goddard, T. D., Huang, C. C., Couch, G. S., Greenblatt, D. M., Meng, E. C., et al. (2004). UCSF Chimera–a visualization system for exploratory research and analysis. *J. Comput. Chem.* 25, 1605–1612. doi: 10.1002/jcc.20084

Pines, G., Zhang, Y., and Kanner, B. I. (1995). Glutamate 404 is involved in the substrate discrimination of GLT-1, a (Na+ + K+)-coupled glutamate transporter from rat brain. *J. Biol. Chem.* 270, 17093–17097. doi: 10.1074/jbc.270.29.17093

Pingitore, P., Pochini, L., Scalise, M., Galluccio, M., Hedfalk, K., and Indiveri, C. (2013). Large scale production of the active human ASCT2 (SLC1A5) transporter in Pichia pastoris–functional and kinetic asymmetry revealed in proteoliposomes. *Biochim. Biophys. Acta* 1828, 2238–2246. doi: 10.1016/j.bbamem.2013.05.034

Sahin-Toth, M., and Kaback, H. R. (2001). Arg-302 facilitates deprotonation of Glu-325 in the transport mechanism of the lactose permease from *Escherichiacoli*. *Proc. Natl. Acad. Sci. U.S.A.* 98, 6068–6073. doi: 10.1073/pnas.111139698

Scalise, M., Pochini, L., Console, L., Losso, M. A., and Indiveri, C. (2018a). The human SLC1A5 (ASCT2) amino acid transporter: from function to structure and role in cell biology. *Front. Cell Dev. Biol.* 6:96. doi: 10.3389/fcell.2018.00096

Scalise, M., Pochini, L., Console, L., Pappacoda, G., Pingitore, P., Hedfalk, K., et al. (2018b). Cys Site-directed mutagenesis of the human SLC1A5 (ASCT2) transporter: structure/function relationships and crucial role of Cys467 for redox sensing and glutamine transport. *Int. J. Mol. Sci.* 19:648. doi: 10.3390/ijms19030648

Scalise, M., Pochini, L., Cosco, J., Aloe, E., Mazza, T., Console, L., et al. (2019). Interaction of cholesterol with the human SLC1A5 (ASCT2): insights into structure/function relationships. *Front. Mol. Biosci.* 6:110. doi: 10.3389/fmolb.2019.00110

Scalise, M., Pochini, L., Panni, S., Pingitore, P., Hedfalk, K., and Indiveri, C. (2014). Transport mechanism and regulatory properties of the human amino acid transporter ASCT2 (SLC1A5). *Amino Acids* 46, 2463–2475. doi: 10.1007/s00726-014-1808-x

Scalise, M., Pochini, L., Pingitore, P., Hedfalk, K., and Indiveri, C. (2015). Cysteine is not a substrate but a specific modulator of human ASCT2 (SLC1A5) transporter. *FEBS Lett.* 589, 3617–3623. doi: 10.1016/j.febslet.2015.10.011

Schrödinger, R. (2020a). *LigPrep, Schrödinger*. New York, NY: LLC.

Schrödinger, R. (2020b). *Maestro, Schrödinger*. New York, NY: LLC.

Scopelliti, A. J., Font, J., Vandenberg, R. J., Boudker, O., and Ryan, R. M. (2018). Structural characterisation reveals insights into substrate recognition by the glutamine transporter ASCT2/SLC1A5. *Nat. Commun.* 9:38.

Scopelliti, A. J., Ryan, R. M., and Vandenberg, R. J. (2013). Molecular determinants for functional differences between alanine-serine-cysteine transporter 1 and other glutamate transporter family members. *J. Biol. Chem.* 288, 8250–8257. doi: 10.1074/jbc.m112.441022

Tetsuka, K., Takanaga, H., Ohtsuki, S., Hosoya, K., and Terasaki, T. (2003). The l-isomer-selective transport of aspartic acid is mediated by ASCT2 at the blood-brain barrier. *J. Neurochem.* 87, 891–901. doi: 10.1046/j.1471-4159.2003.02063.x

Torres-Zamorano, V., Leibach, F. H., and Ganapathy, V. (1998). Sodium-dependent homo- and hetero-exchange of neutral amino acids mediated by the amino acid transporter ATB degree. *Biochem. Biophys. Res. Commun.* 245, 824–829. doi: 10.1006/bbrc.1998.8434

Trott, O., and Olson, A. J. (2010). AutoDock vina: improving the speed and accuracy of docking with a new scoring function, efficient optimization, and multithreading. *J. Comput. Chem.* 31, 455–461.

Utsunomiya-Tate, N., Endou, H., and Kanai, Y. (1996). Cloning and functional characterization of a system ASC-like Na+-dependent neutral amino acid transporter. *J. Biol. Chem.* 271, 14883–14890. doi: 10.1074/jbc.271.25.14883

Vaughn, P. R., Lobo, C., Battaglia, F. C., Fennessey, P. V., Wilkening, R. B., and Meschia, G. (1995). Glutamine-glutamate exchange between placenta and fetal liver. *Am. J. Physiol.* 268, E705–E711.

Yu, X., Plotnikova, O., Bonin, P. D., Subashi, T. A., Mclellan, T. J., Dumlao, D., et al. (2019). Cryo-EM structures of the human glutamine transporter SLC1A5 (ASCT2) in the outward-facing conformation. *Elife* 8:e48120.

Zander, C. B., Albers, T., and Grewer, C. (2013). Voltage-dependent processes in the electroneutral amino acid exchanger ASCT2. *J. Gen. Physiol.* 141, 659–672. doi: 10.1085/jgp.201210948

Zerangue, N., and Kavanaugh, M. P. (1996). Flux coupling in a neuronal glutamate transporter. *Nature* 383, 634–637. doi: 10.1038/383634a0

Conflict of Interest: The authors declare that the research was conducted in the absence of any commercial or financial relationships that could be construed as a potential conflict of interest.

SCIENTIFIC REPORTS
nature research

Check for updates

OPEN

ATP modulates SLC7A5 (LAT1) synergistically with cholesterol

Jessica Cosco[1,4], Mariafrancesca Scalise[1,4], Claire Colas[2], Michele Galluccio[1], Riccardo Martini[2], Filomena Rovella[1], Tiziano Mazza[1], Gerhard F. Ecker[2] & Cesare Indiveri[1,3]✉

The plasma membrane transporter hLAT1 is responsible for providing cells with essential amino acids. hLAT1 is over-expressed in virtually all human cancers making the protein a hot-spot in the fields of cancer and pharmacology research. However, regulatory aspects of hLAT1 biology are still poorly understood. A remarkable stimulation of transport activity was observed in the presence of physiological levels of cholesterol together with a selective increase of the affinity for the substrate on the internal site, suggesting a stabilization of the inward open conformation of hLAT1. A synergistic effect by ATP was also observed only in the presence of cholesterol. The same phenomenon was detected with the native protein. Altogether, the biochemical assays suggested that cholesterol and ATP binding sites are close to each other. The computational analysis identified two neighboring regions, one hydrophobic and one hydrophilic, to which cholesterol and ATP were docked, respectively. The computational data predicted interaction of the ϒ-phosphate of ATP with Lys 204, which was confirmed by site-directed mutagenesis. The hLAT1-K204Q mutant showed an impaired function and response to ATP. Interestingly, this residue is conserved in several members of the SLC7 family.

The human LAT1 transporter (SLC7A5) is one of the seven members of the SLC7 family characterized by the association with ancillary glycoproteins belonging to the SLC3 family, namely SLC3A1 and SLC3A2[1,2]. The formation of these heterodimers represents a peculiar feature for mammalian transporters in terms of both structural and functional properties. The heterodimer is formed via a disulfide (S–S) between a conserved Cys residue of the SLC7 member(s), representing the light subunit, and a conserved Cys residue of the SLC3 member(s), representing the heavy subunit. The actual biological significance of such an interaction is not completely defined neither in terms of evolution nor in terms of regulatory aspects even though it is plausible that the ancillary glycoproteins serve as a chaperone for the light subunit to reach the definitive location in the cell membrane[1,2]. In particular, LAT1 forms a functional heterodimer with SLC3A2, commonly known as CD98 or 4F2hc. Over the years, it has been demonstrated, both in intact cells (ex vivo) and in proteoliposomes (in vitro), that the sole competent subunit for the transport function is LAT1, while CD98 does not play any role for the intrinsic transport function[3]. In good agreement with this observation, CD98 is a multifunctional protein that plays biological roles independently from the interaction with membrane transporters indicating that this protein is not a "simple" chaperone[4]. The functional properties of LAT1 have been investigated for decades and upon the description of its substrate specificity, it is now well assessed that the protein is involved in the distribution of essential amino acids in cells by catalyzing an amino acid antiport. Physiologically, histidine is the substrate preferentially exported from the cell interior to allow the other essential amino acids to be absorbed[3,5]. LAT1 has a quite narrow tissue distribution: it is mainly expressed in placenta and the blood–brain barrier. In these districts, the supply of essential amino acids is fundamental for normal cell growth and development[2]. Indeed, mice embryos KO for LAT1 are not vital, indicating that the absence of this protein is life-threatening or, even, not compatible with life[6]. Besides this experimental observation, the relevance of hLAT1 for the human being is testified by the virtual absence of diseases so far known, characterized by the complete lack of protein expression. In good agreement with this postulate, it has been recently demonstrated, by experiments conducted on mice and in vitro models, that two natural point mutations of LAT1 are responsible for the appearance of a familiar form of autism spectrum disorders (ASD) characterized by a lower supply of essential amino acids in brain[5].

[1]Department of DiBEST (Biologia, Ecologia, Scienze Della Terra) Unit of Biochemistry and Molecular Biotechnology, University of Calabria, via Bucci 4C, 87036 Arcavacata di Rende, Italy. [2]Department of Pharmaceutical Chemistry, University of Vienna, Althanstrasse 14, 1090 Wien, Austria. [3]CNR Institute of Biomembranes, Bioenergetics and Molecular Biotechnologies (IBIOM), via Amendola 122/O, 70126 Bari, Italy. [4]These authors contributed equally: Jessica Cosco and Mariafrancesca Scalise. ✉email: cesare.indiveri@unical.it

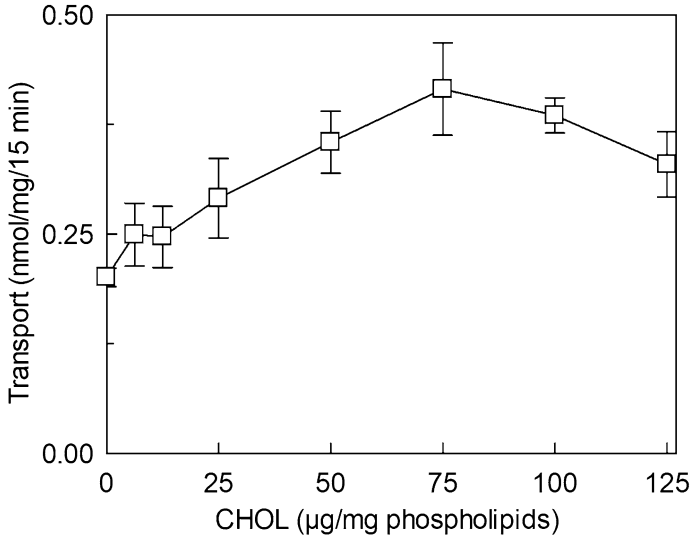

Figure 1. Effect of cholesterol on the transport activity of hLAT1. The purified protein was reconstituted in proteoliposomes as described in "Methods". Transport assay was started adding 5 µM [^{3}H]-histidine to proteoliposomes containing 10 mM histidine prepared with the indicated concentrations of cholesterol (CHOL). The transport was measured in 15 min according to the stop inhibitor method. Transport rate was expressed as nmol/mg in 15 min. Results are means ± SD of at least three independent experiments.

On the other way round, the over-expression of LAT1 is now considered a hallmark of several human cancers even if they originate from tissues that normally do not express LAT1[2,7]. Notwithstanding the high frequency of this phenomenon, its biological significance is not yet completely defined. Over the years, it has been proposed that cancer cells over-express LAT1 for absorbing glutamine and leucine, through a cycle with the glutamine transporter ASCT2, to supply the high demand of these amino acids[8]. Later on, it has been demonstrated that glutamine is not a good substrate of LAT1, in both directions of transport cycle[3]. Therefore, the high expression of LAT1 may be linked to the need for essential amino acids used in protein synthesis under the high proliferation conditions of cancer cells. However, LAT1 is not only required for sustaining cell divisions. It is not trivial that, among the transported substrates, there is likely one or more responsible for the additional role(s) in cancer cells. As an example, leucine is an allosteric regulator of the mitochondrial enzyme GDH that is responsible for the utilization of glutamine carbon skeleton in TCA, a feature typical of cancer cells[9,10]. Leucine is also one of the signals employed by cells to regulate their metabolism: in lysosomes, the master regulator of cell metabolism, mTORC1, senses leucine levels in both physiological and pathological conditions[11]. Furthermore, sestrin 2 has been recently described as the cytosolic sensor of leucine levels, linked to mTORC1[11]. Then, it is not a surprise that LAT1 is considered a hot protein and that over the years, efforts have been made to define structure/function relationships as well as regulatory properties with the main scope to specifically target this protein for pharmacological applications[12–14]. Interestingly, the 3D structure of the complex LAT1/CD98 has been recently solved opening important perspectives for structure/function relationship studies and drug design[15]. So far, only one compound which targets LAT1 reached the clinical trial for cancer treatment, i.e. the tyrosine analogue JPH203[16,17]. In the context of drug development, parallel to inhibitors, also prodrugs are designed given the ability of LAT1 to transport also thyroid hormones, L-DOPA and gabapentin, i.e. non amino-acid substrates[18]. The study of the regulators of LAT1 is, on the contrary, still *in nuce* and this represents a strong restrain for further understanding of LAT1 biology both in physiological and in pathological conditions. Therefore, in the present work, we aimed to investigate the modulation of LAT1 transport activity by physiological effectors, employing the experimental model of proteoliposomes. This tool gives the possibility of easily modifying the lipid composition of the membrane as well as precisely controlling the composition of the external and internal aqueous compartments of the protein-harboring vesicles[19]. We moved from the increasing evidence that cholesterol can regulate the features of several membrane transporters and that LAT1 shows potential binding sites for cholesterol[20]. Interestingly, we identified by in silico and in vitro studies a novel regulation by intracellular ATP which is synergistic with the effect of cholesterol. Moreover, the molecular basis of the pH sensitivity was also described, moving a step forward in completing the knowledge on human LAT1.

Results

Effect of cholesterol on the transport activity of hLAT1 in proteoliposomes. The effect of cholesterol (CHOL) on hLAT1 function was studied using the proteoliposome tool harboring the functionally active recombinant protein and assaying its function as [^{3}H]-histidine$_{ex}$/histidine$_{in}$ antiport. The transport activity increased by increasing the cholesterol content in the proteoliposome lipids up to 75 µg cholesterol/mg phospholipids; at higher cholesterol concentration, the transport activity decreased (Fig. 1). To obtain information on the possible influence of cholesterol on the affinity for the substrate on the external or internal face of the protein, kinetic parameters were measured under the optimal condition of cholesterol concentration. It has to

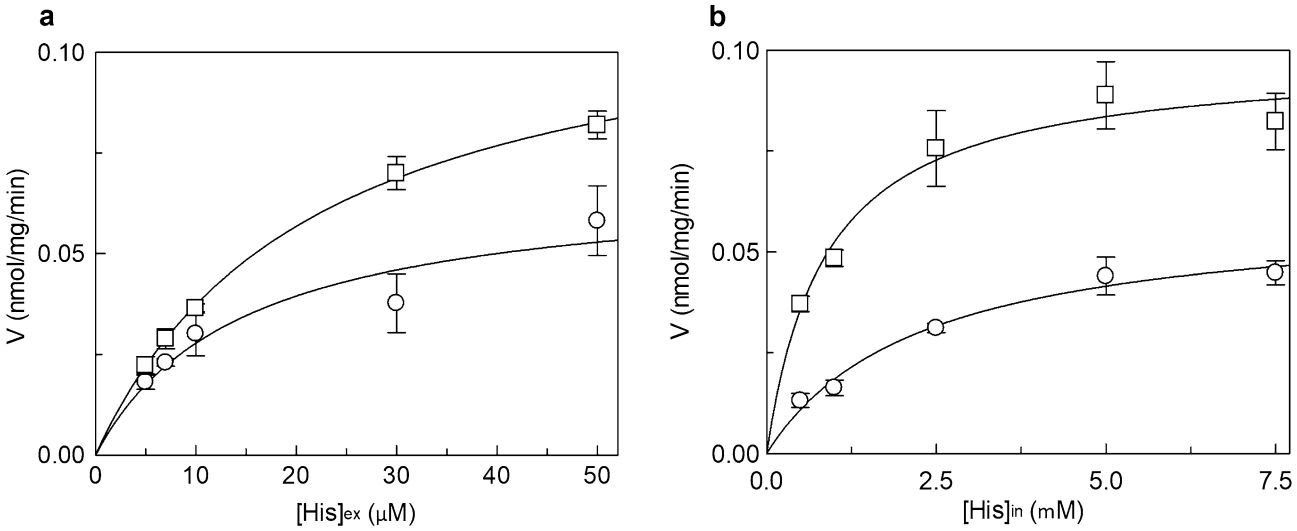

Figure 2. Effect of cholesterol on the kinetics of hLAT1. The purified protein was reconstituted using proteoliposomes prepared without (○) or with 75 μg cholesterol/mg phospholipids (□). The transport was measured in 15 min according to the stop inhibitor method. In (**a**), measurement of external Km. Transport rate was measured by adding [^{3}H]-histidine at the indicated concentrations to proteoliposomes containing 10 mM histidine. Data were plotted according to the Michaelis–Menten equation as transport rate vs histidine concentration. In (**b**), measurement of internal Km. Transport rate was measured by adding 30 μM [^{3}H]-histidine to proteoliposomes containing in the internal side indicated concentrations of histidine. Data were plotted according to the Michaelis–Menten equation as transport rate vs histidine concentration. Results are means ± SD of at least three independent experiments.

be stressed that the transporter is inserted in the proteoliposome membrane with the same orientation as in the cell membrane, therefore, the extraliposomal or the intraliposomal side corresponds to the extracellular or the intracellular side, respectively[3,21]. Figure 2a shows the transport rate dependence on external substrate concentration plotted according to Michaelis–Menten equation; a Km of 22.6 ± 4.3 μM (Fig. 2a, upper curve) was measured which was similar or only slightly higher than the external Km measured in the absence of cholesterol, that is 14.9 ± 2.7 μM (Fig. 2a, lower curve). This small variation correlates well with previous data obtained in cell systems in which the Km of the low-affinity substrate L-DOPA was shown to not be influenced by sequestration of cholesterol by methyl-cyclodextrin[20]. The Vmax of [^{3}H]-histidine$_{ex}$/histidine$_{in}$ antiport increased in the presence of cholesterol (Fig. 2a) from 0.069 ± 0.0094 to 0.12 ± 0.012 nmol/mg/min, in line with the data of Fig. 1. Interestingly, when measuring the internal Km, a different behavior was observed with respect to the external one; indeed, the internal Km significantly decreased from 2.3 ± 0.6 mM in the absence of cholesterol to 0.87 ± 0.12 mM in the presence of cholesterol (Fig. 2b), indicating an increased internal affinity for the substrate. In good agreement with the data obtained when investigating the external side, the Vmax increased from 0.061 ± 0.0087 nmol/mg/min to 0.10 ± 0.0038 nmol/mg/min.

Effect of nucleotides on the transport activity of hLAT1. In the attempt of exploring possible cell regulators linked to the energy metabolism, nucleotides were tested since ATP and other nucleotides were previously found to influence the activity of transporters[22–25]. The [^{3}H]-histidine$_{ex}$/histidine$_{in}$ antiport was measured in the presence of internal ATP under the optimal condition of cholesterol concentration. The transport activity increased by increasing the intraliposomal (intracellular) ATP concentration up to 4 mM and then decreased at higher concentrations (Fig. 3a). Then, other tri-phospho-nucleotides, namely CTP, UTP and GTP were tested in comparison with ATP. CTP, UTP and at a lower extent GTP, stimulated the transport function at a concentration of 4 mM (Fig. 3b). It has to be highlighted that 4 mM is in the range of the intracellular concentration of ATP but is much higher than the concentration of other nucleotides. Indeed, GTP, CTP and UTP did not exert any effect at concentrations from 0.1 to 0.3 mM (Supplementary Fig. 1a) which are closer to the physiological conditions[26–28]. To exclude the possibility that the activation by ATP was due to an osmotic effect or to the Na^+ cation present with the commercial formulation of ATP, sucrose or NaCl were tested as a control. No, or very small effect was observed in either condition indicating that the effect of the nucleotide is specific (Fig. 3b). Very interestingly, the activation by ATP did not occur if cholesterol is omitted from the proteoliposome preparation. In fact, in the absence of cholesterol, the nucleotide exerted only a very small, if any, effect (Fig. 3c). A clear activation was indeed observed in the presence of 75 μg cholesterol/mg phospholipids, in agreement with the data of Fig. 3a. This result suggests that the sites of interaction of cholesterol and ATP may be close to each other. The data reported in Fig. 3b indicates that the base moiety is not crucial for the activation. To investigate if the effect could be influenced by the phosphate groups, the transport activity was measured in the presence of 4 mM AMP, ADP or cAMP in comparison to ATP. As shown in Fig. 3d, the extent of activation decreased by decreasing the number of phosphate groups. This indicates that three phosphates are necessary for the full effect. Interestingly, the effect exerted by ATP is in the same order of magnitude of that exerted by ATP-Magnesium (Supplementary

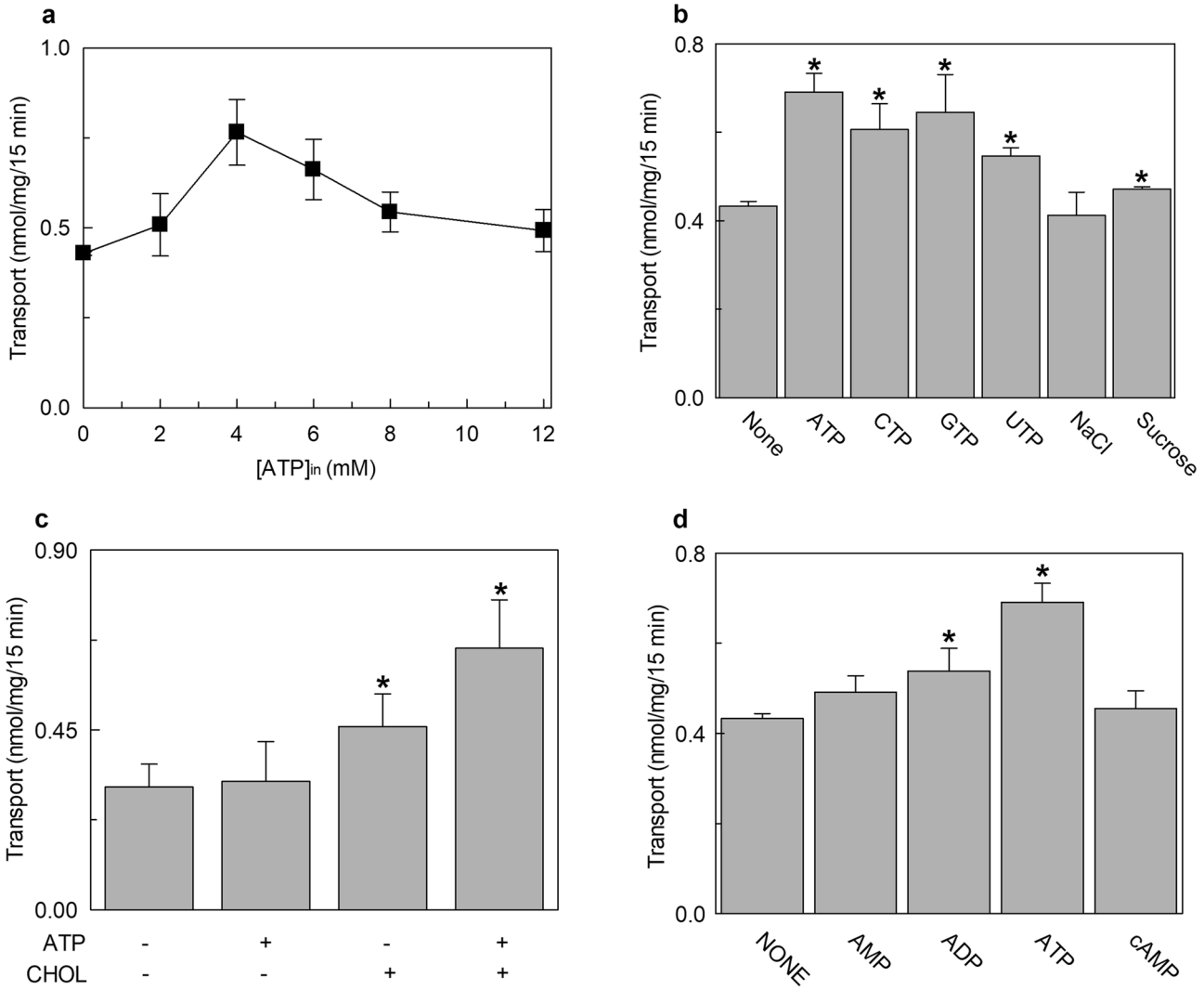

Figure 3. Effect of intraliposomal nucleotides on the transport activity of hLAT1. The purified protein was reconstituted in proteoliposomes prepared with 75 µg cholesterol/mg phospholipids as described in "Methods". Transport assay was started adding 5 µM [^{3}H]-histidine to proteoliposomes containing 10 mM histidine. The transport was measured in 15 min according to the stop inhibitor method. Transport rate was expressed as nmol/mg in 15 min. In (**a**), the dependence of hLAT1 transport activity on intraliposomal ATP. The indicated concentrations of ATP, buffered with 20 mM HepesTris pH 7.0, were added in the internal side of proteoliposomes. In (**b**), the effect of nucleotides on the transport activity of hLAT1. Intraliposomal compartment included 4 mM of the indicated nucleotides, buffered with 20 mM HepesTris pH 7.0. As an osmotic control, 12 mM NaCl or 12 mM sucrose was added in place of nucleotides. In (**c**), transport activity of the recombinant hLAT1. Proteoliposomes were prepared without (−) or with (+) 75 µg cholesterol/mg phospholipids as indicated; 4 mM ATP, buffered with 20 mM HepesTris pH 7.0, was included (+) or not (−) in the intraliposomal compartment as indicated. (**d**) Effect of AMP, ADP and cAMP on the transport activity of hLAT1. Proteoliposomes contained 4 mM of AMP, ADP, cAMP or ATP. Results are means ± SD of at least from three independent experiments. (*) Significantly different from the control (no addition in the intraliposomal compartment, none) as estimated by the Student's t-test ($p < 0.05$).

Fig. 1b). The kinetic parameters were then evaluated in the presence of 4 mM ATP with respect to the control condition without ATP. As shown in Fig. 4a, in the presence of intraliposomal ATP the external Km was slightly increased (33.9 ± 4.4 µM) and the V_{max} was higher than the control, i.e. the condition without ATP. The internal Km was not significantly influenced by the presence of ATP (0.57 ± 0.14 mM), while the Vmax was increased (Fig. 4b). To exclude a possible influence of the ancillary protein CD98 on the effect of cholesterol and ATP on hLAT1, the protein extracted from SiHa cells that is in complex with CD98[3] was employed. As shown in Fig. 5, the transport activity is influenced by cholesterol and/or ATP as the recombinant protein. Indeed, ATP stimulated the transport only in the presence of cholesterol while the nucleotide did not exert any effect in the absence of cholesterol.

The effect of ATP was also evaluated on the external side. The transport activity is 25% inhibited at 4 mM ATP (Supplementary Fig. 2). This concentration value is higher than the extracellular concentration of ATP[27,28],

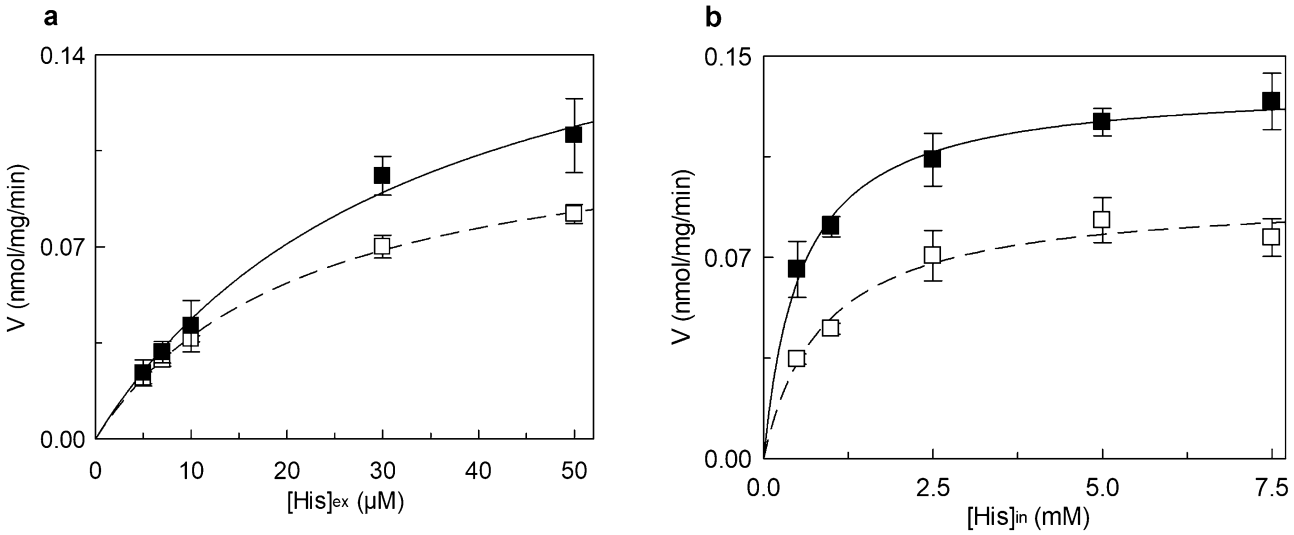

Figure 4. Effect of ATP on the kinetics of hLAT1. The purified protein was reconstituted in proteoliposomes prepared with 75 μg cholesterol/mg phospholipids as described in "Methods", containing (■) or not (□) 4 mM ATP (in dotted line, data from corresponding Fig. 2). The transport was measured in 15 min according to the stop inhibitor method. In (**a**), measurement of the external Km. Transport rate was measured by adding [^{3}H]-histidine at the indicated concentrations to proteoliposomes containing 10 mM histidine. Data were plotted according to the Michaelis–Menten equation as transport rate vs histidine concentration. In (**b**), measurement of the internal Km. Transport rate was measured by adding 30 μM [^{3}H]-histidine to proteoliposomes containing the indicated concentration of histidine. Data were plotted according to the Michaelis–Menten equation as transport rate vs histidine concentration. Results are means ± S.D. of at least three independent experiments.

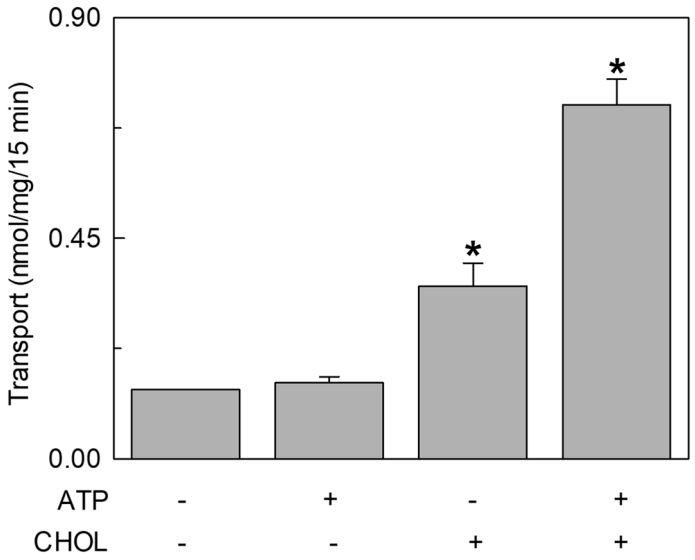

Figure 5. Effect of ATP on the transport activity of hLAT1 extracted from SiHa cells reconstituted in proteoliposomes. SiHa cell extract was prepared as described in "Methods". Transport was started adding 5 μM [^{3}H]-histidine to proteoliposomes containing 10 mM histidine prepared without (−) or with (+) 75 μg cholesterol/mg phospholipids as indicated; 4 mM ATP, buffered with 20 mM HepesTris pH 7.0, was included (+) or not (−) in the intraliposomal compartment as indicated. The transport was measured in 15 min according to the stop inhibitor method. Results are means ± S.D. of at least three independent experiments.

therefore this inhibition cannot be considered physiologically relevant. Moreover, this data confirms that the transporter is asymmetrical and inserted into the proteoliposome membrane with a right-side-orientation with respect to the native membrane as previously described[21].

Computational analysis of cholesterol and ATP interaction with hLAT1. To investigate the interaction of cholesterol and ATP with hLAT1 on a molecular level, computational analysis was performed (Supple-

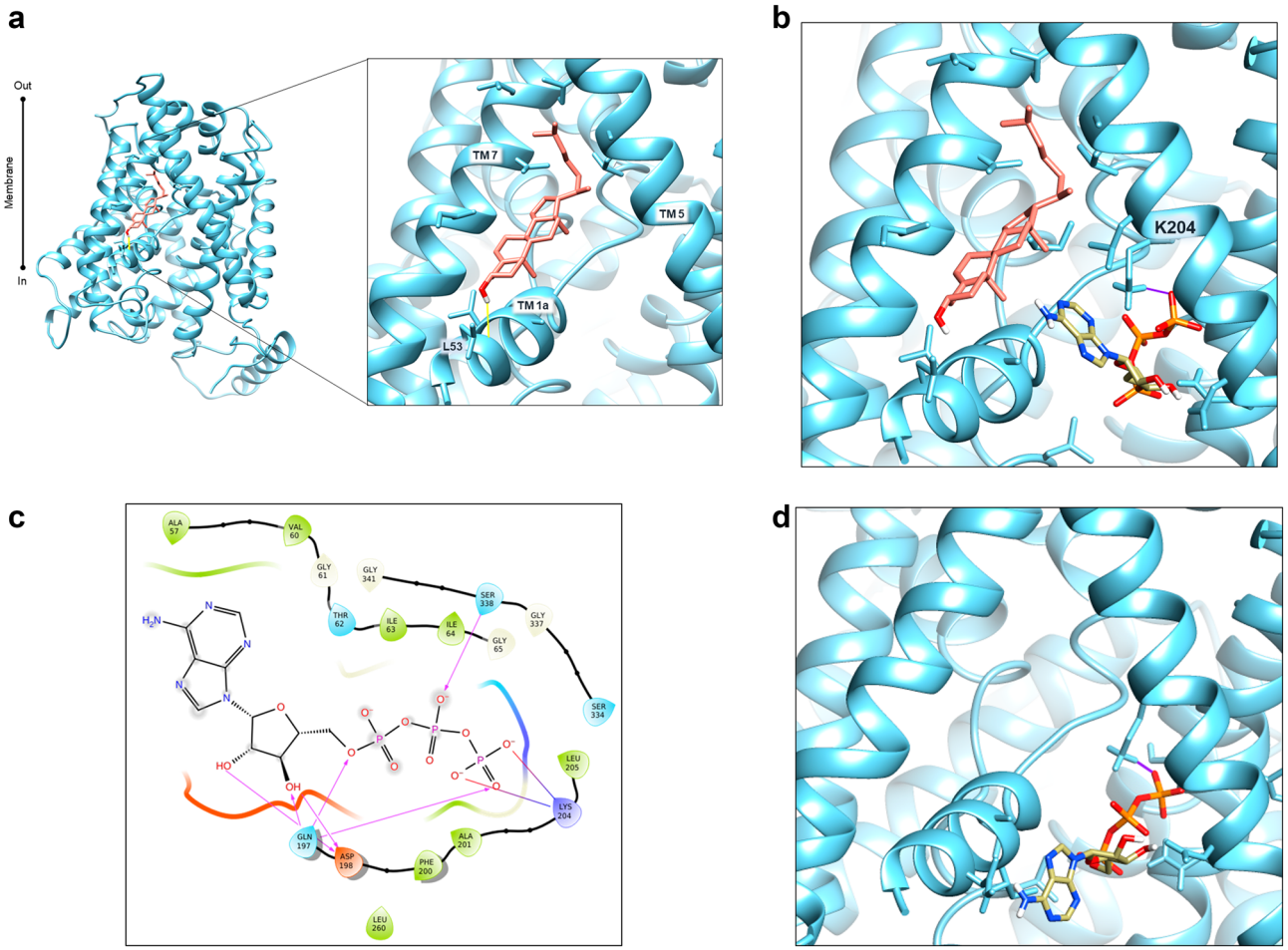

Figure 6. Docking analysis of hLAT1. Docking analysis in site 1 of hLAT1. The cryo-EM structure of hLAT1 in inward conformation (PDB ID: 6IRT, chain B) was represented as ribbon (sky blue) using Chimera v.1.7 software (https://www.cgl.ucsf.edu/chimera). Docking analysis was performed using InducedFit docking from Schrödinger-Maestro v11.3[65] as described in "Methods". In (**a**), molecular docking of cholesterol (in salmon) in the site 1 (TM 1a, TM5 and TM7). Residues belonging to cholesterol site are represented as sticks. This pose has a docking score of -5.54 and a MMGBSA binding energy of − 46.66 kcal/mol. The membrane and intracellular/extracellular environment are indicated. In (**b**), molecular docking of ATP in site 1 in the presence of cholesterol. The best pose from cholesterol docking was used to dock ATP. Lys 204 represented in stick makes an electrostatic bond (in violet) with the γ-phosphate of ATP. This pose has a docking score of − 6.92 and a MMGBSA binding energy of − 8.97 kcal/mol. In (**c**), 2D visualization of hLAT1 interaction with ATP. The arrows indicated the residues involved in the binding of ATP. In (**d**), molecular docking of ATP in site 1 in the absence of cholesterol; in violet, electrostatic bond with Lys 204 represented in stick. The pose has a docking score of − 6.336.

mentary Fig. 3). The structure of the hLAT1 (PDB ID: 6IRT, chain B)[15] has been used for the analysis. The initial step consisted in identifying hydrophobic and hydrophilic regions on the surface of hLAT1 using SiteMap[29,30]. Ten sites have been predicted with a score from 0.888 to 1.015, i.e. the optimal range for a reliable SiteMap prediction (Supplementary Fig. 3)[29]. Interestingly, site **d** corresponded to one of the lipid-like densities observed in the cryo-EM structure of hLAT1 (Supplementary Fig. 4). In this site, the very conserved **LLY**AFS**K** motif is present (Supplementary Fig. 4), well-acknowledged as a cholesterol binding motif CRAC[31]. However, our attention for deepening the analysis of cholesterol and ATP binding sites was focused on site **h,** due to the presence of a hydrophilic surface close to a hydrophobic one (Supplementary Fig. 3). It is worth to note that site **h** includes two hydrophobic subsites, namely subsite 1 and subsite 2. Only subsite 1 is close to a hydrophilic region (identified in red/blue surfaces by SiteMap—Supplementary Fig. 3) thus being in line with our working hypothesis, based on biochemical data, that the binding sites for cholesterol and ATP should be close to each other. Moreover, subsite 1 includes also the residues previously predicted to be involved in cholesterol binding by sequence alignments with the *Drosophila melanogaster* dopamine transporter dDAT, sharing a similar fold and also presenting a cholesterol modulated activity[20]. Subsequently, docking of cholesterol was performed after generating a grid on the subsite 1 of site **h**. To obtain a more reliable result, an Induced Fit docking was performed as it incorporates side chains mobility of the binding site. After clustering of all poses retrieved, the pose with the lowest docking score (− 5.54) was selected from the most populated cluster (Fig. 6a). In this site cholesterol is accommodated

Figure 7. Multiple alignments of SLC7 protein sequences. Indicated SLC7 members were aligned using the software Clustal Omega as described in "Methods" (https://www.ebi.ac.uk/Tools/msa/clustalo). In the yellow box, the conservation of Lys 204 (yellow box) of SLC7A5 is shown in comparison to the other members of the SLC7 family.

by hydrophobic residues of the helices 1a, 5 and 7 such as L53, V56, A57, L208, A209, I212, I284, V288, L291. As described above, subsite 1 has in its vicinity a hydrophilic pocket that might accommodate ATP (Fig. 6a). Thus, Induced Fit docking of ATP was performed on this region (Fig. 6b). The ϒ-phosphate has an electrostatic interaction with the Lys 204. The ribose group was predicted to interact with the residues Gln 197 and Asp 198. Besides the interaction with the ribose group, Gln 197 interacts also with the α-phosphate. The β-phosphate forms a hydrogen bond with Ser 338 and (Fig. 6c). Interestingly, in the absence of cholesterol, the docking of ATP was different with the nucleotide remaining in a more external position (Fig. 6d) indicating that its binding is influenced by the presence of cholesterol in the subsite 1. Next, we conducted a blind docking of ATP in the presence of cholesterol in subsite 1 using AutoDock Vina[32], which resulted in a single cluster located in the region of the hydrophilic surface of pose **h** (Supplementary Fig. 5). These results gave us further confidence in our ATP binding mode prediction.

Basic functional characterization of site-directed mutant hLAT1-K204Q. The docking analysis together with the biochemical data suggested focusing on Lys 204 since this residue establishes an electrostatic interaction with ϒ-phosphate, crucial for the ATP effect (Figs. 3d and 6c). Moreover, Lys 204 is conserved in the SLC7 family members whose transport function is already characterized (Fig. 7). Therefore, Lys was mutated to Gln to retain the hydrophilic nature and the size of the residue, while removing the positive charge. Despite the conserved features, the hLAT1-K204Q at pH 7.0 only exhibited 15% activity when compared to the WT (Fig. 8a). Another peculiar feature of this mutant was the loss of sensitivity towards inhibitors both competitive and covalent ones (Fig. 8b), indicating that the substrate-binding site of hLAT1 might be compromised by the mutation. The importance of Lys 204 for basic transport function of hLAT1 allowed us to hypothesize that its positive charge could be involved in the pH sensitivity of the protein. In contrast with previous findings[1,18,33], we observed that the transport activity of hLAT1 is pH-dependent, being maximal at neutral pH but much lower at acidic pH (Fig. 9). Surprisingly, the hLAT1-K204Q exhibited an inverted pH dependence with the lowest activity at pH 7.5, while the activity at pH 6.0 was comparable to that of the WT at pH 7.0 (Fig. 9). Kinetics of transport was also studied and Km towards histidine was measured at both pH 7.0 and pH 6.0. The Km values were 549 ± 108 μM or 51.4 ± 7.5 μM at pH 7.0 (Fig. 10a) or pH 6.0 (Fig. 10b), respectively. In line with the data of Fig. 9, the V_{max} value at pH 6.0 is one order of magnitude higher than that at pH 7.0. Both the values were higher than that of the WT protein confirming the role of Lys 204 in the transport process and in substrate recognition (Fig. 8). This is in agreement with the location of this Lys residue in the proximity of the substrate-binding site (Supplementary Fig. 6).

Effect of the K204Q mutation on ATP and cholesterol dependence. After the basic functional characterization of the mutant, we investigated the dependence on cholesterol and ATP (Fig. 11). Interestingly, the mutant is activated by cholesterol similarly to the WT protein (Fig. 11a). In contrast, regarding the ATP dependence, the hLAT1-K204Q showed different behavior in comparison to the WT protein. As reported in Fig. 11b, the hLAT1-K204Q showed a shift in the ATP concentration required for transport stimulation. Noteworthy, the activity of the mutant was only slightly stimulated at 4 mM but reached the maximum of activation at 8 mM ATP (Fig. 11b). These results, which are quite different from those of the hLAT1 WT, indicated that the residue Lys 204 is crucial for ATP sensitivity in hLAT1.

Discussion

The role of cholesterol in modulating the transport activity of hLAT1 is described in this work. The interaction of cholesterol with hLAT1 was previously hypothesized based on the identification of conserved motifs within proteins structurally related to hLAT1[20] such as dDAT[34] and hSERT[35]. Then, the recently solved 3D structure of hLAT1 in complex with hCD98 showed some lipid sites probably occupied by cholesteryl hemisuccinate added to the protein during purification[15]. The same authors showed that the addition of cholesterol to proteoliposomes harboring the LAT1-CD98 complex led to stimulation of leucine uptake. Transport modulation by cholesterol revealed to be a particularly interesting issue, since other transporters belonging to different SLC families were found to be modulated by this lipid as well[20,34,36–42]. Therefore, we deepened this aspect by using biochemical

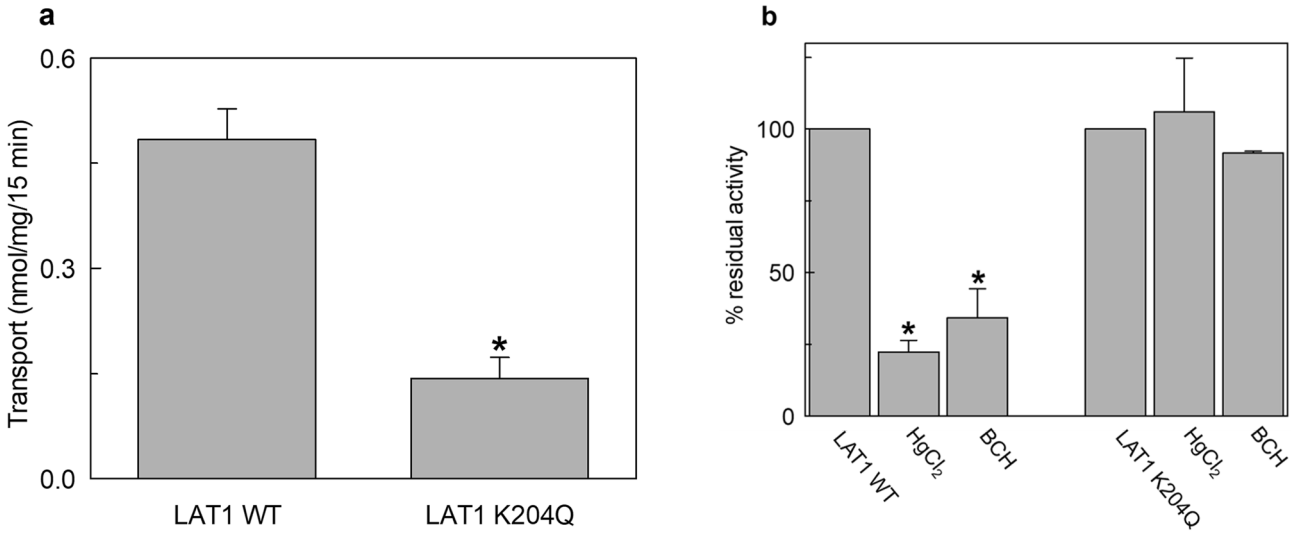

Figure 8. Transport activity of the recombinant hLAT1 WT or hLAT1-K204Q mutant. The mutant protein was prepared as described in "Methods". The purified hLAT1-WT or hLAT1-K204Q proteins were reconstituted in proteoliposomes prepared with 75 μg cholesterol/mg phospholipids as described in "Methods". Transport assay was started by adding 5 μM [^{3}H]-histidine to proteoliposomes containing 10 mM histidine. The transport was measured in 15 min according to the stop inhibitor method. In (**a**), comparison of the transport activity of hLAT1-WT or hLAT1-K204Q mutant. Transport rate was expressed as nmol/mg in 15 min. In (**b**), the effect of $HgCl_2$ and BCH on transport activity of hLAT1-WT or hLAT1-K204Q mutant. During transport assay, 15 μM $HgCl_2$ and 5 mM BCH were added in the extraliposomal side together with the radiolabeled substrate. Transport was indicated as % residual activity with respect to the control (i.e. proteoliposomes with no externally added inhibitor). Results are means ± SD of at least three independent experiments. (*) Significantly different from the control (no externally added inhibitor) as estimated by the Student's t-test ($p < 0.05$).

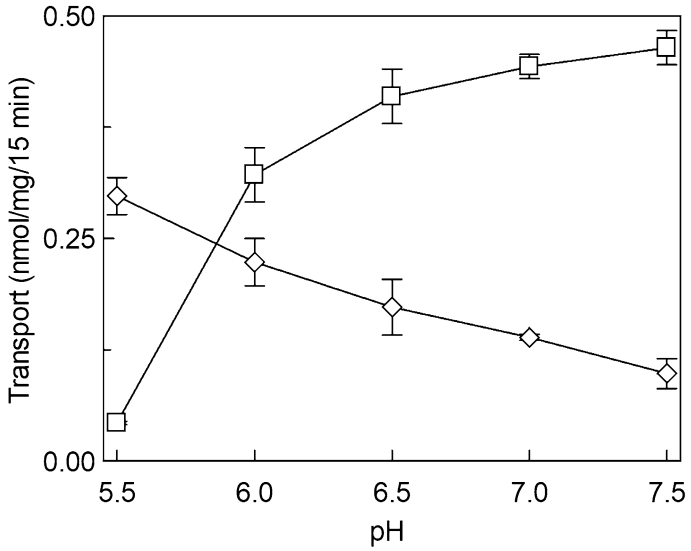

Figure 9. Effect of pH on the transport activity of hLAT1-WT or hLAT1-K204Q mutant. The purified proteins, WT (□) and K204Q (◊), were reconstituted in proteoliposomes prepared with 75 μg cholesterol/mg phospholipids as described in "Methods" and buffered with 20 mM Hepes Tris at the indicated pH. Transport was started by adding 5 μM [^{3}H]-histidine to proteoliposomes containing 10 mM histidine. The transport was measured in 15 min according to the stop inhibitor method. Transport rate was expressed as nmol/mg in 15 min. The pH was equal in both the internal and external sides of proteoliposomes. Results are means ± SD of at least three independent experiments.

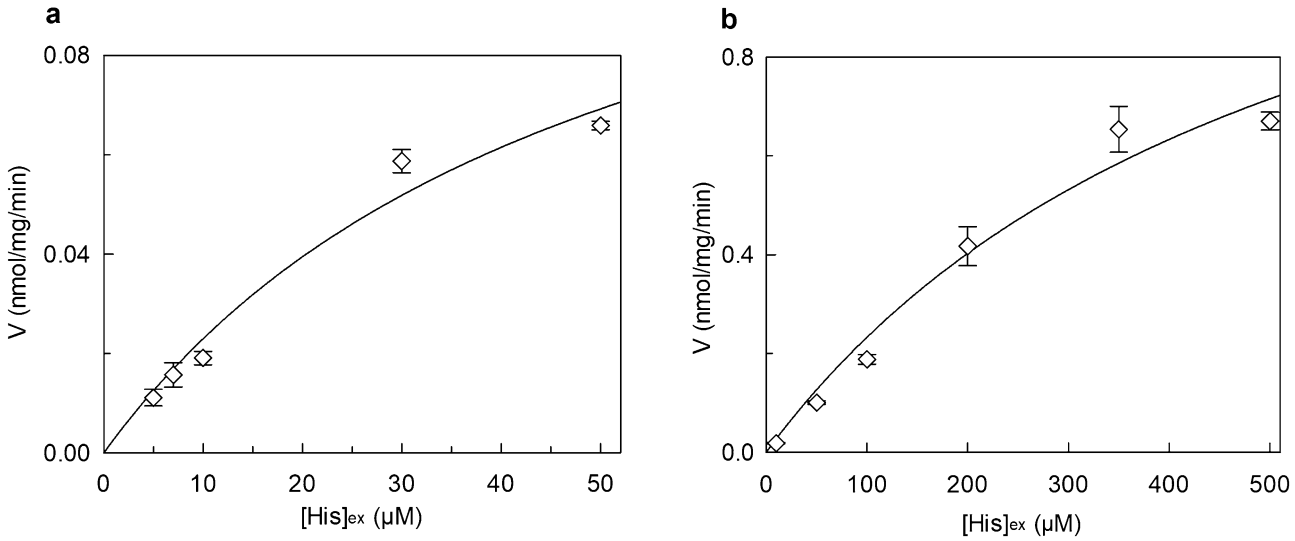

Figure 10. Effect of pH on external Km of hLAT1-K204Q mutant. The purified protein was reconstituted using proteoliposomes prepared with 75 μg cholesterol/mg phospholipids. The transport was measured in 15 min according to the stop inhibitor method. Transport rate was measured by adding [^{3}H]-histidine at the indicated concentrations to proteoliposomes containing 10 mM histidine. Data were plotted according to the Michaelis–Menten equation as transport rate vs histidine concentration. In (**a**), proteoliposomes were prepared at pH 6.0 and substrate was buffered with 20 mM HepesTris pH 6.0. In (**b**), proteoliposomes were prepared at pH 7.0 and substrate was buffered with 20 mM HepesTris pH 7.0. Results are means ± SD of at least three independent experiments.

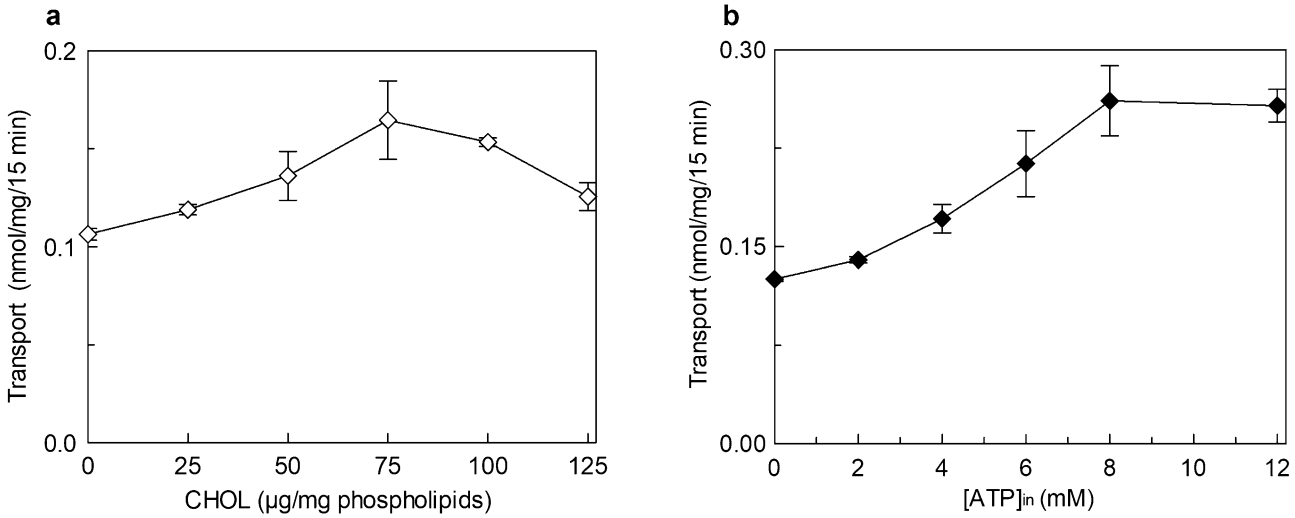

Figure 11. Effect of cholesterol and ATP on the hLAT1-K204Q mutant. The purified protein was reconstituted as described in "Methods". Transport was started adding 5 μM [^{3}H]-histidine to proteoliposomes containing 10 mM histidine. The transport was measured in 15 min according to the stop inhibitor method. Transport rate was expressed as nmol/mg in 15 min. In (**a**), the effect of cholesterol on the transport activity of hLAT1-K204Q mutant. Proteoliposomes were prepared with indicated concentrations of cholesterol (CHOL). In (**b**), the effect of internal ATP on transport activity of hLAT1-K204Q mutant. The indicated concentrations of ATP, buffered with 20 mM HepesTris pH 7.0, were added in the internal side of proteoliposomes prepared with 75 μg cholesterol/mg phospholipids. Results are means ± SD of at least three independent experiments.

approaches together with computational analysis. From the collected data, it emerged that cholesterol added to the proteoliposomes indeed stimulated the transport activity measured as antiport of the high-affinity substrate histidine (Fig. 1). The intrinsic feature of proteoliposome tool allowed us to investigate in further detail the effect of cholesterol on hLAT1 function in terms of kinetic parameters. The affinity for the substrate on the external face of the transporter was not, or only slightly, modified by cholesterol (Fig. 2a). These findings correlate well with previous results on hLAT1, obtained by a different experimental approach consisting in sequestering cholesterol from the cell membrane by methyl-cyclodextrin[20]. Moreover, the internal affinity for the substrate, which

cannot be approached using the intact cell system, was also investigated. Differently from the external side, the internal affinity was strongly increased suggesting a stabilization of the hLAT1 inward open conformation by cholesterol (Fig. 2b). This differs from data on hSERT, obtained by studies performed with inhibitors, showing that cholesterol favours the outwardly open conformation[35]. As in the case of other membrane proteins[22,37–44], cholesterol effects might be not exclusively due to an action on the membrane fluidity/arrangement, but they could be related to a physical interaction with the protein. Very probably, cholesterol binds to hLAT1 in more than one site as suggested by the patch of densities reported in the 3D structure, and in agreement with our computational analysis (Supplementary Fig. 3). At this stage is not possible to evaluate the exact contribution of each cholesterol binding site to the transport activity of LAT1. Interestingly, some of the identified sites, namely **d**, **e**, **f**, **g** and **h** are coincident with those previously predicted[15,20,45] (Supplementary Fig. 3). It is important to highlight that cholesterol can bind to membrane proteins in annular or non-annular sites, engaging distinct types of interaction: (1) annular sites are less specific and devoted to mediate the interaction of a hydrophobic transmembrane segment with the phospholipid bilayer; (2) non-annular sites engage larger protein domains and are involved in the regulation of the protein function[31]. Therefore, it is more likely that the effect on substrate affinity could be due to the interaction of cholesterol with sites showing non-annular features. The selection of the most plausible cholesterol-binding site was supported by the new collateral finding of regulation of transport activity by intraliposomal ATP (Fig. 3). Indeed, the stimulatory effect of ATP was only exerted in the presence of cholesterol, thus strengthening the hypothesis that the respective binding sites are close to each other. The extent of stimulation by cholesterol is similar to that previously described for the same[15,20] or other transporters[37–39,41]. The synergistic effect by cholesterol and ATP reaches a factor higher than 3. In line with a physiological role of such a modulation, ATP-Magnesium is able to exert the same activation of free ATP. This indicates that the LAT1 bound form is ATP, as observed in other cases[46,47]. It has to be stressed that this phenomenon was observed also on the native transporter. This is in line with our previous findings demonstrating that all the transport features are virtually identical in the native and the recombinant hLAT1[3]. Very interestingly, the docking analysis of ATP on the whole hLAT1 structure resulted in a single cluster of interactions coincident with the hydrophilic pocket close to subsite 1 in site **h** (Fig. 6a and Supplementary Fig. 5). Altogether, the described observations indicated that binding of ATP in subsite 1 (of site **h**) might explain the synergistic effect of ATP and cholesterol. It has to be noted that ATP has a secondary role in the transport modulation with respect to cholesterol, since it does not influence substrate affinity, but only the transport rate (Fig. 4). This phenomenon may be interpreted also in terms of docking analysis of ATP performed on the homology model of hLAT1 in an outward open conformation (Supplementary Fig. 7). In fact, the hydroxyl moiety of cholesterol establishes hydrogen bond interactions alternatively with the backbone atoms of Leu 53 (Fig. 6a) or the side chain of Asp 198 (Supplementary Fig. 7) in the inward or outward conformation, respectively. In the outward state, Lys 204 that is the major determinant for ATP coordination is buried. This let us hypothesize that the binding of ATP only occurs in the inward open conformation in line with its accessory role with respect to cholesterol.

As a serendipity event, the residue underlying the ATP effect gave further insights into the hLAT1 structure/function relationships. The homologous residue in bacterial ApcTs has a role in conformational changes and pH response[48–50]. Thus, we investigated the relationships of Lys 204 with the pH response of hLAT1. First, we revealed that, contrarily to previous assumptions[1,18,33], the activity of hLAT1-WT is pH-dependent (Fig. 9). This novel finding may be due to the better suitability of the in vitro system of proteoliposomes for investigating the pH dependence[19]. Interestingly, the loss of the positive charge of Lys 204 in the hLAT1-K204Q triggered an inverted pH dependence with respect to the hLAT1-WT. Moreover, as previously supposed for the bacterial homologue GkApcT[50], Lys 204 has also a crucial role in the layout of the active site: the hLAT1-K204Q shows an impairment of the affinity towards histidine and loses the response to inhibitors targeting the substrate-binding site (Fig. 8). Indeed, Lys 204 is not far from residues involved in the substrate binding and translocation[15,21] (Supplementary Fig. 6). The influence of Lys 204 on the active site may be mediated by the residues present in the kink of helix 1 interposed between the active site and Lys 204 (Supplementary Fig. 6). This correlates with the finding that this helical domain most probably moves during the conformational changes necessary for translocation as also recently proposed[45,51]. The stimulation by ATP may have a biological significance linked to the metabolic state of the cells. It is well known that ATP acts also as a metabolic regulator on a great number of enzymes and, in some cases, of transporters[22–25,42]. To our knowledge, this is the first case of a transporter of the SLC7 family, showing a regulation by ATP. Therefore, hLAT1 could respond to metabolic changes via the interaction with ATP and increasing the distribution of essential amino acids to cells under conditions of energy sufficiency. This may have a relevant role also in the metabolic rewire typical of cancer cells[52]. Furthermore, the accessible hydrophilic pocket identified in this work opens perspectives for the design of potential interactors able to target specifically hLAT1 contributing to the design of drugs for its silencing.

Methods

Materials. *E. coli* Rosetta(DE3)pLysS cells were from Novagen (Rome, Italy); His Trap HP and PD10 columns were from GE Healthcare; L-[^{3}H]histidine was from American Radiolabeled Chemicals (ARC Inc., USA); $C_{12}E_8$, Amberlite XAD-4, egg yolk phospholipids (3-sn-phosphatidylcholine from egg yolk), cholesterol, Sephadex G-75, imidazole, L-histidine and all the other reagents were from Merck KGaA (Germany).

Extraction of hLAT1 from SiHa cells. SiHa cells were maintained in Dulbecco's Modified Eagle Medium as described in[3]. LAT1 was extracted from SiHa pellets, after solubilization with RIPA buffer and incubation for 30 min on ice. Proteins were quantified, after centrifugation (12,000*g*, 15 min, 4 °C), using the colorimetric method Lowry-Folin[3].

LAT1 K204Q Forward	TTTGCGGCGGCGCAGCTGCTGGC
LAT1 K204Q Reverse	GCCAGCAGCTGCGCCGCCGCAAA

Table 1. Sequences of primers used for mutagenesis.

Construction and over-expression of recombinant hLAT1 proteins. hLAT1 has been mutated using PCR overlap extension method as described in[53,54] by using primers reported in Table 1. hLAT1 WT and K204Q mutant have been over-expressed in *E. coli* Rosetta(DE3)pLysS as described in[55].

Protein purification. hLAT1 WT and K204Q mutant were over-expressed in *E.coli* and purified as previously described[55]. ÄKTA start FPLC equipment was used for purification. The supernatant from solubilized cell lysate was loaded on a His Trap HP column (5 mL Ni Sepharose) preequilibrated with a buffer containing 20 mM Tris HCl pH 8.0, 10% glycerol, 200 mM NaCl, and 0.1% sarkosyl (10 mL). The column was washed with a washing buffer containing 20 mM Tris HCl pH 8.0, 10% glycerol, 200 mM NaCl, 0.1% DDM, and 3 mM DTE (10 mL). The protein was eluted by the washing buffer added with 400 mM imidazole (15 mL). Desalt of 2.8 mL of the purified protein was then performed using a PD-10 column. The desalting buffer contained 20 mM Tris HCl pH 8.0, 10% glycerol, 0.1% DDM, and 10 mM DTE.

Liposome preparation. 7.5 mg of cholesterol were added to 100 mg of egg yolk phospholipids and solubilized with 1 mL chloroform. After short incubation under rotatory stirring (1200 rpm, 30 °C, 5 min) open tube is dried O.N. at room temperature[56]. The lipid film was resuspended in 1 mL water (10% final concentration) and sonicated to form unilamellar liposomes as previously described[57].

Reconstitution of the hLAT1 transporter into proteoliposomes. The desalted proteins, hLAT1 WT and mutant K204Q, were reconstituted by removing the detergent from mixed micelles containing detergent, protein, and phospholipids by incubation with Amberlite XAD-4 in a batch-wise procedure, as previously described[21]. In brief: the mixture for reconstitution was composed of 4 µg purified protein in desalting buffer (150 µL), 100 µL of 10% $C_{12}E_8$, 100 µL of sonicated liposomes prepared as described in the above paragraph, 10 mM histidine, 10 mM DTE, and 20 mM HepesTris pH 7.0 (except where differently indicated) in a final volume of 700 µL. Amberlite XAD-4 (0.5 g) was added to this mixture and incubated for 90 min under rotatory stirring (1200 rpm) at 23 °C using a previously pointed out procedure[21]. This methodology allows inserting the structurally asymmetric protein, with an homogeneous orientation (right-side-out) into the membrane[19].

Transport measurements. Transport was assayed as previously described[21]. In brief: proteoliposomes (600 µL) were passed through a Sephadex G-75 column (0.7 cm diameter × 15 cm height) equilibrated with a buffer containing 20 mM Hepes Tris pH 7.0 and 10 mM sucrose. Eluted proteoliposomes were divided into aliquots of 100 µL for transport assay. [^{3}H]-histidine (5 µM) was added to the proteoliposome samples for starting the transport and 15 µM Mercury(II) Chloride ($HgCl_2$) was added to stop the transport according to the stop inhibitor method[21]. To remove the external (not taken up) radioactivity, 100 µL of each sample were passed through a Sephadex G-75 column (0.6 cm diameter × 8 cm height). Samples were eluted with 1 mL 50 mM NaCl in 4 mL of scintillation mixture for radioactivity counting. Calculated specific activity was expressed as nmol/mg at a given time or as nmol/mg/min in the case of transport rate measurement. Kinetic parameters were derived from data fitting in Michaelis–Menten equation using Grafit 5.0.13 software (Erithacus Software, West Sussex, UK).

Computational analysis. *Protein preparation.* The three-dimensional coordinates of LAT1 (PDB ID: 6IRT)[15] were downloaded, refined, and prepared within Maestro v11.3[58] using Schrödinger Protein Preparation Wizard tool[59,60] which consists of three essential steps: addition of hydrogens, optimization of hydrogen bonds by flipping amino side chains, correction of charges, and minimization of the protein complex. Default parameters were used. Chain A, corresponding to CD98 and all ligands in 6IRT were removed.

SiteMap. The hydrophobic and hydrophilic regions on the protein surface were investigated using SiteMap[29,30,61]. The prepared chain B of 6IRT was submitted to SiteMap using default parameters and ranked. 10 sites were identified with a minimum of 15 site points after generating a fine grid (i.e. corresponding of a grid spacing of 0.35 Å) and enabling the detection of shallow binding sites on the surface.

Preparation of ligands. The ligands cholesterol and ATP were downloaded from PubChem in sdf format. Subsequently, they were prepared using LigPrep[62] by optimizing geometries of the ligands and assigning them appropriate protonation states[63]. Epik with default parameters was used[64].

Receptor grid generation. Receptor grids were generated keeping the default parameters of van der Waals scaling factor 1.00 and charge cutoff 0.25 subjected to OPLS3 force field. A cubic box of specific dimensions (30 × 30 × 30 Å) centered around selected residues (L53, V56, V60, F200, K204, A207, L210, I211, I280, I284, L291) was generated for the protein.

Induced fit docking (IFD) extra precision (XP). Docking analysis were performed using Induced Fit XP Docking[65] protocol in Maestro[66,67] . At first, a Glide docking was carried out[68]. On the basis of B-factor, side chains were trimmed and a van der Waals scaling factor of 0.50 was used for both receptor and ligand. The number of poses generated was set to 20. All residues within 5.0 Å of ligand poses were refined and side chains optimized using a Prime structure prediction. This procedure allows the binding site residues to better accommodate the various ligand poses, resulting in more optimized protein–ligand interactions. Finally, structures within 30.0 kcal/mol of the best structure, and within the top 20 structures overall were redocked using Glide XP. The ligand was docked into the induced-fit receptor structure and the results yielded an IFD score for each output pose.

Autodock Vina. Autodock Vina v1.1.2 was used to identifying ATP binding sites in LAT1 transporter in the presence of Cholesterol (pose with docking score − 5.54 of Cholesterol, from Maestro)[32] using a blind docking procedure. The grid box, which covered the whole protein, has a size of 70 × 102 × 74 Å (x, y, and z) with spacing 1.0. After ligand preparation (see above), the ATP molecule was docked into refined LAT1. The best conformation space of the ligand was searched employing the Lamarckian Genetic Algorithm. Default parameters were used and 20 different conformers were generated for the ATP molecule.

Binding energy calculation. Molecular Mechanics Generalized Born Surface Area (MMGBSA) solvation[69] were used to calculate the binding energies for the best poses of LAT1-cholesterol and LAT1-cholesterol-ATP complexes derived from Induced fit docking XP (i.e. docking score). Default parameters with VSGB 2.051 energy model[70] and OPLS3e force field were applied.

Visualization of docking results. Molecular graphics and visualization of docking results were performed with the UCSF Chimera v.1.7 software (Resource for Biocomputing, Visualization, and Informatics, University of California, San Francisco, CA, USA)[71].

Alignment. The amino acid sequence of SLC7 members and other orthologues were downloaded from UniProt and aligned through the Clustal Omega[72].

Homology modeling. We used a previously published homology model of LAT1 described in[73,74]. Briefly, the model was built using MODELLER using the structure of the arginine/agmatine transporter AdiC from *E. coli* in the outward open conformation (PDB ID: 5J4N) as a template[75].

Statistical analysis. Results were analyzed by nonparametric Student's t-test as described in figure legends.

Received: 22 April 2020; Accepted: 17 September 2020
Published online: 07 October 2020

References

1. Fotiadis, D., Kanai, Y. & Palacin, M. The SLC3 and SLC7 families of amino acid transporters. *Mol. Aspects Med.* **34**, 139–158. https://doi.org/10.1016/j.mam.2012.10.007 (2013).
2. Scalise, M., Galluccio, M., Console, L., Pochini, L. & Indiveri, C. The Human SLC7A5 (LAT1): The intriguing histidine/large neutral amino acid transporter and its relevance to human health. *Front. Chem.* **6**, 243. https://doi.org/10.3389/fchem.2018.00243 (2018).
3. Napolitano, L. *et al.* LAT1 is the transport competent unit of the LAT1/CD98 heterodimeric amino acid transporter. *Int. J. Biochem. Cell Biol.* **67**, 25–33. https://doi.org/10.1016/j.biocel.2015.08.004 (2015).
4. Cantor, J. M. & Ginsberg, M. H. CD98 at the crossroads of adaptive immunity and cancer. *J. Cell Sci.* **125**, 1373–1382. https://doi.org/10.1242/jcs.096040 (2012).
5. Tarlungeanu, D. C. *et al.* Impaired amino acid transport at the blood brain barrier is a cause of autism spectrum disorder. *Cell* **167**, 1481–1494.e1418. https://doi.org/10.1016/j.cell.2016.11.013 (2016).
6. Ohgaki, R. *et al.* Essential roles of L-type amino acid transporter 1 in syncytiotrophoblast development by presenting fusogenic 4F2hc. *Mol. Cell. Biol.* https://doi.org/10.1128/MCB.00427-16 (2017).
7. Bhutia, Y. D., Babu, E., Ramachandran, S. & Ganapathy, V. Amino Acid transporters in cancer and their relevance to "glutamine addiction": Novel targets for the design of a new class of anticancer drugs. *Can. Res.* **75**, 1782–1788. https://doi.org/10.1158/0008-5472.CAN-14-3745 (2015).
8. Nicklin, P. *et al.* Bidirectional transport of amino acids regulates mTOR and autophagy. *Cell* **136**, 521–534. https://doi.org/10.1016/j.cell.2008.11.044 (2009).
9. Scalise, M., Pochini, L., Galluccio, M., Console, L. & Indiveri, C. Glutamine transport and mitochondrial metabolism in cancer cell growth. *Front. Oncol.* **7**, 306. https://doi.org/10.3389/fonc.2017.00306 (2017).
10. Broer, S. & Broer, A. Amino acid homeostasis and signalling in mammalian cells and organisms. *Biochem. J.* **474**, 1935–1963. https://doi.org/10.1042/BCJ20160822 (2017).
11. Wolfson, R. L. & Sabatini, D. M. The dawn of the age of amino acid sensors for the mTORC1 pathway. *Cell Metab.* **26**, 301–309. https://doi.org/10.1016/j.cmet.2017.07.001 (2017).
12. Singh, N. & Ecker, G. F. Insights into the structure, function, and ligand discovery of the large neutral amino acid transporter 1, LAT1. *Int. J. Mol. Sci.* https://doi.org/10.3390/ijms19051278 (2018).
13. Singh, N. *et al.* Discovery of potent inhibitors for the large neutral amino acid transporter 1 (LAT1) by structure-based methods. *Int. J. Mol. Sci.* https://doi.org/10.3390/ijms20010027 (2018).
14. Singh, N., Villoutreix, B. O. & Ecker, G. F. Rigorous sampling of docking poses unveils binding hypothesis for the halogenated ligands of L-type Amino acid Transporter 1 (LAT1). *Sci. Rep.* **9**, 15061. https://doi.org/10.1038/s41598-019-51455-8 (2019).

15. Yan, R., Zhao, X., Lei, J. & Zhou, Q. Structure of the human LAT1-4F2hc heteromeric amino acid transporter complex. *Nature* **568**, 127–130. https://doi.org/10.1038/s41586-019-1011-z (2019).
16. Oda, K. *et al.* L-type amino acid transporter 1 inhibitors inhibit tumor cell growth. *Cancer Sci.* **101**, 173–179. https://doi.org/10.1111/j.1349-7006.2009.01386.x (2010).
17. Okano, N. *et al.* First-in-human phase I study of JPH203, an L-type amino acid transporter 1 inhibitor, in patients with advanced solid tumors. *Invest. New Drugs* https://doi.org/10.1007/s10637-020-00924-3 (2020).
18. del Amo, E. M., Urtti, A. & Yliperttula, M. Pharmacokinetic role of L-type amino acid transporters LAT1 and LAT2. *Eur. J. Pharm. Sci. Off. J. Eur. Federation Pharm. Sci.* **35**, 161–174. https://doi.org/10.1016/j.ejps.2008.06.015 (2008).
19. Scalise, M., Pochini, L., Giangregorio, N., Tonazzi, A. & Indiveri, C. Proteoliposomes as tool for assaying membrane transporter functions and interactions with xenobiotics. *Pharmaceutics* **5**, 472–497. https://doi.org/10.3390/pharmaceutics5030472 (2013).
20. Dickens, D. *et al.* Modulation of LAT1 (SLC7A5) transporter activity and stability by membrane cholesterol. *Sci. Rep.* **7**, 43580. https://doi.org/10.1038/srep43580 (2017).
21. Napolitano, L. *et al.* Novel insights into the transport mechanism of the human amino acid transporter LAT1 (SLC7A5). Probing critical residues for substrate translocation. *Biochim. Biophys. Acta General Subjects* **1861**, 727–736. https://doi.org/10.1016/j.bbagen.2017.01.013 (2017).
22. Cosco, J., Regina, T. M. R., Scalise, M., Galluccio, M. & Indiveri, C. Regulatory aspects of the vacuolar CAT2 arginine transporter of *S. lycopersicum*: Role of osmotic pressure and cations. *Int. J. Mol. Sci.* https://doi.org/10.3390/ijms20040906 (2019).
23. Pochini, L. *et al.* The human OCTN1 (SLC22A4) reconstituted in liposomes catalyzes acetylcholine transport which is defective in the mutant L503F associated to the Crohn's disease. *Biochem. Biophys. Acta.* **559–565**, 2012. https://doi.org/10.1016/j.bbamem.2011.12.014 (1818).
24. Levine, K. B., Cloherty, E. K., Hamill, S. & Carruthers, A. Molecular determinants of sugar transport regulation by ATP. *Biochemistry* **41**, 12629–12638. https://doi.org/10.1021/bi0258997 (2002).
25. Echtay, K. S. *et al.* Uncoupling proteins: Martin Klingenberg's contributions for 40 years. *Arch. Biochem. Biophys.* **657**, 41–55. https://doi.org/10.1016/j.abb.2018.09.006 (2018).
26. Fitz, J. G. Regulation of cellular ATP release. *Trans. Am. Clin. Climatol. Assoc.* **118**, 199–208 (2007).
27. Traut, T. W. Physiological concentrations of purines and pyrimidines. *Mol. Cell. Biochem.* **140**, 1–22. https://doi.org/10.1007/bf00928361 (1994).
28. Falzoni, S., Donvito, G. & Di Virgilio, F. Detecting adenosine triphosphate in the pericellular space. *Interface Focus* **3**, 20120101. https://doi.org/10.1098/rsfs.2012.0101 (2013).
29. Halgren, T. New method for fast and accurate binding-site identification and analysis. *Chem. Biol. Drug Des.* **69**, 146–148. https://doi.org/10.1111/j.1747-0285.2007.00483.x (2007).
30. Halgren, T. A. Identifying and characterizing binding sites and assessing druggability. *J. Chem. Inf. Model.* **49**, 377–389. https://doi.org/10.1021/ci800324m (2009).
31. Fantini, J. & Barrantes, F. J. How cholesterol interacts with membrane proteins: an exploration of cholesterol-binding sites including CRAC, CARC, and tilted domains. *Front. Physiol.* **4**, 31. https://doi.org/10.3389/fphys.2013.00031 (2013).
32. Trott, O. & Olson, A. J. AutoDock Vina: improving the speed and accuracy of docking with a new scoring function, efficient optimization, and multithreading. *J. Comput. Chem.* **31**, 455–461. https://doi.org/10.1002/jcc.21334 (2010).
33. Kanai, Y. *et al.* Expression cloning and characterization of a transporter for large neutral amino acids activated by the heavy chain of 4F2 antigen (CD98). *J. Biol. Chem.* **273**, 23629–23632. https://doi.org/10.1074/jbc.273.37.23629 (1998).
34. Penmatsa, A., Wang, K. H. & Gouaux, E. X-ray structure of dopamine transporter elucidates antidepressant mechanism. *Nature* **503**, 85–90. https://doi.org/10.1038/nature12533 (2013).
35. Laursen, L. *et al.* Cholesterol binding to a conserved site modulates the conformation, pharmacology, and transport kinetics of the human serotonin transporter. *J. Biol. Chem.* **293**, 3510–3523. https://doi.org/10.1074/jbc.M117.809046 (2018).
36. Coleman, J. A., Green, E. M. & Gouaux, E. X-ray structures and mechanism of the human serotonin transporter. *Nature* **532**, 334–339. https://doi.org/10.1038/nature17629 (2016).
37. Pochini, L. *et al.* Effect of cholesterol on the organic cation transporter OCTN1 (SLC22A4). *Int. J. Mol. Sci.* https://doi.org/10.3390/ijms21031091 (2020).
38. Scalise, M. *et al.* Insights into the transport side of the human SLC38A9 transceptor. *Biochim. Biophys. Acta* **1558–1567**, 2019. https://doi.org/10.1016/j.bbamem.2019.07.006 (1861).
39. Scalise, M. *et al.* Interaction of cholesterol with the human SLC1A5 (ASCT2): Insights into structure/function relationships. *Front. Mol. Biosci.* **6**, 110. https://doi.org/10.3389/fmolb.2019.00110 (2019).
40. Castellano, B. M. *et al.* Lysosomal cholesterol activates mTORC1 via an SLC38A9-Niemann-Pick C1 signaling complex. *Science* **355**, 1306–1311. https://doi.org/10.1126/science.aag1417 (2017).
41. Hormann, S., Gai, Z., Kullak-Ublick, G. A. & Visentin, M. Plasma membrane cholesterol regulates the allosteric binding of 1-methyl-4-phenylpyridinium to organic cation transporter 2 (SLC22A2). *J. Pharmacol. Exp. Therap.* **372**, 46–53. https://doi.org/10.1124/jpet.119.260877 (2020).
42. Barnes, K., Ingram, J. C., Bennett, M. D., Stewart, G. W. & Baldwin, S. A. Methyl-beta-cyclodextrin stimulates glucose uptake in Clone 9 cells: a possible role for lipid rafts. *Biochem. J.* **378**, 343–351. https://doi.org/10.1042/BJ20031186 (2004).
43. Zeppelin, T., Ladefoged, L. K., Sinning, S., Periole, X. & Schiott, B. A direct interaction of cholesterol with the dopamine transporter prevents its out-to-inward transition. *PLoS Comput. Biol.* **14**, e1005907. https://doi.org/10.1371/journal.pcbi.1005907 (2018).
44. Garcia, A. *et al.* Cholesterol depletion inhibits Na(+), K(+)-ATPase activity in a near-native membrane environment. *J. Biol. Chem.* **294**, 5956–5969. https://doi.org/10.1074/jbc.RA118.006223 (2019).
45. Lee, Y. *et al.* Cryo-EM structure of the human L-type amino acid transporter 1 in complex with glycoprotein CD98hc. *Nat. Struct. Mol. Biol.* **26**, 510–517. https://doi.org/10.1038/s41594-019-0237-7 (2019).
46. Kaczmarski, J. A. *et al.* Structural basis for the allosteric regulation of the sbta bicarbonate transporter by the PII-like protein, SbtB, from Cyanobium sp. PCC7001. *Biochemistry* **58**, 5030–5039. https://doi.org/10.1021/acs.biochem.9b00880 (2019).
47. Bertholet, A. M. & Kirichok, Y. UCP1: A transporter for H(+) and fatty acid anions. *Biochimie* **134**, 28–34. https://doi.org/10.1016/j.biochi.2016.10.013 (2017).
48. Errasti-Murugarren, E. *et al.* L amino acid transporter structure and molecular bases for the asymmetry of substrate interaction. *Nat. Commun.* **10**, 1807. https://doi.org/10.1038/s41467-019-09837-z (2019).
49. Shaffer, P. L., Goehring, A., Shankaranarayanan, A. & Gouaux, E. Structure and mechanism of a Na+-independent amino acid transporter. *Science* **325**, 1010–1014. https://doi.org/10.1126/science.1176088 (2009).
50. Jungnickel, K. E. J., Parker, J. L. & Newstead, S. Structural basis for amino acid transport by the CAT family of SLC7 transporters. *Nat. Commun.* **9**, 550. https://doi.org/10.1038/s41467-018-03066-6 (2018).
51. Palazzolo, L. *et al.* In silico description of LAT1 transport mechanism at an atomistic level. *Front. Chem.* **6**, 350. https://doi.org/10.3389/fchem.2018.00350 (2018).
52. Cantor, J. R. & Sabatini, D. M. Cancer cell metabolism: One hallmark, many faces. *Cancer Discov.* **2**, 881–898. https://doi.org/10.1158/2159-8290.CD-12-0345 (2012).
53. Ho, S. N., Hunt, H. D., Horton, R. M., Pullen, J. K. & Pease, L. R. Site-directed mutagenesis by overlap extension using the polymerase chain reaction. *Gene* **77**, 51–59. https://doi.org/10.1016/0378-1119(89)90358-2 (1989).

54. Galluccio, M. *et al.* Functional and molecular effects of mercury compounds on the human OCTN1 cation transporter: C50 and C136 are the targets for potent inhibition. *Toxicol. Sci. Off. J. Society Toxicol.* **144**, 105–113. https://doi.org/10.1093/toxsci/kfu259 (2015).
55. Galluccio, M., Pingitore, P., Scalise, M. & Indiveri, C. Cloning, large scale over-expression in *E. coli* and purification of the components of the human LAT 1 (SLC7A5) amino acid transporter. *Protein J.* **32**, 442–448. https://doi.org/10.1007/s10930-013-9503-4 (2013).
56. Massey, J. B. Effect of cholesteryl hemisuccinate on the interfacial properties of phosphatidylcholine bilayers. *Biochem. Biophys. Acta.* **1415**, 193–204. https://doi.org/10.1016/s0005-2736(98)00194-1 (1998).
57. Indiveri, C., Prezioso, G., Dierks, T., Kramer, R. & Palmieri, F. Kinetic characterization of the reconstituted dicarboxylate carrier from mitochondria: A four-binding-site sequential transport system. *Biochem. Biophys. Acta.* **1143**, 310–318. https://doi.org/10.1016/0005-2728(93)90202-q (1993).
58. Schrödinger, R. Maestro, Schrödinger, LLC, New York, NY (2019).
59. Schrödinger, R. Protein Preparation Wizard; Epik, Schrödinger, LLC, New York, NY, 2016; Impact, Schrödinger, LLC, New York, NY, 2016; Prime, Schrödinger, LLC, New York, NY (2019).
60. Sastry, G. M., Adzhigirey, M., Day, T., Annabhimoju, R. & Sherman, W. Protein and ligand preparation: Parameters, protocols, and influence on virtual screening enrichments. *J. Comput. Aided Mol. Des.* **27**, 221–234. https://doi.org/10.1007/s10822-013-9644-8 (2013).
61. Schrödinger, R SiteMap, Schrödinger, LLC, New York, NY (2019).
62. Schrödinger, R. LigPrep, Schrödinger, LLC, New York, NY (2019).
63. Halgren, T. A. *et al.* Glide: A new approach for rapid, accurate docking and scoring. 2. Enrichment factors in database screening. *J. Med. Chem.* **47**, 1750–1759. https://doi.org/10.1021/jm030644s (2004).
64. Shelley, J. C. *et al.* Epik: A software program for pK(a) prediction and protonation state generation for drug-like molecules. *J. Comput. Aided Mol. Des.* **21**, 681–691. https://doi.org/10.1007/s10822-007-9133-z (2007).
65. Schrödinger, R. Induced Fit Docking protocol; Glide, Schrödinger, LLC, New York, NY, 2016; Prime, Schrödinger, LLC, New York, NY (2019).
66. Farid, R., Day, T., Friesner, R. A. & Pearlstein, R. A. New insights about HERG blockade obtained from protein modeling, potential energy mapping, and docking studies. *Bioorg. Med. Chem.* **14**, 3160–3173. https://doi.org/10.1016/j.bmc.2005.12.032 (2006).
67. Sherman, W., Day, T., Jacobson, M. P., Friesner, R. A. & Farid, R. Novel procedure for modeling ligand/receptor induced fit effects. *J. Med. Chem.* **49**, 534–553. https://doi.org/10.1021/jm050540c (2006).
68. Friesner, R. A. *et al.* Glide: A new approach for rapid, accurate docking and scoring. 1. Method and assessment of docking accuracy. *J. Med. Chem.* **47**, 1739–1749. https://doi.org/10.1021/jm0306430 (2004).
69. Genheden, S. & Ryde, U. The MM/PBSA and MM/GBSA methods to estimate ligand-binding affinities. *Expert Opin. Drug Discov.* **10**, 449–461. https://doi.org/10.1517/17460441.2015.1032936 (2015).
70. Li, J. *et al.* The VSGB 2.0 model: A next generation energy model for high resolution protein structure modeling. *Proteins* **79**, 2794–2812. https://doi.org/10.1002/prot.23106 (2011).
71. Pettersen, E. F. *et al.* UCSF Chimera—A visualization system for exploratory research and analysis. *J. Comput. Chem.* **25**, 1605–1612. https://doi.org/10.1002/jcc.20084 (2004).
72. Madeira, F. *et al.* The EMBL-EBI search and sequence analysis tools APIs in 2019. *Nucleic Acids Res.* **47**, W636–W641. https://doi.org/10.1093/nar/gkz268 (2019).
73. Chien, H. C. *et al.* Reevaluating the substrate specificity of the L-type amino acid transporter (LAT1). *J. Med. Chem.* **61**, 7358–7373. https://doi.org/10.1021/acs.jmedchem.8b01007 (2018).
74. Sali, A. & Blundell, T. L. Comparative protein modelling by satisfaction of spatial restraints. *J. Mol. Biol.* **234**, 779–815. https://doi.org/10.1006/jmbi.1993.1626 (1993).
75. Ilgu, H. *et al.* Insights into the molecular basis for substrate binding and specificity of the wild-type L-arginine/agmatine antiporter AdiC. *Proc. Natl. Acad. Sci. USA* **113**, 10358–10363. https://doi.org/10.1073/pnas.1605442113 (2016).

Acknowledgements

This work was supported by PRIN (Progetti di Ricerca di Interesse Nazionale) project n. 2017PAB8EM MIUR (Italian Ministry of Instruction, University and Research) to CI. CC, RM, and GFE acknowledge funding from the Innovative Medicines Initiative 2 Joint Undertaking under Grant agreement No. 777372 ("RESOLUTE"). This Joint Undertaking receives support from the European Union's Horizon 2020 research and innovation program and EFPIA.

Author contributions

J.C. and M.S. planned, performed experiments, analyzed data and contributed in writing the paper; J.C. and C.C. performed computational analysis and data interpretation; M.S. performed cell culture experiments; M.G. performed WT and mutant production in *E. coli*; T.M. contributed to proteoliposome experimental set-up; R.M. and F.R. contributed to perform computational analysis; G.E. supervised computational analysis; C.I. supervised the work and wrote the paper; all authors contributed in manuscript revision.

Competing interests

The authors declare no competing interests.

Additional information

Supplementary information is available for this paper at https://doi.org/10.1038/s41598-020-73757-y.

Correspondence and requests for materials should be addressed to C.I.

Reprints and permissions information is available at www.nature.com/reprints.

Publisher's note Springer Nature remains neutral with regard to jurisdictional claims in published maps and institutional affiliations.